Delft University of Technology

Faculty of Civil Engineering and Geosciences
Section Geo-Engineering

MSc Thesis

The capabilities of the Plaxis Shotcrete material model for designing laterally loaded reinforced concrete structures in the subsurface

---

Author:
T.W.P. Maatkamp

Graduation committee:

Prof. Dr. Ir. K.G. Gavin	Delft University of Technology
Dr. Ir. R.B.J. Brinkgreve	Plaxis BV – Delft University of Technology
Ing. H.J. Everts	ABT BV – Delft University of Technology
Ir. P. Lagendijk	Aronsohn raadgevende ingenieurs BV – Delft University of Technology
Ing. N.T. Loonen	ABT BV

24 October 2016

Preface

After eight months of research at ABT b.v. in order to obtain the Master of Science degree in Civil Engineering at Delft University of Technology this is the final report. The thesis regards the subject of designing laterally loaded reinforced concrete structures in Plaxis with the help of the recently developed Shotcrete material model. A practical application is found proving the applicability of the model for different kind of uses.

To complete one of the biggest challenges I had great help and support of friends, family, staff and colleagues. In this preface I would like to mention some in particular which helped me to complete my study and the finalising thesis. However I would like to thank all people which contributed to my student life by means of personal development and career perspective.

First of all I want to thank all graduation committee members for their time, input and critical review during my thesis. Ken Gavin for his scientific view on the subject and his input during each meeting. Ronald Brinkgreve for his Plaxis knowledge, the providence of the material model information and asking the right challenging questions during the committee meetings. Bert Everts for the introduction to the company ABT bv and the subject itself. Paul Lagendijk for reviewing the concept reports in depth and his interest in the subject. Last but not least I would like to thank my daily supervisor, Niki Loonen, at ABT bv. His guidance, critical view and motivating words made it possible to deliver this report.

Furthermore I would like to thank my colleagues from the geotechnical department of ABT in Velp and Delft for the input during the thesis and the pleasant and cosy work environment. I am ABT grateful giving me the opportunity to fulfil the thesis in a practical work environment and contribute in an innovative way to improve the design process.

At last, I would like to thank my family, parents, sister, girlfriend, friends and roommates for their support and positive distraction during my study.

Tom Maatkamp

Delft, October 2016

Summary

A hot topic in the Netherlands is the safety reassessment of dikes. Currently several (river)dikes are being reinforced to withstand a given normative high water level. The environment of those dikes is often characterised by small floodplains and urban areas right next to the dike, wherefore standard geo-technical measures cannot be applied. Installing a diaphragm wall in the crest of the dike is in such a case a measure that can guarantee the safety, by preventing the development of a shear plane when the dike is subjected to a normative high water level. In engineering practice modelling of those structures is simplified by using a linear elastic plate element with a reduced stiffness, to account for concrete cracking upon loading, or a linear elastic-perfectly plastic volume element in the geotechnical finite element code Plaxis.

In this master thesis attention will be paid to the possibility of modelling and designing such (geotechnical) reinforced concrete structures in Plaxis more accurately with the use of a new concrete material model. Recently the Shotcrete material model for volume elements is released by Plaxis. The Shotcrete material model accounts for non-linear and time dependent behaviour, i.e. more realistic behaviour, of concrete. The material model is however only been used for modelling unreinforced shotcrete in a NATM application. The capabilities of using the Shotcrete material model to design laterally loaded reinforced concrete structures in the subsurface is investigated.

At first the theoretical applicability of the Shotcrete material model to design reinforced concrete structures in Plaxis 2D is being researched. Verification against guidelines and model codes for describing concrete behaviour showed that the material model has the prospect to model non-linear concrete material behaviour, including cracking, realistically. By means of analysing a statically determined reinforced concrete bending beam model it is found that using a by elastoplastic plate element(s) reinforced Shotcrete volume element has additional value over the use of a linear elastic and a linear elastic-perfectly plastic material model when modelling a reinforced concrete structure. Nevertheless it is observed that the results given by the Shotcrete model are slightly mesh sensitive.

The use of a by elastoplastic plate element(s) reinforced Shotcrete volume element is subsequently verified by comparing the results to commonly for design used M-κ and M-N-κ hand calculations. It is demonstrated that in case the reinforced concrete structure is subjected to bending, as well as a normal force, the model gives accurate and realistic results. Deviations can be explained by differences in calculation method, hand calculation versus numerical model. When the structure is subjected to a normal force attention has to be paid to pre-stressing of the reinforcement and the resulting stresses in the concrete.

An elastoplastic plate reinforced Shotcrete volume element is used to model a diaphragm wall next to an excavation. Evaluation of an excavation next to a diaphragm wall, such that structural bending failure is the normative failure mode, showed that using an elastoplastic plate reinforced Shotcrete volume element gives improved results with respect to commonly used modelling methods. The other used modelling methods are a linear elastic, respectively equivalent to the reinforced diaphragm wall M-κ, plate element and a linear elastic volume element. A lower bending moment is obtained in the structure

at the same deformation, which is partly the effect of higher (soil-structure) interface shear stresses. During the analysis it is found that obtaining the correct bending moment in the structure is not straightforward. It is found that only by taking an internal force equilibrium at the neutral line in the normative cross-section of the diaphragm wall the correct bending moment can be obtained.

Applying the model in the Kinderdijk-Schoonhovenseveer (KIS) dike reinforcement project demonstrates the advantage of applying a more realistic, nevertheless more complex, way of modelling reinforced concrete structures in Plaxis 2D. The obtained bending moment in the structure increases with 25 % in SLS and decreases with 10 % in ULS with respect to modelling the diaphragm wall by means of a linear elastic plate element with a reduced stiffness, to account for cracking. To conclude, a stepwise approach is proposed to model a laterally loaded reinforced concrete structure in the subsurface realistically, by means of implementing a by elastoplastic plate elements reinforced Shotcrete volume element.

Table of contents

List of Symbols and abbreviations

a	Increase of ϵ_{cp}^{p} with increase of p'
A_c	Cross-sectional area [m^2]
b	Width [m]
D	Diameter [m]
E_c	Concrete stiffness [GPa]
E_{cm}	Mean concrete stiffness [GPa]
E_{oed}	Tangent stiffness modulus for primary oedometer loading [kN/m^2]
E_1/E_{28}	Time dependency of elastic stiffness
E_{28}	Stiffness of cured shotcrete at t_{hydr}
ϵ	(Total) strain
$\epsilon_{cf,28}^{p}$	Compressive plastic failure strain after 28 days
ϵ_{cp}^{p}	Uniaxial compression plastic peak strain at 1h, 8h, 24h
ϵ_{cr}	Creep strain
$\epsilon_{cu,28}^{p}$	Compressive plastic ultimate strain after 28 days
ϵ_e	Elastic strain
ϵ_p	Plastic strain
ϵ_{shr}	Shrinkage strain
ϵ_3^p	Peak strain in major principal direction
ϵ_{∞}^{shr}	Final Shrinkage strain
D	Diameter [m]
$f_{c,1}/f_{c,28}$	Time dependency of strength
$f_{c,28}$	Uniaxial compressive strength of cured shotcrete at t_{hydr} [MPa]
f_{cd}	Concrete design strength [kN]
f_{cfn}	Normalised failure strength (compression)
f_{ck}	Characteristic compressive strength [MPa]
$f_{ck,cube}$	Characteristic compressive cube strength [MPa]
f_{cm}	Mean compressive strength [MPa]
f_{ct}	Uniaxial tensile strength [MPa]
f_{ctk}	Characteristic tensile strength [MPa]
f_{ctm}	Mean tensile strength [MPa]
f_{cun}	Normalised residual strength (compression)
f_{c0n}	Normalised initially mobilised strength
$f_{t,28}$	Uniaxial tensile strength of cured shotcrete at t_{hydr} [MPa]
f_{tp}	Tensile peak strength
f_{tu}	Ultimate tensile strength
f_{tun}	Ratio of residual vs. peak tensile strength
f_{tyn}	Normalised tensile yield strength
f_{yd}	Design yield strength of reinforcement [kN]
f_{yk}	Characteristic yield strength of reinforcement [kN]
G	Shear modulus [kN/m^2]
$G_{c,28}$	Compressive fracture energy of cured shotcrete at t_{hydr} [kN/m]
$G_{t,28}$	Tensile fracture energy of cured shotcrete at t_{hydr} [kN/m]
h	Height [m]
H_c	Compressive hardening parameter

H_t	Tensile hardening parameter
I	Moment of inertia [m^4]
K_{IC}^2	Critical stress intensity factor [$MN/m^{3/2}$]
k_1, k_2, k_3, k_4	Constants regarding crack distance
$\kappa_r, \kappa_y, \kappa_{c,pl}$ and κ_{rd}.	Curvature [m^{-1}], at respectively rupture, yielding, plasticity and failure
L	Length [m]
l_{eq}	Equivalent length (if no regularisation is used)
$M, M_r, M_y, M_{c,pl}$ and M_{rd}	Moment [kNm], respectively at respectively rupture, yielding, plasticity and failure
N_p	Allowable Normal force in rebar (till plasticity) [kN]
$\rho_{p,eff}$	Effective reinforcement percentage
ϕ_{cr}	Ratio between creep and elastic strains
ϕ_{max}	Maximum friction angle
ψ	Dilantancy angle [^{0}]
q	Line load [kN/m]
$s_{r,max}$	Maximum distance between two cracks [m]
σ	Stress [kN/m^2]
σ_c	Concrete stress [kN/m^2]
σ_{ct}	Concrete tensile stress [kN/m^2]
σ_s	Stress in steel [kN/m^2]
σ_{xx} , σ_{yy} , σ_{zz}	Stress in x, respectively y and z-direction [kN/m^2]
σ_3	Stress in major principal direction
t_{hydr}	Time for full hydration (usually 28 days) [d]
t_{50}^{cr}	Time for 50% of creep strains
t_{50}^{shr}	Time for 50% of shrinkage strains
τ_{xy}	Shear stress on x-y plane [kN/m^2]
u	Perimeter of the member in contact with atmosphere [m]
u_y	Displacement in y-direction [m]
ν	Poisson's ratio
w	Bending deformation [m]
γ_{fc}	Safety factor for compressive strength
γ_{ft}	Safety factor for tensile strength
$\varnothing$	Diameter of reinforcement [mm]

FEM	Finite element model
LEPP	Linear elastic-perfectly plastic
MC	Mohr-Coulomb
NHW	Normative high water level
SC	Shotcrete
SLS	Serviceability limit state
ULS	Ultimate limit state

1 Introduction

1.1 Reading guide

Chapter 1 gives an introduction in the research. In this first chapter, at first a motivation for the research to be carried out is given. Thereafter the problem to be solved is defined. The objective is outlined in order to clarify the scope of the research. In the introductory chapter also an overview of the limitations of the research is stated.

In chapter 2 the theoretical background of the subject to be covered is given. This chapter consists of 4 main parts and is finalised with a conclusion, linking the different aspects. The first part of the theoretical background gives insight in the behaviour of reinforced concrete. In the appendix more details about unreinforced concrete behaviour and other theoretical background used for verification of the Shotcrete material model is given. The second part contains a model description of the Shotcrete material model. The model features as well as the input parameters and values for reinforced concrete structures are given. The third part contains a short introduction in the behaviour of laterally loaded structures in the subsurface, which can be linked in a further stage to the applicability for modelling reinforced concrete structures in the subsurface. The last paragraph gives information about the different (current) options to model reinforced concrete structures. To conclude the theoretical background a conclusion about the theoretical applicability of modelling reinforced concrete structures with the Plaxis Shotcrete material model is drawn.

In chapter 3 a preliminary model setup is presented. A single stress-point analysis and a parameter sensitivity analysis are carried out in order to be able to fit the Shotcrete material model such that it represents commonly used (C30/37) structural concrete. Again additional detailed insight in the model behaviour is given in the appendix. After a good fit is found, a first reinforced bending beam model on two hinges is evaluated. The Shotcrete material model results, deformation, stress distribution and rebar force, are compared to those of other material models and hand calculations. Furthermore the Shotcrete material model results for a reinforced concrete bending beam test case are evaluated against theory. A mesh sensitivity analysis is carried out to be able to evaluate the applicability of the model for soil-structure interaction cases. Afterwards a comparison is made with proven design hand calculation, M-κ and M-N-κ diagram, for a reinforced concrete structure subjected to bending (and normal force). At last a conclusion is formed about the Shotcrete material model's applicability for modelling laterally loaded reinforced concrete beams.

In chapter 4 a soil-structure interaction case, where an excavation takes place next to a diaphragm wall is considered. In this case, plate elements as well as reinforced volume elements are tested on deformation and bending moments. The Shotcrete material model results are compared with M-κ based calculations. The to be used method to realistically back calculate the occurring bending moment is researched (in the appendix). Furthermore a in depth analysis of the behaviour of the reinforced

Shotcrete volume element is carried out. A conclusion is drawn about the use, applicability and capabilities of the Shotcrete material model for such cases.

In chapter 5 a case study showing the applicability of the Shotcrete material model in design cases is considered. A dike, in the KIS project, is subjected to a normative high water level with a probability of occurrence of 1/2000. To guarantee safety and the fact that commonly used applied dike (stability) reinforcement measures were not possible, a diaphragm wall is installed in the crest of the dike. An SLS and ULS design analysis are carried out, comparing the current design method with a by plate reinforced Shotcrete volume element equivalent to the (real) installed diaphragm wall. Differences in obtained results are analysed and the capabilities of the Plaxis Shotcrete material model to design such a case in engineering practice are evaluated.

Chapter 6 contains the conclusion regarding the capabilities of the Plaxis Shotcrete material model to design laterally loaded reinforced concrete structures in the subsurface. Besides in this chapter the found results are discussed and recommendations for further research are given.

The structure of the report is given in Figure 1.

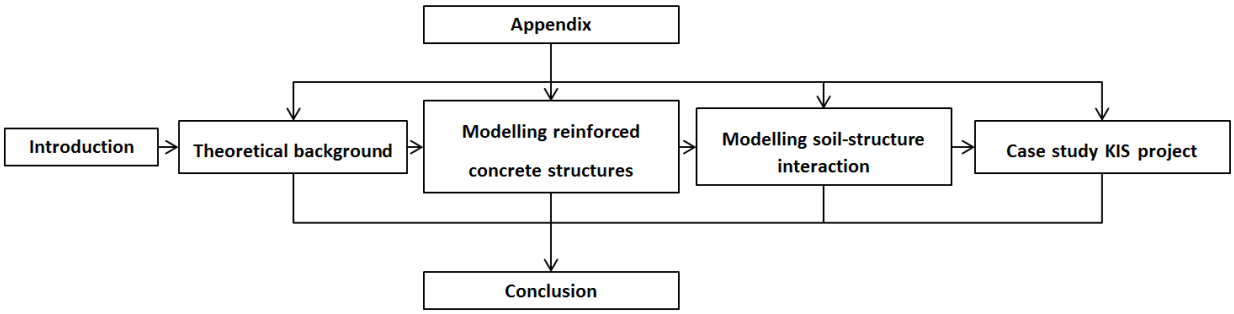

Figure 1: Report structure.

1.2 Research motivation

A hot topic in the Netherlands is the safety reassessment of dikes, resulting from the fact that new standards have to be adopted. The focus is changed from the perspective of probability of failure to a risk based safety approach. Risk is defined as the likelihood and the consequence of an event (Van Staveren, 2006). Besides hydraulic safety, probability of overtopping, geotechnical safety plays also an important role in the overall safety assessment. Geotechnical failure mechanisms have influence on the dike safety and therefore on the risk of flooding.

Currently several (river)dikes are being reinforced in the Netherlands. The environment of those dikes is often characterised by small floodplains and urban areas right next to the dike. In some cases houses are even built on the dike. The past decades the focus of safety of the area behind the dike was considered by the peak discharge combined with the cross-sectional area of the river. To enlarge the discharge of the river during high water levels the river was dredged or other measures were taken to increase the river's cross-sectional area and or velocity. This resulted in the fact that erosion increased and the river

bottom reached the level of the Pleistocene sand layer. A typical cross-sectional profile of a dike in such an environment is given in Figure 2.

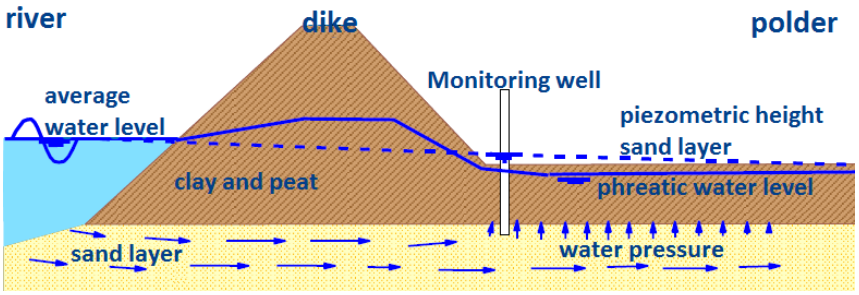

Figure 2: Characteristic lay-out of dike environment (Janssen, 2016).

When the river makes contact with the Pleistocene sand layer, the river influences the piezometric head and pore pressures in that layer due to the highly permeable character. In many river/dike environments in the Netherlands the layers formed on top of the Holocene sand layer consist of soft soils such as peat and clay. The volumetric weight of these soft soil layers is considerably smaller than that of sand. Another difference in properties concerns the permeability. The soft soil layers on top of the Pleistocene sand layer can be regarded as impermeable, while sand is (highly) permeable. The high permeability of the sand layer causes that the water pressure in the sand layer will rise during high water levels. The increase in water pressure in the sand layer during high water levels causes uplift of the impermeable soft soil layer on top. Uplift is the result of a sharp drop of effective stress at the layer interface. Besides uplift, a geo-technical failure mechanism for dikes, slide planes and circular shear planes are more probable to occur (Figure 3). The stability of the dikes in such environments is thus highly influenced during high river discharges. In Figure 3 this situation is visualised, taking into account a normative high water level with a 1/2000 probability of occurrence (NHW 1/2000).

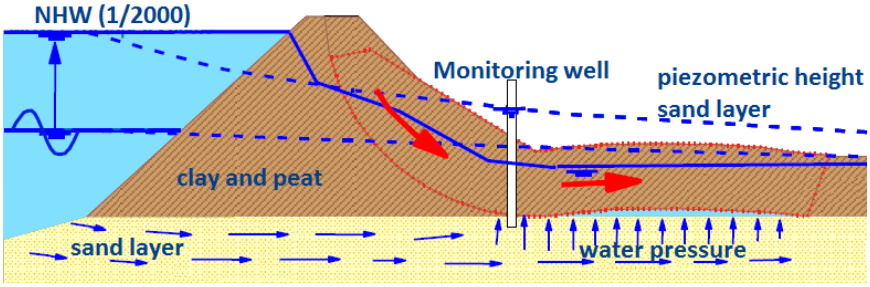

Figure 3: Development of shear plane in dike environment due to high water (Janssen, 2016).

To prevent a circular shear plane several measures can be taken. A common measure is to increase the weight of the inner berm by adding sand layers (embankments). This leads to an increase of effective stress at the layer interface and therefore reduces the probability of a shear plane to occur. Though when houses are present in this area just behind the dike, another solution has be thought of. An alternative measure is to reinforce the dike with structures, such as diaphragm walls or bored piles. These structures have to be able to prevent the development of a circular shear plane. Anchored piles,

installed at the inner toe of the dike, will be used when the houses are present in the near but not on the dike. In this case these piles are subjected to a lateral load caused by a moving soil body. Diaphragm walls are used as a fully water retaining structure and are for this reason installed in the crest of the dike. Attention has to be paid to the fact that the concrete structure in those cases is watertight. Diaphragm walls are constructed in the case that a house is built at the inner toe of the dike. In this master thesis attention will be paid to the possibility of modelling and designing such geotechnical reinforced concrete structures in Plaxis more accurately with the use of a new concrete material model.

1.3 Problem definition

Currently, different modelling programs and calculation methods are used in order to model geotechnical reinforced concrete structures. Modelling the subsurface behaviour is commonly done with the use of Plaxis (FEM). While for the reinforced concrete structure programs such as Technosoft, DIANA (FEM) or Scia are used. Plaxis and DIANA are both capable of modelling the integral design, although both have their specific use and limitations. In Plaxis 2D commonly plate models are implemented to model structural behaviour. However volume elements can be used to model structural behaviour and simultaneously get more insight in the stress distribution. In Plaxis 3D volume elements are used, characterised by a simplified (reinforced) concrete material model. When performing a very detailed structural analysis, DIANA is often used due to its ability to implement a detailed design of the reinforcement as well as the possibility to model non-linear behaviour of concrete. DIANA has also the possibility to model subsurface behaviour, nevertheless it has its limitations in this field compared to Plaxis. By the fact that specific structural respectively subsurface modelling programs have both their limitations, a combination has often to be used during the design process. The coupling between the different programs introduces extra (unwanted) uncertainty. Optimisation is required in order to reduce these uncertainties and come to a more economic design.

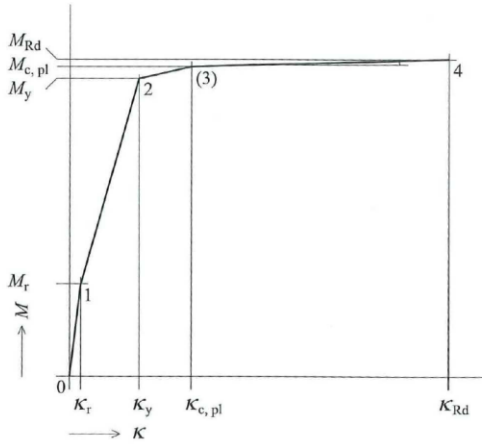

Figure 4: M-κ diagram (Braam & Lagendijk, 2010).

In Plaxis three types of material models can be used when modelling 2D plate elements: elastic, elastoplastic and (non-linear) elastoplastic (M-κ diagram (Figure 4)). Modelling the material behaviour according to an elastoplastic material model with the use of a user defined M-κ diagram gives more

accurate results, concerning the theoretical behaviour of reinforced concrete structures subjected to bending. A simplified linear elastic description of the material behaviour can lead in some cases, laterally loaded piles and diaphragm walls, to a (unrealistically) high occurring bending moment. This unrealistically high occurring bending moment in the model is caused by the fact that cracking (at M_r (Figure 4)) of the concrete material, resulting in a stiffness reduction of the structure, is not taken into account. For this reason using an elastoplastic M-κ material description for plate elements, which considers the reduction of stiffness due to cracking, is a better approximation of reality. Nevertheless it is wished to get more insight in the cracking process and other output results of the reinforced concrete structure subjected to bending. This can be achieved by using a concrete specific material model for a volume element.

The release of a new Plaxis material model for volume elements, Shotcrete material model, has the possibility to model concrete material behaviour more realistically (Schütz, Potts, & Zdravkovic, 2011; Schädlich & Schweiger, 2014b; Witasse, 2016). Shotcrete is a kind of concrete, which can be sprayed onto a surface. This kind of concrete is particularly used for the NATM. NATM is a tunnelling method based on sequential excavation at the tunnel front (Figure 5). Sequential advance of the tunnel face requires stabilisation of the tunnel surface where no permanent (secondary) lining is applied yet. To stabilise those areas, prevent loosening and excessive rock deformation, shotcrete is used. The Shotcrete material model is developed to describe the behaviour of the sprayed concrete for this application. Currently the Shotcrete material model is only used for modelling shotcrete, while it has the prospect to be used for other concrete modelling cases (Witasse, 2016).

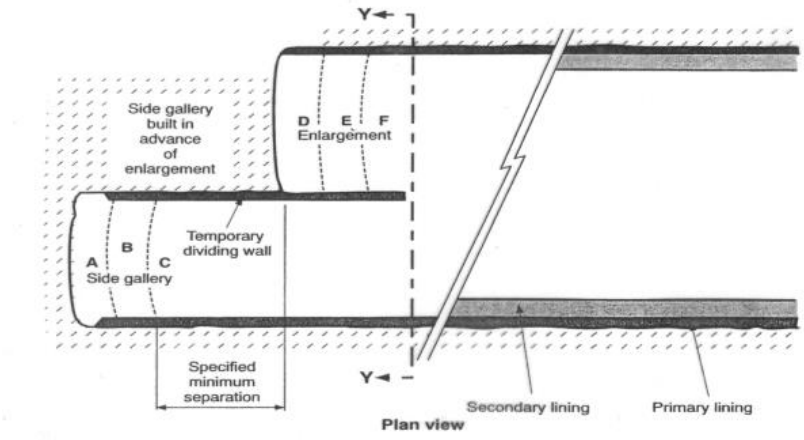

Figure 5: NATM. Primary lining consists of reinforcement and shotcrete. Secondary lining is permanent (Bakker, 2015).

The behaviour of shotcrete, and in general concrete, is non-linear and differs in time due to hydration and hardening of the concrete. The Shotcrete material model is able to describe time dependent and non-linear material behaviour correctly, using normalised hardening and softening parameters (Schütz, Potts, & Zdravkovic, 2011). By the fact that the Shotcrete material model is able to model concrete behaviour in detail, it has to prospect to be used for other applications than only modelling shotcrete as is recently demonstrated by Witasse (2016). Currently in most cases a linear elastic-perfectly plastic

(LEPP) material model with a tension cut-off is used when modelling reinforced concrete structures in the subsurface in Plaxis (Ardiaca, 2009). However the behaviour of in-situ and prefab reinforced concrete is time dependent. Besides, the behaviour is largely determined by age at loading time, relative humidity and the concrete mixture/composition. Furthermore, properties such as stiffness and strength depend on ageing, hydration, creep, shrinkage and thermal deformation. The Shotcrete material model is able to take these processes and the effect on material properties into account (Schädlich & Schweiger, 2014b). Using the Shotcrete material model for designing reinforced concrete structures could therefore be of additional value with respect to a LEPP material modelling approach. In addition, by using the Shotcrete material model for a volume element more realistic visualisation of stress concentrations in structures could be obtained. It provides after all the prospect to use Plaxis for an integral subsurface structure design. An overview of the by Plaxis possible options and material models to model (reinforced) concrete structures are given in Figure 6.

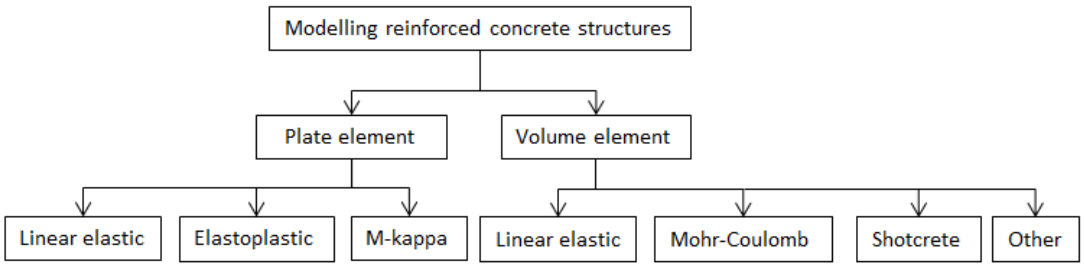

Figure 6: Overview of by Plaxis possible elements and material models to model (reinforced) concrete structures.

A challenging aspect of modelling reinforced concrete structures using the Shotcrete material model in Plaxis is to include reinforcement. The model is, as mentioned before, initially developed for shotcrete, which is typically unreinforced. The major difference between reinforced and unreinforced concrete is the tensile strength of the material. In unreinforced concrete the tensile strength is governed by the tensile strength of the concrete, which is only about 5-10% of the compressive strength of concrete (Braam & Lagendijk, 2010). However for reinforced concrete, as soon as the tensile concrete material strength is reached, initiating cracking, the steel reinforcement will take up the tensile forces. The tensile strength of the steel reinforcement is significantly larger than the tensile strength of concrete, causing that the tensile strength of reinforced concrete is on its turn much larger than the tensile strength of unreinforced concrete. The Shotcrete material model is not designed for taking into account such high tensile strength properties for a continuum. To take the tensile strength properties of reinforced concrete into account a solution has to be found. Rrecent research of Witasse (2016) implies that an option is to incorporate beam/plate elements in a Shotcrete volume element to account for reinforcement. This possibility is further researched and evaluated. Attention has to be paid to the interaction between concrete and reinforcement, for example to the occurring stresses in both elements.

Summarised, research has to be carried out in order to examine the capabilities of the Shotcrete material model in Plaxis to design reinforced concrete structures in the subsurface.

1.4 Objective

The objective of this research is to assess the capabilities of the Shotcrete material model in Plaxis, when designing laterally loaded reinforced concrete structures in the subsurface. The problem stated in paragraph 1.3 has to be tackled in this master thesis. Plaxis is widely used to solve geotechnical numerical problems, however the Shotcrete material model is not extensively used to model concrete yet. It is only used for the designed purpose, modelling the behaviour of shotcrete used in the NATM. Currently reinforced concrete structures in Plaxis (in the subsurface) are modelled by a time independent LEPP material model, although behaviour of concrete is (highly) dependent on time and besides non-linear. An improvement regarding concrete modelling can be made when considering more realistic non-linear behaviour instead of LEPP material behaviour. The capabilities of using Plaxis with non-linear plastic strain hardening and softening Shotcrete material model for other purposes than NATM have to be researched for this reason. In this research only the non-linear aspect of the Shotcrete material model is used. Time dependent behaviour is out of the scope. To accomplish the described objective, several sub objectives are defined:

- Evaluate the theoretical applicability of the Shotcrete material model to model reinforced concrete structure in Plaxis.
- Evaluate the possibilities and limitations of modelling reinforced concrete structures in the subsurface subjected to bending.
- Evaluate simple reinforced concrete bending beam constructions with the use of a linear elastic, a Mohr-Coulomb and a Shotcrete material model in Plaxis.
- Verify a Shotcrete reinforced concrete beam model subjected to bending, respectively bending and normal force with the use of M-κ and M-N-κ diagrams hand calculations.
- Evaluate and validate a diaphragm wall (2D) soil-structure interaction case and an engineering case study with the Shotcrete material model.

1.5 Scope and limitations

This report focusses on the mechanical time independent behaviour of the Shotcrete material model and its applicability in designing laterally loaded reinforced concrete structures. A limited amount of time is available for the thesis, resulting in the limitations concerning the research given below:

- Time dependent concrete behaviour is excluded in the modelling analysis. The Shotcrete material model offers, based on the literature research done, the ability to model time dependent behaviour such as ageing, hydration, creep, shrinkage and thermal deformation correctly. It coops with the effect of increasing brittleness of concrete by increased stiffness and strength during hardening. Standard input values for the parameters influencing time dependent behaviour are found during the literature study. Nevertheless these are excluded in the modelling analysis.
- Only one option to model reinforcement is considered in this research. In this research reinforcement is modelled by means of plate element(s). In Plaxis it is also possible to use

embedded beams. Embedded beams offer the opportunity to include different reinforcement bars and moreover give the opportunity to include bond-slip modelling.

- The option to give the Shotcrete volume element such characteristics that additional elements within a volume element would not be necessary to account for reinforcement is not investigated.
- This research focusses on laterally loaded reinforced concrete structures, while also vertical loading situations may be of interest and worth researching.
- To illustrate the applicability for modelling laterally loaded structures attention is paid to diaphragm wall modelling. However also plates on the subsurface, piles and underwater concrete floors could be illustrative cases and possible applications.
- Designing laterally loaded structures with the help of the Shotcrete material model is only researched in Plaxis 2D. 3D cases such as laterally loaded reinforced piles are not researched.
- The research mainly focusses on comparing model results to proven design calculations, rather than a pure experimental and monitored (case study) validation. This is done by Plaxis (Witasse, 2016).
- The evaluation of the case study mainly focusses on the structural behaviour of the diaphragm wall and the applicability of the Shotcrete model to design such a structure. Less attention is paid to the detailed effect of using the Shotcrete material model on the soil-structure interaction behaviour.

2 Theoretical background

In this chapter the relevant theoretical background is given. The aspects covered, are an introduction in reinforced concrete material behaviour, an introduction in the Shotcrete material model and an overview of the design aspects and calculation methods for laterally loaded reinforced concrete structures. Additional detailed theoretical background on the behaviour of plain structural concrete can be found in appendix A.1. More insight in design aspects of reinforced concrete structures can be found in appendix A.2. Also the time dependent features and further background considering the Shotcrete material model can be found in appendix A.3. Furthermore, additional background information about the modelling of diaphragm walls, respectively laterally loaded piles and details about the appropriate available modelling software can be found in appendix A.4.

2.1 Reinforced concrete

In this paragraph at first the concrete reinforcement characteristics are evaluated, whereafter insight in the behaviour of reinforced concrete under loading is given.

2.1.1 Steel for reinforced concrete material behaviour

The stress-strain material behaviour of the steel reinforcement is visualised in Figure 7 (1). Steel reinforcement behaves linear under stress till the moment of yielding, the moment at which irreversible plastic strains are generated, is reached. When yielding the material hardens till the ultimate failure strength is reached. For calculation purposes the behaviour of the steel reinforcement is simplified (Figure 7 (2)). The behaviour is schematised by a linear-elastic perfectly plastic (LEPP) model. In Figure 7, A is the schematised behaviour dependent on characteristic values while both B branches can be used for design calculation purposes. The upper B branch is based on characteristic values including a partial safety factor. The horizontal B branch is based on design values. The horizontal B branch can be used in the design process without doing a check on the maximum strain. For the upper B branch, the sloping line, such a check has to be performed in order to be sure that overestimation of strength is prevented. The stiffness in the linear part can be assumed to be equal to 200 GPa or 200 000 N/mm^2, respectively 210 GPa or 210 000 N/mm^2 (NEN-6008, 2008). The characteristic strength, minimum yield strength, of the reinforcement is 500 N/mm^2 (NEN-6008, 2008). The design strength, taking into account a proposed safety factor of 1.15 by NEN-6008 (2008), of reinforcement is approximately 435 N/mm^2. Besides the modulus of elasticity E_s and the characteristic yield strength f_{yk} (or the characteristic value of 0.2% proof strength, $f_{0.2k}$), ductility parameters are used in the stress-strain diagram for design purposes. The ductility parameters are represented by the characteristic strain at maximum force ϵ_{uk} and the characteristic ratio between tensile and yield strength $(f_t/f_y)_k$. The plastic strain parameter ϵ_{ud} can assumed to be 0.9 ϵ_{uk}. In the design process it has to be checked additionally that the reinforcement has to yield before the concrete starts to fail in compression, in order to prevent sudden failure.

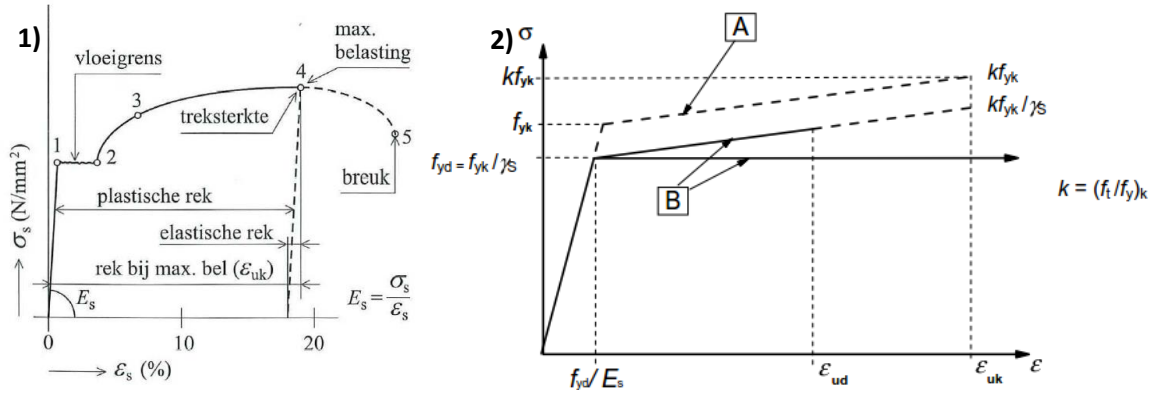

Figure 7: Material behaviour of steel (Braam & Lagendijk, 2010) and the schematised diagram for design purposes according to NEN-EN 1992-1-1 (2011).

Three different types of steel reinforcement can be applied according to NEN-6008 (2008): B500A, B500B and B500C. The characteristics including minimum straining at maximum load of the different types of reinforcement are given in Table 1 below.

Table 1: Reinforcement Characteristics (NEN-6008, 2008).

Type of reinforcement steel	B500A	B500B	B500C
Minimum yield strength [MPa]	500	500	500
Minimum ratio between tensile strength and Minimum yield strength	1.05	1.08	1.15 ≤1.35
Minimum strain at maximum load (%)	3.0	5.0	7.5

2.1.2 Reinforced concrete material behaviour

In principle the tensile strength of concrete is relatively limited with respect to its compressive strength, only 5-10 % (Braam & Lagendijk, 2010). When considering a simple beam structure on two hinges subjected to a lateral line load, the concrete beam experiences compressive stresses in the top part while in the bottom part of the beam tensile stresses are generated (Figure 8). To withstand the tensile stresses in the lower part of the bending beam, the beam has to be reinforced. Considering reinforced concrete; as soon as the concrete starts to crack in the tensile zone, the reinforcement takes the tensile load (almost) immediately.

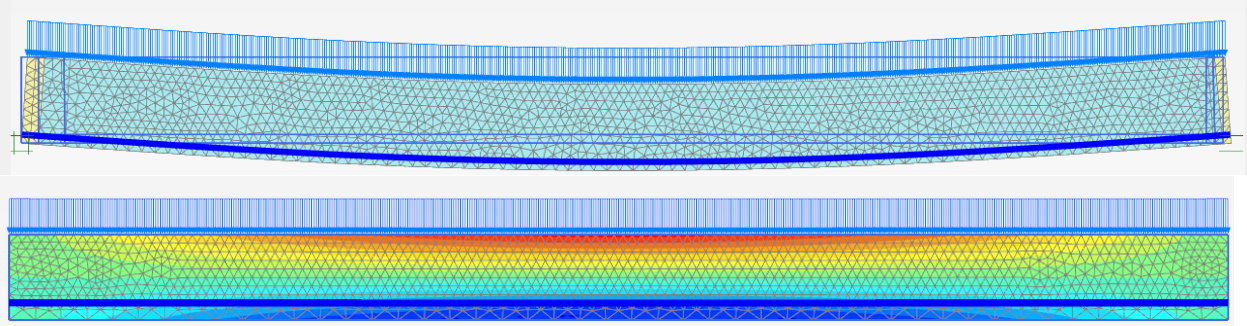

Figure 8: A Beam on two hinges: (a) Deformation (b) stress distribution; compression (red) and tension (blue).

The occurring tensile stresses are highest in the lowest part of the reinforced concrete beam. Therefore the reinforcement is placed as far from the neutral line (the transition between compression and tension stresses) as possible. However in the design process also attention has to be paid to the fact that the concrete cover is sufficient in order to prevent corrosion of the reinforcement and besides a loss in functionality of the structure. Corrosion of the reinforcement leads to a decrease of the surface area, which on its turn results in a strength decrease. Corrosion causes the fact that the volume of the reinforcement inside the cracks increases, forcing the crack to expand. This results in a longitudinally growth of the crack. Growth of the present cracks leads subsequently to increased corrosion, inducing a vicious circle. A check on the concrete cover has to be performed in order to prevent extensive cracking, a loss of functionality, progressive corrosion and ultimately failure.

2.1.2.1 Pure bending

Pure bending is the phenomenon describing a (bending) reinforced concrete beam (schematisation of reality) under a constant moment without experiencing shear forces. Different stages (1,2,3,4) of a reinforced concrete beam with a strength class <C55 under pure bending, considering ultimate limit state, are visualised in Figure 9. The different stages, with number between brackets referring to the different stages in Figure 9, are explained below.

When the applied load on the reinforced concrete beam is relatively limited the concrete material itself will take all the tensile stresses, till the moment that $\sigma_{ct} = f_{ctm}$ (Figure 9 (1)). Increasing the load any further, the tensile stress becomes larger than the tensile strength of the concrete ($\sigma_{ct} > f_{ctm}$), causing cracking of the concrete material in the tensile zone (Figure 9(2)). The bending moment at which this occurs, is indicating the rupture moment (M_r). The reinforcement takes all tensile stresses at the moment the concrete starts to crack. During the design process it has to be taken into account that the reinforcement has to be able to resist the stresses complying with the rupture moment, in order to prevent sudden failure. It is possible to increase the load, as the steel reinforcement has not reached the yield point yet. At yielding ($\sigma_s = f_{yd}$) the moment is indicated as the yield moment (M_y) (Figure 9(3)). The failure moment is reached when the compressive stress is equal to the compressive strength; $\sigma_c = f_{cd}$ and corresponding to a concrete strain of 3.5 ‰ (Figure 9(4)) (assuming LEPP and <C50). In Figure 9 the described behaviour of a reinforced concrete beam under pure bending, for a concrete strength till C50 and taking into account a LEPP material characterisation, is visualised.

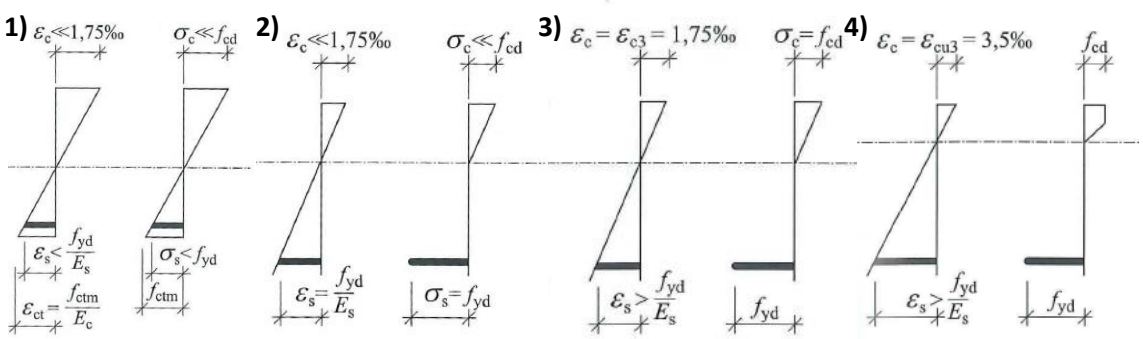

Figure 9: Stress-strain diagram for the different stages (1), (2), (3) and (4) (modified from Braam & Lagendijk (2010)).

For several reasons cracking of concrete structures (in the subsurface) has to be limited. On the one hand to be able to resist high tensile forces while on the other hand there are requirements regarding functionality and sustainability. Both subjects considering crack width limitation are treated in depth in appendix A.2.

2.1.2.2 Bending stiffness

The bending stiffness (resistance against deformation) is not only important for calculating the magnitude of bending, but also plays a major role in the distribution of stresses in the structure. The bending stiffness EI (equation 2.1) can be defined as the ability of the structure to resist deformation/curvature (κ). Deformation requirements (limitations) normally coincide with serviceability limit state conditions. However for the deformation case to be considered, failure is the governing criterion. This implies the use of ultimate limit state conditions for the calculations to be done.

$$EI = \frac{M}{\kappa} \quad (2.1)$$

The bending stiffness of reinforced concrete differs with the magnitude of the applied moment. A different bending stiffness is measured between un-cracked and cracked reinforced concrete. Four different stages of bending stiffness can be identified when considering ultimate limit state design. The points of interest are: at the moment rupture, yielding, plasticity and respectively failure takes place. In a moment and curvature relationship these points are given as $M_r, M_y, M_{c,pl}$ and M_{rd} respectively $\kappa_r, \kappa_y, \kappa_{c,pl}$ and κ_{rd}. The relation between moment and curvature is visualised in Figure 10. The first part of the curve, till M_r is reached,(Figure 10) can be described by the concept of linear elasticity. For this part of the curve the stiffness can be defined as: $EI = E_c * \frac{1}{12} * b * h^3$. When analysing reinforced concrete beams a ratio between the modulus of elasticity concrete and reinforcement has to be used to account for the effect of present reinforcement in the concrete beam.

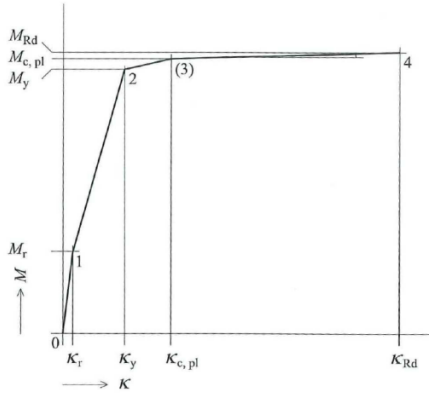

Figure 10: M-κ diagram (Braam & Lagendijk, 2010).

The behaviour between the start of loading and the moment of yielding can divided by using two different linear lines. Describing the behaviour of the un-cracked concrete and subsequently cracked concrete. The shaded area between a bilinear and a linear based concrete material description (Figure 11) can be characterised by two material behaviour properties (Figure 11). At the moment when

concrete cracks, the behaviour is determined by partly cracked (zero stiffness) and partly un-cracked material. The un-cracked areas are relatively stiff, causing the fact that the deformation stays rather limited. This phenomenon is called tension-stiffening. The tension-stiffening area can be described as the contribution of the bending stiffness in-between the cracks by partial relief of the reinforcement, resulting in a stiffening/hardening character of the material. The other part, till rupture, of the shaded area represents the tensile strength of concrete. Given the fact that the bending moment and the curvature are not constant over the full length of the beam, without considering the spatially effect of cracking on the bending stiffness, the bending stiffness also varies over the length of the beam for this reason. In appendix A.2.2 more details regarding bending stiffness of a laterally loaded reinforced concrete beam are given.

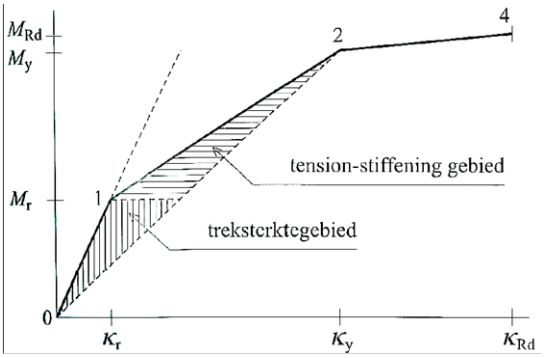

Figure 11: Schematised M-κ diagram including material behaviour (Braam & Lagendijk, 2010).

2.2 Shotcrete material model

To model shotcrete (concrete) a new material model is developed for Plaxis. In this paragraph an overview of the model background based on Schütz, Potts & Zdravkovic (2011), Schädlich and Schweiger (2014a) and Schädlich & Schweiger (2014b) is given. In appendix A.3 additional information considering the model background, time dependency and other model details, can be found.

2.2.1 Introduction

The Shotcrete material model is designed to model shotcrete linings more realistically. Shotcrete linings experience directly after installation a high load. In this stage of maturity the concrete is not fully hardened yet, resulting in the fact that the model has to take time dependent behaviour into account. Current models assume linear elastic material behaviour of the concrete lining with a stepwise increase of the modulus of elasticity (Schädlich & Schweiger, 2014b). The result of using such models is that calculated bending moment is higher than the occurring magnitude in practice. This is the result of the fact that the reduction in stiffness due to cracking of the concrete is not considered. Especially when structures are subjected to (high) bending forces such a material model does not give accurate results, leading to over-dimensioning of the structure. The Shotcrete model has the ability to take loading history, cracking, time dependency and non-linearity into account. This results in more realistic modelling of concrete tunnel lining, as is validated by Saurer et al. (2014) for a NATM application. However the Shotcrete material model features give also opportunities to model cast concrete, jet grout and other cement-based materials more realistic (Schädlich & Schweiger, 2014b). In this thesis the

opportunities regarding the use of Shotcrete material model in Plaxis for reinforced concrete structures is researched.

2.2.2 Model formulation

The Shotcrete material model is based on elastoplastic strain hardening/softening. The total strain in the model is determined by an elastic term, a plastic term, a creep term and a shrinkage term (equation 2.2)

$$\epsilon = \epsilon_e + \epsilon_p + \epsilon_{cr} + \epsilon_{shr} \quad (2.2)$$

To account for plasticity a Mohr-Coulomb yield surface for deviatoric loading and a Rankine yield surface for tensile loading is adopted (Figure 12).

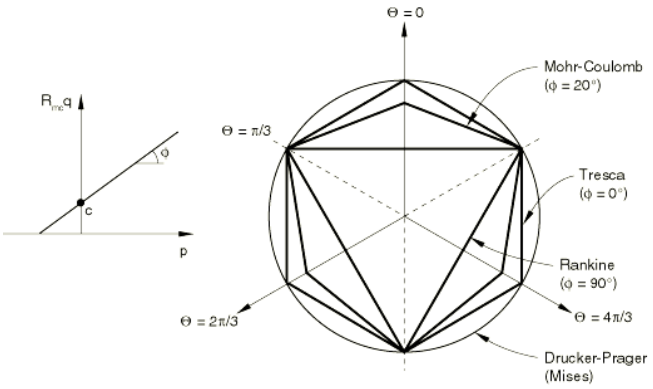

Figure 12: Mohr-Coulomb and Rankine yield surfaces in meridional and deviatoric planes (Hibbit, Karlsson, & Sorensen, 2014).

The Mohr-Coulomb yield surface is determined by the internal friction angle and the cohesion (Figure 12). The internal friction angle determines the slope of the yield envelope while the cohesion determines the (allowable) shear stress at zero normal stress, no compressive/tensile stresses. The Rankine criterion specifies where tensile failure occurs, in other words when the maximum principal stress reaches the uniaxial tensile strength f_{ct} (CEB-FIP, 1990). Using the Mohr-Coulomb failure envelope in combination with a Rankine tensile criterion, the compressive strength is underestimated slightly when high strength concrete is considered. While the tensile strength, assumed to be 10% of the compressive strength, in the model matches quite good with experimental data of Kupfer et al. (1969). By the fact that the main failure mode of shotcrete lining and bending beams is in tension, this does not have significant influence on the reliability of the model results. In cases when compressive failure is the dominant failure mode, the results have to be analysed with care.

Compression

Schutz et al. (2011) proposed four phases to describe the behaviour of shotcrete in compression (Figure 13). In the figure normalised values are used to describe the stress-strain relationship. This is the result of the time dependent nature of the stress-strain curve. The time dependent nature of the model is governed by the fact that shotcrete becomes increasingly brittle by increasing stiffness and strength in time. To account for this, normalising in terms of peak strength and strains is required. On the horizontal

axis in Figure 13 a normalised strain hardening/softening parameter ($H_c = \epsilon_3^p / \epsilon_{cp}^p$) is used to account for the decrease in peak strain with hydration time. ϵ_3^p represents the minor principal plastic strain and ϵ_{cp}^p represents the plastic peak strain in uniaxial compression. The vertical axis is determined by a ratio between the principal stress σ_3 and the concrete strength f_c. Several different stress values are distinguished on the vertical axis: f_{c0n}, f_{cfn} and f_{cun}. The graph starts at a value of f_{c0n}, which represents the point at which yielding starts. In the paper of Schädlich & Schweiger (2014b) this is called "Normalized initially mobilised strength". Therefore the graph only contains the part of the stress-strain behaviour where plastic strains are generated simultaneously with elastic strains. The next value described, met after peak strength, is the failure strength $f_{cf,n}$. The last strength parameter used for the description of the stress-strain behaviour, $f_{cu,n}$, is the residual strength after failure. The compressive fracture energy G_c under the curve in phase II is equal to the area between peak and failure strength/strain. It describes the energy needed before the concrete starts to fail after reaching peak strength and is a determining factor for describing the concrete stress-strain behaviour. When using the Shotcrete material model the fracture energy has to be chosen such that the right values of strain are obtained at the different stresses.

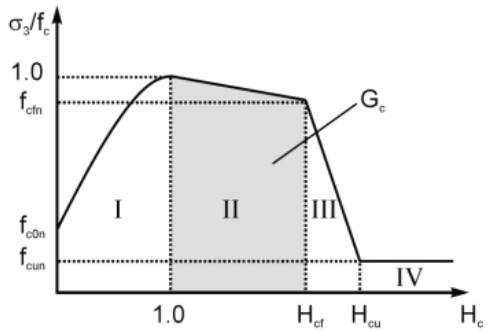

Figure 13: Normalised (time dependent) stress-strain behaviour of the shotcrete material model (Schädlich & Schweiger, 2014b).

The first part (I) of the stress-strain curve is described by quadratic strain hardening. When the current stress state touches the yield surface the behaviour is characterised by elasto-plasticity, indicating the generation of plastic strains next to elastic strains. The normalised stress-strain curve will follow a parabolic path in this region. In mind should be taken that the purely elastic part of the behaviour is not visualised in Figure 13.

The second phase (II) in Figure 13 describes the behaviour of linear softening and occurs when reaching peak strength, $\epsilon_3^p = \epsilon_{cp}^p$ and $\sigma_3 = f_c$. Linear softening characterises the material behaviour at the moment micro-cracking are formed in the rupture zone. The destruction of inter-particle bonding causes a decrease in strength and an increase in strain rate. For a correct description of the linear softening part in compression, a specific procedure regarding mesh dependency is adopted in the Shotcrete material model. The third phase (Figure 13) describes the behaviour when failure strength f_{cfn} is reached. For numerical purposes a linear reduction in stress after failure and a constant stress strain

rate close to zero in phase IV is adopted. In reality concrete is assumed to be completely crushed in the fourth phase, causing a (immediate) reduction in stresses till zero.

The compressive peak strain $\epsilon^{p}_{cp,28}$ can be estimated from a uniaxial compression test, but the strain at failure $\epsilon^{p}_{cf,28}$ and the ultimate strain $\epsilon^{p}_{cu,28}$ cannot be estimated accurately. This is the result of excessive cracking after peak strength and non-uniform material behaviour. With the help of the concept of fracture mechanics (energy), which is explained in appendix A.1.4, the compressive failure strain $\epsilon^{p}_{cf,28}$ can be estimated from the compressive fracture energy G_c (Figure 13). The total fracture energy in compression G_c represents the energy required to propagate a crack of unit area until complete crack opening. Therefore it is equal to the area beneath the graph between peak and failure strength/strain. Using normalisation with respect to the equivalent length of the finite element, the area below the stress-strain curve from peak until failure remains in every situation equal to the compressive fracture energy. For the linear softening behaviour in the third part (Figure 13), an equation is adopted based on the modulus of elasticity. In the model, cracking is governed by the adoption of the smeared crack concept.

The softening behaviour is governed by a decrease in cohesion, also called cohesion softening. Softening is strength reduction due to plastic straining. This can be seen by the downward movement of the stress-strain behaviour in phase II and III (Figure 13). This is the effect of the Mohr-Coulomb yield envelope translating to the right in principal stress space. When load is applied the translation in yield envelope causes the fact that at lower stress states the envelope is reached. When reaching the envelope, plastic straining will occur. The concept of cohesion softening therefore implies that at a lower stress state the strength reduces and more plastic straining will be initiated.

Tension

The behaviour of concrete (shotcrete) is captured by a linear elastic formulation until the tensile (peak) strength f_{tp} of the material is reached. A Rankine yield criterion is adopted as described by Thomée (2005), with the addition to include rounding near the apex to avoid numerical problems. When the tensile (peak) strength of the material (f_{tp}) after a linear elastic stress path is reached, linear softening takes place. This results in an increase of strain with a decreasing strength (Figure 14). The strength decreases from the initial tensile strength f_{tp} to the ultimate tensile strength f_{tu}, characterised by softening behaviour. The softening behaviour is crucial to incorporate cracking in the model.

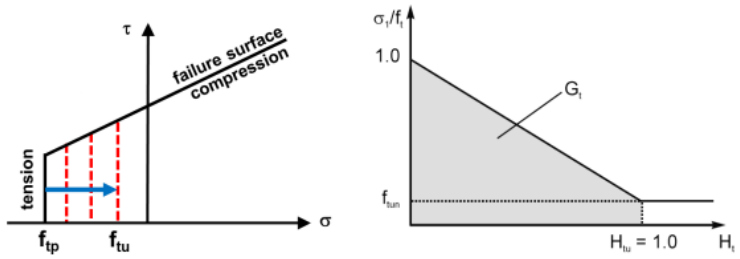

Figure 14: Shotcrete model tension behaviour (Schädlich & Schweiger, 2014b).

Due to the fact that the material is governed by time depending properties, also the tension behaviour is determined by those. The normalised dimension parameters $f_{t,y,n}, f_{tu,n}$ and H_{tu}, equivalent to those in compression, are calculated from the uniaxial tensile strength and strain values at 28 days. The material is softening linearly till the residual (ultimate) strength f_{tu} is reached (Figure 14). The according strain $\epsilon_{tu,p}$ is calculated from the fracture energy G_t. Once the residual strength f_{tun} is reached softening will not occur any longer. This is represented by the horizontal line in the (normalised) stress-strain diagram (Figure 14). For the fracture energy in tension the same considerations and concepts are adopted as in case of compression. In Figure 14 it is shown that the tensile fracture energy represents the area under the (normalised) stress-strain curve. Furthermore, also the fracture energy in tension is made mesh independent. The model is therefore able to correctly describe the linear softening behaviour.

2.2.3 Input parameters

To capture the non-linear and time dependent behaviour of concrete, the Shotcrete material model requires the input of 26 parameters (Table 2). In Table 2 the parameters are listed and the proposed values by Schädlich & Schweiger (2014b) for these parameters are given. Each input parameter will be explained with respect to its physical meaning and the range of realistic input values after being introduced in Table 2. In appendix B.3 (/E.1) a parameter sensitivity analysis will be carried out in order to give additional information and verification about the model parameters. Realistic input values will be tested and the boundaries of (stable) input is investigated.

Table 2: Model parameters including recommended values by Schädlich & Schweiger (2014b).

Parameter	Description	Recommended values for shotcrete/concrete	Unit
E_{28}	Young's modulus of cured shotcrete at t_{hydr}	25 – 30 GPa	Stress
ν	Poisson's ratio	0.15 – 0.25	--
$f_{c,28}$	Uniaxial compressive strength of cured shotcrete at t_{hydr}	Depending on strength class	Stress
$f_{t,28}$	Uniaxial tensile strength of cured shotcrete at t_{hydr}	0.05 – 0.1 $f_{c,28}$	Stress
ψ	Dilantancy angle	0 – 10	0
E_1/E_{28}	Time dependency of elastic stiffness	1 no time dependency 0.5 – 0.7 for shotcrete	--
$f_{c,1}/f_{c,28}$	Time dependency of strength	1 (no time dependency 0.2-0.3 for cast concrete	--
f_{c0n}	Normalised initially mobilised strength	0.1 – 0.25	--
f_{cfn}	Normalised failure strength (compression)	0.1 (1 for no softening)	--
f_{cun}	Normalised residual strength (compression)	0.1 (1 for no softening)	--
ϵ_{cp}^{p}	Uniaxial plastic failure strain at 1h, 8h, 24h	1h: -0.01 – -0.03 8h: -0.001 – -0.0015 24h: -0.0007 – -0.0012	--
$G_{c,28}$	Compressive fracture energy of cured shotcrete at t_{hydr}	30 – 70 kN/m	Force/length
f_{tun}	Ratio of residual vs. peak tensile strength	0 (1 for no softening)	--

$G_{t,28}$	Tensile fracture energy of cured shotcrete at t_{hydr}	0.05 – 0.15 kN/m for plain shotcrete	Force/length
l_{eq}	Equivalent length (if no regularisation is used)	0 in FE-calculations	Length
a	Increase of ϵ_{cp}^{p} with increase of p'	16 – 20	Length
ϕ_{max}	Maximum friction angle	35 – 43 depending on σ	^{0}
ϕ_{cr}	Ratio between creep and elastic strains	2 – 3 for tunnel linings, for cast concrete EC 2	--
t_{50}^{cr}	Time for 50% of creep strains	1 – 5 d	Time
ϵ_{∞}^{shr}	Final Shrinkage strain	-0.0005 – -0.0015	--
t_{50}^{shr}	Time for 50% of shrinkage strains	28 – 100d	Time
γ_{fc}	Safety factor for compressive strength	Depending on standard	--
γ_{ft}	Safety factor for tensile strength	Depending on standard	--
t_{hydr}	Time for full hydration (usually 28 days)	28 d	Time

The following concrete properties will be considered when researching the applicability of the Shotcrete material model for modelling structural reinforced concrete (Table 3).

Table 3: Concrete class C30/37 properties (NEN-EN 1992-1-1, 2011).

Parameter	Concrete class (C30/37)	Unit
f_{ck}	30	MPa
$f_{ck,cube}$	37	MPa
f_{cm}	38	MPa
f_{ctm}	2.9	MPa
f_{ctk}	2	MPa
E_{cm}	33	GPa
E_c	29.7	GPa

The first input parameter is the modulus of elasticity after 28 days (age). The modulus of elasticity is, as mentioned before, dependent on the concrete class used. The modulus of elasticity of concrete class C30/37 has a value of 29.7 GPa. The characteristic compressive and tensile strength are 30 MPa respectively 2 MPa. For the Poisson's ratio of non-fissured concrete a value of 0.2 can be assumed. All these values are in compliance with NEN-EN 1992-1-1 (EC 2) (2011).

The dilatancy angle of structural concrete is according to Vermeer & de Borst (1984), after researching test results of Green & Swanson (1973), around 13 degrees (12.6^{o}) under normal conditions. Plaxis recommends for the Shotcrete material model a dilatancy angle of 0-10 degrees. For modelling structural (plain/reinforced) concrete the dilatancy angle proposed by Vermeer & de Borst (1984) is taken into account. The angle of internal friction is according to Vermeer & de Borst (1984) 35 degrees, while according to Candappa et al. (2001) the angle of internal friction is 43 degrees. In the to be tested Shotcrete material model a value of 35 degrees will be used.

According to Reinhardt (1985) the stiffness at day 1 compared to the reference material stiffness is approximately 60%. The strength at day 1 with respect to the reference strength is approximately 25%.

For shotcrete a test on the hardening and hydration is performed, by Chang (1994). Analysing this experimental data a same ratio in hardening as Reinhardt proposed is found. The hardening, increase in elasticity modulus with time, in the Shotcrete material model with factors of 0.5, 0.6 and 0.7 is compared to the experimental data validating the CEB-FIP model code (1990) formulation. A time dependent ratio of 60% for the modulus of elasticity and 25% for the strength ratio are found to be correct.

The normalised initially mobilised strength is expressed as a percentage of the peak strength. The initial ratio between the compressive peak and compressive yield strength is representative for this parameter. The compressive yield strength according to NEN-EN-1992-1-1 and the CEB FIP model code (2010) is 1/3 of the uniaxial compressive strength. The normalised failure strength is another ratio which functions as an input parameter for this model. It is the ratio between the failure strength and peak strength. According to Kwak & Filippou (1990) the failure strength is around 85 % of the peak strength. A third ratio needed to describe the behaviour in compression is the magnitude of the residual strength with respect to the peak strength. The residual strength in compression is derived from P-CMOD curves by Reinhardt and Xu (1999). From five different samples it is estimated that the residual compressive strength is around 10% of the peak strength. The residual strength in tension with respect to the peak strength in tension is according to Dai & Gao (2014) only 5%. While according to Hossain and Weiss (2004) the tensile residual strength is 5-10 %. However in the experimental results of Cornelissen et al. (1986) no residual tensile strength is recognised. The tensile residual strength will be considered as (almost) zero in the model. Exactly zero is not possible for numerical reasons.

The peak plastic strain limit determines the strain at failure. The proposed values by the Eurocode (NEN-EN 1992-1-1, 2011) for C30/37 is 3.5 ‰. This value has to be adopted in the model. However additionally it has to be taken into account that after peak strain, failure strain and subsequently ultimate (residual) strain is considered in the model. These are taken with respect to corresponding strength (ratios) and fracture energy. Correct values have to be adopted for these parameters in order to get a correct representation at peak and failure strength. The fracture energy can be calculated according to the CEB-FIP model code (2010) based on the mean compressive strength as described in appendix A.1.4. The compressive fracture energy for concrete class C30/37 is, considering this calculation method, 140.5 kN/m. Nevertheless conformity with occurring strains at the different strength ratios has to be guaranteed. This is researched in more detail in the sensitivity analysis in appendix B.3 (E.1). The tensile fracture energy for plain concrete (without reinforcing fibers) can be assumed to be 0.1 kN/m according to test data of Barros & Figueiras (1999).

The creep factor according to CEB-FIP (2010) recommendations is 1.9 to 2.7 depending on the cross-sectional area A_c and the perimeter of the member in contact with the atmosphere u. The halftime value of creep can be taken as suggested by Schädlich and Schweiger (2014b), between 1 and 5 days. The shrinkage strain can also be determined based on CEB-FIP (2010) recommendations. Reasonable values for the shrinkage strain are -0.61‰ to -0.49‰ depending on the cross-sectional area and the perimeter. Concluded from evaluated data of Granger by Bazant (2001) is that the halftime of shrinkage

strains can be estimated at 200 days. The hydration time is 28 days as defined by for instance Reinhardt (1985).

In Table 4 the values of each parameter for plain concrete, considering all literature, are summerised. In the practical model research these values are taken into account. However when the parameter sensitivity analysis concludes something different those results are governing above the ones found in literature.

Table 4: Proposed values for concrete modelling based on all literature described in this chapter next to recommended values by Plaxis.

Parameter	Proposed value for concrete	Recommended values for shotcrete/concrete	Unit
E_{28}	29.7	25 – 30 GPa	GPa
ν	0.2	0.15 – 0.25	--
$f_{c,28}$	30	Depending on strength class	MPa
$f_{t,28}$	2	0.05 – 0.1 $f_{c,28}$	MPa
ψ	13	0 – 10	Deg
E_1/E_{28}	0.6	1 no time dependency 0.5 – 0.7 for shotcrete	--
$f_{c,1}/f_{c,28}$	0.25	1 (no time dependency 0.2-0.3 for cast concrete	--
f_{c0n}	0.33	0.1 – 0,25	--
f_{cfn}	0.85	0.1 (1 for no softening)	--
f_{cun}	0.10	0.1 (1 for no softening)	--
ϵ_{cp}^{p}	-0.0035	1h: -0.01 – -0.03 8h: -0.001 – -0.0015 24h: -0.0007 – -0.0012	%
$G_{c,28}$	140.5	30 – 70	kN/m
f_{tun}	0	0 (1 for no softening)	
$G_{t,28}$	0.1	0.05 – 0.15 kN/m for plain shotcrete	kN/m
l_{eq}	--	0 in FE-calculations	--
a	No confinement	16 – 20	--
ϕ_{max}	35	35 – 43 depending on σ	Deg
ϕ_{cr}	1.9 – 2.7	2 – 3 for tunnel linings, cast concrete EC 2	--
t_{50}^{cr}	3	1 – 5	d
ϵ_{∞}^{shr}	-0.00049 – -0.00061	-0.0005 – -0.0015	%
t_{50}^{shr}	200	28 – 100	d
γ_{fc}	--	Depending on standard	--
γ_{ft}	--	Depending on standard	--
t_{hydr}	28	28	d

2.3 Laterally loaded structures

Two types of laterally loaded structures are distinguished; laterally loaded diaphragm walls and laterally loaded piles. By means of the theory of laterally loaded piles, the concept of laterally loaded structures is explained. The general behaviour of diaphragm walls and piles is almost the same, as both can be simplified by a laterally loaded beam element with a difference in 2D/3D effects. Therefore the general aspects of both can be described at once. Besides introducing the behaviour of laterally loaded structures, in appendix A.4 insight will be given in the difference between modelling piles and diaphragm walls.

2.3.1 Laterally loaded piles

Laterally loaded piles can be divided into two groups (Figure 15) based upon the type of loading: by external load, also called actively loaded (Fleming, Weltman, Randolph, & Elson, 1992; Reese & Van Impe, 2010) and by laterally displacing soil, called passively loaded (Basu, Salgado, & Prezzi, 2008).

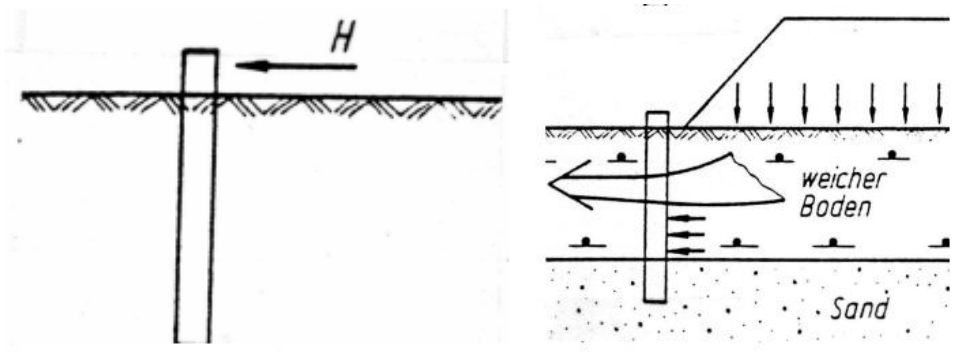

Figure 15: Laterally loaded piles, active respectively passive (Everts, 2015).

An actively loaded pile is loaded at the top, pile cap or head, of the pile by for example wind or traffic loads. Typically those loads are important for abutment, quay wall and high-rise building designs. A passively laterally displacing soil load on a pile is experienced when the soil displaces and excites a force over the whole length of the pile. This is the case when piles are near or in an embankment and in case earth-retaining structures are considered. In such circumstances almost no vertical loading is experienced by the structure. Therefore the horizontal loading will be the critical one during for the design. A lot of research, for example Brinch Hansen (1961), Broms (1965), Begemann & De Leeuw (1972) Poulos & Davis (1980) and API RP 2A-WSD (2010), through the past decade is carried out in order to come to design methods for the lateral soil-structure interaction. However besides the soil-structure interaction, also a structural analysis of the laterally loaded piles for the design is important.

A laterally loaded pile can be schematised as a transversely loaded beam structure. Loading laterally will lead to an increase of normal stress in the soil in the front of the pile, the soil body in the direction of the load, while the normal stress behind the pile will decrease. Compression will occur in front of the pile while relaxation will occur behind the pile. Different failure modes can take place due to the difference in soil behaviour. The possible failure modes are: rotation, bending (including shear deformation failure of the structure) and or translation (Figure 16) (Fleming, Weltman, Randolph, &

Elson, 1992; Salgado, 2008). In more detail, the bending failure mode also includes the occurrence of shear deformation. Despite a linear increase of shear deformation with length it is commonly not the dominating failure mode within bending failure due to the fact that deformation caused by a bending moment increases with a third power (Blodgett, 1991). Therefore only in case of extremely short span shear deformation plays an important role (Blodgett, 1991). In the design shear reinforcement has to be considered in any case to be able to resist the occurring shear forces caused by bending.

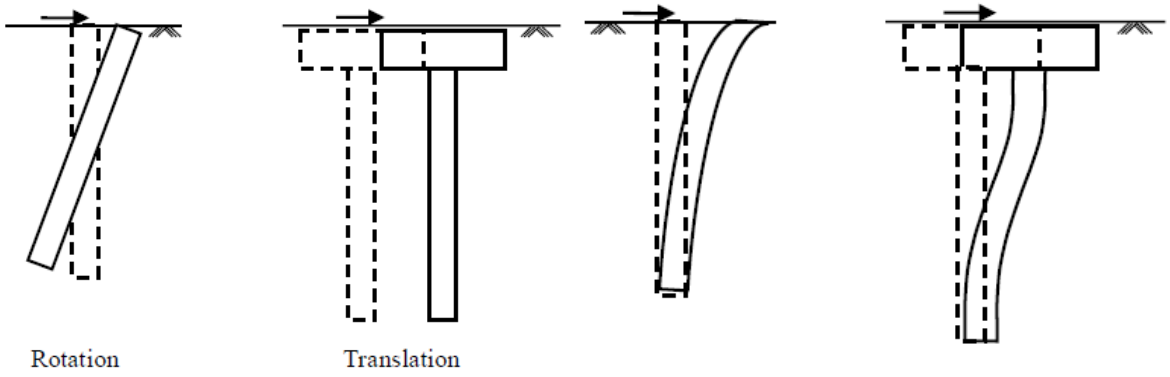

Figure 16: For rigid piles (left 2) and for flexible piles (right 2) (Basu, Salgado, & Prezzi, 2008).

At surface level a gap, due to wedge forming, will occur behind the pile while at depth the soil will fail and will flow around the pile. The failure mechanism is highly dependent upon the type of laterally load, the stiffness and the length of the pile. For flexible piles, relatively long and slender, soil-structure interaction is determining the behaviour. The deflection is mostly dependent on soil resistance versus pile deflection in such cases, causing high lateral deflection and bending. This can result in the occurrence of excessive bending moments and lead to the formation of plastic hinges with collapse at worst case (Basu, Salgado, & Prezzi, 2008). Long stiff piles have a high resistance against bending, wherefore failure of soil around the pile is probable to occur. This will subsequently lead to (plastic) flow of soil around the pile (Fleming, Weltman, Randolph, & Elson, 1992). Flow of soil around the pile can cause large lateral deflection, translation or rotation of the pile. This type of failure is governing in the ultimate limit state for a laterally loaded pile. Flowing of soil around the pile is a 3D problem, which can be modelled in (numerical) FEM programs as Plaxis. Although the mentioned failures, both ultimate limit state, do not have to be governing during the design as other aspects of the structure can already fail in serviceability limit state conditions. Failure in serviceability limit state conditions can be the result of for instance a restriction in the allowable deformation or deflection.

When a single pile is modelled or the distance in a pile group is larger than eight times the pile diameter, this conceptual description of loading conditions and failure is applicable. Otherwise also group effects have to be taken into account. In this research a single pile (row) is examined, wherefore the effects of less resistive forces of a trailing-row (Salgado, 2008) and the effect of additional vertical forces due to lateral deflection/movement are not considered. Detailed insight in the differences and considerations regarding modelling of diaphragm walls and laterally loaded piles is given in appendix A.4.

2.4 Calculation methods

Designing subsurface reinforced concrete structures involves many aspects which can be modelled with different programs. Several modelling programs are 2D and others can be used in 3D modelling. The structure being designed determines if 3D modelling has added value above a simplified 2D approach. In this chapter several different programs are mentioned, each designed with a different purpose and therefore applicability in the design.

2.4.1 Designing reinforced concrete structures in the subsurface

D-series programs, D-Pile Group or D-Sheet piling can be used for modelling the soil-structure interaction for piles and earth-retaining structures by taking into account calculation methods according to the API and Eurocode. A Finite Element Modelling (FEM) program used for 2D and 3D calculations of the subsurface including (basic) structural analysis is Plaxis. In FEM analysis constitutive models are used to represent the material behaviour. For the structural design of reinforced concrete structures a simplified 2D approach can be done with Technosoft, which also uses calculation methods according to standards and codes. Finite Element Modelling (FEM) from a structural perspective is possible with the use of DIANA. This FEM software package is besides also able to model subsurface behaviour in addition to detailed structural modelling. An overview and evaluation of these software programs is given in appendix A.5. Attention in this chapter is paid to features of DIANA and Plaxis to be able to model reinforced concrete structures as both can be considered as applicable to model reinforced concrete structures in the subsurface in detail.

2.4.2 Modelling reinforced concrete beams in FEM

DIANA is originally designed for modelling structural behaviour, while Plaxis is originally designed for modelling subsurface behaviour. Both programs include possibilities to model soil-structure interaction and the specific parts in more detail. To give insight in the capabilities considering the modelling of reinforced concrete the features of both programs are analysed below. This gives more insight in the capability of the Plaxis Shotcrete model and its additional value in modelling reinforced concrete structures.

2.4.3 DIANA

DIANA is originally designed for finite element analysis of reinforced concrete structures. It includes features as embedded reinforcements with grids. Besides reinforcement bars can be defined independently from the finite element mesh. Also bond-slip reinforcement, pre and post tensioning, hardening of concrete and dedicated post-processing of crack patterns can be taken into account. Additionally ambient, thermal and construction-staged analysis can be carried out. Furthermore, material models as Mohr-Coulomb, Von-Mises and other specific material models accounting for cyclic behaviour and plasticity of reinforcement can be used. Additionally creep and shrinkage models, discrete cracking with interface elements and other total-strain or multi-directional cracking are included with the reference to international design codes. In summary can be concluded that detailed and specific material models are included to model reinforced concrete behaviour.

2.4.4 Plaxis

In Plaxis reinforced concrete structures are usually modelled with the use of plate elements. These plate elements can be given linear elastic, elastoplastic and elastoplastic (M-κ) material behaviour in order to represent the real behaviour of the structure. Other specific structural elements can be used to cover a whole range of different structures, as anchors or piles. Though most elements can be given realistic parameters including interface parameters to model the soil-structure interaction, using a volume element gives more realistic results. Many different constitutive relations (models) can be used in Plaxis. For concrete the Mohr-Coulomb model is a good first order approximation, despite it does not take non-linear or time-dependent behaviour into account. The new Shotcrete model gives the opportunity to incorporate such behaviour by the use of CEB-FIP (1990) and partly other code recommendations. Furthermore, it also takes cracking into account improving the accuracy of modelling concrete behaviour. As Plaxis is in base a modelling program for soil, no detailed reinforcement can be modelled in the concrete element. Structural elements as plates or embedded beams have to be used to model reinforcement, which leads to that fact that the structure has to be simplified when modelled. However it is possible to give the characteristics of the whole (detailed) reinforcement to a single element, wherefore the difference in model outcome should be rather small.

2.5 Conclusion literature research

The introduction of the non-linear time dependent Shotcrete material model in Plaxis gives prospect to model concrete more realistically than a Mohr-Coulomb model with a tension cut-off. The Shotcrete model formulation is in compliance with the recommendations for concrete modelling by the CEB-FIP model code and other literature as the Eurocode 2. However the most recent version of the CEB-FIP model code is not used as a base. Hardening and softening behaviour in compression as well as in tension is included in such way that a realistic (non-linear) stress-strain curve can be obtained. Especially due to the fact that cracking is taken into account more realistic behaviour (results) can be obtained. Nevertheless the tensile stress-deformation curve suggested by Hordijk (1991) based on experimental results of Cornelissen et al. (1986) is more sophisticated than the linear approach of the Shotcrete material model. The use of fracture energy G_c and G_T and its mesh independency give the ability to account for cracking of concrete realistically. As this plays an important role in the stress-deformation behaviour of concrete, it should give additional value over the use of other methods to model structures in Plaxis. Cracking is modelled according to the smeared cracking concept in the Shotcrete model, which is defined as appropriate by the CEB-FIP model code (2010) in case many cracks are likely to be formed. However it seems that an even more sophisticated crack propagation analysis by using a cohesive model is not feasible. This method allows by a traction-separation law to model the propagation of a crack and distribution of stresses, near the formed cracks in detail. The continuum element is not damaged, while crack opening is realised by disconnection of interface elements. Nevertheless, the introduction of time dependent parameters based on CEB-FIP model give the model the ability to model strength and stiffness evolution, creep and shrinkage effects accurately.

A drawback of using the Shotcrete material model for modelling normal strength structural concrete is the fact that many input parameters are required. The input parameters require sufficient theoretical

background, which is hard to find for normal strength concrete in contrast to shotcrete. Especially parameters needed to determine the exact stress-strain and time-dependent behaviour are difficult to find for normal strength structural concrete. However as mentioned before for most parameters standard input values are found, which can be used in any case. Another point of discussion concerning the additional value of using the Shotcrete material model to model reinforced concrete structures in Plaxis concerns the modelling of reinforcement. Plaxis does not include the ability to define detailed reinforcement. Beam (embedded) elements have to be included in the continuum element to account for reinforcement.

Practical research has to be carried out in order to find if the use of the Shotcrete material model over a Mohr-Coulomb model has additional value in actual modelling. Besides, the model results have to be compared to proven reinforced concrete bending beam calculations such as M(-N)-κ diagrams, to be able to verify the results for laterally loaded structures. Another aspect of research concerns the use and correctness of the proposed values of the input parameters. Additionally the ability of the model to take cracking and the simultaneous stress take up by the reinforcement has to be researched. This process is important when modelling reinforced concrete beams correctly.

3 Modelling reinforced concrete structures

This chapter consists of five paragraphs. The concept of a single stress-point analysis, simulating a uniaxial compression test, is covered in the first paragraph. After the theory of a single stress-point analysis is explained, it is applied by means of simulating a uniaxial compression test on the Shotcrete material model in the soil-test facility in Plaxis. A sensitivity analysis of the Shotcrete material model can be found in appendix B. Moreover in appendix B a first insight in fitting the Shotcrete material model to model structural concrete is given. The sensitivity analysis is used to get insight in the model behaviour as well as in the right input values. To be able to get realistic modelling results the Shotcrete material model is fitted against experimental data of a uniaxial compression test such that the model behaviour matches the behaviour of C30/37 (reinforced) concrete. In the second paragraph a reinforced concrete beam, schematisation of real structures, subjected to bending (and a normal force) is compared to other modelling methods, including the use of other material models. Furthermore, the results of the Shotcrete beam model are analysed and evaluated in depth in this paragraph, concerning also aspects as mesh sensitivity. In the third and fourth paragraph the results of using the Shotcrete material model to model a reinforced concrete structure subjected to bending and a normal force is verified against trusted hand calculations. At last a conclusion is formed about the applicability of the Shotcrete material model to model reinforced concrete structures subjected to bending and a normal force.

3.1 Single stress-point constitutive modelling

A material model uses a constitutive relation, which defines the stress-strain relationship for a particular material. The relationship between stress and elastic respectively plastic strain rates is given by the constitutive model M as shown in equation 3.1.

$$\sigma = M * \epsilon \quad (3.1)$$

Input in a material model is given by model parameters, such as strength and stiffness parameters. Model parameters give the quantification of deformation behaviour. Material models can be formulated by linear as well as non-linear equations relating stress and strain. Non-linear material behaviour description does not always involve plasticity, also non-linear elastic behaviour can cause non-linear model behaviour. Analytical solutions are limited to a single stress point. A single stress point analysis can be carried out in order to simulate standard lab tests and stress paths. The purpose of such tests is to gain insight in local behaviour such as stress-strain relationship of the material. Also the model formulation can be analysed in depth with for instance a stress path analysis. A single stress point analysis is moreover used for verification of computer model implementation. For the purpose of this research a uniaxial compression test is simulated at a single stress-point in the soil-test facility in Plaxis. The boundary conditions are given in Table 5 and Table 6 as well as other test configurations, considering phase description. The direction of stresses and strains comply with Cartesian stress directions as described in FigureA-5 and A-6 appendix A.1.2.

Table 5: Boundary conditions uniaxial compression test in soil test facility (Plaxis).

Initial	Initial stresses (kN/m^2)	Boundary conditions
σ_{xx}	0	Stress inc XX
σ_{yy}	0	Strain inc YY
σ_{zz}	0	Stress inc ZZ
τ_{xy}	0	Stress inc XY

Table 6: Test configurations of a uniaxial compression test, strain driven.

Phase 1		**Increments**	**Value**
Duration	1 Day	$\Delta\sigma_{xx}$	0 kN/m^2
Steps	1	$\Delta\epsilon_{yy}$	0 %
		$\Delta\sigma_{zz}$	0 kN/m^2
		$\Delta\tau_{xy}$	0 kN/m^2
Phase 2			
Duration	0 Day	$\Delta\sigma_{xx}$	0 kN/m^2
Steps	1000	$\Delta\epsilon_{yy}$	-1 or -10 %
		$\Delta\sigma_{zz}$	0 kN/m^2
		$\Delta\tau_{xy}$	0 kN/m^2

3.1.1 Curve fitting with strain controlled compression test

Uniaxial compression strain controlled lab tests are not commonly done. However for the purpose of analysing and fitting a material model (stress-strain relationship) such test results are useful. Van Mier (1984) did research to strain-softening of concrete under multiaxial loading conditions. In this research also uniaxial lab tests on concrete samples are performed. In Figure 17 the results of the performed uniaxial strain controlled compression tests are visualised.

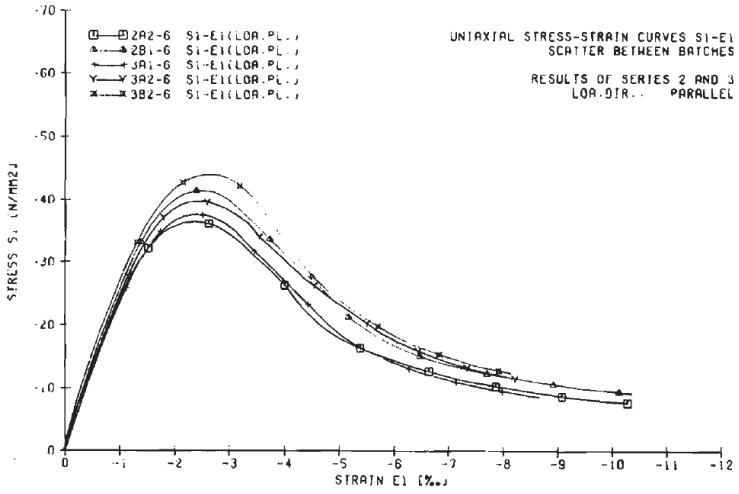

Figure 17: Strain controlled uniaxial compression test results (stress-strain curve) by Van Mier (1984).

The lower line in Figure 17 is used as reference to fit the Shotcrete material model. A test sample with a strength of 30 MPa, complying with the C30/37 modelling consideration, is not available. However analysing the results of the sample with a strength of 37 MPa gives a good indication. The first thing to notice, not concerning the absolute magnitude of the compressive strength, is that the peak strength is reached at a higher strain value than proposed by NEN-EN-1992-1-1 (2011). The peak strength occurs at a strain of 2.3 ‰, while the mostly in engineering practice used method (method 3) described in NEN-EN-1992-1-1 (2011) prescribes that the peak should be occurring at 1.75 ‰. Nevertheless the results are in accordance with the parabola method prescribed in NEN-EN-1992-1-1 (2011). A strain of 2.2 ‰ is used for ϵ_{c1} when using the parabola method. At a strain of 1.75 ‰ in Figure 17 the strength is at 95% of the peak strength. For safety and engineering practice the recommendation of method 1 proposed in NEN-EN-1992-1-1 (2011) is considered for the Shotcrete model.

The second model stage to be fitted to the lab test results is the moment at which failure occurs. According to NEN-EN-1992-1-1 (2011) failure occurs at a strain of 3.5‰. By literature, paragraph 2.2.3, is proposed that failure of the concrete occurs at 85 % of the peak strength. Analysing the results (Figure 17) of Van Mier (1984) leads to the conclusion that at a strain of 3.5 ‰, the strength of the concrete is approximately 84% of the peak strength. Therefore it can be concluded that the proposed by literature values can be taken into account for a realistic failure analysis.

The parameter describing the area under the stress-strain curve and determining the strain occurring between the peak strength and the point of failure is the fracture energy G_c. The compressive facture energy G_c should be fitted such that the stress-strain behaviour of the model corresponds to the lab test results. By trail-and-error it is found that the fracture energy indeed has to have a value of 1.55 kN/m, as is found in the sensitivity analysis (appendix B.3 (/E.1)). It has to be taken in mind that this value is ten times lower than proposed in literature, which is remarkable. Nevertheless, in the next modelling stage the value found in the sensitivity and this analysis is governing.

The last two parameters to be fitted are the strength (% of peak strength) at which plastic strains are generated and the residual strength of the concrete after failure. Plastic straining of concrete is by literature proposed, paragraph 2.2.3, to be at 33% of the peak strength. Comparing this assumption to the lab test results of Van Mier (1984) leads to the conclusion that this is a good approximation. The residual strength on the other hand is not similar. Van Mier (1984) suggests that at a strain of 8 ‰ a residual strength of 11 MPa is reached. Regarding the lower line in Figure 17 a percentage of 22% of the peak strength has to be considered for the residual strength. In literature, paragraph 2.2.3, a residual strength of only 10% of the peak strength is suggested. For safety the by literature proposed value is considered in further modelling with the Shotcrete material model.

The stress-strain curve of the Shotcrete model after fitting to the strain controlled uniaxial compression lab test results by Van Mier (1984) is given in Figure 18. This stress-strain behaviour will be governing in the following analysis.

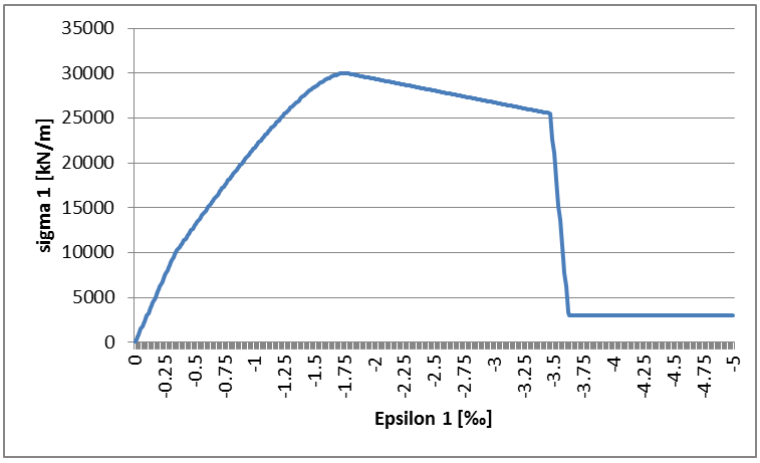

Figure 18: Shotcrete model stress-strain diagram of fitted to literature and Van Mier (1984) lab test results.

3.2 Bending beam analysis

After fitting the Shotcrete material model such that it represents C30/37 concrete, a reinforced concrete beam model subjected to bending can be modelled and analysed. The bending beam model consists of a reinforced concrete beam on two hinges subjected to a lateral line load. A simple beam construction is used in order to be able to validate the results. Besides this makes it possible to easily evaluate the additional value of using a Shotcrete model over a first-order approximation material model, such as Mohr-Coulomb. Furthermore, in this paragraph the ability of adding reinforcement to the (Shotcrete volume element) beam model by using a plate element in Plaxis is tested. Another analysis carried out in this chapter concerns the practical use of the Shotcrete material model for modelling reinforced concrete structures subjected to bending. The calculation time using a Shotcrete material model instead of a Mohr-Coulomb material model for the volume element is evaluated. Additionally the mesh sensitivity of the Shotcrete material model on the model outcome, such as stress distribution and deformation, is researched.

3.2.1 Model setup (initial values, boundary conditions and restrains)

A first problem encountered regarding the modelling of a reinforced concrete beam on two hinges, considers the hinges. In Plaxis two point fixities have to control the movement. In the situation that one hinge is completely fixed, vertical as well as in horizontal direction, and the other hinges is only fixed in vertical directions, the bending behaviour is concentrated at those point. The area of the hinges is that small that the stresses rise to infinite. This causes model failure almost instantly under loading when using the Shotcrete material model over the whole length of the volume element. A solution found is to use a linear elastic transition element with the same deformation characteristics, although no failure criterion, at both hinges. The width of those elements is chosen such that the influence area of the hinges on the stresses is completely covered. This has the effect that the model does not fail due to the occurrence of unrealistically high stresses at the hinges. The practical explanation for the right to use linear elastic material properties at the hinges is the fact that in reality the surface at which the beam rests is not infinitely small as in the Plaxis model. The beam is supported over a larger surface in reality.

The use of a linear elastic element at each hinges solves this inequality with the real situation. The model with a single plate element as reinforcement looks therefore as shown in Figure 19.

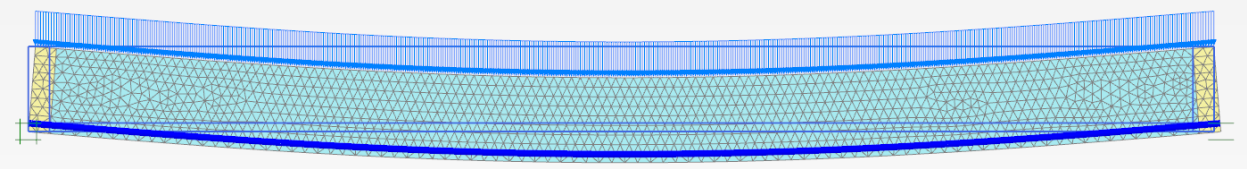

Figure 19: Model setup, including linear elastic transition elements at the hinges.

The model consists of a reinforced concrete beam with the dimensions given in Table 7. The length of the beam between the two hinges is 14 meter. Both elastic elements have a width of 0.25 meter. The beam is implemented in Plaxis 2D with a very fine mesh to give detailed insight in the structural behaviour and be able to compare the results to realistic hand calculations. The line load applied on top is varied to be able to evaluate the whole range of bending behaviour of a reinforced concrete beam.

Table 7: Dimensions and properties of the reinforced concrete C30/37 beam.

Parameter	Value	Unit
Length reinforced concrete beam	14	m
Length elastic elements	0.25	m
Mohr-Coulomb/Shotcrete element length	13.5	m
Width concrete element	1000	mm
Height concrete element	1000	mm
Concrete properties	C30/37	-
Reinforcement	1	%
Rebar yield strength	435	N/mm^2

A second point of attention when evaluating and comparing deformation and stress results from the Plaxis model is that there will always be a difference in results with respect to hand calculations, which consider the concept of forget-me-nots (Vergeet-mij-nietjes). The difference results from the fact that in finite element modelling by Plaxis shear deformation is taken into account, while in the forget-me-nots the effect shear deformation is not considered. When applying the concept of a statically determined structure the moment can be calculated as follows: $M_{ed} = \frac{1}{8} * q * l^2$. The corresponding deformation in the middle of the span is in that case equal to: $w = \frac{5}{384} qL^4/EI$.

Another point of attention comparing the results to hand calculations is the fact that the Shotcrete material model takes non-linear behaviour into account which is in contrast to hand calculations. The mentioned points of attention indicate that differences in results are likely to occur and cannot be explained as the result of a single factor.

3.2.1.1 Material properties

To model a reinforced concrete beam a plate element is included at a reasonable distance from the centreline of the concrete continuum element. A concrete cover of 5 centimetres is regarded. The plate

element is given the characteristics of B500B/C reinforcement. The plate element, reinforcement, material characteristics are given in Table 8. Two different cases are tested using a single plate as reinforcement. In one case the reinforcement behaviour is linear elastic, while in the other case the reinforcement behaviour is elastoplastic. The second case is more realistic as yielding of the rebar can be taken into account. Both cases are researched to be able investigate the influence of including rebar yielding in the model.

Table 8: Reinforcement model characteristics.

Parameter	Value	Unit
Modulus of elasticity	210 000 000	kN/m^2
Area	0.01	m^2
Moment of Inertia	$8.33*10^{-8}$	m^4
EI	17.49	kNm^2/m
EA	210 000 000	kN/m
N_p*	4350	kN

*Used in modelling Elastoplastic rebar behaviour, not in linear elastic rebar behaviour.

The characteristics of the elastic transition elements at the hinges should match the correct and equivalent concrete material properties. Nevertheless failure/plastic properties are excluded. This results in the material properties given in Table 9.

Table 9: Properties linear elastic transition elements at hinges.

Parameter	Value	Unit
Modulus of elasticity	29 700 000	kN/m^2
ν	0	-
G	14 850 000	kN/m^2
E_{oed}	29 700 000	kN/m^2

The volume element between the elastic transition parts at the hinges considers material behaviour such that the concrete in the model is represented realistically, wherefore also failure properties have to be included. Two optional material models, representing the concrete behaviour, are considered for this volume element characterising the bending beam behaviour. The first option is to apply Mohr-Coulomb model characteristics (LEPP), which is also considered in NEN-EN-1992-1-1 (2011). The Mohr-Coulomb parameters as found in the single stress-point analysis (appendix B.1) are adopted for that case).

The second option is to give this determining model element the characteristics based on the Shotcrete material model. The Shotcrete material model parameters applied in this case are given in Table 10. Applying both models makes it possible to compare both in detail for a reinforced concrete bending beam test case. Time dependent behaviour is excluded in this study as is focussed on comparing Mohr-Coulomb and Shotcrete model results and making a comparison with hand calculations which do not include time dependency of the results.

Table 10: Input for the Shotcrete model bending beam analysis.

Parameter	Value	Unit
E_{28}	29 700 000	kN/m^2
ν	0.2	-
$f_{c,28}$	30 000	kN/m^2
$f_{t,28}$	2 000	kN/m^2
ψ	13	^{o}
E_1/E_{28}	1	-
$f_{c,1}/f_{c,28}$	1	-
$f_{c0,n}$	0.33	-
$f_{cf,n}$	0.85	-
$f_{cu,n}$	0.1	-
ϵ_{cp}^{p}	-0.75	‰
$G_{c,28}$	1.55	kN/m
$G_{t,28}$	0.1/0.15*	kN/m
$f_{tu,n}$	0	-
ϕ^{max}	35	^{o}
Time dependent parameters	0	-/day

(*)
During the modelling process a modification had to be made in order to be able to get model convergence at high loads, respectively to get results in ultimate limit state cases. In this chapter a tensile fracture energy of 0.1 kN/m is used for serviceability limit state calculations as the deformation is slightly more realistic. For ultimate limit state cases, a applied line load higher than 120 kN/m, a tensile fracture energy of 0.15 kN/m is governing. The results using both input values for the tensile fracture energy are compared at a line load of 120 kN/m to indicate the difference in model outcome. It is found that the difference in bending deformation is approximately 4%, while the stress distribution and the occurring rebar force only deviate 1% from each other. Therefore it can be concluded that it is justifiable to use a higher tensile fracture energy for ULS design.

3.2.2 Comparing Mohr-Coulomb and Shotcrete

A first analysis of the reinforced concrete bending beam considers the comparison between the usage of a first order approximation material model, Mohr-Coulomb, and the Shotcrete material model. The model used for the comparison is visualised in Figure 19. The comparison contains an analysis of the stress-strain behaviour, the stresses, the deformation and the rebar force. Besides also the models are compared in terms of calculation time.

3.2.2.1 Stress-strain behaviour

To compare the results using the Mohr-Coulomb respectively the Shotcrete model a spectrum of load is applied. The loads applied range from uncracked concrete in the tensile zone (10 kN/m) to model failure (146.4 kN/m). At each applied load the results are analysed and compared to each other as well as to literature. The analysis of the reinforced concrete bending beam behaviour regards evaluation of the stress-strain output, the normal force in the reinforcement, the magnitude of deformation in the Y-

direction and the generation of plasticity. When loading approximates failure also utilisation of compressive and tensile strength is analysed. Shortcomings, deviations from expected behaviour according to theory, of both models are also indicated when present.

To start with a line load of 10 kN/m is applied to analyse uncracked behaviour, as the tensile strength is not reached yet. For an unreinforced concrete beam a symmetric stress distribution over the cross-section should be obtained according to theory. In Figure 20 it is visualised that for an unreinforced beam the stresses are indeed symmetrically distributed over the cross-section and the tensile stress occurring is lower than the tensile strength. Introducing reinforcement, a plate element, leads to deviations from the symmetric stress behaviour (Figure 21).

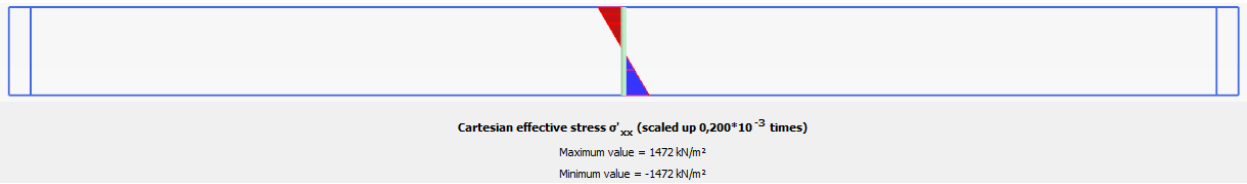

Figure 20: Stresses in the middle of an unreinforced concrete (Mohr-Coulomb) beam subjected to a line load of 10 kN/m.

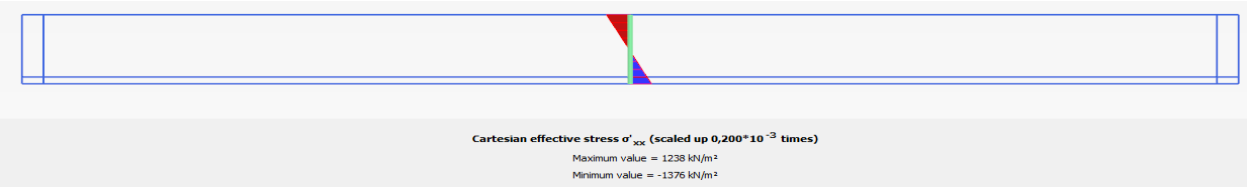

Figure 21: Stresses in the middle of a single plate reinforced concrete (Mohr-Coulomb) beam subjected to a line load of 10 kN/m.

However these deviations can be explained. The stiffness of the reinforcement is higher than the stiffness of the concrete volume element causing a non-symmetric and unequal distribution of stresses in the cross-section (Figure 21). This is the result of the fact that the lay-out of the beam is non-symmetric and the stiffer reinforcement plays a role in the behaviour. When applying the same reinforcement in the top as the bottom part of the beam (Figure 22), the stress-strain diagram should become equal again, which can also be seen in Figure 22. However for simplicity an analysis with reinforcement in the compressive and tensile zone is only carried out in case of a beam subjected to a normal force in addition to the applied lateral load (paragraph 3.4 and appendix E.4).

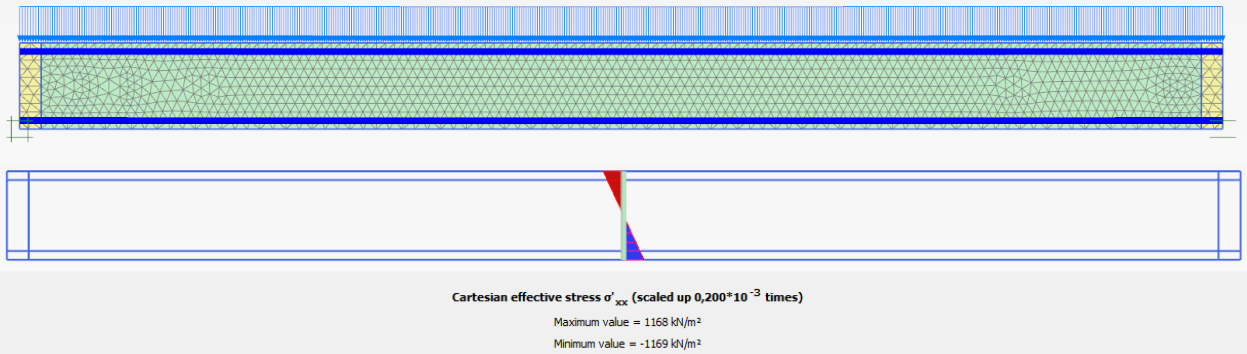

Figure 22: Double plate reinforced concrete beam model with equal effective stresses at a applied line load of 10 kN/m.

The material model formulation of the Mohr-Coulomb and Shotcrete model are similar for situations in which the tensile strength of the material is not reached. It is indeed found that the obtained model results are also similar (appendix E.2/3). As soon as the moment is reached when the tensile stress becomes higher than the tensile strength, the Shotcrete material model starts to initiate cracks while in the Mohr-Coulomb model this is not the fact. In the Mohr-Coulomb model the tension cut-off takes care that the tensile stress does not become higher than the tensile strength, resulting in a stress redistribution over the element in combination with an increase in normal stress in the rebar. In a stress distribution diagram this phenomenon can be observed by the fact that a straight vertical stress line is present in the tensile area, while the transition point between tensile and compressive stress moves upward with the application of higher loads (Figure 23).

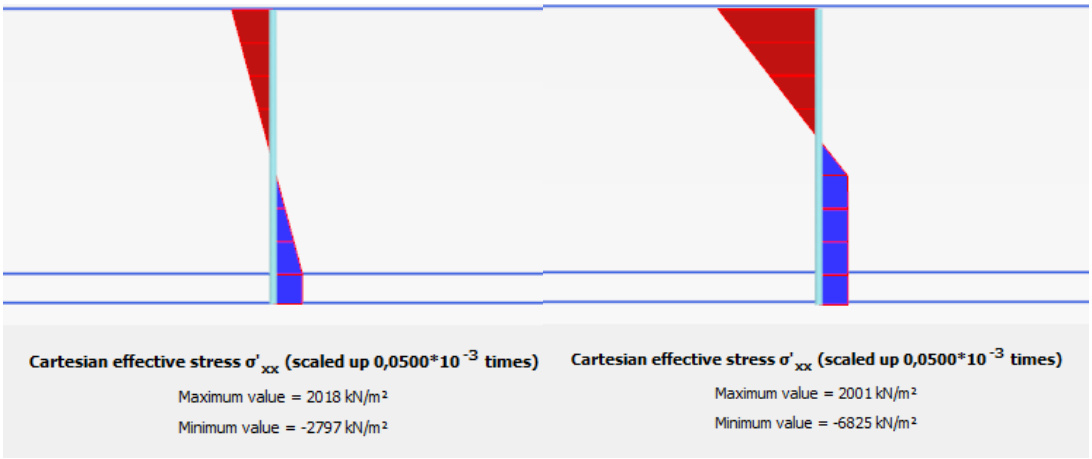

Figure 23: Stress distribution in the middle of a reinforced concrete (Mohr-Coulomb) bending beam at 20 kN/m and 40 kN/m.

The force in the reinforcement sharply increases at the moment when the tensile strength of the material is reached, as the material is no longer possible to withstand any (/more) tensile stress. In reality cracking is caused by locally complete loss of tensile strength when the tensile stress is equal to the tensile strength. In such a case the tensile stresses have to be completely taken by the reinforcement, as explained and visualised in paragraph 2.1.2 (Figure 9). As mentioned, the Shotcrete material model tries to capture such behaviour. The tensile stress in the concrete material drops as soon

as the tensile strength is reached. In Figure 24 the stress distribution in the middle of the Shotcrete volume element at a load beyond the rupture moment is given.

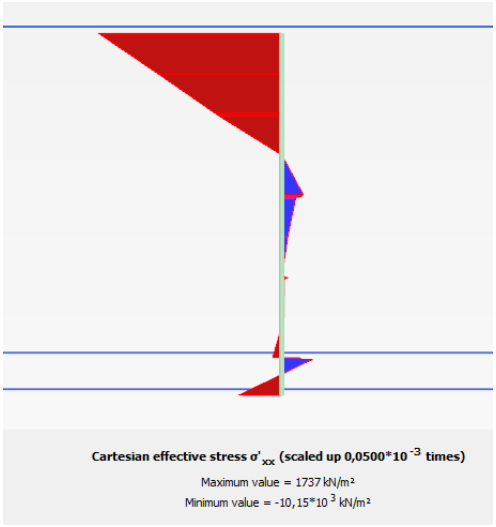

Figure 24: Stress distribution in the middle of a reinforced concrete (Shotcrete model) bending beam at 50 kN/m.

Unfortunately it is observed that the tensile stress in the material is not completely gone when the tensile strength is reached (Figure 24). Besides it is found that significant compressive stresses are generated in the part where no stress is expected at all. The observed "noise" can be the result of a crack nearby as well as numerical difficulties with the redistribution of stresses among a crack. Furthermore it is observed that the first and widest crack is not initiated exactly in the middle of the beam, which is in contrast from what to be expected according to the theory. An explanation for this phenomenon is that the increase in load during a single (loading) step is too large around the crack initiating moment. The tensile strength is reached over a larger area in the bottom of the beam than only exactly in the middle, wherefore the model has to choose where to initiate cracking. However reducing the maximal percentage of Mstage in Plaxis does not solve this problem. In summary it can be concluded that the results differ slightly from what is expected according to theory for a homogeneous uniform cracked reinforced bending beam. Nevertheless, in general the results match the theory quite well. It is observed that increasing the load stepwise, the tensile stress decreases in the concrete material and simultaneously the normal force in the reinforcement increases.

To illustrate the difference in model output using a Mohr-Coulomb or the Shotcrete material model, the tension cut-off points (tensile stress>strength) are visualised in Figure 25. In this figure also the occurring deviatoric strains are given, to be able to visualise the cracking in case of using the Shotcrete material model. Furthermore, the normal (axial) force in the reinforcement is given, such that the effect of the cracking process on the reinforcement is visualised. It can be observed that the cracking pattern coincides with the normal force pattern obtained in the reinforcement, as is expected when the Shotcrete material model is used. A detailed analysis of the results considering Shotcrete material model behaviour for the concrete is given in paragraph 3.2.3.

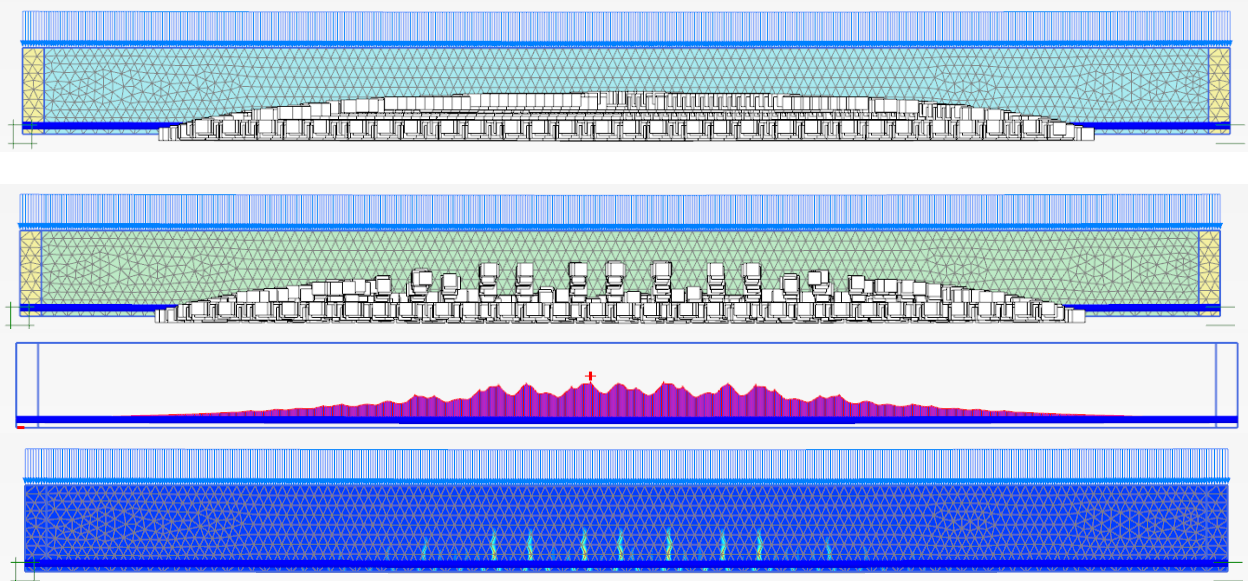

Figure 25: Tension cut-off points in MC and SC model when subjected to a line load of 40 kN/m, the occurring normal (axial) force in the reinforcement and the developed cracks in the SC model.

3.2.2.2 Stress, deformations and rebar force

A distinction is made in two categories analysing the stresses, deformations and rebar forces. The first category contains analysis of the reinforced concrete bending beam, before cracking takes place. In appendix E.2.1-5 (MC) E.3.1-5 (SC) under different loads, before cracking takes place, the stress-strain diagrams, the corresponding deformations and the rebar forces are given. In appendix E.2.6-16 (MC) E.3.6-17 (SC) the stress-strain diagrams, the deformations and the rebar forces of the reinforced bending beam at higher loads can be found. In appendix E.3 considering the Shotcrete model results, a difference is made between ultimate limit state (ULS) and serviceability limit state (SLS) loads. Besides a difference is made in this appendix by which way, linear elastic respectively elastoplastic, the rebar is modelled. The difference in ULS and SLS is indicated with an additional term for the increased tensile fracture energy G_t. The normal force in the reinforcement is only given for ULS model situations.

A selection of the full comparison using the Mohr-Coulomb (MC), Shotcrete (SC) and a linear elastic (LE) material model for concrete is given in appendix B.4/E and in Figure 26, Figure 27 and Figure 28. In Appendix B.4 the results of using an unreinforced beam are given, which gives the opportunity to investigate the influence of adding reinforcement in the model before cracking takes place. The model results of unreinforced concrete are only displayed in Table A-13 (appendix B.4) as their visibility is limited in the graphs on the next page. Additionally, the results of a hand calculation, u_y, σ_{xx} (considering no reinforcement) and N (considering reinforcement) are given in the mentioned figures. The hand calculated deformations and stress give an upper bound to the Plaxis output before cracking occurs and a lower bound after cracking takes place, due to the fact that cracking is not taken into account in the hand calculations. The hand calculated rebar force (Appendix B.4.2) can be considered as an upper bound for the modelled results. However conservative assumptions are taken into account for the hand calculation. The following parameters are used in the figures below: u_y the maximum

deformation in the y-direction, σ_{xx} the tensile (positive) as well as the compressive (negative) stress in the centre/middle of the beam and N the maximum normal force in the rebar.

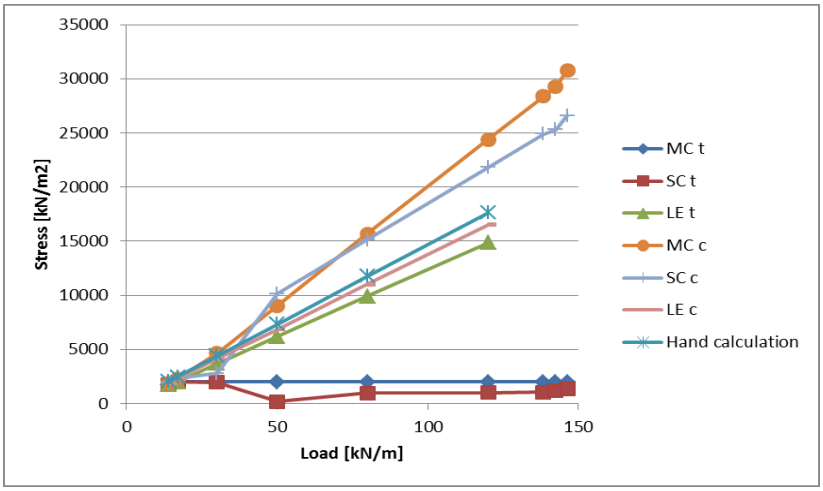

Figure 26: Load-stress distribution (σ_{xx}) comparison between different calculation/modelling methods in compression (c) and in tension (t).

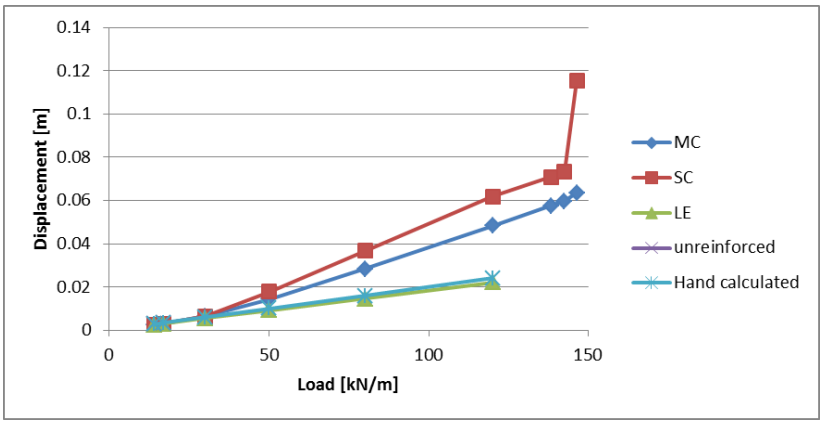

Figure 27: Load-displacement u_y comparison between different calculation/modelling methods.

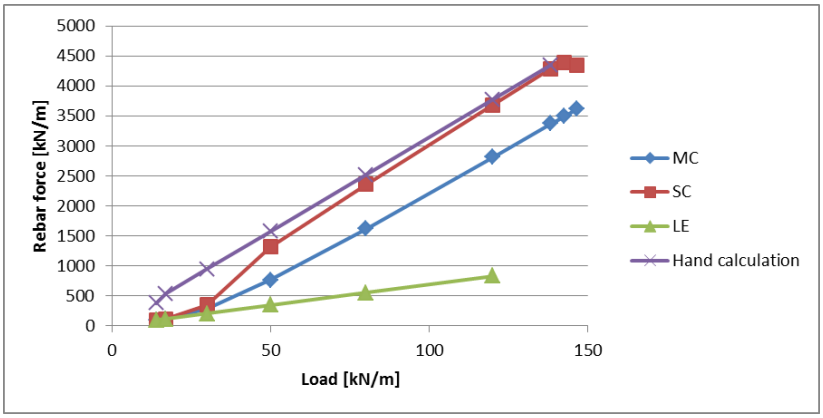

Figure 28: Load-Rebar Force (N) comparison between different calculation/modelling methods.

Analysing the results given in appendix B.4/E and the visualised results in Figure 26, Figure 27 and Figure 28 gives several points of interest. A first point of interest is that under low loads, meaning before concrete cracking, the bending deformation in the Shotcrete model is 3.5 % lower than in the Mohr-Coulomb model. This is not caused by a difference in occurring stresses as these are equal. The model formulation is exactly the same for un-cracked concrete as mentioned in paragraph 2.2.2, wherefore (consistent) deviations are not to be expected.

After cracking takes place the bending deformation obtained by using the Shotcrete material model are up to almost 2 times higher than when the Mohr-Coulomb material model is used (Figure 27). According to theory (paragraph 2.1.2) this is to be expected due to the fact that the Shotcrete material model in contrast to the Mohr-Coulomb model takes cracking into account, involving a decrease in bending stiffness. Subsequently, a decrease in bending stiffness causes larger occurring deformations. The significantly higher deformation observed is therefore reasonable and closer to the real deformation (behaviour). By the fact that the Mohr-Coulomb model does not take cracking into account but uses instead a tension cut-off to simulate tensile failure the stresses in the tensile part of the concrete beam remain (Figure 26, Figure 29, Appendix B.4 and E.2). In Figure 29 an example of the difference between the stress-distribution at higher load in the Mohr-Coulomb model and the Shotcrete model is given. A remark has to be made regarding the Shotcrete material model output: tensile stress (and compressive stress) is present in the area where no tensile stress after cracking is expected (Figure 26, Figure 29). Nevertheless it simulates concrete cracking behaviour quite accurately.

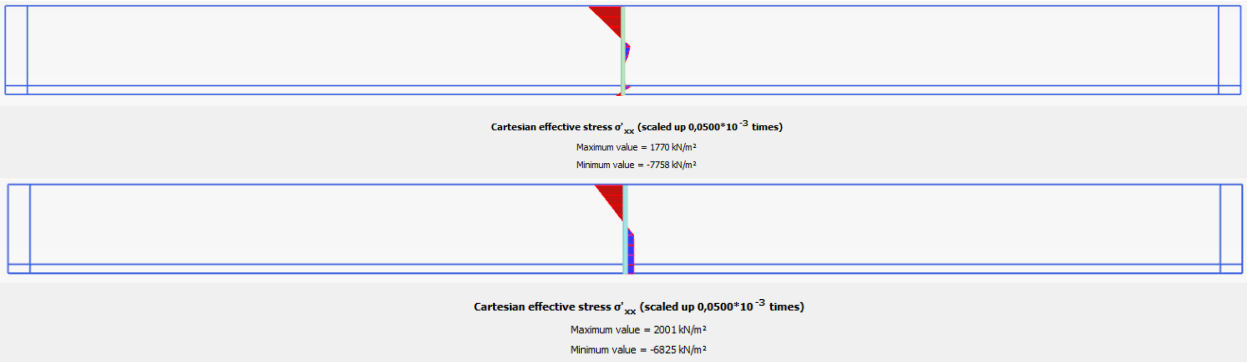

Figure 29: Concrete stresses at 40 kN/m line load by the Shotcrete model (1) respectively Mohr-Coulomb model (2).

It is possible to include simulated cracking in the Mohr-Coulomb model by introducing different layers over the thickness of the concrete volume element and give the ones which should crack a tensile strength of zero. Unfortunately on forehand it is not known till which height the tensile strength has to be taken zero, wherefore an iterative procedure has to be adopted. It might be considered as a solution, but however it is not suitable for engineering practice. In this way the modelling process takes a lot of time, especially when also covering soil-structure interaction situations.

Furthermore, it is observed that all results including normal force in the reinforcement, stress-strain behaviour in the concrete and the occurring model deformation, are correlated. This can be concluded from the fact that when higher concrete stresses occur, the deformation as well as the normal force in

the reinforcement is becoming larger (Figure 26, Figure 27 and Figure 28/appendix B.4, E.2 and E.3). Another observation confirming the validity of using the Shotcrete (and Mohr-Coulomb) material model results is that the deformation when using a linear elastic material model, not considering plasticity, is significantly smaller. Moreover, the stress obtained in the compression side of the beam is higher than when considering linear elastic model behaviour as this is not limited by a tension cut-off or by a certain tensile strength capacity. The stresses have to be in equilibrium, including normal force in the reinforcement, at all time. Therefore the compressive strength has to be lower than obtained without a limitation on the allowable tensile stress. When using a Mohr-Coulomb or Shotcrete model the normal force in the reinforcement has to be significantly higher as plasticity occurs. This is also observed in the model results. The observations support the hypothesis that application of the Shotcrete material model has additional value for modelling the structure when considering a soil-structure interaction situation.

Another point of interest which confirms the additional value of using the Shotcrete model over the use of a Mohr-Coulomb material model is the fact that the obtained forces in the single plate rebar are higher and comply with hand calculated results (appendix B.4). Especially at high applied loads (ULS calculations) the stresses in the rebar approximate those which should occur according to hand calculations. This observation is analysed and explained in more detail in paragraph 3.2.3.3.

Two other rough calculation methods are used to give a general indication of the occurring deformations, the stresses in the concrete cross-section and the normal force in the reinforcement. The two other rough calculation methods, unreinforced model calculations, respectively hand calculations are used as a first order comparison. These calculations support the theoretical background of the difference between reinforced and unreinforced concrete (modelling) results. Especially the results at loads before cracking is initiated give a good indication of in which extent the reinforced concrete models are able to model uncracked reinforced concrete. It is shown that in case when reinforcement is modelled in Plaxis, the deformations and stresses in the concrete are lower compared to a unreinforced model (Figure 26, Figure 27). This is caused by the fact that the reinforcement already takes some stresses when the concrete bending beam is still uncracked (Figure 28). On its turn, this is the result of a higher stiffness of the reinforcement with respect to the concrete material in the model. At higher loads, the reinforced Mohr-Coulomb and Shotcrete model give larger deformations and (compressive) stresses (Figure 26, Figure 27) than simple (uncracked) hand calculation results. Indicating the effect of taking “cracking” into account. The hand calculated normal force in the reinforcement gives an upper bound to the predicted occurring rebar forces in the Shotcrete model. Nevertheless, at high loads the results are comparable. In mind should be kept that the hand calculations are based on conservative assumptions, considering the height of the compressive stress area in the concrete. Therefore the results can (still) be regarded as valid.

Another noticeable fact is that the maximum deformation does not coincide with the place where the maximum stresses and maximum rebar force occur when using the Shotcrete material model. The maximum deformation occurs exactly in the middle of the beam as is expected. However the maximum stresses and the maximum occurring rebar force occur at the coordinates where the largest crack is initiated in the model. Due to numerical (too) large steps around the crack initiation moment, the crack

is initiated a couple of centimetres out of the middle. A confirmation for the validity of the model is that at the coordinates where the first and largest cracks are initiated, also the occurring stress and normal force in the reinforcement are the highest. It should be taken into account that the first and largest crack is not initiated exactly in the middle when analysing and comparing the results. Another fact that should be taken in mind when comparing the model results to analytical results concerns the including of shear deformation in Plaxis model results, while in hand calculations this phenomenon is not considered.

3.2.2.3 Calculation time

To be able to derive a conclusion about the applicability of the Shotcrete material model over the Mohr-Coulomb material model a comparison based on calculation time is made. In engineering practice accurate results are wished for but the calculation time should be reasonable in any case. The calculation time increases with the mesh size and the complexity of the used material model, respectively the model itself. One of the aspects of influence is checked in this paragraph, namely the consequence on the calculation time when using a more complex material model (Shotcrete) instead of a first order approximation model (Mohr-Coulomb model). In the analysis the mesh size, defined in Plaxis as Very fine, is kept equal. This mesh involves the use of 2442 elements for the analysis. The model setup, a single plate reinforced concrete beam (Figure 19), is also kept the same during the analysis, to be certain that the deviations in calculation time can be related to the use of the different material model.

Both models are tested at five different loads to give insight in the calculation time with respect to different (behaviour) situations. In Table 11, visualised in Figure 30, the results of the analysis are given.

Table 11: Comparison of calculation time using a Mohr-Coulomb or a Shotcrete material model.

Load	Calculation time Mohr-Coulomb	Calculation time Shotcrete	Difference (Absolute and %)
20 kN/m	7 s	83 s	76 s / 1186 %
40 kN/m	420 s	2300 s	1880 s / 548 %
80 kN/m	1020 s	9600 s	8580 s / 941 %
120 kN/m	1860 s	14100 s	12240 s/ 758 %
Failure (146.4 kN/m)	1980 s	6300* s	4320 s/ 318 %

*Influence of G_t=0.15 kN/m instead of 0.1 kN/m, leading to less calculation time.

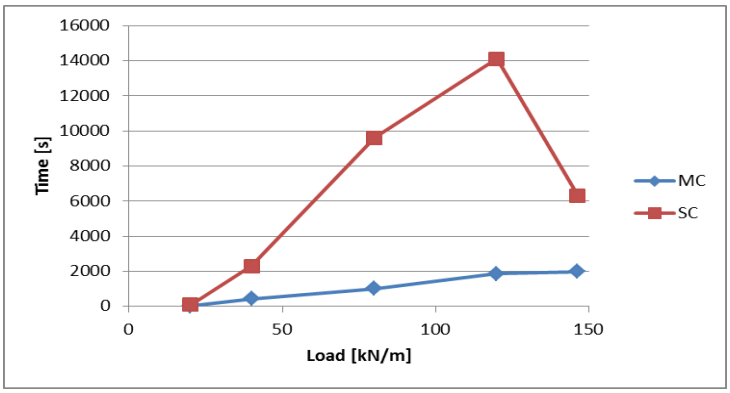

Figure 30: Calculation time using a Mohr-Coulomb or a Shotcrete material model.

In Table 11, respectively Figure 30, it can be observed that the load as well as the model complexity (material model) plays a role in the calculation time. The higher the load, the more calculation steps are needed and because plasticity is involved the calculation time is increased rapidly. In mind has to be kept that a model change was necessary to converge the Shotcrete model at ULS loads. The result is that a relatively lower calculation time is obtained. This demonstrates that using low fracture energies in the model cause a significant increase in calculation time. Nevertheless it can be concluded that the calculation time using the Shotcrete material model is significantly higher, especially for ULS calculations. The relative differences in calculation time between the models range from 3 to almost 12 times more calculation time needed when using the Shotcrete material model instead of a Mohr-Coulomb material model (using a very fine mesh). This can be explained by the fact that when cracking occurs a lot of detailed calculations have to be performed by Plaxis. A decrease in calculation time of the Shotcrete model can be obtained by increasing the fracture energy slightly. This also enhances the model stability. Though the accuracy decreases a bit instead.

3.2.3 Modelling results of the Shotcrete material model

The results of the Shotcrete material model are already used in the previous paragraph in order to investigate the additional value of the Shotcrete model when modelling reinforced concrete structures. The results indicate that at first sight this is the fact. Therefore in this paragraph more detail is paid to the in depth analysis of the results regarding the reinforced concrete bending beam analysis with the use of the Shotcrete material model. In this paragraph specific results are used for the analysis, while all modelling results by each aspect are given in appendix E.3.

3.2.3.1 Stress-strain

In appendix E.3 the applied loads on the reinforced concrete bending beam with the Shotcrete material model are given. Stepwise the load is increased and analysed. The analysis focusses in detail on the moment of cracking of the concrete, the moment at which the rebar yields and the moment of failure are also researched. According to Plaxis at a load of 18.15 kN/m, corresponding to a back calculated, by the statically determined structural concept, bending moment of 445 kNm, cracking is initiated. The moment of cracking in the Mohr-Coulomb model is equal to the one in the Shotcrete model which is expected as explained in paragraph 2.2. However according to the hand calculation cracking should only

be taking place when a line load higher than 22 kN/m is applied. This can partly be explained by the fact that during the hand calculation no shear deformation is taken into account.

After the first crack is initiated, more cracks will follow. By applying intermediate loads between rupture and yielding moment, the evolution of cracking over the beam can be investigated. In Figure 31 the cracking pattern at four different intermediate loads is visualised by means of visualising the deviatoric strain. The cracking pattern at line loads of 20, 40, 70 and 120 kN/m is visualised in this figure. Only at a line load of 20 kN/m another parameter, the normalised tension parameter, is used to indicate cracking. This is because of the fact that cracking is just initiated and when displayed in deviatoric strain the small cracks are not visible.

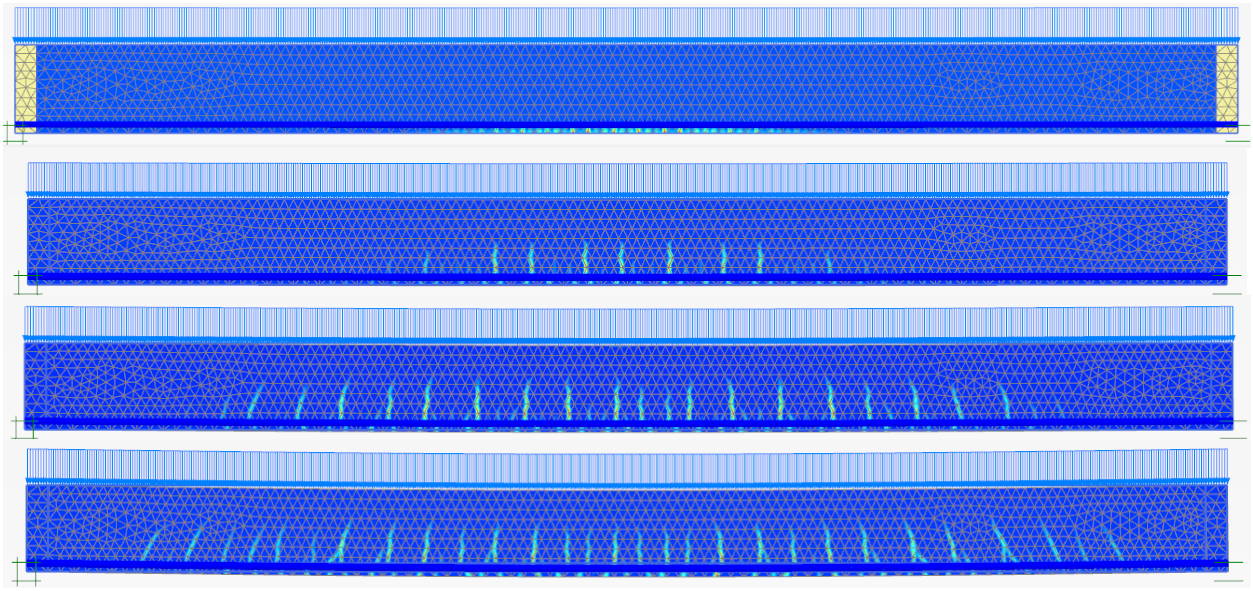

Figure 31: Cracking pattern (deviatoric strain) of reinforced bending beam at line loads of 20, 40, 70 and 120 kN/m.

In Figure 31 is observed that the progression as well as the crack pattern over the beam is equal to what is expected from theory. A lot of small cracks are present below the reinforcement while above the reinforcement less but larger cracks are formed. The development of cracking is also matched with theory. Just above the critical cracking load a small crack is formed near the centre. With increasing load the cracks develop gradually towards the hinges and the first developed cracks will simultaneously grow higher into the beam. An arc pattern is observed in both theory and results of the Plaxis model (Figure 31 and Figure 32).

Figure 32: Experimental crack pattern reinforced concrete beam subjected to bending (and ultimately shear cracking) (Leonhardt & Walther, 1962).

In depth also the validity of the cracking pattern is research. NEN-EN-1992-1-1 (2011) is used to calculate the distance between the occurring cracks. The crack distance can be calculated in two different ways. One giving an accurate indication, however needs a lot of input, and one giving a rough estimation. The rough estimation is giving an upper bound for the maximum to be expected distance between the cracks (equation 3.4). X is the distance from the reinforcement to the centreline of the cross-section.

$$s_{r,max} = 1.3 * (h - x) = 1.3 * (1 - 0.4) = 0.78\ m\ (3.4)$$

The maximum distance between the cracks by the more accurate calculation is given in equation 3.5.

$$s_{r,max} = k_3 c + k_1 k_2 k_4 \varnothing / \rho_{p,eff} = 0.345\ m\ (3.5)$$

Where k_3 (3.4) and k_4 (0.425) are given by the NB of the Eurocode, k_1(0.8) is dependent on the concrete cover of the rebar and k_2 (0.5) depends whether the failure is due to bending or pure tension. Besides, the diameter of the rebar (∅=32 mm) and the "effectiveness" of the reinforcement ($\rho_{p,eff}$) influence the outcome.

In large structures the more accurate formula according to NEN-EN-1992-1-1 (2011) is still not sufficient as a check. Another lower bound for the distance between cracks has to be adopted according to TGB Betonconstructies (2013), which is considered in equation 3.6.

$$s_{r,max} \leq \max(15\phi, (50 - 0.8 f_{ck})\phi) = 26\ \phi\ \ (3.6)$$

The crack distance in Plaxis is around 40 centimetres wherefore it may be assumed to be accurate. The NEN-EN-1992-1-1 (2011) should cover a whole range of different setups, wherefore a slight deviation is not considered to be wrong or inaccurate.

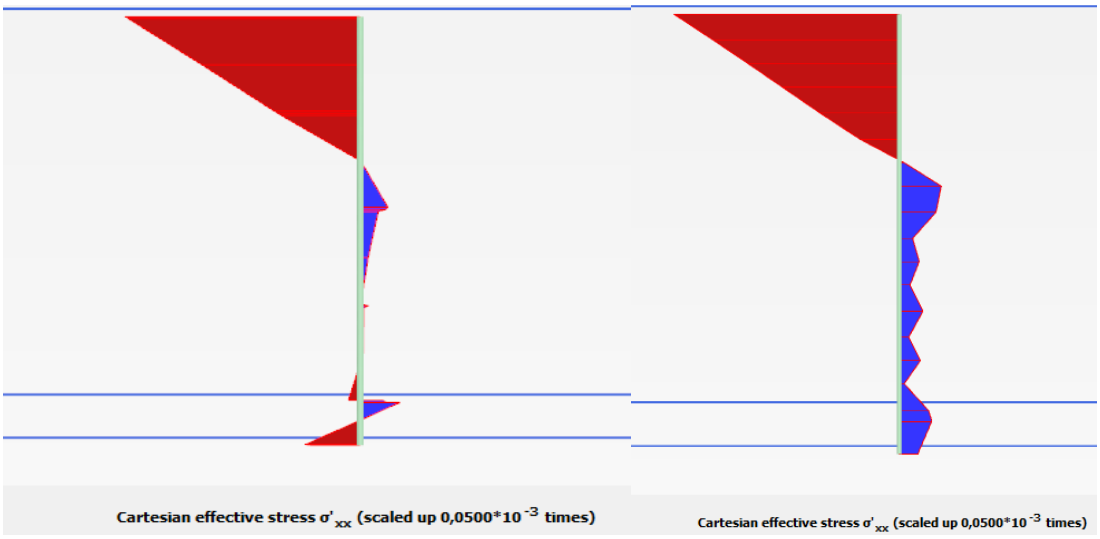

Figure 33: Example of occurring "Noise" in stress-distribution in the middle of the beam and in a crack.

Another aspect to be paid attention to is the "noise" in the cross-sectional obtained stresses in the concrete. In Figure 33 two different detailed cross-sections are given. The first is made in the middle of the span of the beam. As mentioned before, still some stresses remain in the cross-sectional area. Unfortunately not only tensile stresses remain after cracking, also compressive strains are suddenly generated below the neutral line. These compressive stresses are possibly the cause of numerical processes, which is in definition not wrong. A possible cause of these numerical processes can be the results of the smeared crack model, which "smears" the crack over a certain area. To test this assumption another cross-section is made crossing a virtual crack (Figure 33). In this cross-section it is shown that only tensile stresses are occurring below the neutral line. No tensile stresses are expected to occur when the cross-section crosses a crack. It is observed that the tensile stress drops in the model every time a crack crosses the cross-section, which conforms the validity of the model. Another possible cause of these numerical difficulties concerns the tensile fracture energy. Schädlich and Schweiger (2014b) mention that low values for the tensile fracture energy in large models can lead to unpredictable behaviour. It must be remarked that the occurring stresses relatively balance each other and probably have minor influence on the overall model behaviour, especially regarding soil-structure interaction situations. In mind has to be taken that the distribution of stresses around a meandering crack is hard to predict and verify. Nevertheless further research in the occurrence of these numerical processes is whished for.

3.2.3.2 Deformations

Besides a in depth stress-strain analysis, also the deformations can be evaluated in detail. The deformation of the bending beam is directly correlated to the bending stiffness. Therefore deviations in magnitude of bending with the same load conditions can be related to a difference in bending stiffness. A non-linear increase in bending deformation with loading indicates a changing bending stiffness with loading. A (non-linear) difference in bending stiffness can according to theory (paragraph 2.1.2.2) be related with the phenomenon of cracking or yielding.

In paragraph 3.2.2 and appendix E.3 the deformations for a certain spread of applied line loads are given. Intermediate loading steps are performed, Table 12, between yielding and failure to investigate the sharp decrease in bending stiffness according to the M-κ diagram (Figure 10). Two remarks have to be made analysing Table 12. The first remark considers the change in fracture energy to guarantee convergence at ULS loads, as mentioned before. Another remark considers the difference between the defined material behaviour of the reinforcement. The difference in the use of a linear elastic or an elastoplastic material model for the reinforcement is researched. The difference found is significant at the yielding moment, which is also to be expected. This confirms the need of an elastoplastic reinforcement formulation when modelling a reinforced concrete bending beam. Furthermore it confirms the model validity for these model setups. In Figure 34 the load-displacement curve is given based on the data in Table 12.

Table 12: Load-Deformation for the Shotcrete model.

Load [kN/m]	Deformation [m]
15	$-2.658*10^{-3}$
20	$-3.718*10^{-3}$
40	-0.0119
50	-0.0179
70	-0.0304
80	-0.0367
120	-0.0618/-0.05943*
138.3	-0.07092**/-0.07090
140	-0.07194**/-0.07196
142.5	-0.07345**/-0.07344
146.4	-0.07613**/-0.08825
150**/146.6	-0.07844**/-0.1157

*Influence of G_t=0.15 kN/m instead of 0.1 kN/m.
** Linear elastic rebar instead of Elastoplastic rebar.

In Figure 34 it can be observed that based on the results given in Table 12 the load-displacement graph matches the theory of loading a reinforced concrete beam laterally. At first the behaviour is linear elastic, but as soon as cracking takes place the stiffness is reduced and the displacement increases more rapidly. The use of linear elastic (LE) reinforcement leads to a linear load-displacement curve, while the use of elastoplastic (EP) reinforcement leads to yielding. The model simulates realistic load-displacement behaviour quite well using an elastoplastic formulation for the rebar. The difference in results when using a different tensile fracture energy is displayed at a load of 120 kN/m. It can be observed that an increase in fracture energy reduces the amount of displacement, by 4 %.

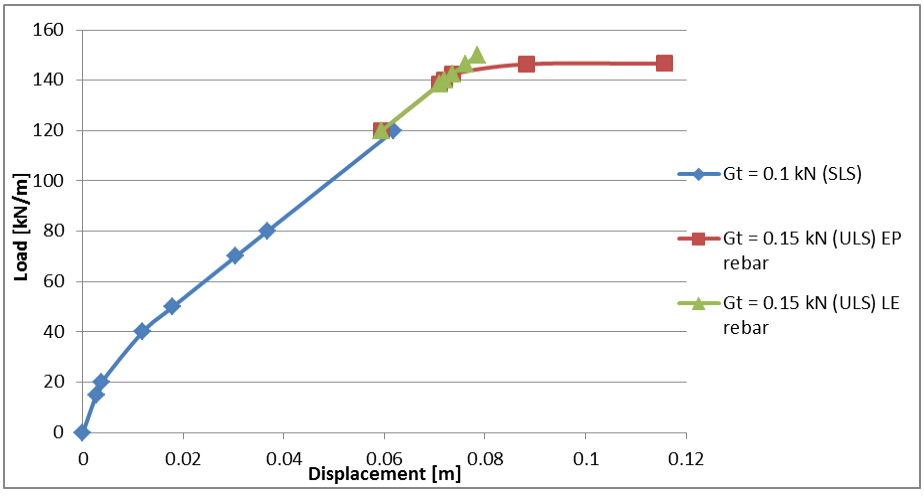

Figure 34: Load-displacement curve in SLS and ULS with different tensile fracture energy based and rebar characteristics.

Another option to check the validity the load-displacement behaviour of the concrete (Shotcrete) reinforced bending beam behaviour is to directly use the output of Plaxis. A single check with G_t = 0.15 kN/m and elastoplastic reinforcement behaviour is performed. A single point in the middle (bottom

part) of the beam is analysed in Figure 35. It is shown that the three stages concerning a reinforced beam subjected to bending can be indicated. The linear elastic part till rupture, the decreased stiffness after rupture corresponding with the phenomenon called tension stiffening (paragraph 2.1.2) and the further decreased stiffness until failure due to yielding of the reinforcement. The load can only increase a fraction when yielding occurs, as progressive generation of plasticity takes place in Plaxis.

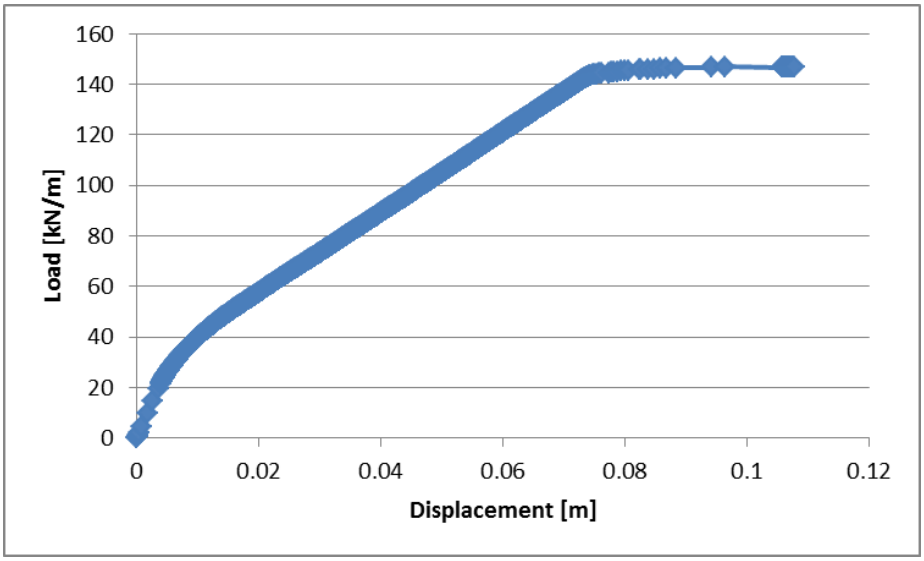

Figure 35: Load-displacement output of Plaxis in the middle of the reinforced beam subjected to a line load.

3.2.3.3 Reinforcement

The normal force in the reinforcement is another output of the model. In paragraph 3.2.2 and appendix E.3 the normal force in the reinforcement is given for a certain range of the laterally applied line loads on the reinforced concrete beam. However for the interest of analysing the accuracy/correctness of occurring reinforcement forces, additional attention is paid to the load at which yielding takes place. In Table 13 especially results around the moment at which the reinforcement should yield are given. The graph in Figure 36 (Load-Normal force) corresponds with the use of a fracture energy equal to G_t = 0.15 kN/m and an elastoplastic reinforcement material model formulation.

Table 13: Load-Rebar force for the shotcrete model.

Load	Rebar force [kN/m]
15	100
20	146
40	926
50	1318
70	1991
80	2362
120	3686/3621*
138.3	4286**/4285
140	4337**/4338

142.5	4405**/4387
146.4	4542**/4381
150**/146.6	4652**/4373

*Influence of G_t=0.15 kN/m instead of 0.1 kN/m.
** Linear elastic rebar instead of Elastoplastic rebar.

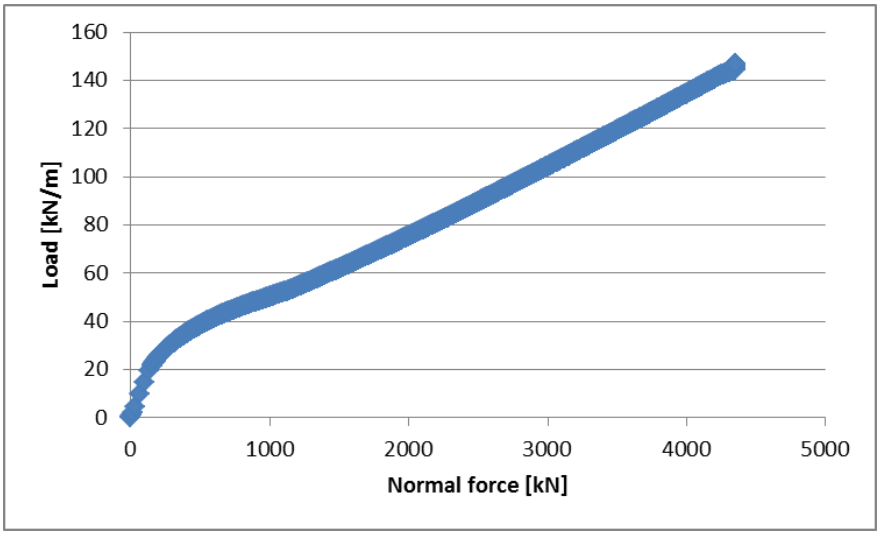

Figure 36: Load-Normal force (rebar) Plaxis output in the middle of the beam.

The three recognised stages in the load-displacement graph are also present in Figure 36. At first the concrete material is capable of handling the tensile stresses, but from the moment of cracking of the concrete material the normal force in the reinforcement increases more rapidly. All additional tensile stresses in the still extended tensile part of the beam are taken by the reinforcement. With increased loading an equilibrium is reached between the tensile force uptake by the reinforcement and the increased load. This can be observed by the fact that at the start of cracking the normal force increases more rapidly increases than at higher loads. The process of cracking evolves such that a linear relation between force increase in the rebar and the increasing load can be recognised. At yielding suddenly the normal force in the reinforcement does not increase anymore. “Failure” of the reinforcement occurs, due to the linear elastic perfectly plastic material formulation. This is also slightly visible in Figure 36. The load is still increased a little bit as the reinforcement reaches its ultimate capacity at a normal force of 4350 kN.

Another observation done considers the distribution of the normal force over the length of the reinforcement. In theory it is described that the normal force in the reinforcement is the highest at a place where the concrete is cracked. In between the cracks, the concrete has still its limited tensile strength capacity. This phenomenon is visualised in Figure 37.

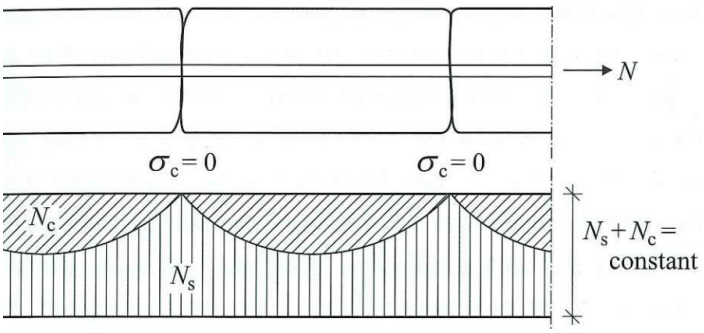

Figure 37: Force distribution in cracked reinforced concrete (Braam & Lagendijk, 2010).

In Figure 38 it can be seen that the Shotcrete model output takes the difference between cracked and uncracked areas into account. The normal force in the reinforcement is the highest where the largest crack is initiated and the irregular pattern of peaks indicate the difference between the cracked and uncracked ("valley") areas.

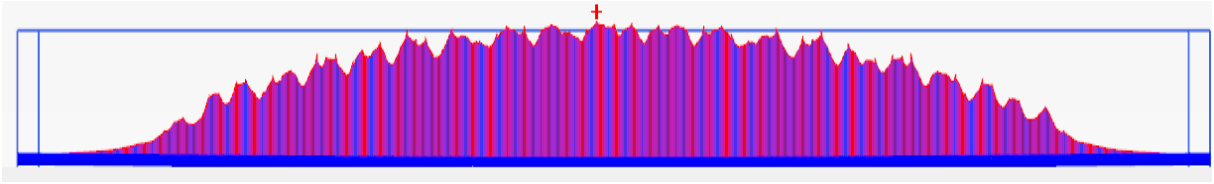

Figure 38: Normal force distribution in the reinforcement in the Shotcrete reinforced bending beam.

3.2.3.4 Mesh sensitivity analysis

Another aspect determining the applicability of a model concerns the calculation time versus the accuracy. A mesh sensitivity analysis is carried out in order to determine if a coarser mesh can be applied without losing too much accuracy. Besides, an analysis is carried out to evaluate the effect of using a coarser mesh on calculation time. During the mesh sensitivity analysis the model itself is kept similar to the set-up given in Figure 19. The mesh sensitivity analysis is carried out for two different applied lateral line loads; 40 kN/m, respectively 60 kN/m. This magnitude of load applied gives a for analysis interesting case, namely a moderately cracked beam. It has to be taken into account that the deviations between the model results will probably increase at higher loads than analysed due to the fact that cracking is mesh dependent. Results of using a applied line load of 40 kN/m are given in appendix E.5.1, while results for a applied line load of 60 kN/m are given in appendix E.5.2. A detailed analysis is done on the results of the case when a line load of 40 kN/m is applied, while 60 kN/m results are mainly used for confirmation. The mesh options to be analysed with Plaxis are: Very fine, Fine, Medium, Coarse and Very coarse. In Figure 39 the reinforced bending beam with the different mesh sizes is visualised.

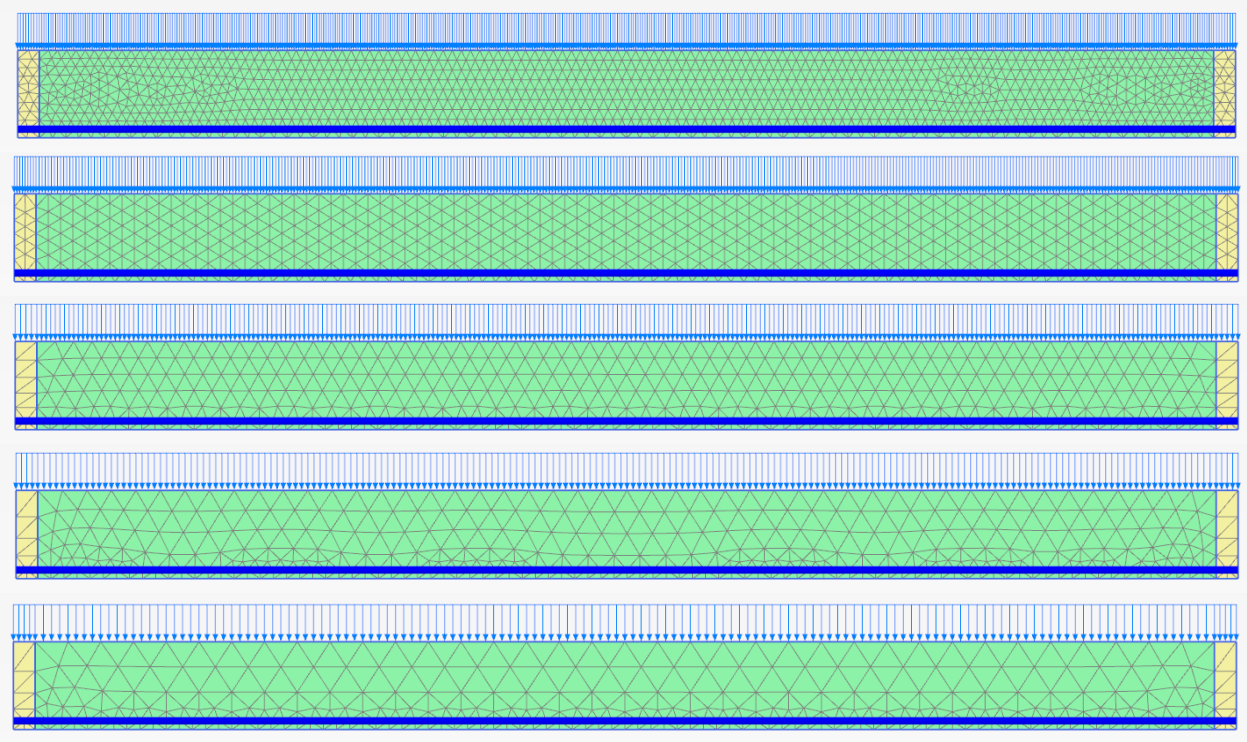

Figure 39: Different mesh sizes used for the mesh sensitivity analysis.

The first aspect of this analysis covers the accuracy of the model. The occurring stresses in the concrete are analysed with respect to the Very fine reference mesh results. In appendix E.5, respectively Table 14, for different mesh sizes the stress distributions at the centre of the beam are given. The in Table 14 given values and relative differences with respect to the results using a very fine mesh cannot be interpreted on itself. Consequently the in appendix E.5 given results have to be analysed. It is observed that only with the use of the very fine mesh size accurate insight in the stress distribution after cracking can be obtained. The use of the coarser meshes cause an over estimation of tensile capacity. The very fine mesh size approximates reality, by the fact that almost over the whole mobilised tensile area the tensile stress is reduced. The other meshes come to a similar result as the Mohr-Coulomb model, with the difference that only in the very bottom part the tensile stresses are reduced (till zero). Analysing the results of an applied line load of 60 kN/m confirms most conclusions. However the coarser meshes (Fine and Medium) seem also applicable for obtaining a correct insight in the occurring stresses. Therefore it can be stated that probably the stress-distribution and especially the governing stress for model failure are not dependent on mesh size. Possibly a coarser mesh can be used for the reinforced concrete structure during a soil-structure interaction model.

Table 14: The influence of the mesh size on the tensile (and compressive) stresses obtained in the middle of the reinforced concrete (Shotcrete) bending beam with a 40 kN/m line load.

Mesh size	Stresses [kN/m^2]	Difference
Very Fine (2442 elements)	1770/-7760	Reference
Fine (1294 elements)	1920/-7388	+8%/ -5%
Medium (876 elements)	1825/-7923	+3%/+2%
Coarse (750 elements)	1564/-7798	-13%/+0.5%
Very coarse (626 elements)	2005/-7374	+12%/-5%

Another important model output considering the accuracy is the deformation. The spread in deformation result ranges from 11.8 mm to 12.1 mm for a applied line load of 40 kN/m (Table 15). This is only a deviation of 2.2 % with respect to the reference (very fine mesh). The figures corresponding to the deformation are given in appendix E.5. It is observed that using a fine mesh for a deformation analysis has only slight influence. The deformation will only slightly reduce with increasing mesh refinement, in both the case of an applied line load of 40 kN/m and 60 kN/m. However in specific cases this can be of importance. Taken in mind has to be that all design aspects together determine the need of a finer mesh. Therefore all aspects, stress distribution, reinforcement force and cracking pattern, have to be considered during a full analysis. But using a coarser mesh does not influence the obtained deformation results heavily.

Table 15: The influence of the mesh size on the deformation of the reinforced concrete (Shotcrete) bending beam with a 40 kN/m line load.

Mesh size	Deformation [m]	Difference
Very Fine (2442 elements)	-0.01180	Reference
Fine (1294 elements)	-0.01206	+2.2 %
Medium (876 elements)	-0.01199	+1.5 %
Coarse (750 elements)	-0.01185	+0.5 %
Very coarse (626 elements)	-0.01207	+2.2 %

The occurring force in the reinforcement for a applied line load of 40 kN/m can also be evaluated for the different mesh sizes. The results are given in Table 16. The differences in the calculated rebar force with respect to the reference calculation are ranging from -3% when a coarse mesh is used to +7.5 % when a very coarse mesh is used (Table 16). This seems to correspond partially with the occurring stresses in the concrete element itself (Table 14). However it should be taken into account that a lower obtained tensile stress in the concrete material has to correspond with a high force occurring in the reinforcement. In literature (paragraph 2.1.2) is described that as soon as the concrete cracks the tensile capacity is lost locally and the reinforcement has to take up these forces. In the modelling results an opposite relation is found, which is not to be expected. This possibly indicates that results of coarser meshes are inaccurate. Analysing the results of applying a line load of 60 kN/m (appendix E.5.2) leads to approximately the same results.

Table 16: The influence of the mesh size on the rebar force of the reinforced concrete (Shotcrete) bending beam with a 40 kN/m line load.

Mesh size	Rebar force [kN/m]	**Difference**
Very Fine (2442 elements)	921	Reference
Fine (1294 elements)	971	+5 %
Medium (876 elements)	979	+6 %
Coarse (750 elements)	892	-3 %
Very coarse (626 elements)	995	+7.5 %

Not only quantitative analysis is used in the evaluation to the appropriateness of using a coarser mesh, but also a qualitative analysis is carried out. In Figure 40 the crack patterns of the reinforced concrete bending beam subjected to a line load of 40 kN/m are visualised. It is shown that only in the case of using a very fine mesh, the results of the crack pattern are reasonable. When coarsening the mesh the cracking pattern becomes unstable. At some place suddenly the crack becomes very long, the crack mouth becomes wider and vague and the arc pattern disappears (Figure 40). This is the result of less elements used in the calculation. Furthermore this is caused by less boundaries over which the crack can propagate. The path to be followed is more prescribed than in case a very fine mesh is used, which allows the crack to choose its own path. For an applied line load of 60 kN/m, the cracking pattern is somewhat wider. Nevertheless also in this case only using a Very Fine mesh will give favourable results.

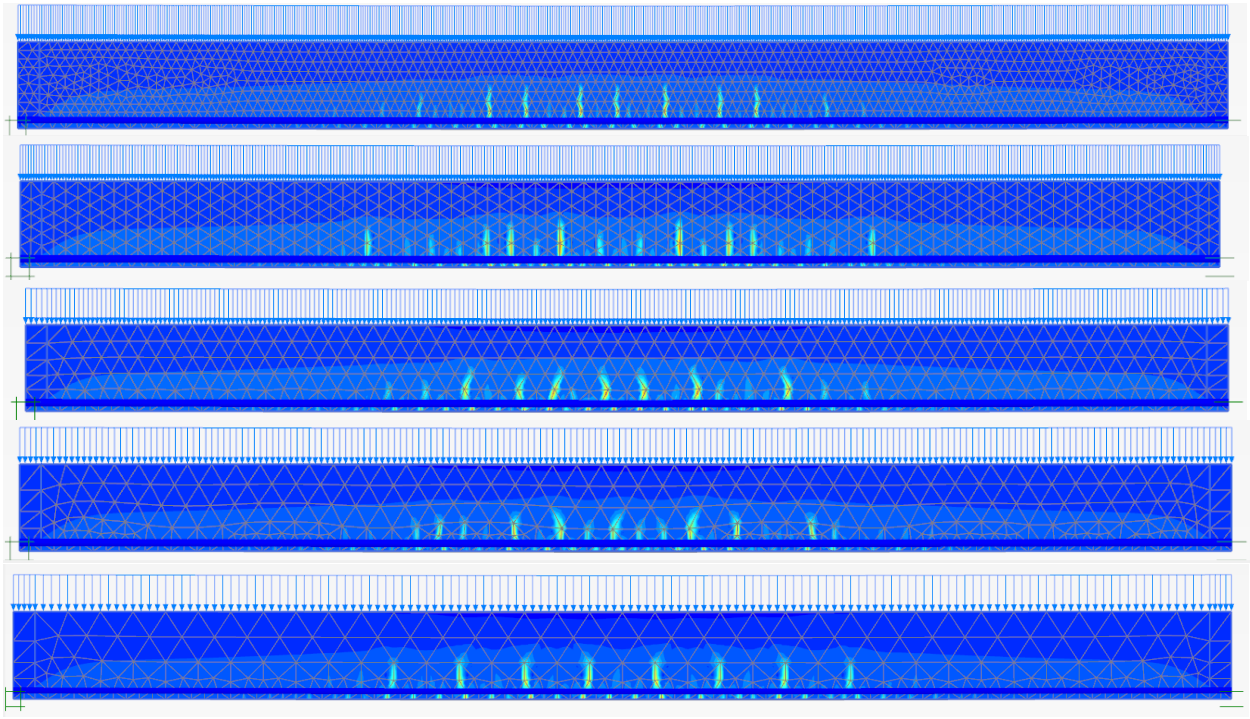

Figure 40: Cracking pattern at different mesh sizes (from very fine tot very coarse) at a applied line load of 40 kN/m.

A second aspect of the quantitative analysis concerns the results of a Plaxis build in function, which gives the quality of each element in the mesh. This output is given in appendix E.5. It is observed that a finer

mesh will not give a better quality absolutely. Although, when looking closer to the results, it is found that using a finer mesh leads to a better overall model (mesh) quality. In the Very fine mesh only a couple of elements have a low quality, while in coarser meshes significantly more elements have a relatively low quality. Especially elements next to the reinforcement have a lower quality in the coarser meshes. This influences the accuracy of the model significantly as those areas are governing for the overall model results.

Not only the accuracy of the results is an important model feature. Also the calculation time needed for a single model calculation when applying a line load of 40 kN/m, respectively 60 kN/m is important. It is wished for that an optimum is found between accuracy and calculation time in engineering practice. Below in Figure 41 the calculation time with increasing mesh refinement is given.

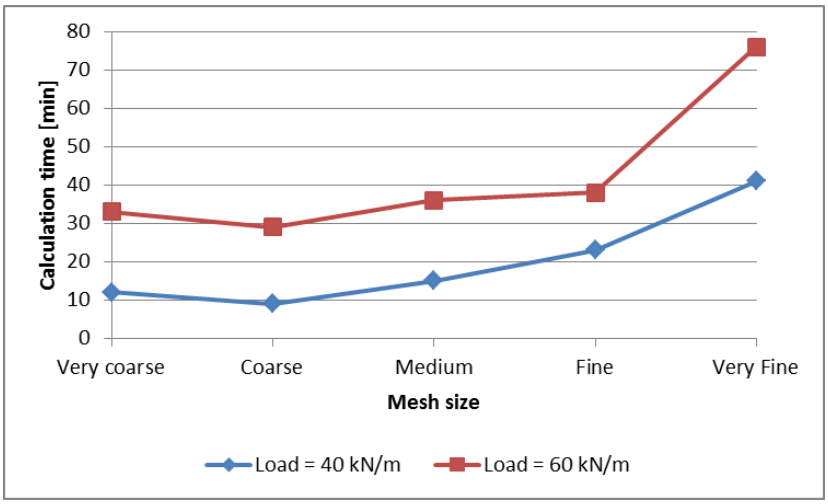

Figure 41: Calculation time for different mesh sizes applying a line load of 40 kN/m and 60 kN/m to the model.

It is shown that the coarsest mesh does not involve the least calculation time, which might be expected on forehand. The inaccuracies when modelling are becoming high when using this mesh, wherefore the calculations required increase. The difference in calculation time between the different mesh sizes is relatively limited, with the exception of the finest mesh. The calculation time is almost doubled between the Fine and Very Fine mesh. It should be taken in mind that when increasing the load, the calculation time significantly increases causing an even larger absolute difference in time. The difference in calculation time between the other mesh sizes is that small that the Fine mesh, increasing the accuracy with respect to the other mesh sizes significantly, is the best choice. Taking in mind that the accuracy of using a Fine mesh with respect to the Very Fine mesh is somewhat lower. Cracking is a complex process, which requires a very fine mesh for cases in which the cracking pattern really matters. To get appropriate model results it should be checked that at the final load the differences caused by meshing is relatively limited. Therefore calculation time may not always be the governing factor deciding the appropriate mesh size.

3.3 Comparison with M-κ diagram by hand

The model results of the reinforced concrete beam subjected to bending can be compared to a hand calculation, which is also able to account for cracking of a reinforced concrete element. On forehand it is known that the results will deviate somewhat due to the fact that in Plaxis shear deformation is taken into account which is in contrast to the hand calculation. In the hand calculation it is besides assumed that the cross-section of the beam stays undeformed while in Plaxis the cross-section deforms. Another deviation that should be taken into account when analysing the results is that the Shotcrete model allows the concrete to have tensile strength above the crack in the tensile zone of the beam. Moreover in the Shotcrete model some residual strength after cracking is taken into account. In the hand calculation these properties are not taken into account, wherefore the curvature (κ) in the Shotcrete model will probably be lower. Despite the mentioned deviations, a comparison with a M-κ hand calculation gives the opportunity to verify the model results. In this paragraph an insight in the hand calculation is given and the results are compared subsequently. The detailed hand calculation can be found in appendix C.

3.3.1 M-k diagram by hand

The M-κ diagram (Figure 42) describes the behaviour under bending of a reinforced concrete beam with the help of several points. The first point to be determined is the moment at which rupture occurs. The second point indicates the moment at which yielding (of the rebar) occurs. The third point indicates the moment at which the concrete material starts to yield and the last point indicates failure. Failure occurs according to NEN-EN-1992-1-1 (2011) at a concrete strain of 3.5 ‰. The points indicated are based on the moment applied and the resulting curvature of the beam. The curvature is dependent on the moment applied but also on the (bending) stiffness of the beam as mentioned before in paragraph 2.1.2. The slope in between the different points becomes more gradual with increasing moment, less additional moment has to be applied to cause an increase in curvature. Therefore it can be concluded that the (bending) stiffness decreases with increasing moment. The Plaxis Shotcrete reinforced bending beam model has to be able to model the behaviour described and visualised in Figure 42. The model set-up used in the M-κ diagram calculation is equal to those used for the Plaxis calculation. A concrete beam of 1000x1000 m with a concrete strength of C30/37 is used. The reinforcement is situated 900 mm from the top and has the characteristic values of B500A/B reinforcement.

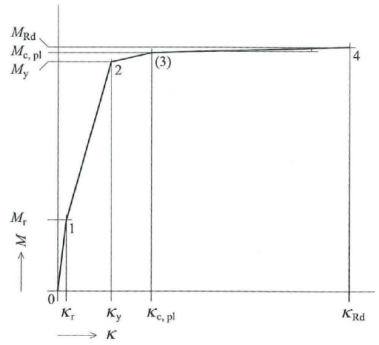

Figure 42: M-κ diagram (Braam & Lagendijk, 2010).

The rupture moment is determined by the tensile strength of the concrete material and the stiffness of the (combined) reinforced concrete material. Rupture occurs at a moment of 442 kNm, which is similar to an applied line load of 18 kN/m in the Plaxis model. The line load is back calculated according to the Forget-me-nots. This causes a small deviation from the real (to be) applied line load in Plaxis, due to the assumptions used for this calculation. Yielding occurs at a moment of 3387 kNm, which coincides approximately with a applied line load of 138 kN/m. A stress of 435 N/mm^2 has to occur in the reinforcement to cause yielding. A strain of 2.1 ‰ occurs at yielding in the reinforcement while a strain of 1.4 ‰ takes place in the concrete material. It is therefore checked and verified that the concrete strain is below the strain at which plasticity occurs. Meeting this criterion prevents sudden failure of the structure. Yielding of the concrete material occurs at a defined strain (1.75 ‰) according to NEN-EN-1992-1-1 (2011). The occurring moment at this state is 3493 kNm, corresponding to a applied line load of 142.6 kN/m. The moment of failure, a strain of 3.5 ‰ in the concrete material, is 3586 kNm. The (to be) applied line load in that case equals 146.4 kN/m. The stiffness decreases with increasing moment as is expected according to theory. Detailed insight in the M-κ calculation itself is given in appendix C. In Table 17 the given moments and corresponding (to be applied) line loads (in Plaxis) for each point of the graph is given. In Figure 43 the M-κ diagram is visualised. In the next sections the calculated corresponding line loads are used as input for the Plaxis model. The curvature resulting from the Plaxis calculations will be back calculated and the differences with respect to the hand calculated values will be evaluated.

Table 17: M-k diagram values and corresponding model line loads.

Moment	Moment Value [kNm]	Corresponding line load [kN/m]
Rupture	442	18
Yielding of rebar	3387	138.3
Yielding of concrete	3493	142.6
Failure	3586	146.4

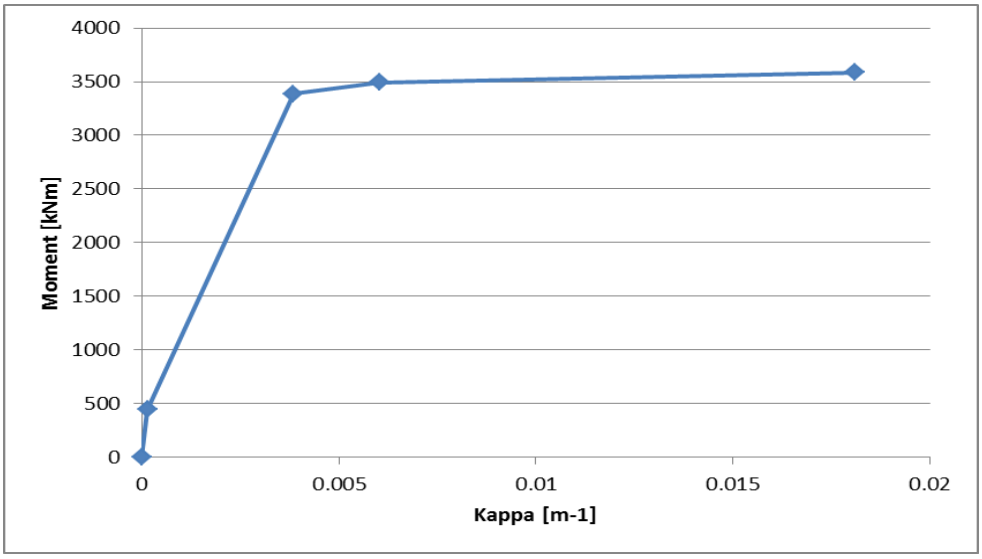

Figure 43: Hand calculated M-k diagram of considered reinforced concrete beam.

3.3.2 M-k diagram by Plaxis

In a volume element in Plaxis it is not possible to output the curvature directly. This is due to difficulties with the varying occurring concrete strain, which is the effect of the smeared cracking concept, and the fact that it is not possible to directly output the strain in the reinforcement (plate element). Therefore a solution has to found. It is known on forehand that the neutral line of the reinforced concrete beam will be approximately at the center. At the neutral line a plate element with almost zero stiffness is created, a so-called dummy element. The dummy element deforms exactly as the neutral line of the beam without influencing the overall model behaviour. The deformation of the dummy element is used to calculate the curvature. From mathematics it is known that the curvature is the second derivative of the deformation of a line. A fourth order polynomial function is fitted at the deformation curve of the dummy element over the whole length. The second derivative of the polynomial function is calculated and the coordinates at which the deformation is maximal, the middle, is filled in in the function. This gives the curvature at maximum deformation. An example of a polynomial fit to a deformation curve is given in appendix C.2. This process is repeated for different applied bending moments.

As mentioned before, problems with the model convergence have led to the fact that the fracture energy had to be increased during the process. This will result in some small deviations (<5%) from the proposed real situation. Another small deviation comes from the fact that the obtained moment is back calculated using the rules for a statically determined structure, not taking into account shear deformation, which is accounted for by Plaxis. Taking these deviations into account besides the ones mentioned before, the results can be analysed properly.

Two situations are analysed from the perspective of the behaviour of concrete. In the first case parameter values as proposed in Table 10 are used in the calculation. Thereafter, to investigate the influence of the model to coop with remaining and residual tensile strength in the concrete after cracking, the tensile strength of the material is reduced to 25 % of its original. The results of the second case have to approximate the hand calculation better as in the hand calculation no tensile strength is taken into account above the cracked zone, respectively after cracking.

The comparison between the M-κ diagram by hand and by Plaxis is based on the line load values at the points indicating a change in behaviour from Table 17. It appeared however that the failure load according to hand calculations was not critical enough to initiate model failure. Therefore a failure analysis in Plaxis is carried out. The failure at a higher load than expected according to the hand calculation is probably the result of the fact that Plaxis takes residual tensile strength and tensile strength above a crack into account increasing the overall strength.

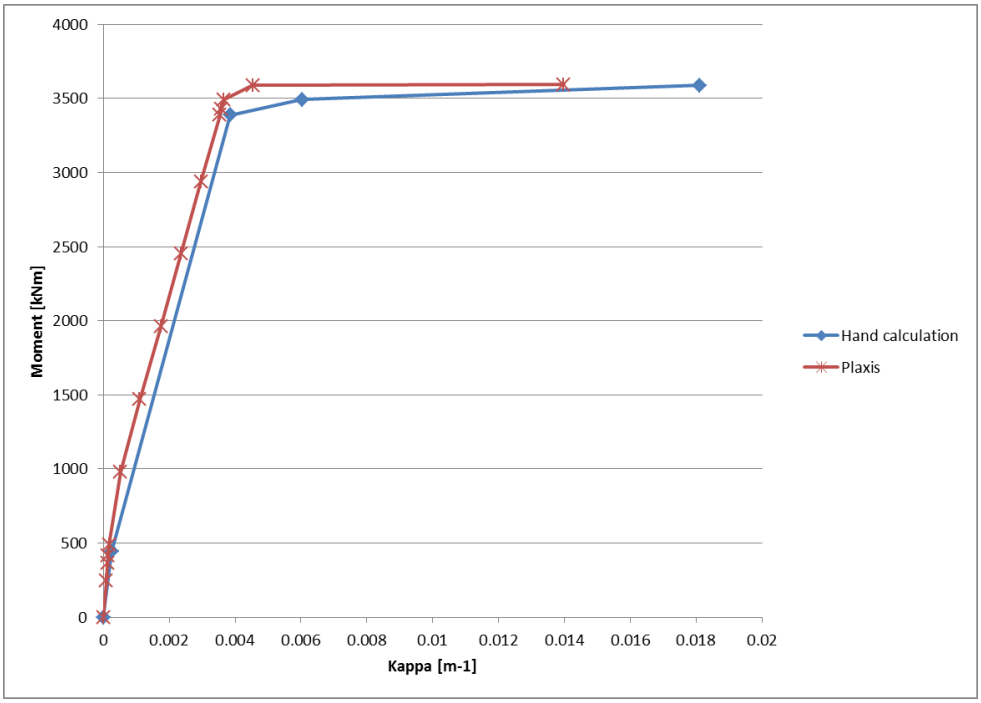

Figure 44: Comparison of modelled and hand calculated M-κ diagram.

The M-κ diagram based on Plaxis output regards a value of 0.15 kN/m for the tensile fracture energy as 0.1 k/m did not lead to convergence at high loads. This will lead to a small deviation from reality. It can be observed that the Plaxis model output results match quite well the hand calculated moments at which the bending stiffness changes (Figure 44). The absolute magnitude of the curvature (κ) is different and consistently smaller. However the shape and the important moments of change of behaviour correspond. It turns out that the moment of failure deviates only 0.1 % from the calculated value by hand. The moment at which yielding occurs, deviates 2 % from the hand calculation. This is both within the bounds of a reliable calculation.

The reason for the fact that the curvature (κ) is consistently smaller is already stated before. This is the result of the way in which the model accounts for the influence of cracking on the overall beam behaviour. At failure the difference in the occurring curvature is larger. This is the effect of the back calculation of the curvature by fitting to a curve, the aspects regarding the tensile strength mentioned and the way in which failure is defined in the model. Back calculation of the curvature is tricky at failure as a polynomial fit has to be made to the plastic buckling of the beam in the middle. A sixth order polynomial fit is used around the middle, rather than over the whole length. Though the R-value, which gives an indication of the accurateness of the fit, remains slightly lower than 1. A perfect fit is not possible due to the bending shape (not round) of the beam. Furthermore, model failure is obtained in Plaxis when large strains are occurring without the possibility to increase the load/stress slightly. Therefore the model failure criterion will not always lead to as high strains as calculated by hand.

To test the influence of the model tensile strength behaviour, the tensile strength is reduced to 25% of the proposed C30/37 value. In Figure 45 the model results are given regarding the moment curvature relation. Noted has to be that not all load results are given in Figure 45 for the reduced tensile strength case. This is the effect of the change in failure mode, to shearing, due to a change in properties of the beam. It can be concluded that the curvature increases when decreasing the tensile strength in the model, which was expected on forehand. The obtained curvature after the moment of cracking is found to be almost equal to the hand calculation. Therefore it can be concluded that the model takes tensile strength behaviour more realistic and accurately into account. The difference in obtained results by the model and the hand calculated M-κ relationship of this reinforced concrete beam can be fully explained by the difference in taking into account tensile strength behaviour, the influence of failure definition in the model and the accuracy of back calculating the model curvature. Summed up, the Shotcrete results are found to be reliable.

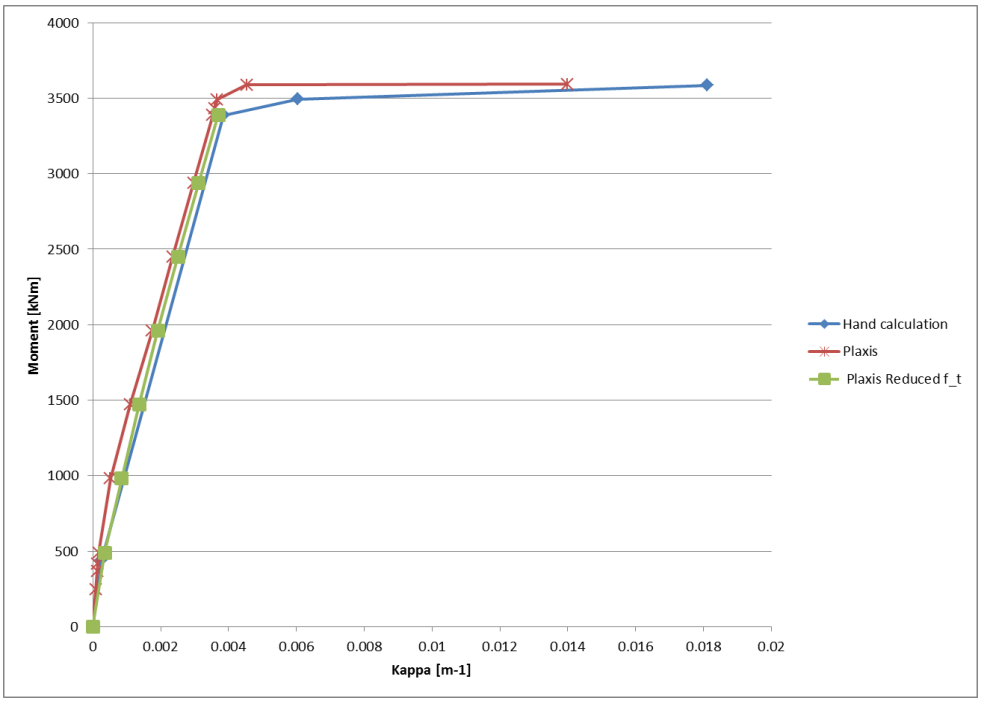

Figure 45: M-κ diagram with the influence of reduced model tensile strength properties.

3.4 Comparison with M-N-κ diagram by hand

In some cases, not in particular in this case, diaphragm walls are subjected to a normal force additional to a lateral force. By hand a similar calculation to the case in which no normal force is present can be made to account for the presence of a normal force. The way in which such a calculation is done can be found in Braam & Lagendijk (2010). A similar approach as given in appendix C.2 is used for calculating the curvature κ from the output results of Plaxis results. The starting points will be described below, whereafter the results of the hand calculation and the results of the Plaxis can be compared. In Table 18 the starting points for the calculation are stated. The model characteristics are similar to the ones used for the M-κ comparison, despite the difference in problem lay-out.

Table 18: Input for M-N-κ diagram comparison

Input (parameter)	Value	Unit
Concrete properties	- C30/37 - Shotcrete model input	-
Width concrete beam	1	m
Height concrete beam	1	m
Concrete cover	0,05	m
Reinforcement characteristics	- B500B - Plate element input	-
Rebar yield strength	435	N/mm^2
Reinforcement tensile zone	1	%
Reinforcement compressive zone	1	%
Line load	Variable	kN/m
Normal force	2000	kN

Two differences with respect to the M-κ (previous) model are present. In addition to the previous model set-up, it is also chosen to add reinforcement in the compressive zone as this commonly the case in practice. This will cause by definition a stiffer reaction than in the M-κ model set-up. Another difference with respect to the M-κ model set-up is that a normal force, line load, of 2000 kN/m^2 is applied perpendicular to the cross-section of 1 m^2. The normal force is applied at both hinges (for symmetry) (Figure 46). The magnitude of the normal force is chosen such that a realistic load case for a diaphragm wall is represented. The beam element present in the center of the concrete beam is a dummy element, which makes it possible to calculate the curvature of the beam.

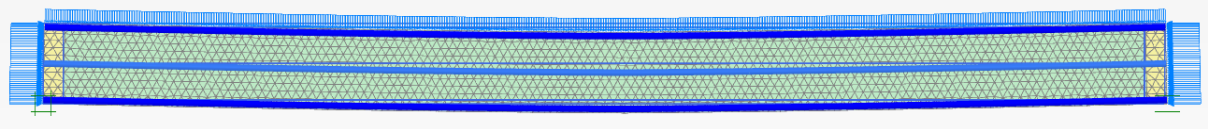

Figure 46: Situation/beam lay-out for M-N-κ diagram.

The M-N-κ diagram has the same shape as the M-κ diagram calculated in paragraph 3.3. However due to the additional normal force the moments of rupture, yielding and failure are different. The moments will become higher as the added normal force leads to additional resistance against bending. The moment at which rupture, yielding and respectively failure occur are given in Table 19. The corresponding curvature related to the moments is also given in this table. The M-N-κ diagram is shown in Figure 47.

Table 19: M-N-κ diagram values and corresponding model line loads.

Moment	Moment Value [kNm]	Corresponding line load [kN/m]
Rupture	962	39.2
Yielding of rebar	4404	179.8
Yielding of concrete	4727	192.9
Failure	4839	197.5

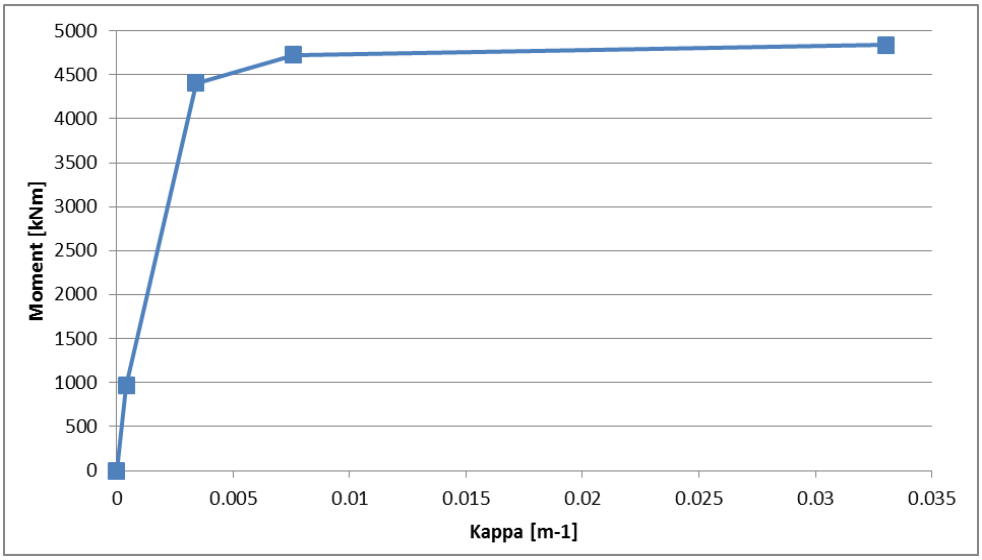

Figure 47: M-N-κ diagram based on hand calculation.

The Plaxis model to obtain the M-N-κ diagram consists of three phases. In the first phase the model, without loads, is initialised. In the second phase the normal force is applied (stepwise). Due to the fact that the load in Plaxis is applied stepwise, a third phase is needed in order to be sure that the normal force is fully applied before applying any lateral load. In the third phase the lateral line load, normative force for bending failure, is applied in addition to the existing normal force. This represents a realistic case in practice as the lateral load is governing for failure. The lateral line load is during the analysis varied such that a smooth M-N-κ diagram is able to draw. The normal force is kept constant during this procedure. The moment (applied) is back calculated using the rule for a statically determined structure for this model: $M = \frac{1}{8} * q * l^2$. In Plaxis shear deformation occurs wherefore this assumption is not completely accurate (± 2%), however it is checked that it gives a good indication of the occurring moment in the Plaxis model. To obtain the occurring curvature corresponding to each applied moment, the procedure described in appendix C.2 is adopted. In this procedure it is described that by taking the second derivative of a deformation (function) of a dummy element at the neutral line the curvature can be back calculated. Below, the M-N-κ diagram based on Plaxis results is compared to the hand calculated M-N-κ diagram (Figure 48).

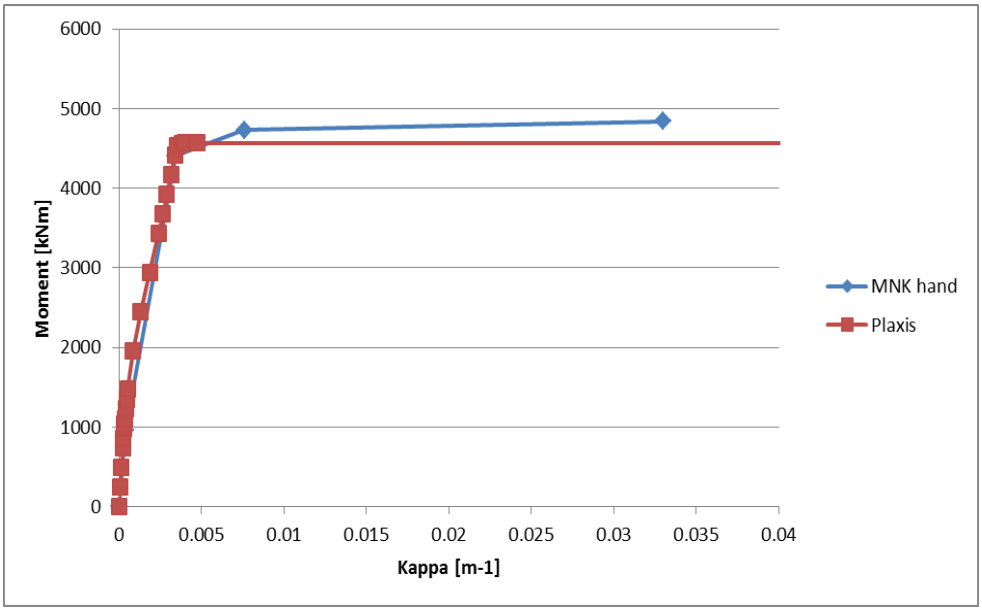

Figure 48: M-N-κ diagram comparison between hand calculation and Plaxis results.

It is observed that the curve based on the Plaxis calculation matches the hand calculation quite good. The deviation in uncracked and cracked concrete until rebar yielding is very limited. Though the moment at which rupture occurs is significantly higher (approximately 40 %). Due to the fact that rupture is initiated at a higher moment the curvature is more limited. Remarked has to be that after cracking takes place in the Plaxis model, the response is less stiff than in the hand calculation. This leads to convergence of the results at higher moments. Furthermore it can be observed that the curvature in Plaxis is far higher at model failure. This is the effect of the formation of a plastic hinge, where the curvature has to be determined. Accurate determination is not possible at a plastic hinge. It can be stated that the curvature calculated is unrealistic and at the moment the reinforcement is yielding the model fails.

It is shown in Figure 48 that failure in terms of bending moment is occurring earlier in Plaxis than according to the hand calculation. A first explanation for this difference is the fact that the obtained normal force after application does not result exactly in a normal force of 2000 kN/m. This is the result of the pre-tensioning effect in the reinforcement. The two reinforcement plates each take up 199.6 kN/m. An applied normal force of 2000 kN/m at the hinges results therefore in a load of 1761 kN/m obtained in the middle of the beam over the whole cross-section. Taking into account the 'real' occurring normal force in the beam, the positive pre-tensioning effect in the reinforcement (tension side) and the negative effect in the reinforcement (compressive side), a better match is obtained concerning the moment of failure (Figure 49). This makes it clear that attention has to be paid to the output of the previous loading phase in Plaxis when analysing the final result.

A second explanation for model failure at a lower load than expected by the hand calculation considers the influence of reinforcement yielding. It turned out that, as well in the hand calculation as in Plaxis, for this situation reinforcement yielding occurs before concrete yielding. At the moment the reinforcement

starts to yield in the Plaxis model, the strain increases dramatically. The rapidly increased straining of the reinforcement causes on its turn a rapid increase of concrete strains and ultimately failure. A rapid increase of straining is the criterion for Plaxis to define failure. The beam "immediately" fails for this reason and the hand calculated failure moment is not reached. The curvature becomes in such a situation really high as can be seen in Figure 48 and Figure 49.

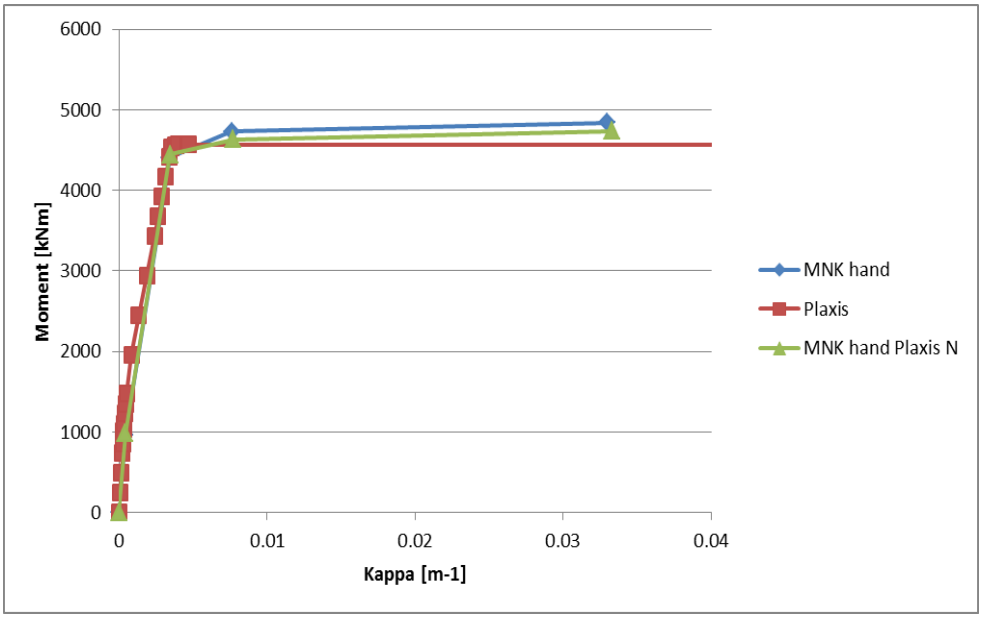

Figure 49: M-N-κ comparison with a to Plaxis occurring normal force adjusted hand calculation.

Another noticeable fact coming forward in the analysis concerns the difference in Plaxis and the M-κ and M-N-κ diagram among results between yielding of the reinforcement and concrete. When the difference between those two moments and corresponding curvature in the hand calculation is rather large, Plaxis has difficulties predicting this part of the behaviour. However this does not mean that Plaxis is less accurate. The M(-N)-κ diagram is a method to simulate the influence of cracking on the curvature behaviour and does for example not take into account the (shape) change in the cross-section while bending.

Furthermore, attention has to be paid to the fact that a small difference in loading in Plaxis around failure can lead to large differences in obtained curvature. Nevertheless the moment at which failure occurs is only 3 % different taking into account the reduced (occurring) normal force. This might be regarded as a satisfying result considering also the differences, model features as well as assumptions, between the two calculation methods.

3.5 Conclusion

The Shotcrete material model needs the input of many parameters to be able to model concrete behaviour in detail. With the help of the by literature, theoretical as well as experimental, and by sensitivity analysis proposed (standard) input values the stress-strain behaviour of the Shotcrete model can be fitted to represent structural concrete correctly. In this research a fit is made to commonly used

normal strength structural concrete (C30/37). The fit is concrete class specific, meaning that whenever another concrete class has to be used in the model the material model has to be refitted.

To model a statically determined reinforced concrete beam properly a volume element, including elastic transition elements, with a plate element as reinforcement is created on two hinges. Different material models, linear elastic, Mohr-Coulomb and Shotcrete, are applied for the volume element to validate the use of the Shotcrete material model. The results are besides compared to hand calculations. Evaluating all results give the indication that using the by a single elastoplastic plate reinforced Shotcrete material model gives realistic modeling results concerning the bending deformation, stress-distribution in the material and normal force in the reinforcement of a reinforced concrete beam. The calculation time is found to be significantly higher than when using a Mohr-Coulomb model, 3 to almost 12 times depending on the limit state. The model stability can be enhanced by increasing the tensile fracture energy. The calculation time decreases significantly when increasing the tensile fracture energy.

A in depth research of the by Shotcrete material model modelled reinforced concrete beam showed that the output, bending, normal force in the reinforcement and cracking pattern correspond to theory. The distance between the formed cracks complies with hand calculations from the Eurocode. With increasing load the cracks develop gradually towards the hinges and the first developed cracks will simultaneously grow higher into the beam. An arc pattern is observed in both theory and results of the Plaxis model. The three phases in a progressively laterally loaded reinforced concrete structure; linear elastic behaviour, loss of stiffness due to cracking and significant loss of stiffness at yielding/failure, can subsequently be observed when using the Shotcrete material model. The normal force in the reinforcement coincides with the by theory described pattern; high rebar force at the place of a crack and less rebar force in between to cracks. A qualitative as well as a quantitative analysis is carried out regarding mesh sensitivity. Both proved that using a coarser mesh does not influence the results heavily. Nevertheless using a finer mesh gives more realistic cracking patterns and more accurate deformation and stress-distribution results.

The bending behaviour of the reinforced Shotcrete beam is evaluated with the help of a M-κ and M-N-κ diagram. The curvature in Plaxis cannot be directly outputted, wherefore the second derivative to the polynomial fit of the occurring deformation (curve) has to be taken. It turned out that in the case without applying a normal force on the structure the results were within the bounds of a reliable calculation (<2%). Especially when taking in mind the difference in accounting for remaining tensile strength between the hand calculation and Plaxis. In case a normal force is acting on the beam, the results of Plaxis also match the hand calculation quite good. Nevertheless, the moment of cracking is found to be deviating significantly. This can be partly explained by the fact that adding a model phase before bending causes pre-tensioning of the reinforcement, decreasing the normal force in the concrete material. When taking this effect into account in the hand calculation, a good match is obtained. Summed up, evaluating a statically determined reinforced concrete beam modelled with the use of a Shotcrete material volume element reinforced by an elastoplastic plate element demonstrates the applicability of the Shotcrete material model to design reinforced concrete structures subjected to bending.

4 Modelling soil-structure interaction

In this chapter a soil-structure interaction case is evaluated. The model consists of a diaphragm wall in the subsurface. A simplified situation is considered, where the subsurface consists of a single stiff sand layer. The diaphragm wall can be assumed to be endlessly long which implies that a 2D model can be used. Furthermore the diaphragm wall tip is at such depth that stability will not be the governing failure mode, but bending will be the normative failure mode. For this research particularly the ability of a reinforced Shotcrete volume element to model realistic bending behaviour in a soil-structure case is interesting. A Shotcrete volume element of 1 meter thickness including a single plate as reinforcement is used to approximate the behaviour of a diaphragm wall up to bending failure. A plate element representing the structure in Plaxis is extensively tested and proven accurate, wherefore it is used as a reference in this chapter.

4.1 Model setup

A simplified single-layered subsurface case is considered in the soil-structure analysis. Bending has to be the normative failure mode for the diaphragm wall to test the reinforced Shotcrete model, wherefore the diaphragm wall is installed deep in the subsurface such that stability will not play a role in the failure analysis. Furthermore, due to the fact that only bending deformation and the occurring bending moment in the diaphragm wall are of interest, a subsurface consisting of one layer is satisfying. The area of the subsurface is chosen such that model boundary conditions do not influence the behaviour. The situation is visualised in Figure 50. In Figure 50 for the demonstration of the cases to be analysed on the left side of the excavation a plate element is used for the diaphragm wall, while on the right side of the excavation a volume element is used. Around the diaphragm wall an interface is created in order to allow for proper modelling of soil-structure interaction, simulating the contact area between a structure and surrounding soil..

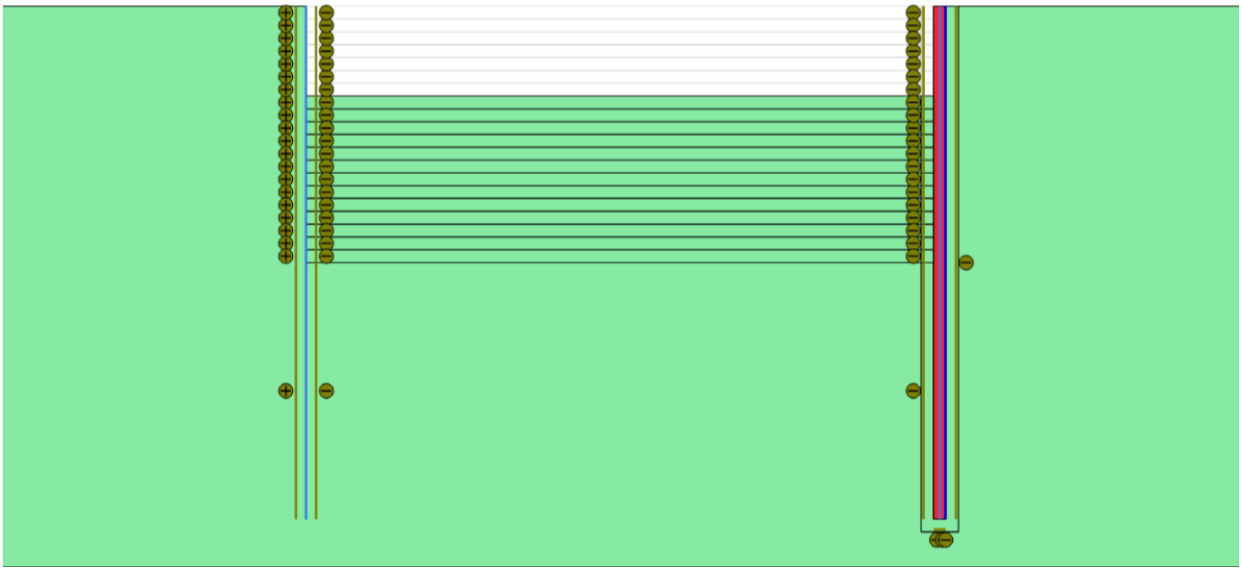

Figure 50: Model set-up excavation with for demonstration; left a Plate element and right a reinforced volume element.

4.1.1 Subsurface

The subsurface consists of a single sand layer in this case. For the purpose to model an excavation situation realistically, a Hardening Soil model in Plaxis is chosen. Due to its characteristics and features the Hardening soil model is well suited for unloading situations with simultaneous deviatoric loading (excavations) as is mentioned by Brinkgreve (2015). Detailed insight in the material model and its features can be found in the Plaxis 2D Material models manual (Brinkgreve, Kumarswamy, & Swolfs, 2016). The characteristics of the subsurface for this case are given in Table 20.

Table 20: Subsurface characteristics.

Parameter	Name	Sand	Unit
Material model	Model	Hardening Soil	-
Type of material behaviour	Type	Drained	-
Soil unit weight unsaturated	γ_{unsat}	17	kN/m^3
Soil unit weight saturated	γ_{sat}	20	kN/m^3
Initial void ratio	e_{init}	0.5	-
Secant stiffness in standard drained triaxial test	E_{50}^{ref}	40 000	kN/m^2
Tangent stiffness for primary oedometer loading	E_{oed}^{ref}	40 000	kN/m^2
Unloading / reloading stiffness	E_{ur}^{ref}	120 000	kN/m^2
Power for stress-level dependency of stiffness	m	0.5	-
Cohesion	$c_{ref}{}'$	0	kN/m^2
Friction angle	ϕ	32	^{0}
Dilatancy angle	ψ	2	^{0}
Poisson's ratio	ν_{ur}'	0.2	-
K_0-value for normal consolidation	k_0^{nc}	0.4701	-
Permeability	$k_{x,y}$	1	m/day
Strength reduction factor interface	R_{inter}	0.67	-
Over-consolidation ratio	OCR	1	-
Pre-overburden pressure	POP	0	kN/m^2

For simplicity the influence of normally present groundwater is excluded. No groundwater is present in the model, wherefore flow conditions and (excess) pore pressures can be disregarded. In Table 20 it can also be seen that a strength reduction factor at the interface is applied. Interfaces are present between the diaphragm wall and the soil next to it. For a common diaphragm wall excavation it can be assumed that the strength of the soil to the strength at the interface is 2/3 of the initial strength.

4.1.2 Structure

The characteristics of the reinforced diaphragm wall are given in Table 21. Translating the reinforcement material characteristics to a linear elastic-perfectly plastic material model gives the input as mentioned in Table 22. Reinforcement is present in each diaphragm wall, respectively model set-up.

Table 21: Characteristics of the reinforced diaphragm wall.

Parameter	Value	Unit
Length reinforced diaphragm wall	41	m
Width concrete element	1000	mm
Height concrete element	1000	mm
Concrete properties	C30/37	-
Concrete cover	0.05	m
Reinforcement properties	B500B	
Reinforcement	1	%
Rebar yield strength	435	N/mm^2

Table 22: Reinforcement model characteristics.

Parameter	Value	Unit
Modulus of elasticity	210 000 000	kN/m^2
Area	0.01	m^2
Moment of Inertia	$8.33*10^{-8}$	m^4
EI	17.49	kNm^2/m
EA	210 000 000	kN/m
N_p	4350	kN

Translating the concrete properties to material model characteristics give the input as is given for the linear elastic case (Plate and Volume element) in Table 23, the M-κ plate element case in Table 24 and for the Shotcrete model case in Table 23. In chapter 3 is explained that there is a difference in modelling results of a first hand-calculated M-κ diagram and a Shotcrete diaphragm wall. Therefore a (correct) fit is made upon the rupture moment in the Shotcrete volume element. The fitted M-κ plate element characteristics are given in Table 24.

Table 23: Linear elastic volume and plate element input parameters and input parameters Shotcrete volume element.

Material Model	Parameter	Value	Unit
Linear elastic	Modulus of elasticity	29 700 000	kN/m^2
	ν	0.2	-
(Plate)	EA	29 700 000	kN/m^2
	EI	2 994 000	$kN\ m^2/m$
Shotcrete	γ	Surrounding soil	kN/m^3
	E_{28}	29 700 000	kN/m^2
	ν	0.2	-
	$f_{c,28}$	30 000	kN/m^2
	$f_{t,28}$	2 000	kN/m^2
	ψ	13	^{o}
	E_1/E_{28}	1	-
	$f_{c,1}/f_{c,28}$	1	-
	$f_{c0,n}$	0.33	-

	$f_{cf,n}$	0.85	-
	$f_{cu,n}$	0.1	-
	ϵ_{cp}^{p}	-0.75	‰
	$G_{c,28}$	1.55	kN/m
	$G_{t,28}$	0.15	kN/m
	$f_{tu,n}$	0	-
	ϕ^{max}	35	o
	Time dependent parameters	0	-/day

Table 24: Input parameters M-κ plate element.

Material Model	**Parameter**	**Value**	**Unit**
M-κ	Modulus of elasticity	29 700 000	kN/m^2
	ν	0.2	-
	EA	29 700 000	kN/m^2
	EI	2 994 000	kN m^2/m
	M_r - κ_r	442 - 0.1476*10^{-3}	kNm - 1/m
	M_y - κ_y	3387 - 3.854*10^{-3}	kNm- 1/m
	$M_{c,pl}$ - $\kappa_{c,pl}$	3493 -6.038*10^{-3}	kNm- 1/m
	M_{rd} - κ_{rd}	3586 - 0.01811	kNm- 1/m
M-κ fit	M_r - κ_r	416.5 - 0.1441*10^{-3}	kNm - 1/m
	M_{y1} - κ_{y1}	3430 - 3.591*10^{-3}	kNm- 1/m
	M_{y2} - κ_{y2}	3491 - 3.664*10^{-3}	kNm- 1/m
	$M_{c,pl}$ - $\kappa_{c,pl}$	3587 - 4.532*10^{-3}	kNm- 1/m
	M_{rd} - κ_{rd}	3593 - 0.01398	kNm- 1/m

The unit weight of the volume element is equal to the unit weight of the subsurface, to exclude deformations caused by self-weight of the reinforced concrete structure. This is a simplification of reality, however for the purpose of this research case it does not have influence on the results of interest.

To obtain the governing bending moment in the structure, several options are available. In appendix D.1 it is shown that only using an internal force equilibrium method around the neutral reliable results can be obtained. In Figure 51 the to be used plate element and the volume element including reinforcement for the calculation are visualised.

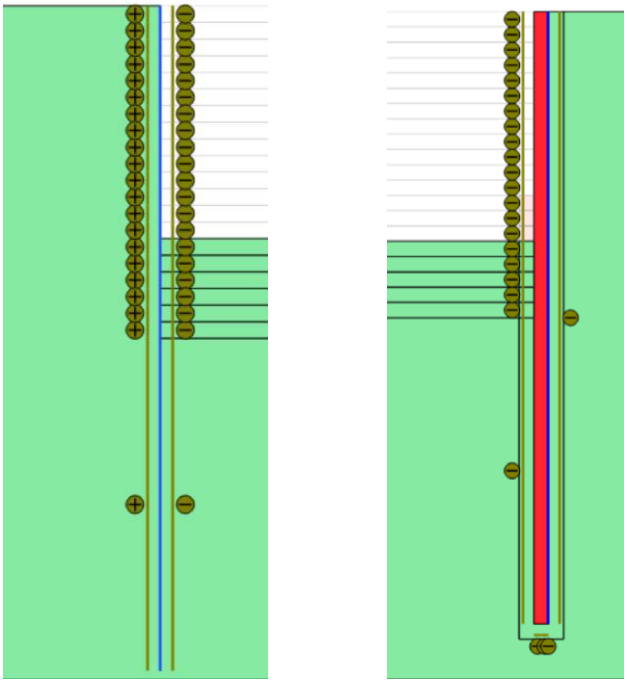

Figure 51: On the left a single plate element as diaphragm wall. On the right a volume element with a single plate as reinforcement represent a diaphragm wall.

To get a reasonable comparison between different options of modelling, several cases are tested. The cases to be evaluated for a diaphragm wall subjected to bending in a sandy subsurface are:

- Linear elastic plate element
- M-κ plate element
- Fitted to Shotcrete diaphragm wall M-κ plate element
- Linear elastic volume element with a single elastoplastic plate as reinforcement
- Shotcrete volume element with a single elastoplastic plate as reinforcement

4.1.3 Loading

An endlessly long diaphragm wall is installed in the subsurface. Subsequently the soil next to the diaphragm wall is excavated. Excavation takes place till the diaphragm wall will structurally fail under bending. The type of loading applied can be characterised as a passively applied lateral load. Several phases in Plaxis are adopted to model this case. After an initial phase, where the subsurface is initiated and a phase where the structures are created in the subsurface, a first sand layer of 1 meter thickness is excavated. In every following phase a subsequent sand layer of 1 meter thickness is excavated, leading to a horizontal deformation inwards the excavation. The excavation progresses as is shown in Figure 52.

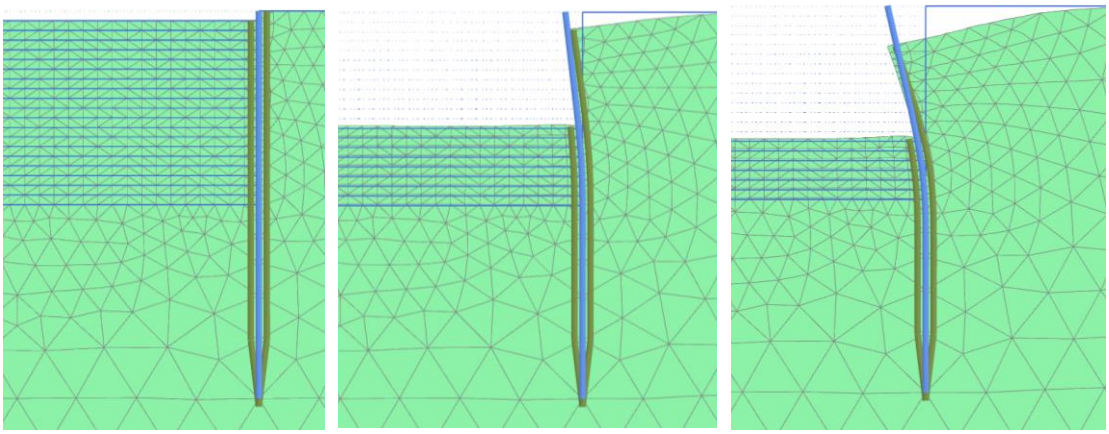

Figure 52: Excavation (loading) process with a plate element (example).

4.2 Results

In this paragraph the modelling results of the subsequent excavation are given. This paragraph contains a subdivision in analysis of the results. At first in specific the difference between modelling a volume and plate element is regarded. Afterwards more detail will be paid to analysing the resulting displacement and bending moments of the different cases. At last the results of using a reinforced Shotcrete volume element are evaluated more specifically.

4.2.1 Plate element versus volume element

In theory the results of using a plate element and a volume element of equivalent thickness, with the same properties, should lead to the same obtained results. To test this assumption, excavation till a depth of 15 meters takes place next to the diaphragm wall. In Figure 53 the displacement in the x-direction, towards the excavation, regarding the subsequent excavation is given. The plate element and volume element used in this analysis are both characterised by linear elastic material properties (Table 23), wherefore structural failure has not to be regarded.

Serious inward deformation of the diaphragm wall occurs after an excavation of five meters. In Figure 53 it is shown that the deformations of the equivalent volume and plate element correspond. The deformation of the plate element is somewhat higher than the of the volume element but due to the fact that the deformation is measured by a dummy element, some slight deviations can occur. Another explanation for small deviations found, is the tolerated error of 1% in the numerical solving. The difference in phase 10 can besides be partly explained by a difference in obtained wall friction ((interface) shear stresses acting on the wall) in that particular phase. The wall friction for the linear volume element is almost 10 % higher than for the plate element, which can result in a small decrease in obtained structural moment. Summed up, it is demonstrated that the deformations of the plate and volume element match and it is reasonable to use a dummy element for measuring displacements/bending moments in case of using a linear elastic material model to represent the behaviour of the structure.

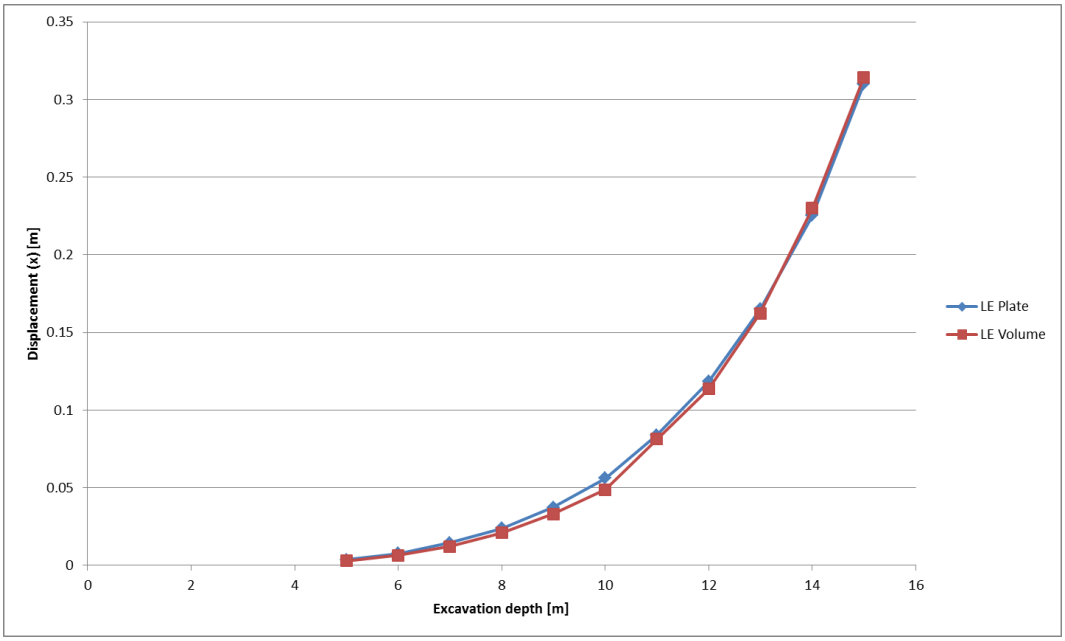

Figure 53: Displacements linear elastic volume element versus equivalent plate element.

Another comparison can be made regarding the obtained moments at subsequent excavation. The bending moments at each excavation depth are given in Figure 54. The results also prove the similarity between both calculation methods when considering linear elastic behaviour. Assumed is that the results of using the M-κ plate element, equivalent to the structure, can be compared to a by plate reinforced Shotcrete volume element.

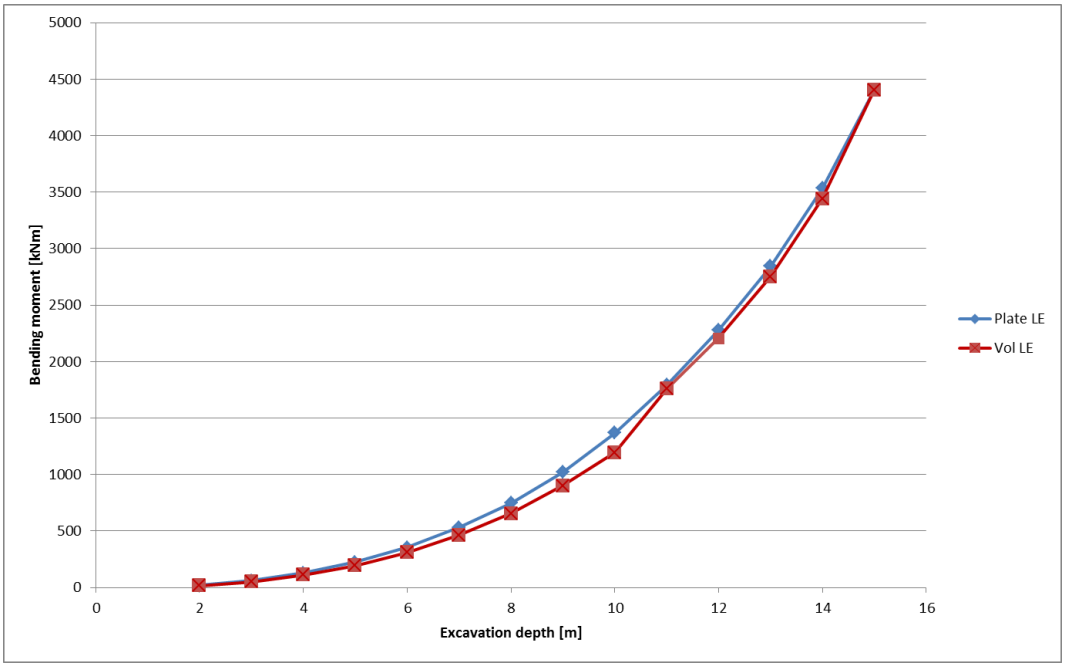

Figure 54: Bending moments obtained for a linear elastic volume element and an equivalent plate element.

4.2.2 Displacement

In appendix D.1 is explained that using a dummy element for the Shotcrete (material) model does not work correctly for obtaining of the bending moments of the reinforced volume element. This is probably due to the influence of shear stresses acting on the volume element (wall friction), remaining tensile stresses in the "cracked" zone, a deforming cross-section, change of the neutral line and the influence of self-weight of the structure. Furthermore in appendix D.1 is shown that the way to obtain the correct bending moment is by using an internal force equilibrium at the neutral line. Explanation in detail about this method and other possible methods to obtain the bending moment of a non-linear (reinforced) volume element, including a Plaxis built in function, is given in appendix D.1.

To get an overview of the applicability of the Shotcrete material model, the results are analysed and compared to linear elastic calculation results as well as M-κ diagram based results. The displacements, in x-direction, for each case (paragraph 4.1.2) are given in Figure 55.

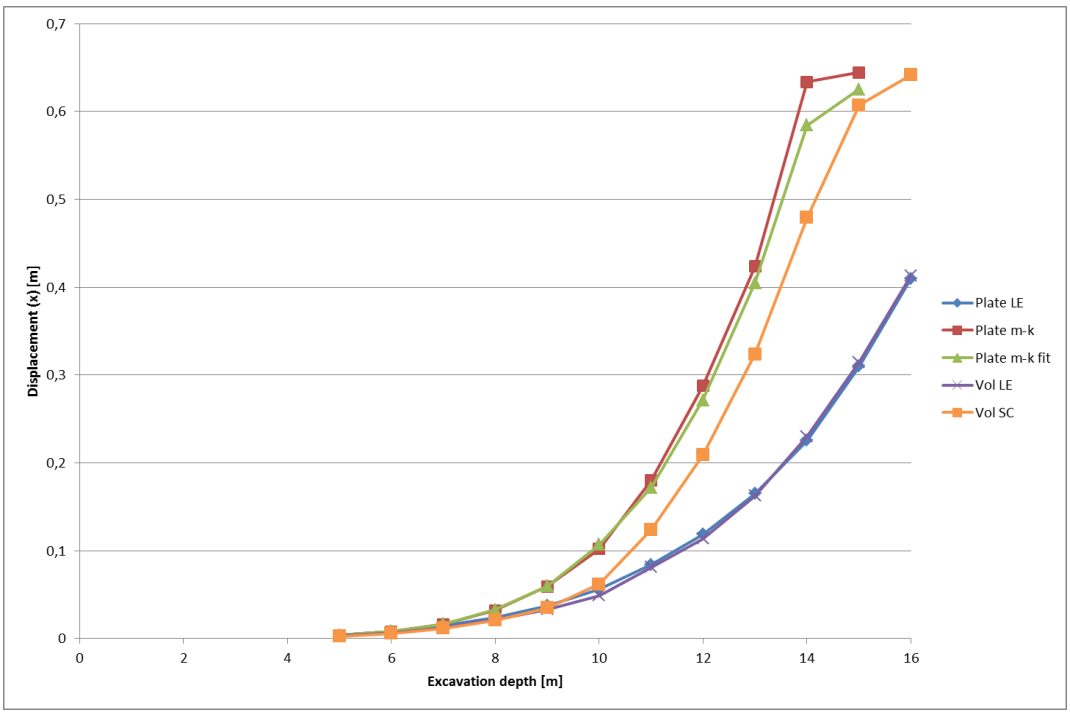

Figure 55: Displacement results for all cases including Shotcrete volume element results.

In Figure 55 is shown that the displacements for the linear elastic plate and volume element are similar as proven before. The displacements when taking into account cracking, for the reinforced Shotcrete volume element as well as for an M-κ diagram based plate element, are significantly larger than obtained in a linear elastic calculation. This corresponds to theory, cracking decreases the stiffness of the structure leading to larger structural deformation. The displacements using a reinforced Shotcrete volume element are lower throughout the excavation than for the M-κ diagram based plate elements, even when taken into account the corrected "fit" M-κ case. This implies that the reduction of stiffness due to cracking in case when using the Shotcrete material model is more limited. An explanation is that

in the Shotcrete model some tensile strength capacity remains when the cracking pattern is not completely developed. Furthermore when the cracking pattern is fully developed the Shotcrete model takes the remaining concrete tensile strength in between the cracks into account, causing an increased stiffness with respect to the M-κ based plate element.

Cracking in the Shotcrete model occurs at a higher bending moment than in both M-κ diagram based plate element calculations. This shown by the fact that the reinforced Shotcrete volume element longer follows the behaviour of the linear elastic cases. The stiffness is however reduced with the same amount as in the M-κ diagram based plate elements. This can be observed by the fact that the Shotcrete volume element line is progressing parallel to the M-κ diagram based plate elements.

The single plate reinforced Shotcrete volume element fails at a larger excavation depth with respect to the M-κ based cases. The bending (moment) capacity of the diaphragm wall is reached at higher excavation depth when modelling with the Shotcrete model. The difference is partly caused by significantly higher interface shear stresses (wall friction). The shear stresses at the interface of the Shotcrete volume element are 33 % higher at an excavation depth of 10 meters. At lower excavation depths this increases up to 90 % and for higher excavation depths up to 40 %. A higher magnitude of interface shear stresses (wall friction) leads to delayed cracking of the structure due to an 'increase in moment capacity of the structure'. This is a possible explanation for the fact that cracking occurs at higher excavation depth when using a Shotcrete volume element instead of in the M-κ plate element cases. The difference in obtained bending moments can also be explained by the remaining tensile capacity during and after cracking and the fact that a deforming cross-section is taken into account in the Shotcrete model. The displacements at failure are corresponding. Summed up, this proves the ability to perform a failure analysis with the use of the Shotcrete material model including a single elastoplastic plate element to represent the reinforcement. Moreover it shows that using a Shotcrete volume element has (beneficial) effect, more accurate and realistic, for modelling soil-structure interaction.

4.2.3 Bending moment

Besides the importance of presenting the displacement behaviour of the diaphragm wall accurate, also the resulting bending moment is important to know when designing a laterally loaded diaphragm wall. The occurring bending moment is important for as well the design of the reinforcement as for the design of the whole structure. The bending moment results of the different cases as mentioned in paragraph 4.1.2 are shown in Figure 56.

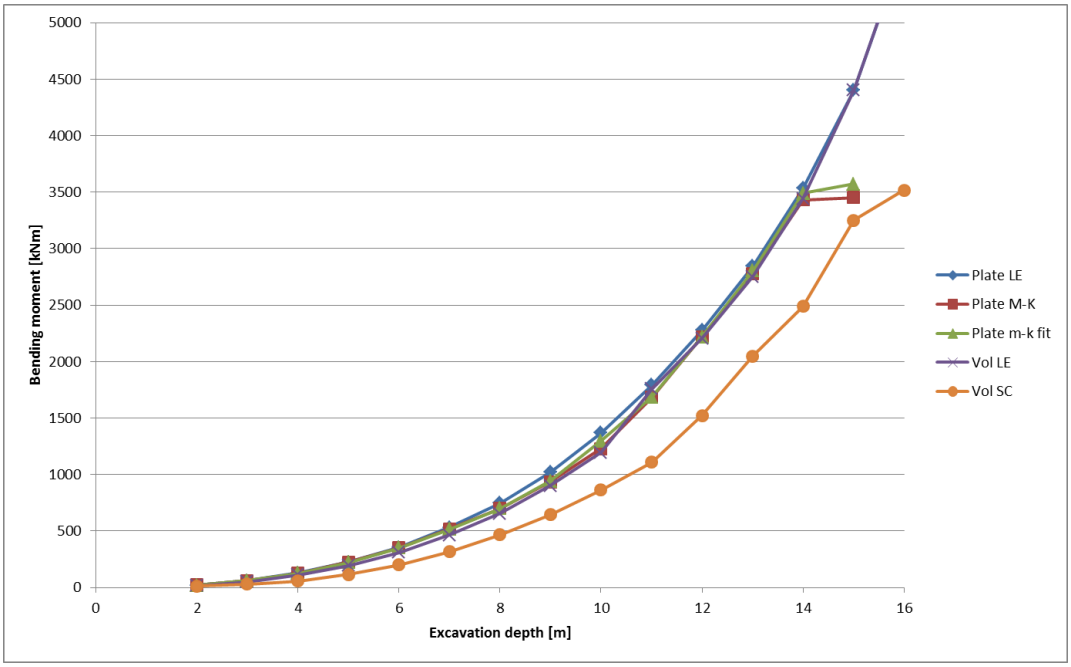

Figure 56: Bending moments for all cases.

The bending moments displayed in Figure 56 at each excavation depth show a clear trend, exponential increase with excavation depth. It is moreover clearly shown that all plate elements and the linear elastic volume element with the conventional dummy element give the same bending moments up to failure. However, the bending moment obtained in the reinforced Shotcrete volume element is subsequently lower. The difference is probably the result of the significantly observed higher interface shear stresses, as mentioned and explained in the previous paragraph (4.2.2). These interface shear stresses reduce the bending moment in the structure, not only directly but also due to the fact that crack initiation takes place at a later stage. The indirect effect can be seen by the fact that when reaching a larger excavation depth than 11 meters the increase in bending moment is equal. Another explanation for the differences in bending moments between the Shotcrete volume element and the other cases are the remaining of tensile strength above and in between the formed cracks. Furthermore it is observed that the (ultimate) failure moment of the reinforced Shotcrete volume element is similar to those of the pre-hand calculated M-κ plates, wherefore the results can be considered as valid.

Combining the separate results from the displacement and bending moment analysis against excavation depth results in the relation between displacement and bending moment for the different cases. These results are visualised in Figure 57.

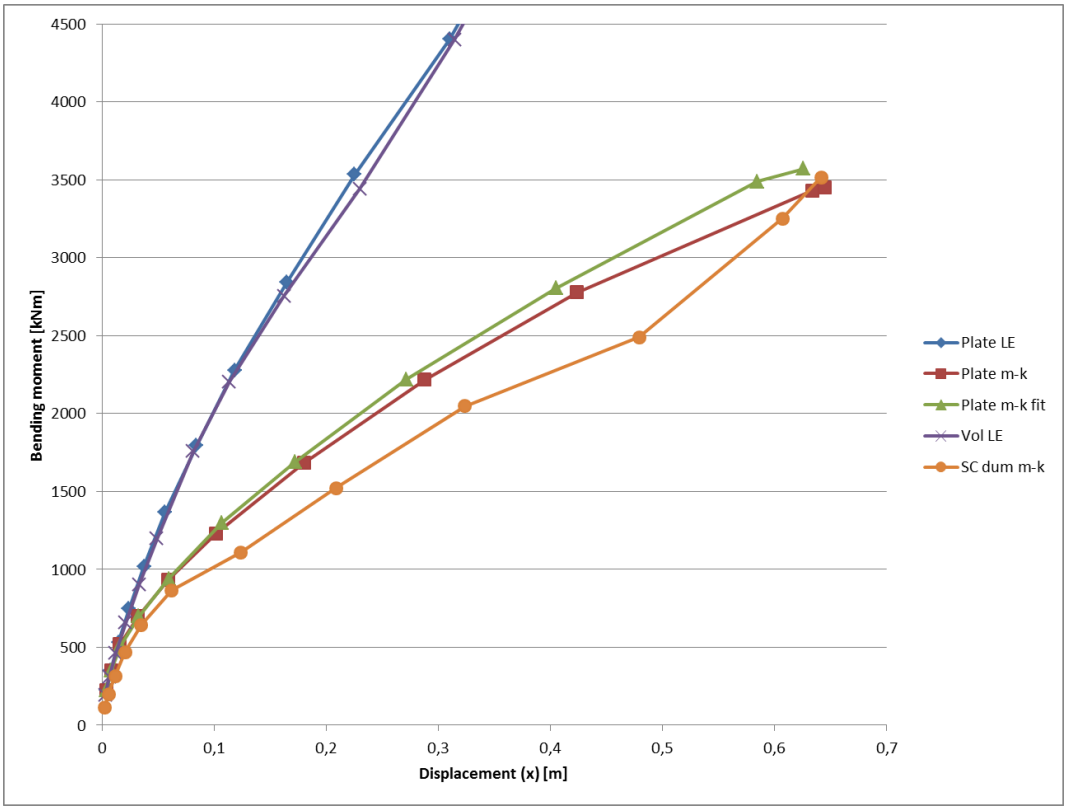

Figure 57: Bending moment – displacement relationship for the different cases.

In Figure 57 is shown that not taking into account cracking, linear elastic plate and volume element, overestimates the occurring moment at a certain deformation. The applicability of a model that takes cracking into account for designing laterally loaded structures in the subsurface is therefore proven. It can also be concluded that the reinforced Shotcrete volume element gives a lower bending moment at the same displacement with respect to a (hand calculated) M-κ based plate element. This is mostly the result of the increased shear stresses at the soil-structure interface. Another explanation is that in the plate element calculation it is assumed that there is no tensile strength after the first crack is initiated.

4.2.4 Reinforced Shotcrete volume element

The results given before prove the applicability of a by elastoplastic plate reinforced Shotcrete volume element to model a diaphragm wall. Several detailed aspects of using the model are not mentioned yet. One of the aspects considers the ability to model cracking realistically. In paragraph 3.2.3 is shown that the alignment of cracking is sensitive to the cracks. A point of attention is that the element boundaries should not be exactly parallel to the lateral loading. The best cracking pattern achieved in this case, by local refinement, is given in Figure 58. A finer mesh is achieved by creating an extra box of refinement around the diaphragm wall. Another observation is that the cracks remain in the volume element when refilling the excavation, indicating the validity of the material model.

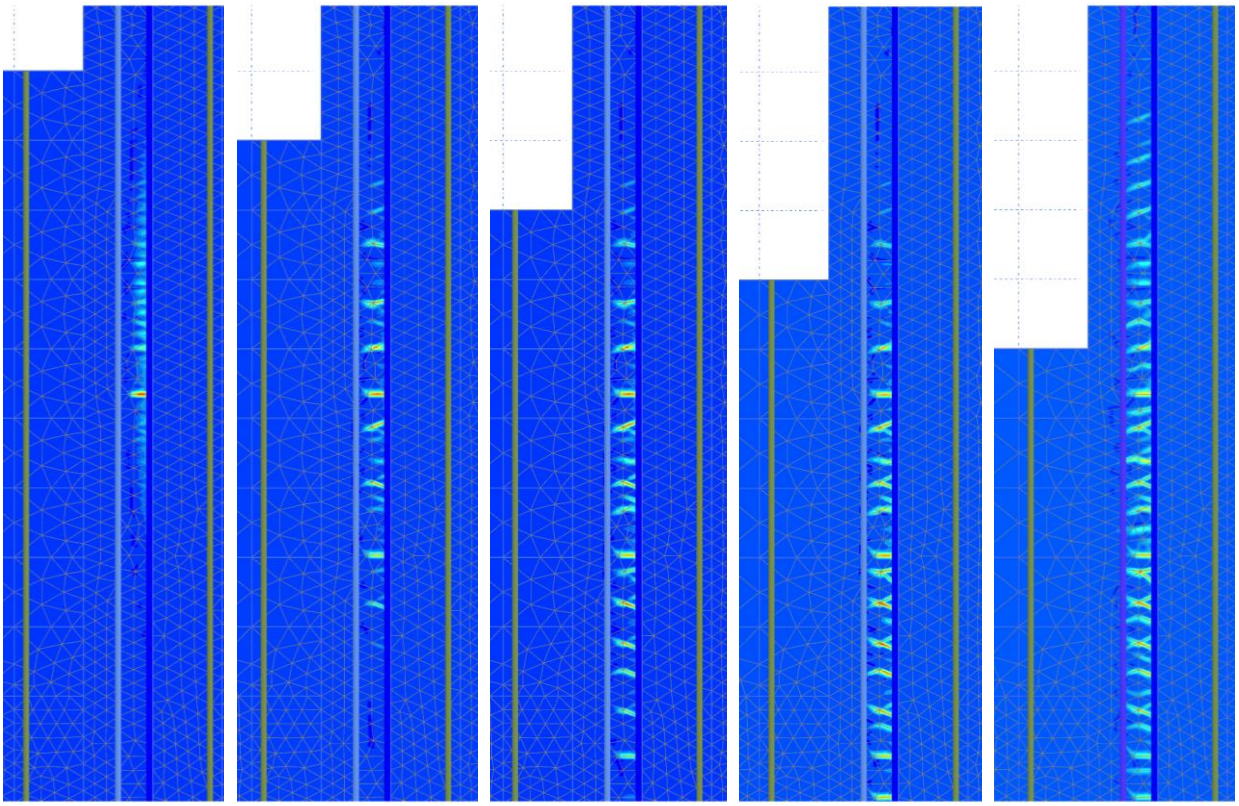

Figure 58: Cracking pattern (H_t) for progressing excavation depth.

Coupled to the mesh-sensitivity of the cracking pattern is the influence of the mesh-sensitivity on the output. In chapter 3 is explained that using a coarser mesh for the structural element causes deviations from the obtained results of the same model with a finer mesh. The deviations between the results obtained in reinforced Shotcrete model and a plate element case cannot be explained only by the mesh-sensitivity of the Shotcrete volume element. There are, as already mentioned, many factors that cause deviations between the results obtained by a reinforced Shotcrete volume element and a plate element.

A last aspect that influences the choice to use a Shotcrete volume element instead of a plate element is the calculation time. The calculation time in both cases is similar, although the Shotcrete volume element case needs mesh refinement and involves non-linearity. The calculation time when using plate element is approximately 40 minutes, while the calculation time when using a reinforced Shotcrete volume element with the same mesh size is 45 minutes. The slightly higher calculation is mainly caused in the phase when failure is almost initiated. Approximating failure leads to an increase of needed iterations.

4.3 Conclusion

The perspective of using the Shotcrete material model for designing a laterally loaded diaphragm wall is researched. It is found that the results, bending moments as well as deformation, of using a (linear elastic) plate element and a (linear elastic) volume element when modelling a diaphragm wall are similar. Furthermore the results show that the obtained bending moment and displacement when using a elastoplastic plate reinforced Shotcrete volume element are lower than in case a plate element with a M-κ based material model is used. The difference is mainly the result of higher interface shear stresses in the reinforced Shotcrete volume element case. The bending moment when using the Shotcrete model can only be back calculated in one way (appendix D.1). The governing bending moment should be back calculated by means of an internal force equilibrium at the neutral line given by the equivalent force, of the stresses in the cross-section, with its arm to the neutral line and the normal force in the reinforcement with its arm to the neutral line (appendix D.1).

The higher, with respect to plate element cases, acting interface shear stresses in the Shotcrete model cause a delay in rupture moment. The influence on the obtained displacement and bending moment at each excavation depth is significant. Both the displacement and bending moment are subsequently lower. It also results in the fact that structural failure takes place at a larger excavation depth. Other factors that explain the difference, between the M-κ plate element and Shotcrete model, in obtained bending moments and displacement are the fact that the (pre-hand calculated) M-κ diagram considers a non-deforming cross-section upon loading and furthermore assumes that the tensile strength after cracking is zero. In the Shotcrete model the cross-section deforms under loading and residual tensile strength above and in between cracks is present. The use of a single elastoplastic plate reinforced Shotcrete volume element with the proper back calculation of the occurring bending moment can be regarded as an appropriate option to model diaphragm walls. It has to prospect to take more realistic soil-structure interaction behaviour into account. Furthermore using the Shotcrete model in the design process gives insight in the cracking process, the stresses in the concrete and normal force in the reinforcement throughout all modelling stages.

5 Case study KIS project

To verify the appropriateness and applicability of using the Shotcrete material model to design a reinforced concrete diaphragm wall, a case study is done. The case study consists of designing a diaphragm wall in the crest of a dike in order to prevent the development of a shear plane during high water levels. In Figure 59 this situation is visualised, taking into account a normative high water level with a 1/2000 probability of occurrence (NHW 1/2000). The governing (for failure and therefore design) situation to be considered is mentioned before in the research motivation (paragraph 1.2). The case study is a project executed by Besix and Mourik in collaboration with ABT bv. along the dike trajectory Kinderdijk-Schoonhovensveer (KIS). The analysis of the situation will mostly be limited to the analysis of the advanced way of diaphragm wall modelling rather than the geotechnical character of the problem. More about the geotechnical aspects of the case study can be found in Janssen (2016).

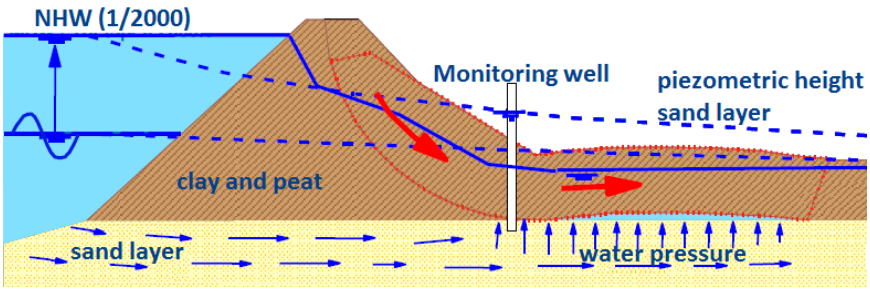

Figure 59: Development of shear plane in dike environment due to high water (Janssen, 2016).

5.1 Problem lay-out

In order to prevent the development of a shear plane in the dike a diaphragm wall is built in the middle of the crest of the dike. The crest of the dike is 16 meters wide and from toe to toe the dike has a width of approximately 64 meters. The height of the dike from surface level is 5 meters. The soft cohesive layers on top of the Pleistocene sand layer have a total thickness of 12.5 meters. The model in Plaxis to schematise this situation is shown in Figure 60 and Figure 61. In Figure 60 the situation before installing the diaphragm wall, including the scale, is visualised. In Figure 61 the situation, with installed diaphragm wall and normative high water level, governing for failure, is shown. The failure situation is such that the normative failure mode takes place, failure of the inner berm of the dike rather than local failure. The diaphragm wall has to be a fully water retaining structure on its own. More information is provided by Janssen (2016) and the guidelines for dike safety calculations; “Leidraad rivieren” (LR) (Barneveld, 2007) and “ontwerp zelfstandige waterkerende constructies (type I) dijkversterking KIS” (Havinga & Larsen, 2013).

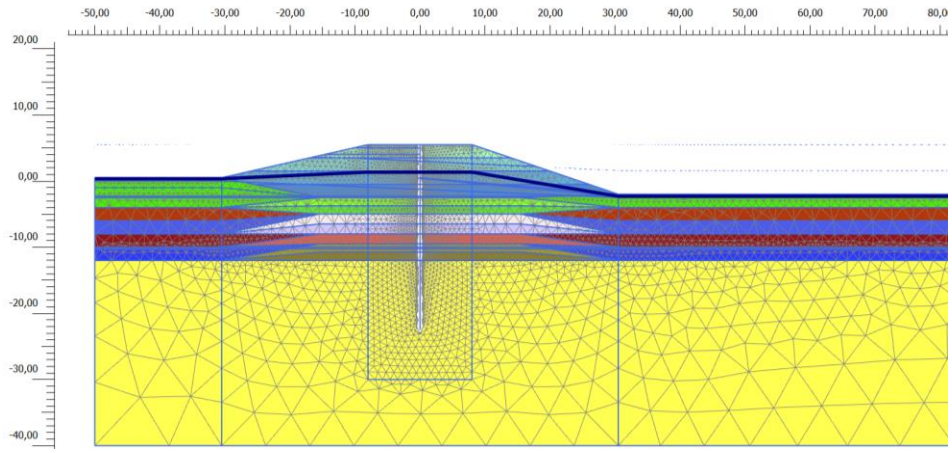

Figure 60: Site situation before installing the diaphragm wall and applying a normative high water level; scale in meters.

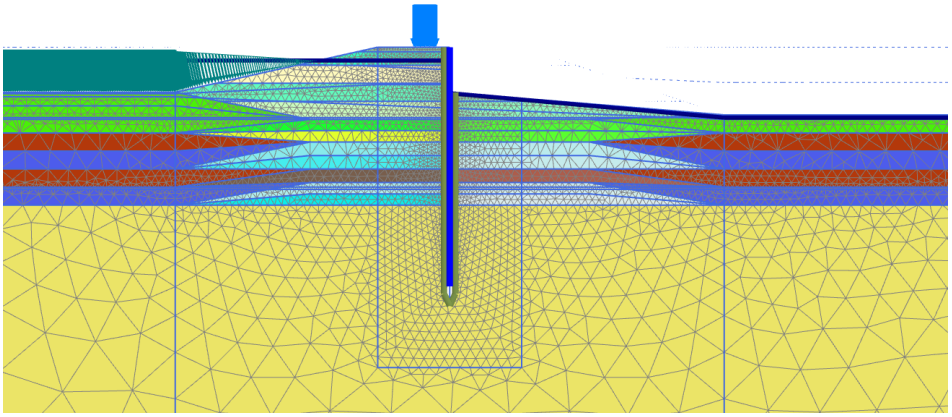

Figure 61: Normative (design) situation for failure analysis.

The characteristics of the diaphragm wall located in the middle of the crest of the dike are given in Table 25. The reinforcement drawings are given in Appendix F.

Table 25: Diaphragm wall characteristics KIS project.

Parameter	Value	Unit
Thickness wall	0.8	m
Concrete cover	0.1	m
Width panel	7.2	m
Length panel	26.65	m
Concrete class	C30/37	-
Reinforcement cage	2	number
Reinforcement compression zone	11-ϕ25	
Reinforcement tensile zone bed 1	25-ϕ32	
Reinforcement tensile zone bed 2	25-ϕ32	
Reinforcement tensile zone bed 3	25-ϕ32	
Distance between each bed	60	mm
Design moment	3065	kNm/m

Currently for modelling the diaphragm wall a linear elastic plate element is used in Plaxis, with a (slight) reduced stiffness of 20.000 MPa to account for (partial) cracking (Havinga & Larsen, 2013). In this research this model setup for the diaphragm wall is used as the reference case. In this research also an equivalent to the real design of the diaphragm wall M-κ plate element will be used and analysed. Furthermore the diaphragm wall will be modelled using a Shotcrete volume element with a reinforcement configuration representing the design as mentioned in Table 25 and appendix F. Reinforcement can be modelled in two different ways in the Shotcrete volume element. One way is to add the plates to the equivalent of each reinforcement bed (Figure 62). The other way is to calculate one equivalent plate, with different sections accounting for the change in reinforcement over the height (Figure 62). The equivalent plate has to be calculated as is proposed in Appendix D.2. Taking in mind the numerical stability of the mesh it is preferable to use just one plate for the tensile reinforcement and one for the compressive reinforcement. It is furthermore found that using only two plates instead of five to account for reinforcement gives approximately the same result. In the calculation therefore only the case in which one equivalent plate element is modelled, is used. Therefore the cases (Figure 62) to be used for modelling the diaphragm wall are:

- Linear elastic plate with reduced modulus of elasticity according to Havinga & Larsen (2013) as is currently used in the design (reference situation).
- M-κ plate element consisting of five sections to account for differing reinforcement. Section 1 and 5 (blue) are the single tensile reinforced section, section 2 and 4 are double bedded (dark red) in the tensile zone and section 3 (red) consists of 3 tensile reinforcement beds.
- Shotcrete volume element with exact reinforcement input by means of two equivalent elastoplastic plate elements; one including three section for the tensile reinforcement and one equivalent in the compressive reinforcement.

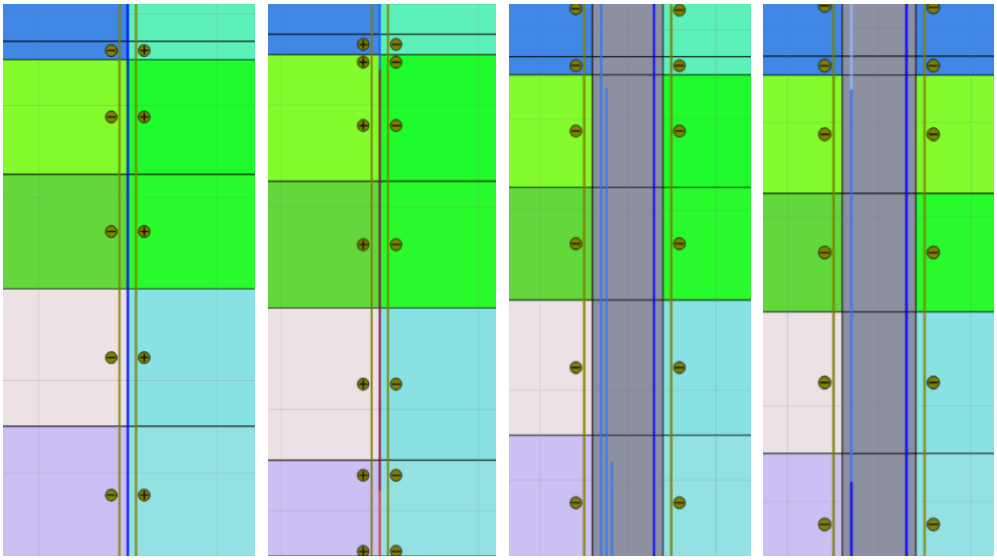

Figure 62: Cases modelling diaphragm wall KIS project. From left to right: Linear elastic plate, M-κ plate, bedded reinforced Shotcrete volume element and equivalent sectioned plate reinforced Shotcrete volume element.

Translating the characteristics to representative model input for the diaphragm wall, regarding a linear elastic respectively M-κ plate, gives the parameters and corresponding values summed up in Table 26.

Table 26: Input values for the diaphragm wall equivalent plate element models.

Material Model	Parameter	Value	Unit
Linear elastic	Modulus of elasticity	20 000 000	kN/m^2
	ν	0.15	-
(Plate)	w	19.20	kN/m/m
	EA	16 000 000	kN/m^2
	EI	853 300	kN m^2/m
M-κ (Plate) section 1 and 5. (1)	Modulus of elasticity	29 700 000	kN/m^2
	ν	0.2	-
	w	19.20	kN/m/m
	EA	9 688 000	kN/m^2
	EI	516 700	kN m^2/m
	M_r - κ_r	162.2 - 0.3140*10^{-3}	kNm - 1/m
	M_y - κ_y	1406 - 4.980*10^{-3}	kNm- 1/m
	$M_{c,pl}$ - $\kappa_{c,pl}$	1484 -6.710*10^{-3}	kNm- 1/m
	M_{rd} - κ_{rd}	1527 - 0.02114	kNm- 1/m
M-κ (Plate) section 2 and 4. (2)	Modulus of elasticity	29 700 000	kN/m^2
	ν	0.2	-
	w	19.20	kN/m/m
	EA	11 110 000	kN/m^2
	EI	592 600	kN m^2/m
	M_r - κ_r	162.2 - 0.3430*10^{-3}	kNm - 1/m
	M_y - κ_y	1990 - 4.605*10^{-3}	kNm- 1/m
	$M_{c,pl}$ - $\kappa_{c,pl}$	2501 - 5.924*10^{-3}	kNm- 1/m
	M_{rd} - κ_{rd}	2762 - 9.989*10^{-3}	kNm- 1/m
M-κ (Plate) section 3. (3)	Modulus of elasticity	29 700 000	kN/m^2
	ν	0.2	-
	w	19.20	kN/m/m
	EA	11 570 000	kN/m^2
	EI	617 400	kN m^2/m
	M_r - κ_r	219.2 - 0.3550*10^{-3}	kNm - 1/m
	M_y - κ_y	2073 - 4.349*10^{-3}	kNm- 1/m
	$M_{c,pl}$ - $\kappa_{c,pl}$	2864 - 6.203*10^{-3}	kNm- 1/m
	M_{rd} - κ_{rd}	3147 - 8.117*10^{-3}	kNm- 1/m

For the Shotcrete (material) model a sequence of steps (appendix D.2) has to be carried out in order to come to the governing parameters (Table 27) for the diaphragm wall. For accurate modelling it is wished to make a distinction between SLS and ULS modelling. In SLS characteristic strength parameters have to

be used, while in ULS design strength parameters have to be used. It is important to fit the model such that it represents C30/37 (strength) parameters. Not only the governing strength has to be inputted, also the plastic peak strain and the fracture energy have to be changed such that the peak strength and moment of failure match the Eurocode standards. This implies that the peak strength, for a conservative assumption, has to correspond to a strain of 1.75 ‰ and failure has to correspond to a strain of 3.5 ‰. Fitting the stress-strain behaviour has to be done with the help of the Plaxis soil-test facility.

Table 27: Input parameters Shotcrete volume element.

Material Model	Parameter	Value	Unit
Shotcrete	γ	24	kN/m^3
	E_{28}	29 700 000	kN/m^2
	ν	0.2	-
	$f_{c,28}$ (characteristic/SLS)	30 000	kN/m^2
	$f_{t,28}$ (characteristic/SLS)	2 000	kN/m^2
	$f_{c,28}$ (design/ULS)	20 000	kN/m^2
	$f_{t,28}$ (design/ULS)	1 333	kN/m^2
	ψ	13	^{o}
	E_1/E_{28}	1	-
	$f_{c,1}/f_{c,28}$	1	-
	$f_{c0,n}$	0.33	-
	$f_{cf,n}$	0.85	-
	$f_{cu,n}$	0.1	-
	ϵ_{cp}^{p} (characteristic/SLS)	-0.75*10^{-3}	‰
	ϵ_{cp}^{p} (design/ULS)	-1.090*10^{-3}	‰
	$G_{c,28}$ (characteristic/ULS)	1.55	kN/m
	$G_{c,28}$ (design/ULS)	3.4	kN/m
	$G_{t,28}$	0.1	kN/m
	$f_{tu,n}$	0	-
	ϕ^{max}	35	^{o}
	Time dependent parameters	0	-/day

To design the diaphragm wall with the Shotcrete volume element, elastoplastic plate reinforcement is added. Different reinforcement characteristics for the tension respectively compression side are considered. On the tensile side the three proposed reinforcement beds are taken into account, by means of one equivalent sectioned plate, as mentioned before. In the compressive area the applied reinforcement is different. The input parameters for the plate elements are given in Table 28.

Table 28: Input parameters Plate elements for reinforcement of Shotcrete volume element.

Parameter	Value	Unit
Modulus of elasticity	210 000 000	kN/m^2
Area tensile reinforcement (1 bed equivalent)	5.58*10^{-3}	m^2
Area tensile reinforcement (2 bed equivalent)	0.01	m^2

Area tensile reinforcement (3 bed equivalent)	0.016	m^2
Area compressive reinforcement	$1.5*10^{-3}$	m^2
Moment of Inertia tensile reinforcement (1 bed equivalent)	$2.266*10^{-8}$	m^4
Moment of Inertia tensile reinforcement (2 bed equivalent)	$4.079*10^{-8}$	m^4
Moment of Inertia tensile reinforcement (3 bed equivalent)	$6.526*10^{-8}$	m^4
Moment of Inertia compressive reinforcement	$4.395*10^{-10}$	m^4
EI tensile reinforcement (1 bed equivalent)	4.759	kNm^2/m
EI tensile reinforcement (2 bed equivalent)	27.70	kNm^2/m
EI tensile reinforcement (3 bed equivalent)	65.75	kNm^2/m
EI compressive reinforcement	0.0923	kNm^2/m
EA tensile reinforcement (1 bed equivalent)	1 172 000	kN/m
EA tensile reinforcement (2 bed equivalent)	2 108 000	kN/m
EA tensile reinforcement (3 bed equivalent)	2 812 000	kN/m
EA compressive reinforcement	315 000	kN/m
N_p	4350	kN

In appendix D.2 the stepwise approach needed to implement the by elastoplastic plates reinforced Shotcrete volume element in Plaxis 2D is given. The in appendix D.2 given approach is applicable for every case of modelling a reinforced (normal strength) concrete structure in Plaxis.

5.2 Loading

Two situations regarding dike safety have to be considered, the serviceability limit state (SLS) and the ultimate limit state (ULS). For both situations a calculation is done in order to obtain the overall safety and the bending moment, respectively displacement. In short both situations are described below. In Janssen (2016) and Havinga & Larsen (2013) both are explained in more detail, in terms of present guidelines and future improvements to those. The calculations done in this research are according to the governing guidelines at this moment.

The required safety is given in terms of a factor in which the strength of the dike (soil) can be reduced before failure occurs. The required safety level against geotechnical failure of the dike when applying the normative high water level is 1.27 (Larsen, Lubking, & Breedeveld, 2013). For the diaphragm walls in this project the required safety is considered to be 1.17. The bending moment and the deformation in ULS of the diaphragm wall are calculated taking into account the reduced, by a factor of 1.17, soil strength properties (parameter set M3). The reduced (by factor of safety 1.17) design parameter set M3 includes non-associative plasticity ($c \neq \phi$). In SLS the characteristic soil strength properties are not reduced (parameter set M1). Parameter set M2 consists of associative ($c = \phi$) design parameters.

5.2.1 Serviceability Limit State

To calculate the serviceability limit state several stages in Plaxis have to be modelled. Background information on the serviceability limit state is given in Janssen (2016). The stages to be modelled including the type of subsurface behaviour are stated in Table 29. The serviceability limit state is governing for design, regarding displacement. The soil parameter set is M1.

Table 29: Modelling stages SLS in the Plaxis model.

Phase	Description	Type of subsurface behaviour
S1a	Initial phase: build original dike body without own weight, with a horizontal phreatic line equal to the polder pile (PL0).	Drained
S1b	Activate volumetric weight of dike.	Drained
S1c	Set phreatic line according to normal circumstances (PL1), including any capillary rise in soil layers.	Drained
S2a	Apply the water line under normal circumstances (PL3) in the sand layer and in the intrusion layer. Interpolate water stresses in the soft soil layer.	Drained
S2b	Activate structural element (characteristic parameters).	Drained
S2b2	Apply the normative high water level as q-load. Apply the water line under extreme circumstances in the sand layer. Interpolate the water stresses in the soft soil layer under the water level. Activate the residual dike profile, eliminating local inner berm failure (Figure 61). Change constitutive soil model to Mohr-Coulomb of all layers in/under residual profile.	Drained
S2c	Apply the normative high water level as q-load.	Undrained
S2d	Apply the traffic load next to the diaphragm wall on the crest of the dike.	Undrained

5.2.2 Ultimate Limit State

The model phases to calculate the ultimate limit state are given in Table 30. The ultimate limit state is governing for the normative/design moment of the structure and the overall dike stability. The start soil parameter set is M2.

Table 30: Modelling stages ULS Plaxis.

Phase	Description	Type of subsurface behaviour
U1a	Initial phase: build original dike body without own weight, with a horizontal phreatic line equal to the polder pile (PL0).	Drained
U1b	Activate volumetric weight of dike.	Drained
U1c	Set phreatic line according to normal circumstances (PL1), including any capillary rise in soil layers	Drained
U2a	Apply the water line under normal circumstances (PL3) in the sand layer and in the intrusion layer. Interpolate water stresses in the soft soil layer.	Drained
U2b	Activate structural element (Design parameters).	Drained
U2b2	Activate the residual dike profile, eliminating local inner berm failure (Figure 61). Change soil parameter set from M2 to M3. From associative design parameters to non-associative reduced (by factor of safety 1.17) design parameters. Change constitutive soil model to Mohr-Coulomb of all layers in/under residual profile.	Drained

U2c	Apply the real normative water line. Apply the water line under extreme circumstances in the sand layer. Interpolate the water pressures in the cohesive layers under the water level.	Drained
U2d	Apply the traffic load next to the diaphragm wall on the crest of the dike.	Undrained

Until the structure is applied in the crest of the dike (phase (S/U)2b) in both SLS and ULS the calculation phases are the same. However the parameter sets differ, characteristic values are used in case of SLS and associative design values in case of ULS. A first difference is that in the ULS model the pore pressures in the sand layer is changed in phase 2c, directly with the application of the Normative High Water level. In the SLS model the pore pressures in the sand layer are changed in S2b2, while in phase 2c the normative high water level is modelled by means of a q-load (undrained situation). In the ULS situation the real occurring normative water level is modelled with a drained analysis. Phase 2d is equal for both, a traffic load of 13.3 kN/m^2 is applied over the road width of 2.5 meters.

5.3 Results

The results, bending moments and corresponding deformations, are compared in both SLS and ULS. In Table 31 and Table 32 the deformations in SLS respectively ULS (at structural design failure) are shown. The differences between the four possible methods to obtain the bending moment of the diaphragm wall are given in appendix D.1.5. In this appendix it is found that only one way to back calculate the occurring bending moment is correct (appendix D.1.6), which is by taking a force equilibrium at the neutral line (Figure 63). Figure 63 is a illustrative case as in the cases tested only N1 and N4 are present. The justification of using this method to obtain the governing bending moment and the details can be found in appendix D.1. In the recommendations is stated that a check on bending moment is not by definition necessary. Back calculating the bending moment is equal to doing a check on the normal force in the reinforcement (no yielding) and a check on the occurring strains in the compressive zone of the structure. Both can be done directly in the reinforced Shotcrete volume element, wherefore back-calculation of the occurring bending moment is by definition not necessary. Despite for convenience, of the in nowadays used engineering practice checks, a check on the bending moment is performed.

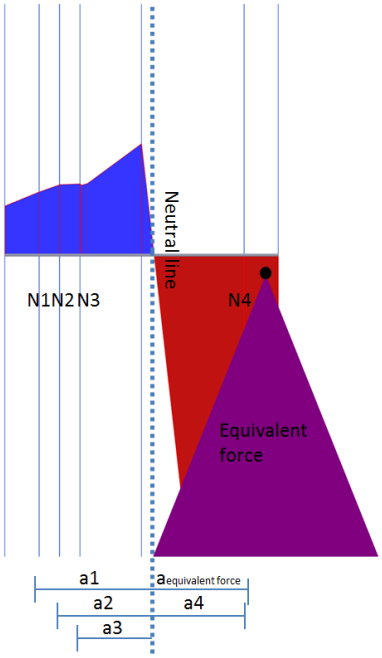

Figure 63: Illustrative (correct) back-calculation of the bending moment by a force equilibrium at the neutral line with 4 reinforcement plates.

In Table 31 the results, occurring bending moments and corresponding displacements, of the three cases in SLS are given. The difference rows indicate the difference between the use of the M-κ plate, respectively reinforced Shotcrete volume element model with respect to the reference linear elastic (reduced stiffness) plate case. The case in which a linear elastic plate element with reduced stiffness is used to model the diaphragm wall is considered as reference case, due to the fact that this is the base for the design made in practice.

Table 31: SLS Bending moments and displacements for the different cases of diaphragm wall modelling.

Case	Bending moment [kNm/m]	Displacement [m]
Linear elastic (reference) (1)	249	0.071
M-κ (2)	196	0.080
Shotcrete (3)	310	0.057
Difference 1-2 [%]	-21.3	12.6
Difference 1-3 [%]	24.5	-19.7

It can be observed (Table 31) that the obtained bending moment in SLS for the M-κ plate element is 21.3 % lower, while the obtained bending moment for the reinforced Shotcrete volume element is 24.5% higher with respect to the reference case. The obtained lower bending moment for the M-κ plate can be explained by the fact that the displacement is 12.6 % larger than in the reference case. It is observed that the stiffness is reduced (by local cracking), causing a larger displacement and therefore a lower obtained bending moment. The reinforced Shotcrete volume element gives a 24.5 % higher bending moment, while the displacement reduces with almost 20 % with respect to the reference case.

This is the effect of the higher initial stiffness compared to the linear elastic plate element. The almost 50% higher initial stiffness of the Shotcrete volume element causes a significant decrease in displacement with a subsequent increase in bending moment. This proves the additional value of using the Shotcrete model in such cases over the design methods nowadays used. Especially when taking in mind the capabilities of the material model to reduce the stiffness after rupture moment.

In **Fout! Verwijzingsbron niet gevonden.** the results in ULS are given for the three different cases. The difference row again indicates the difference in percentage between the results of the linear elastic reference case and the model in which the M-κ plate element, respectively Shotcrete volume element is used.

Table 32: ULS Bending moments and displacements for the different cases of diaphragm wall modelling.

Case	Bending moment [kNm/m]	Displacement [m]
Linear elastic (reference) (1)	1963	0.528
M-κ (2)	1688	0.714
Shotcrete (3)	1766	0.495
Difference 1-2 [%]	-14.0	35.2
Difference 1-3 [%]	-10.0	-6.3

It is found that the mean bending moment obtained in ULS is 10.0 % lower with respect to the reference in case the reinforced (by plates) Shotcrete volume element is used and 14.0 % when a M-κ based plate element is used. This shows that using the by elastoplastic plates reinforced Shotcrete volume element is beneficial in the design process. The way of back calculating the bending moment in the diaphragm wall can be found in appendix D.1. The deformation of the by Shotcrete material model represented diaphragm wall is 6.3 % lower with respect to the reference case. This means that when considering the same displacement as in the reference linear elastic (reduced stiffness) case, the bending moment is even lower. The lower obtained displacement is the result of taking partial cracking of the diaphragm into account. Also factors such as the higher interface shear stresses increase the bending moment capacity of the diaphragm, reducing the displacement. It is shown by both the reduction in displacement and bending moment that using the Shotcrete material model instead of the linear elastic (reduced stiffness) reference case is beneficial and more realistic.

Furthermore it is found that the bending moment obtained by using an equivalent to appendix F diaphragm wall M-κ plate element is 14 % lower, while the deformation increases drastically with 35.2 %. This indicates that the bending moment reduces due to a decrease in stiffness of the plate element. On its turn the stiffness decrease causes a significant increase in displacement of the diaphragm wall. The high deformation is caused by the fact that somewhere over the height of the diaphragm wall the ultimate capacity is almost reached, resulting in progressive plastic deformation. It is also observed that the overall failure mode, when further reducing the soil strength properties, corresponds with plastic deformation of the diaphragm wall. This is in contrast to the case when using the linear elastic plate element and the reinforced Shotcrete volume element. In those cases translation of the diaphragm wall

is the governing failure mode. Other factors influencing the difference in obtained results are already explained in chapter 4 and in appendix D.1.4, by means of a soil-structure interaction case. It is shown that lots of soil-structure interaction factors are influencing the behaviour, which are not accounted for in the pre-calculated M-κ diagrams. Factors that are not accounted for are: the effect of interface shear stresses (wall friction), a deforming cross-section, the influence of self-weight of the structure and the remaining tensile stress around and in between formed cracks. It can therefore be stated that using a M-κ plate element instead of a linear elastic plate element does not give by definition more realistic results.

5.4 Conclusion

This case study shows the capabilities and the result of using a by plates reinforced Shotcrete volume element for designing a laterally loaded reinforced concrete structure in the subsurface. A diaphragm wall similar to a by elastoplastic plates reinforced Shotcrete volume element is compared to the in design used linear elastic plate element with reduced stiffness and a M-κ plate (sectioned) element. It is found that using a M-κ plate element containing of five sections, does not give by definition more favourable results than the linear elastic plate element with reduced stiffness. The overall model safety is possibly affected observed by the fact that the governing failure mode, translation of the diaphragm wall, changes into plastic deformation of the structure when the soil parameters are reduced further than the required safety factor. In the situation used this is not of importance, however in cases where less reinforcement is applied in the diaphragm wall or the situation itself is more extreme this is a possible disadvantage of using the M-κ (sectioned) plate element. Besides the use is not justifiable as the influence of wall friction, a deforming cross-section, self-weight of the structure and a realistic way of cracking (residual and remaining tensile stresses) are not accounted for.

Using the by elastoplastic plates reinforced Shotcrete volume element to model the diaphragm wall takes into account all mentioned effects on the structural behaviour, as is shown in chapter 4. The results in this case study show that the governing bending moment for the structural design decreases with 10 % in ULS compared to reference case (linear elastic plate with reduced stiffness). The displacements decrease with 6 %. The reduction in obtained bending moment in ULS can directly related to the use of the Shotcrete material model. For SLS design it is also proven that the use of the reinforced Shotcrete model is justified. The results show that the bending moment increases with 25 %, while the deformation decreases with 19 % with respect to the reference case. This is the result of the higher initial stiffness, which is more realistic, compared to the linear elastic plate with reduced stiffness.

The stepwise approach used in this case study is applicable for every case in which a reinforced concrete structure, by means of an elastoplastic plate elements reinforced Shotcrete volume element, has to be modelled in Plaxis. The sequence of steps needed to implement the Shotcrete material model and the equivalent elastoplastic plate elements for reinforcement correctly is given in appendix D.2. The method found can be used by most Plaxis users and therefore has the prospect to be implemented widely for structural design.

6 Conclusions, discussion & recommendations

This chapter consists of a conclusion regarding the capabilities of the Plaxis Shotcrete material model for designing laterally loaded reinforced concrete structures in the subsurface. The results are summarised, reflected and discussed. Furthermore recommendations regarding the use of the material model in such cases and recommendations for further research are given.

6.1 Conclusion

Theoretical verification of the Shotcrete material model against CEB-FIP model code (2010), Eurocode 2 (NEN-EN 1992-1-1, 2011) and other scientific literature shows that the material model has the theoretical base to accurately model non-linear realistic concrete material behaviour, including cracking. It is moreover found that for most parameters of the Shotcrete material model standard values can be used when modelling structural concrete. The found standard values consider also the capability of the material model to account for realistic modelling of time dependent behaviour. Fitting the input parameters of the Shotcrete material model in the Plaxis soil-test facility to experimental data of a uniaxial compression test and evaluating the parameter sensitivity analysis proved that only the strength parameters, the modulus of elasticity, the plastic peak strain and the compressive fracture energy are concrete class specific. It is possible to make a database, containing each concrete class and the different stress-strain design considerations according to Eurocode 2 (NEN-EN 1992-1-1, 2011) for wide implementation of the material model regarding modelling (reinforced) normal strength structural concrete in Plaxis.

A statically determined reinforced concrete bending beam test showed that using the Shotcrete material model has additional value over the use of first order approximation models. Throughout the process of progressively loading the beam more realistic (concrete) behaviour is obtained than by using a Mohr-coulomb or linear elastic material model. In more detail, a realistic representation of the failure behaviour of a laterally loaded reinforced beam is observed. The resulting cracking pattern due to loading matches the pattern found in theoretical experiments and besides lies within bounds of the governing guidelines. The required calculation time compared to other material models for the bending beam case is rather high. However it is found that in a practical application the additional required calculation time is negligible. Another observation regards the mesh sensitivity of the Shotcrete material model. A relatively fine mesh is required, due to the mesh sensitivity of cracking (softening behaviour), in order to give reliable and realistic results. A detailed analysis regarding the capabilities of the Shotcrete material model to design laterally reinforced concrete structures, by means of a comparison with a M-κ and M-N-κ diagram, showed that the model can be considered as appropriate and accurate. The M-κ and M-N-κ diagram are in daily engineering practice often used to design a reinforced concrete structure subjected to bending (and normal force). In both cases a close match to the results is found. In case the structure is subjected to a normal force, attention has to be paid to pre-stressing of the reinforcement and the resulting effect on the internal concrete stresses. The differences found between the M-(N-)κ hand calculations and the Plaxis Shotcrete material model can be explained by the fact that the Plaxis Shotcrete material model takes in contrast to a hand calculation shear deformation and remaining tensile strength above and in between the formed cracks upon loading into account.

Evaluation of an excavation next to a diaphragm wall, such that structural bending failure is the normative failure mode, showed that using a single plate reinforced Shotcrete volume element to represent the diaphragm wall gives improved modelling results with respect to commonly used methods. Taking the found benefits into account, it is shown that by using a single plate reinforced Shotcrete volume element instead of a linear elastic plate, respectively volume element, or a M-κ based plate element, soil-structure interaction can be modelled more realistically. Moreover, additional benefits in a soil-structure interaction case by using such a representation of the structure are that the effect of interface shear stresses (wall friction) and the influence of self-weight on the structural behaviour can be taken into account accurately. These benefits result in a lower obtained bending moment at similar excavation depth, respectively deformation of the diaphragm wall. The bending moment in a by plates reinforced Shotcrete volume element can only be back calculated correctly with one method. It is demonstrated that by using an internal force equilibrium at the neutral line in the normative cross-section of the diaphragm wall the correct bending moment can be obtained.

The effect of using the Plaxis Shotcrete material model for a by plates reinforced volume element, equal to the realised diaphragm wall, is shown for the KIS project. The present guidelines propose to use a linear elastic plate element with a reduced stiffness to model the diaphragm wall in the crest of the dike (reference case). Application of an equal to the structure by plates reinforced Shotcrete volume element shows that the obtained bending moments are 10 % lower, with a 6 % lower displacement, for ULS design compared to the reference case. The obtained bending moment in SLS is found to be 25 % higher, with a 19 % lower deformation, when using a reinforced Shotcrete volume instead of a linear elastic plate element with reduced stiffness. Deviations are the result of the fact that the Shotcrete model only reduces the stiffness after rupture moment, while in the linear elastic plate element case the initial stiffness is reduced. It is furthermore demonstrated that using the (sectioned) M-κ plate element does not give by definition more realistic results than the reference case, due to the fact many factors are not accounted for. Summed up, this research proves the capabilities and advantage of using the Shotcrete material model, with the addition of plate elements in the volume element to represent reinforcement, to design laterally loaded reinforced concrete structures in the subsurface. A simple guide consisting of 8 steps is proposed for correct implementation of the Shotcrete material model in a soil-structure interaction case.

6.2 Discussion

Discussion on the conclusions mainly focusses on the points of attention regarding the use of the Shotcrete material model for soil-structure interaction cases. Besides also the results of this research are critically discussed.

Back calculating the bending moment occurring in a by plates reinforced volume element is rather difficult and subjected to several factors which might decrease the accuracy of the obtained result. In this research is demonstrated that only by taking an internal force equilibrium, between the equivalent force and the normal force in the reinforcement, at the neutral line of the normative cross-section will give satisfying results. Similar results are obtained to the by hand calculated bending moment for a statically determined structure, proving the validity. Nevertheless the following points can lead to

deviations between the occurring and back calculated bending moment when using the proposed method to back calculate the bending moment.

- Finding the correct normative cross-section. Normally this corresponds with the coordinates at which the maximum normal force in the reinforcement can be found. For a statically undetermined structure it is not possible to calculate the normative cross-section on forehand.
- Using the exact coordinates of the normative cross-section. It is necessary to draw a cross-section at the exact coordinates of the normative cross-section of the structure, which subjects this method to possible reading errors.
- The main crack in the structure will be formed at the normative cross-section. The trajectory of the crack is not completely perpendicular to the structure, when subjected to bending, leading to the fact that the crack does not entirely follow the path of the normative cross-section to be drawn.
- The coordinates of the neutral line have to be found exactly in the normative cross-section. The stresses obtained in the normative cross-section are influenced by the height and position of the crack. Both determine the exact coordinates of the neutral line in the cross-section, wherefore numerical instabilities around the crack influence the back calculated bending moment.
- Another point of attention regarding the exact coordinates of the neutral line is that the neutral line is defined at the point in the stress-distribution where the stresses are zero. Currently the determination of the coordinates of this point is subjected to reading errors.

For as far as possible these points are taken into account in this research, although a small deviation from perfectly obtaining the bending moment remains. Another point of discussion regards the back calculation of the bending moment in the statically determined bending beam case. The bending moment is back calculated according to the correct formula for statically determined structures. This method of back calculating the bending moment assumes that the normative cross-section remains undeformed, while in Plaxis the cross-section deforms upon progressively loading. It is found that this can cause a deviation of approximately 3 % in the obtained results. However compared to other factors of influence, such as the fact that the Shotcrete material model accounts for residual tensile strength above and in between the cracks in the concrete, the influence is limited.

Another point of attention when using the Shotcrete material model follows from the M-N-κ comparison. The normal force applied on the structure does not cause the equivalent normal force (/stress) in the structure. The reinforcement plate elements are pre-stressed wherefore an intermediate check is required. Nevertheless the comparison proves that a situation in which a vertical and a horizontal load are applied on a structure can be modelled correctly. In this report this is shown by the resulting (minor) effect of interface shear stresses in the soil-structure interaction case. Additionally, in the case study a pre-calculated M-κ diagram is used for the equivalent plate element. For more accurate and realistic results it is advised to re-calculate the M-κ diagram taking the influence of interface shear stresses as well as self-weight into account.

The results obtained in the case study are partly subjected to (small) mesh sensitivity of the Shotcrete material model. It is demonstrated that the mesh size influences the results obtained when using the

Shotcrete material model to represent a reinforced bending beam. As it is not feasible to refine the mesh of the structure in a soil-structure interaction case to the equivalence of a very fine mesh in the reinforced bending beam model, it may be assumed that the results are influenced by a small effect of mesh sensitivity.

Evaluating and interpreting the structural results, especially clarifying the effect of each influencing factor on the obtained bending moment is difficult. Many factors are of influence in a complex soil-structure interaction case. This makes it hard to clarify the effect of each and compare the results to other calculation methods. Factors that influence the structural behaviour and therefore the results are: the interface shear stresses (wall friction), the effect of taking into account a deforming cross-section, the influence of the self-weight of the structure and the effect of taking into account remaining tensile stress around and in between formed cracks.

6.3 Recommendations

Recommendations following from the research done regarding the use of the Shotcrete material model are:

- Use a refined mesh for the by plates reinforced Shotcrete volume element in order to limit the influence of mesh sensitivity and be able to obtain an accurate stress distribution in the normative cross-section, required when back calculating the resulting bending moment in the structure.
- In appendix D.1 is demonstrated that only one way to obtain the bending moment of a reinforced concrete structure, represented by a Shotcrete volume element with plate elements within, is correct. It is recommended to use the found method, an internal force equilibrium at the neutral line.
- In engineering practice, first use a first-order approximation model such as a linear elastic plate element with reduced stiffness to represent the reinforced concrete structure. After a first analysis a detailed structural design can be made by the structural engineer. Subsequently the design can be optimised, using a by plate(s) reinforced Shotcrete volume element.
- The implementation of a library consisting the related input for time (in)dependent modelling of the by Eurocode stated concrete classes, different stress-strain design methods and parameter sets is wished to make the use of the Shotcrete material model, for structural concrete, widely possible.
- The stepwise approach regarding the use of the Shotcrete material model in a soil-structure interaction case proposed in appendix D.2 is recommended to be used.
- Calculating the bending moment is equivalent to a check on the strain in the compressive zone and the normal force in the reinforcement of the concrete structure. The rather complex way of back calculating the bending moment can for this reason be excluded in the stepwise approach. Both individual components are directly outputted and can be checked directly in Plaxis. Failure in Plaxis is based on these two individual components and therefore also concerns the (ultimate occurring) bending moment. By checking these components in the calculation, back calculation of the bending moment is not necessary as is proven in chapter 3.

Recommendations for further research are:

- The possibility to include reinforcement characteristics in the Shotcrete material model's input instead of using plate elements to account for reinforcement. This will not only ease the input of the model, but also the bending moment could probably be obtained correctly with the Plaxis built-in function. However at first eye it seems that including reinforcement in the material model's input leads to a simplification of reinforced concrete behaviour. The Shotcrete material model will act linearly under tension and the ability of the material model to account for cracking is not used. This possibly limits the advantage of using the Shotcrete material model over other modelling approaches to design reinforced concrete structures.
- A possible improvement for even more realistic modelling of reinforced concrete, can be made by using embedded beams instead of plate elements to represent reinforcement. By using embedded beams bond-slip behaviour can be considered and reinforcement bars can be physically distinguished. Witasse (2016) showed that an embedded beam is a feasible option to model reinforcement in a Shotcrete volume element.
- Determining the structural bending moment is at this moment dependent on the structural mechanics knowledge of the user and the accurateness of reading the required coordinates. It is therefore advised to implement a function in Plaxis to output the bending moments directly, using the proposed method in appendix D.1(.4).
- In this research is focussed on designing laterally loaded reinforced concrete structures in 2D, by means of a diaphragm wall. It should be further investigated if also fibre reinforced structures can be modelled more realistically by using the Shotcrete material model. The Shotcrete material model has the prospect to model fibre reinforced concrete, due to the fact that the fracture energy can be used for extending the stress-strain relationship to account for higher residual strength after reaching peak strength. Possible applications are (fibre reinforced) underwater concrete floors, large diameter (fibre) reinforced concrete bored piles and diaphragm walls. In such cases the use of the Shotcrete model is beneficial compared to a standard M-κ approach. Hybrid reinforced concrete structures can possibly be modelled with the Shotcrete material model.
- It should be further researched if adopting an iterative way to determine the M-κ diagram based plate element is feasible. In this way effects such as the influence of interface shear stresses on the bending behaviour of the structure could be taken into account.
- It is also recommended to research the material model's applicability in cases where a vertical load or a high normal force is acting on the reinforced concrete structure.
- The capabilities of the material model in 3D situations have to be researched in order to find if it is possible to model pile behaviour more accurate. A first investigation on a statically determined by beams reinforced concrete (Shotcrete) beam (in Plaxis 3D) showed that this might be able.

7 Bibliography

ACI 209R-92. (1992). *Prediction of creep, shrinkage and temperature effects in concrete structures.* Detroit: American Concrete Institute, Committee 209.

API RP 2A-WSD. (2010). *Planning, designing and constructing fixed offshore platforms - working stress design.* Washington: API Publishing service.

Ardiaca, D. (2009). Mohr-Coulomb parameters for modelling of concrete structures. *Plaxis Bulletin, 25*, 12-15.

Bakker, K. (2015). Bore Tunnels Construction Techniques I - NATM Tunnelling [lecture]. *CIE 5305: Bored and Immersed Tunneling*. TU Delft: CiTG, Geo-engineering.

Barneveld, H. (2007). *Leidraad rivieren.* Den Haag: Ministerie van Verkeer en Waterstaat.

Barros, J., & Fogueiras, J. (1999). Flexural behaviour of SFRC: testing and modelling. *Journal of Material in Civil Engineering, 11*(4), 331-339.

Basu, D., Salgado, R., & Prezzi, M. (2008). Analysis of Laterally Loaded Piles in Multilayered Soil Deposits. *Joint Transportation Research Program*, 330.

Bazant, Z. (2001). Prediction of concrete creep and shrinkage: past, present and future. *Nuclear Engineering and Design, 203*(1), 27-38.

Begemann, H., & De Leeuw, E. (1972). Horizontal Earth Pressures on Foundation Piles as Result of Nearby Soil Fills. *Proceedings 5th Euro Conference Soil Mechanics & Foundation Engineering*, (pp. 1-9). Madrid.

Blodgett, O. (1991). *Design of welded structures* (14 ed.). Cleveland: The James F. Lincoln Arc Welding Foundation.

Braam, C., & Lagendijk, P. (2010). *Constructieleer Gewapend Beton* (6de ed.). Boxtel: Aeneas.

Brinch Hansen, J. (1961). The Ultimate resistance of rigid piles against transversal forces. *The Danish geotechnical institute bulletin*.

Brinkgreve, R. (2015). Elasticity [Lecture]. *CIE 4362: Behaviour of Soils and Rocks*. Delft: TU Delft: CiTG, Geo-engineering.

Brinkgreve, R. (2015). Failure criteria [Lecture]. *CIE4362: Behaviour of Soils and Rocks*. Delft: TU Delft: CiTG, Geo-engineering.

Brinkgreve, R. (2015). Hardening Soil [Lecture]. *CIE4362: Behaviour of soils and rocks*. Delft: TU Delft: CiTG, Geo-engineering.

Brinkgreve, R., Kumarswamy, S., & Swolfs, W. (2016). *PLAXIS 2D Material Models Manual.* Delft: Plaxis.

Brinkgreve, R., Kumarswamy, S., & Swolfs, W. (2016). *PLAXIS 2D Reference manual.* Delft: Plaxis bv.

Broms, B. (1965). Design of laterally loaded piles. *Journal of soil mechanics and foundation devision, 91*(3), 77-99.

Byfors, J. (1980). *Plain strain concrete at early ages.* Stockholm: Swedish Cement and Concrete Institute.

Candappa, D., Sanjayan, J., & Setunge, S. (2001). Complete Triaxial Stress-Strain Curves of High-Strength Concrete. *Journal of Materials in Civil Engineering, 13*(3), 209-215.

CEB-FIP. (1990). *model code. Design code - comite Euro-international du Beton.* London: Thomas Telford.

CEB-FIP. (2010). *fib Model Code for Concrete Structures.* Berlin: Ernst & Sohn.

Chang, Y. (1994). *Tunnel support with shotcrete in weak rock - a rock mechanics study.* Stockholm: Royal Institute of Technology, Department of Civil and Environmental Engineering, Division of Soil and Rock Mechanics.

Cornelissen, H., Hordijk, D., & Reinhardt, H. (1986). Experimental determination of crack softening characteristics of normalweight and lightweight concrete. *Heron, 31*(2), 45-56.

Dai, J., & Gao, W. (2014). FE modeling of FRP-strengthened RC beams subjected to standard fire exposure. In H. Furuta, D. Frangopol, & M. Akiyama, *Life-Cycle of Structural Systems: Design, Assessment, Maintenance and Management* (pp. 1313-1322). Leiden: CRC Press/Balkema.

Everts, H. (2015). Laterally loaded piles [Lecture]. *CIE4362: Soil-structure interaction*. TU Delft: CiTG, Geo-engineering.

Fleming, W., Weltman, A., Randolph, M., & Elson, W. (1992). *Piling Engineering.* Blackie & Son Ltd.

Green, S., & Swanson, S. (1973). *Static constitutive relations for concrete.* TERRA TEK INC SALT LAKE CITY UT.

Griffith, A. A. (1921). The phenomena of rupture and flow in solids. *Philosophical Transactions of the Royal Society of London. Series A, containing papers of a mathematical or physical character, 221*, 163-198.

Grübl, P., Weigler, H., & Karl, S. (2001). *Beton: Arten, Herstellung und Eigenschaften.* Berlin: Ernst & Sohn.

Havinga, H., & Larsen, H. (2013). *Ontwerp zelfstandig waterkerende constructies (type I) dijkversterking KIS.* Delft: Deltares.

Hibbit, K., Karlsson, B., & Sorensen, P. (2014). *ABAQUS Theory manual.* Providence : Dassault Systèmes.

Hillerborg, A., Modéer, M., & Petersson, P. (1976). Analysis of crack formation and crack growth in concrete by means of fracture mechanics and finite elements. *Cement and Concrete research, 6*(6), 773-781.

Hordijk, D. (1991). *Local approach of fatigue of concrete.* Delft: TU Delft, PhD dissertation.

Hossain, A., & Weiss, J. (2004). Assessing residual stress development and stress relaxation in restrained concrete ring specimens. *Cement & Concrete Composites, 26*(5), 531-540.

Janssen, J. (2016). *Research on the safety level of a diaphragm wall in river dikes, using a Montecarlo analysis.* Delft University of Technology: M.Sc. Thesis Geo-Engineering Section.

Kupfer, H., Hilsdorf, H., & Rusch, H. (1969). Behavior of Concrete Under Biaxial Stresses. *Journal Proceedings, 66*(8), 656-666.

Kwak, H., & Filippou, F. (1990). *Finite Element Analysis of Reinforced Concrete Structures Under Monotonic Loads (pp. 33-39).* Berkeley, CA: Department of Civil Engineering, University of California.

Larsen, H., Lubking, P., & Breedeveld, J. (2013). *Ontwerp stabiliteitsschermen (type II) in primaire waterkeringen (groene versie).* Delft: Deltares.

Leonhardt, F., & Walther, R. (1962). *Schubversuche an Einfeldrigen Stahlbeton-Balken mit und ohne Schubbewehrung zur ermittlung der Schubtragfähigkeit under der Oberen Schubspanningsgrenze.* Berlin: Ernst und Sohn.

Meschke, G., Kropik, C., & Mang, H. (1996). Numerical analysis of tunnel linings by means of a viscoplastic material model for shotcrete. *International Journal Numerical Methods in Engineering, 39*(18), 3145-3162.

NEN-6008. (2008). *Steel for the reinforcement of concrete.* Delft: Nederlands Normalisatie Institute.

NEN-9997-1. (2012). *Geotechnisch ontwerp van constructies - Deel 1: Algemene regels.* Delft: Nederlands Normalisatie Instituut.

NEN-EN 1992-1-1. (2011). *Eurocode 2: Design of concrete structures.* European Committee for Standardization.

Poulos, H., & Davis, E. (1980). *Pile foundation analysis and design.* New York: Wiley.

Reese, J., & Van Impe, W. (2010). *Single piles and pile groups under lateral loadings.* Rotterdam: A.A. Balkema.

Reinhardt, H. (1985). *Beton als constructiemateriaal: eigenschappen en duurzaamheid.* Delft: Delftse Universitaire Pers.

Reinhardt, H., & Xu, S. (1999). Crack extension resistance based on the cohesive force in concrete. *Engineering Fracture Mechanics, 64*(5), 563-587.

Rollins, K., Olsen, K., Jensen, D., Garrett, B., Olsen, R., & J., E. (2006). Pile Spacing Effects on Lateral Pile Group Behavior: Analysis. *Journal of Geotechnical and Geoenvironmental Engineering, 132*(10), 1272-1283.

Salgado, R. (2008). *The engineering of foundations.* New York: The McGraw-Hill Companies Inc.

Saurer, E., Marcher, T., Schädlich, B., & Schweiger, H. (2014). Validation of a novel constitutive model for shotcrete using data from an executed tunnel. *Geomechanics and Tunnelling, 7*(4), 353-361.

Schädlich, B., & Schweiger, H. (2014a). A new constitutive model for shotcrete. In M. Hicks, R. Brinkgreve, & A. Rohe, *Numerical Methods in Geotechnical Engineering* (pp. 103-108). London: Taylor & Francis Group.

Schädlich, B., & Schweiger, H. (2014b). *Internal report shotcrete model: Implementation validation and application of the shotcrete model.* Delft: Plaxis.

Scheider, I. (2001). *Cohesive model for crack propagation analysis of structures with elastic-plastic material behaviour Foundations and implementation.* Geesthacht: GKSS research centre.

Schubert, P. (1988). Beitrag zum rheologischen Verhalten von Spritzbeton. *Felsbau, 6*(3), 150-153.

Schütz, R., Potts, D., & Zdravkovic, L. (2011). Advanced constitutive modelling of shotcrete: model formulation and calibration. *Computers and Geotechnics, 38*(6), 834-845.

Sluis, J. (2012). *Validation of embedded pile row in Plaxis 2D.* Delft: MSc. Thesis, TU Delft.

Tanaka, E., & van Eijden, T. (2003). Biomechanical Behavior of the Temporomandibular Joint Disc. *Critical Reviews in Oral Biology & Medicine, 14*(2), 138-150.

TGB Betonconstructies. (2013). Varce 10, Grootte van de scheurafstand. *Cement*, 2-5.

Thomée, B. (2005). *Physikalische nicht-lineare Berechnung von Stahlfaserkonstruktionen.* PhD thesis, Technical University Munich.

Van Breugel, K. (1980). *Artificial cooling of hardening concrete.* Delft: Delft University of Technology, Faculty of Civil Engineering and Geosciences.

Van Mier, J. (1984). *Strain-softening of concrete under multiaxial loading conditions.* Eindhoven: Technische Hogeschool Eindhoven.

van Mier, J. (1998). Failure of concrete under uniaxial compression: An overview. In H. Mihashi, & K. Rokugo, *Fracture Mechanics of Concrete Structures: Proceedings FraMCoS-3* (pp. 1169-1182). Freiburg: AEDIFICATIO.

Van Staveren, M. (2006). *Uncertainty and Ground Conditions: A Risk Management Approach.* Oxford: Butterworth-Heinemann.

van Tol, A. (2006). *Foundation Engineering and Underground Construction (CT5330).* Delft: TU Delft.

Vermeer, P., & de Borst, R. (1984). Non-associated plasticity for soils, concrete and rocks. *HERON, 29*(3).

Walraven, J., & Reinhardt, H. (1981). Theory and Experiments on the Mechanical Behaviour of Cracks in Plain and Reinforced Concrete Subjected to Shear Loading. *HERON, 26*(1a), 1-68.

Wischers, G. (1978). Aufnahme und Auswirkungen von Druckbeanspruchungen auf Beton. *Beton Technische Berichte*(19), 31/56.

Witasse, R. (2016). *On the Use of the ShotCrete UDSM for Modelling Concrete.* Delft: Plaxis bv.

Xu, X. (2007). *Investigation of the end bearing performance of displacement piles in sand.* Perth: PhD dissertation, University of Western Australia.

8 Appendices

Appendix A: Theoretical background

A.1 Concrete material behaviour

In this appendix the behaviour of (reinforced) concrete will be explained based on the theory described by Byfors (1980), Reinhardt (1985), Braam & Lagendijk (2010), CEP-FIP (2010) and NEN-EN 1992-1-1 (2011).

Concrete can be produced in different strength classes. It ranges from C12 to C50 for normal strength concrete (NSC) and for high strength concrete (HSC) up to C120. Even stronger concrete can be produced, which is called ultra-high performance concrete (UHPC). Commonly used for in-situ concrete is a strength used is C30/37. The C stands for strength under compression, while the first number stands for cylinder compressive strength, the second number stands for cubic compressive strength. The cylinder compressive strength is according to NEN-EN 1992-1-1 (2011) used as characteristic compressive strength value. To calculate the design value a partial material safety factor, accounting for material safety and long-term loading, has to be applied on the characteristic value. In NEN-EN 1992-1-1 it is stated that up to strength class C90/105, calculation methods and properties are described by the code for design purposes. For the purpose of this

research the properties described by this code will be taken in mind (Table A-1).

Table A-1: Characteristics of concrete of different strength classes according to NEN-EN 1992-1-1 (2011).

Strenght classes for concrete														
f_{ck}(Mpa)	12	16	20	25	30	35	40	45	50	55	60	70	80	90
$f_{ck,cube}$(Mpa)	15	20	25	30	37	45	50	55	60	67	75	85	95	105
f_{cm}(Mpa)	20	24	28	33	38	43	48	53	58	63	68	78	88	98
f_{ctm}(Mpa)	1.6	1.9	2.2	2.6	2.9	3.2	3.5	3.8	4.1	4.2	4.4	4.6	4.8	5
$f_{ck,0,05}$(Mpa)	1.1	1.3	1.5	1.8	2	2.2	2.5	2.7	2.9	3	3.1	3.2	3.4	3.5
$f_{ck,0,95}$(Mpa)	2	2.5	2.9	3.3	3.8	4.2	4.6	4.9	5.3	5.5	5.7	6	6.3	6.6
E_{cm}(Gpa)	27	29	30	31	33	34	35	36	37	38	39	41	42	44
ϵ_{c1} (‰)	1.8	1.9	2	2.1	2.2	2.25	2.3	2.4	2.45	2.5	2.6	2.7	2.8	2.8
ϵ_{cu1}(‰)	3.5									3.2	3	2.8	2.8	2.8
ϵ_{c2}(‰)	2									2.2	2.3	2.4	2.5	2.6
ϵ_{cu2}(‰)	3.5									3.1	2.9	2.7	2.6	2.6
η	2									1.75	1.6	1.45	1.4	1.4
ϵ_{c3}(‰)	1.75									1.8	1.9	2	2.2	2.3
ϵ_{cu3}(‰)	3.5									3.1	2.9	2.7	2.6	2.6

A.1.1 Time dependency of material properties at early stage

Time and temperature dependent processes, determined by hydration, lead to a change in material properties over time. Hydration is a exothermic chemical reaction process leading to bonding and hardening of the material. A first material property that changes in time is the strength. The strength of concrete increases with time and temperature (maturity). After just three days the compressive strength is between 40 and 60% of its final compressive strength (Figure A-1). Byfors (1980) found that the reference compressive concrete strength at 28 days represents 70 to 90% of its final strength. The tensile strength development is somewhat different from the compressive strength.

The evolution of the elasticity modulus, the compressive and the tensile strength are given in Figure A-1.

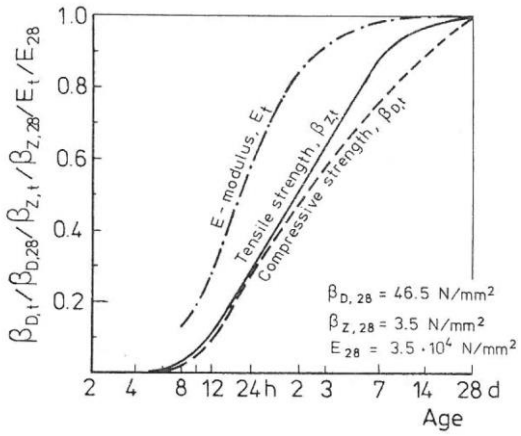

Figure A-1: Evolution of modulus of elasticity, the compressive and the tensile strength (Byfors, Plain strain concrete at early ages, 1980).

A second material property which changes in time is stiffness (Grübl, Weigler, & Karl, 2001). Stiffness or also called modulus of elasticity describes the resistance against deformation. The modulus of elasticity reaches 60% of its final value after just 1 day and after just 3 days 90% of the final value is reached (Figure A-1). The absolute value of the modulus of elasticity is dependent on the concrete class, which is elaborated in the section 0. Poisson's ratio (Figure A-2) is the ratio between the strain in perpendicular directions (equation A.1) and is therefore also used to describe the behaviour of concrete.

$$\nu = -\frac{\epsilon_{xx}}{\epsilon_{yy}} = -\frac{\delta\epsilon_3}{\delta\epsilon_1} \quad (A.1)$$

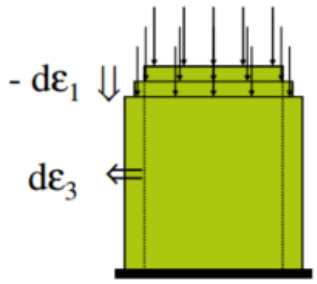

Figure A-2: Poisson's ratio (Brinkgreve, 2015).

Poisson's ratio, which is explained in more detail in paragraph A1.10, starts at a value of 0.5 when the compressive strength of the concrete is nearly zero, representing fully plastic behaviour, and evolves to 0.25 for fully hardened un-cracked concrete (Figure A-3).

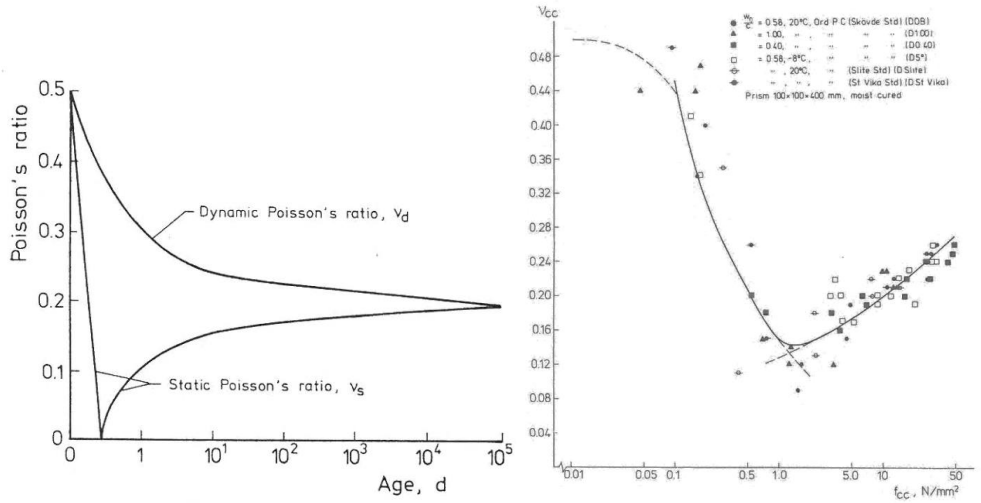

Figure A-3: Static and dynamic Poisson's ratio with age, respectively concrete strength (Byfors, Plain strain concrete at early ages, 1980).

A value of 0,5 for Poisson's ratio, representing incompressible behaviour (infinite modulus of compression), seems unrealistic as it is at the limit of possible values of Poisson's ratio ($-1 \leq \nu \leq 0{,}5$). Though when considering fresh concrete as a fluid, it should be close to 0,5 but will never exceed this value. From the start deformation under sustained load takes place. This phenomena can be defined as creep. Creep effects can be accounted for using a creep coefficient (ϕ_{cr}). The creep coefficient is determined by a ratio between the creep strain and the elastic strain. Van Breugel (1980) found an expression for the creep coefficient within the timeframe of hardening. It relates the evolution of the modulus of elasticity to the modulus of elasticity at the time of loading. A decrease of the creep coefficient is obtained with loading time (age) and relative compressive strength. Relaxation, the decrease in stress at a constant strain rate, can be described similarly as creep. A relaxation factor ψ can be obtained from an expression which only depends on the evolution of creep during time and temperature. Young concrete has the ability to relief more stress in a shorter timespan than 28 days old concrete. This means that the cracking potential at early stages is lower, which complies with the higher plasticity and a lower material strength.

Concrete at an age of 28 days is not fully hardened yet. Though this age is used as reference for material properties. It is shown in Reinhardt (1985) that concrete is able to fill up very small fissures to an age of approximately 1 year. The filling of small fissures is governed by the process of hydration. The larger pores and the small fissures are filled with hydration products, leading to an increase in strength till the concrete is fully hardened. Due to the fact that hydration decreases in time, the ability to fill up small fissures is also decreased in time. Therefore the rate of strength increase, decreases in time (Figure A-4).

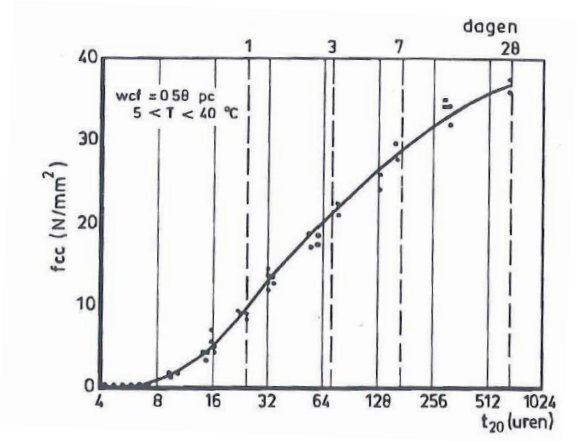

Figure A-4: Compressive strength evolution in time (Reinhardt, 1985).

The strength of concrete differs for different types of loading, depending on the loading rate. Strength behaviour upon (detailed) cyclic loading is outside the scope. For compressive and tensile loading of hardened (28 days old) concrete, the strength can be described according to the concrete class (Table A-1) as mentioned before. In this research these strength properties will be taken into account.

A.1.2 Compressive loading

The concept of stresses on an element such as compression or tension can be explained with the help of the Cartesian stress directions (Figure A-5).

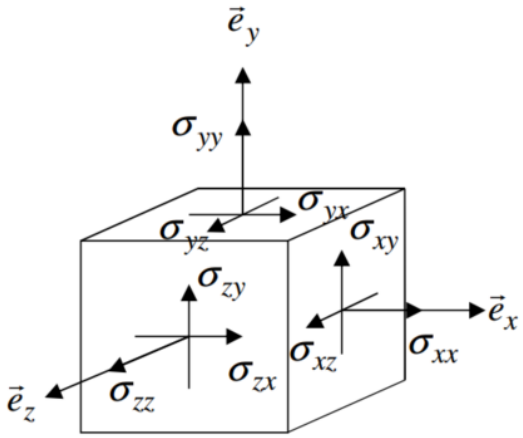

Figure A-5: Cartesian stress directions (In Plaxis 2D) (Brinkgreve, Kumarswamy, & Swolfs, 2016).

The three main stress directions (xx,yy,zz) can be defined as the normal stresses on the arbitrary cubic element. The other stress directions (displayed on the plane) are shear stresses. When the main stress directions are taken such that the corresponding shear components are equal to zero, the stress directions are called principal stresses. Looking in 2D stress space to the cubic element, the compressive stress can be visualised as is done in Figure A-6. The arrows are inward, giving a negative sign in Cartesian stress space, for compression. In tension the arrows will be outwards, giving a positive sign in Cartesian stress space.

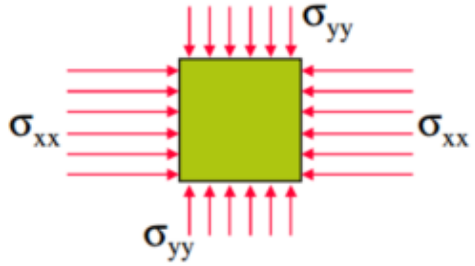

Figure A-6: Compression in 2D (Brinkgreve, 2015).

The compressive strength of concrete is the base for defining almost all other mechanical and physical properties. The compressive strength can be determined by doing a compression test on a cylinder or cube. The values for standard concrete mixtures/strength classes are given in Table A-1. A typical stress-strain diagram of a compression test is given below in Figure A-7.

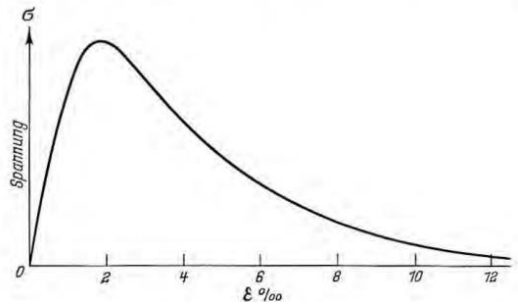

Figure A-7: Stress-strain diagram of normal strength concrete (Wischers, 1978).

The concrete material behaviour can be characterised by three different parts. At first the concrete behaves linear elastic, according to Hooke's law. The stress and strain are linear related by the modulus of elasticity (paragraph A.1.9). At the point of yielding, plastic (irreversible) strains are generated and straining is not linear anymore to the applied stress. The accumulated plastic strains can be determined by unloading before failure occurs. However, it should be noted that not only plastic strains can cause non-linearity. Non-linearity can also be caused by elastic strains. In unloading the elastic strains, reversible strains, disappear. While the generated plastic strains stay in the material, irreversible, after unloading. When reloading again, the curve will follow elastic behaviour till the stress state is reached when the unloading started. At that moment plastic strains will again be generated together with elastic strains. The behaviour of concrete can be defined as non-linear as soon as plastic strains are generated.

To give more insight in non-linear behaviour of concrete at macroscopic level, a description of the processes at meso-level is useful. Aggregates are floating in a matrix of cement, which besides contains small sand particles. An interfacial transition zone encloses the larger aggregates. The interfacial transition zone is characterised by a constant strength and stiffness over the whole volume. Under uniform loading conditions the soft matrix will flow around the stiffer aggregate, which leads to lateral tension and interfacial cracking. Due to the fact that lateral deformation in the soft matrix is larger than in the stiff, shear stresses will develop in front and behind the aggregates. This results in the observed shear cones as presented in Figure A-8.

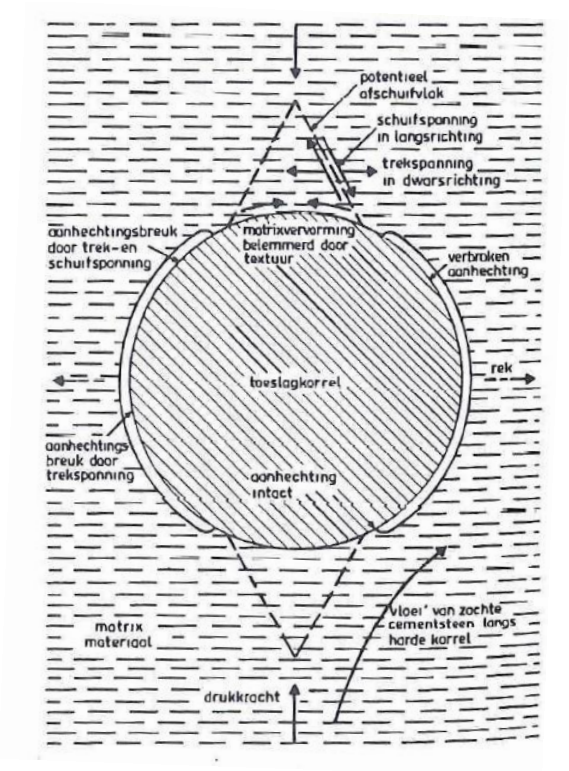

Figure A-8: Compression analysis at meso-level (Reinhardt, 1985).

Failure proceeds along the sides of the shear cones. The overall sample failure mode is strongly dependent on the stiffness ratios between matrix and inclusion. When the concrete hardens, observed in the stress-strain diagram (under compression), de-bonding cracks may already develop. The non-linearity in the stress-strain diagram increases with increasing number and size of (micro)cracks. However when the ratios between aggregate, matrix and interface strength are almost the same, the stress-strain behaviour will approximate linearity. A compressive stress-strain analysis can be done in a compression test. This test can either be load controlled or strain controlled. When load controlled, (sudden) brittle failure is observed, while when strain controlled the softening character can be observed. Boundary conditions and size effects (in testing) are important around and after reaching peak strength. Cracking has significant influence on the stress-strain relation, though the micro cracks in the regime before peak strength are small enough to have no influence (van Mier, 1998).

At peak strength the material fails, denoted by magnitude zero of the modulus of elasticity, as plastic strains accumulate rapidly (Figure A-7). Stress is released and (plastic) strains are generated rapidly. Just before reaching peak strength, at 80-90%, the volume is at minimum. At minimum volume the material will start to dilate and the initiated lateral (micro) cracks become so large that the volume increases despite of the large axial compaction. After reaching minimum volume (of the sample) by compaction and subsequently reaching peak strength cracking has become unstable in that phase. At peak the critical crack length is thus reached. The behaviour occurring after reaching peak strength (Figure A-7) is called softening. Softening is increased straining with a decrease in strength, which is the result of cracking. Softening can only be observed when a the compression test is strain controlled instead of load controlled. The load that can be carried by the concrete decreases with an increase of crack propagation (as in the softening regime). One of the processes that occurs in the softening regime is, unloading occurs in un-cracked regions. Besides, localisation of strains, leading to

a shear crack, occur in the post-peak regime under uniaxial compression. It can be stated that highly non-uniform deformation occurs, which can be related to the evolution strength capacity after reaching peak strength. At last the concrete sample under compressive loading completely fails by the excessive formed cracks. The material strength after failure is in that case governed by the residual strength.

A.1.3 Tensile loading

Tensile loading is the opposite of compressive loading. In Cartesian stress space it means that the major and or minor principle stress have a positive sign instead of a negative sign. A similar stress-strain curve during tensile loading as in compressive loading is followed as shown by Cornelissen, Hordijk and Reinhardt (Figure A-9) (1986).

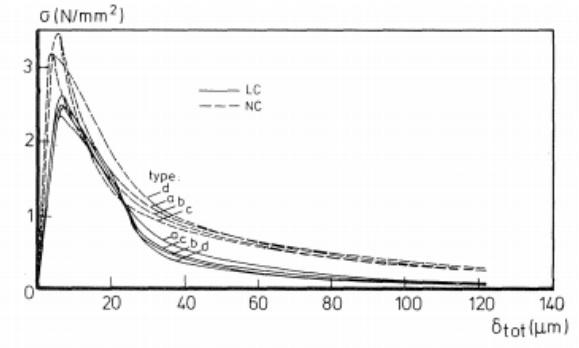

Figure A-9: Stress-deformation results of concrete under tension by experiments of Cornelissen, Hordijk and Reinhardt (1986).

Though, besides the difference in absolute magnitude of tensile and compressive strength, cracking plays a (more) dominant role during tensile loading. Tensile failure is always a discrete phenomenon. Describing tensile loading for the part till cracking occurs a stress-strain relation should be used. While for cracked concrete material a stress-crack opening relation has to be used as proposed by Hordijk (1991) (Figure A-10).

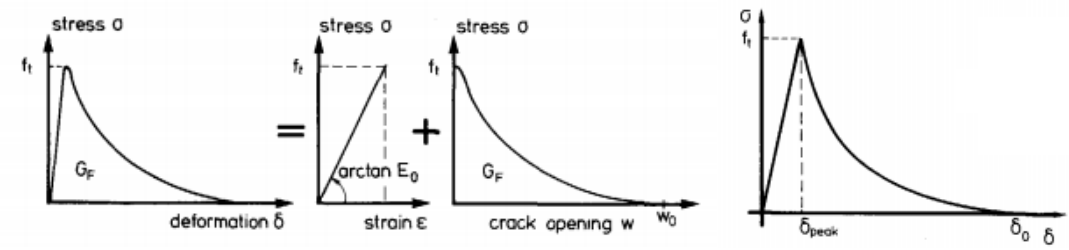

Figure A-10: Theoretical and non-linear modelling of stress-strain/crack opening behaviour of concrete subjected to tensile loading (Hordijk, 1991).

The mathematical un-cracked stress-strain relationship under tensile strength can be described as in equation A.2, and A.3 when the stress exceeds 0,9 f_{ctm}.

$$\sigma_{ct} = E_{ci} * \epsilon_{ct} \; for \; \sigma_{ct} \leq 0.9 f_{ctm} \; (A.2)$$

$$\sigma_{ct} = f_{ctm} * \left(1 - 0.1 * \frac{0.00015 - \epsilon_{ct}}{0.00015 - \frac{0.9 f_{ctm}}{E_{ci}}} \right) for \; \sigma_{ct} \geq 0.9 f_{ctm} \; (A.3)$$

When the tensile stress is around 90% of the tensile strength micro-cracks start to develop, reducing the stiffness. Applying a higher load results to the fact that micro-cracks start to turn into discrete cracks. During the fracture process the fictitious crack opening w can be used as a governing parameter for the stresses and deformations in the material. For a cracked section a bi-linear relationship can be found between stress and crack width, as is also described by the equations given above. The bi-linear relation between tensile stress and crack width is determined by the fracture energy. The concept of fracture energy will be explained in more detail in paragraph A.1.4. The un-cracked stress-strain relationship as well as the stress-crack opening relation are visualised in Figure A-11.

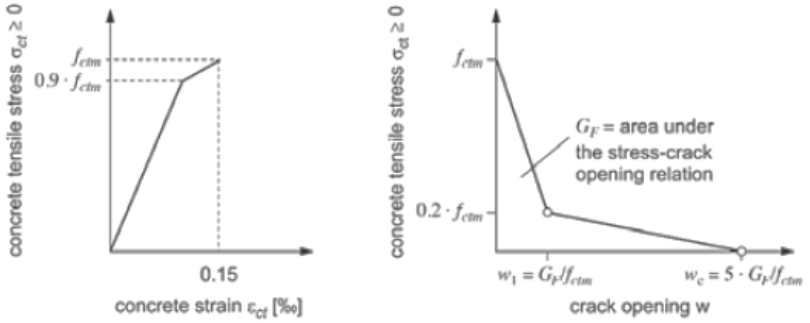

Figure A-11: un-cracked stress-strain diagram and stress-crack opening diagram under tension (CEB-FIP, 2010).

The cracks caused by tensile stresses will grow, in principle, perpendicular to the loading direction. A difference between cracking due to tensile stresses and compressive stresses, is the cause. Under tensile loading pores play a major role in concentration of (tensile) stresses, increasing the cracking rate. In contrast to compressive loading failure under tensile loading is local. In certain areas cracking will be initialised, while in other areas the concrete remains intact. Due to the fact that cracking under excessive tensile loading is a local phenomenon, straining is localised in the cracking zone. When forces are still transferred through (micro-)cracks, the crack is called fictive. The presence of a fictive crack does not have a significant influence on the material behaviour. Though when significant softening takes place due to cracking, the strength drops to (nearly) zero. In those cases the material behaviour is certainly determined by cracking.

Furthermore, if somewhere in the material a crack is initiated, it can be considered that that crack is present over the whole length of the cross-section. Taking this into account it can be supposed that the material will not have tensile strength anymore. The reinforcement has to be able take up the tensile forces as soon as a crack is initiated. A small delay in transfer of the tensile stresses from the material to the reinforcement causes the propagation of the crack over the length of the whole cross section. As soon as the reinforcement takes over the tensile stresses, the crack is limited and partly closed by the pressure in the concrete and the effect of the reinforcement. The crack will therefore not be visible but as in the concept of fracture mechanics, the crack will be present. Detailed insight in the phenomenon of cracking can be provided by means of the concept of fracture mechanics (energy).

A.1.4 Fracture mechanics

A basic principle in fracture mechanics is that a crack is always present. A crack will grow under circumstances and will finally lead to failure of the material. Two different criteria for determining the growth of a crack can be adopted. The first criterion is based on the stress distribution near a

sharp crack in a particular disk cross-section. This criterion is not used in the description of the behaviour of concrete by the shotcrete material model and will therefore not elaborated any further. The second criterion used in fracture mechanics to describe the occurrence and growth of cracking is based on an energy principle (Figure A-12).

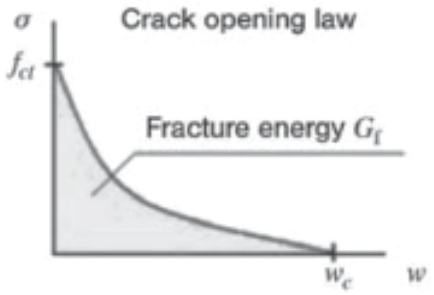

Figure A-12: Crack opening law based on the energy principle (CEB-FIP, 2010).

When using the energy criterion, an energy balance is used to predict (the growth of) cracking. If the initial crack length (a) grows by with δa, the force decreases and elastic energy will be released (Figure A-13). If the crack a grows with length δa, the force decreases and the energy 0AC is released.

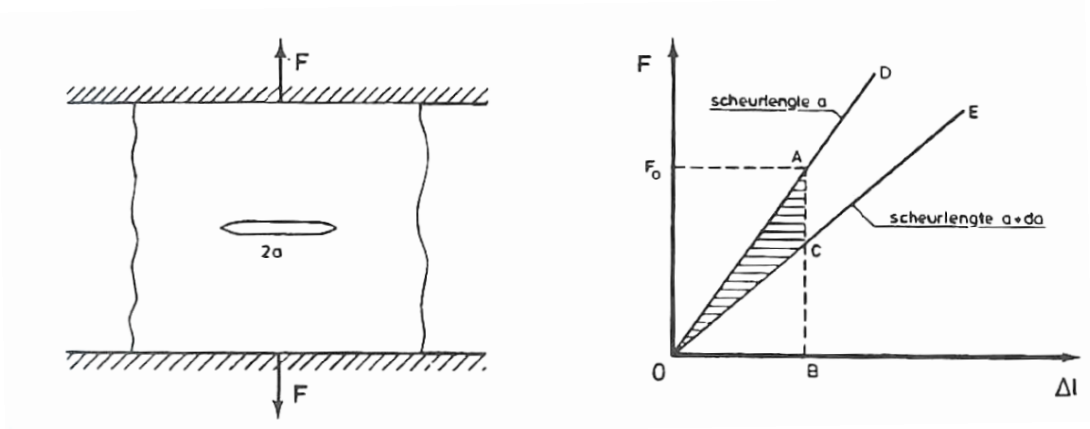

Figure A-13: Elastic energy 0AB with crack length a and 0CB at crack length $a + \delta a$ released in 0AC (Reinhardt, 1985).

Increasing the load leads consequently to a higher magnitude of energy release. Griffith (1921) found that the energy released by the growth of the crack is equal to the energy needed for an increase in cracking. In mathematical terms this relationship can be described as follows:

$\frac{\delta U}{\delta a} = \frac{\delta W}{\delta a}$ with $U =$ the elastic energy (released) and $W =$ the energy required (for a δa increase in length). $\frac{\delta W}{\delta a}$ can be called R and is defined as the crack resistance.

The energy release rate G can be described by $\frac{1}{2}\frac{\delta U}{\delta a}$. The crack resistance can assumed to be constant, wherefore the energy release rate has to meet a critical value before the crack will grow. The critical energy release rate in elastic material for an elliptical crack is described in equation A.4.

$$G_{Ic} = \frac{\pi\sigma^2 a}{E} \; or \; \sigma_c = \sqrt{\frac{EG_{Ic}}{\pi a}} \quad (A.4)$$

When considering elasto-plastic material, the deformation energy is much larger than the surface energy, called the energy requirement to initialise a crack. In common fracture mechanics, the work has to be used. Assuming linear elastic facture mechanics, the fracture criterion is given in equation 2.5.

$$G_{IC} = \frac{K_{IC}^2}{E} \quad (A.5)$$

The problem using a linear elastic or elasto-plastic approach is that the real behaviour is characterised by a softening branch, including fracture work. In Figure A-14 the different constitutive behaviour descriptions, linear elastic, elasto-plastic and elasto-plastic including strain softening, are visualised.

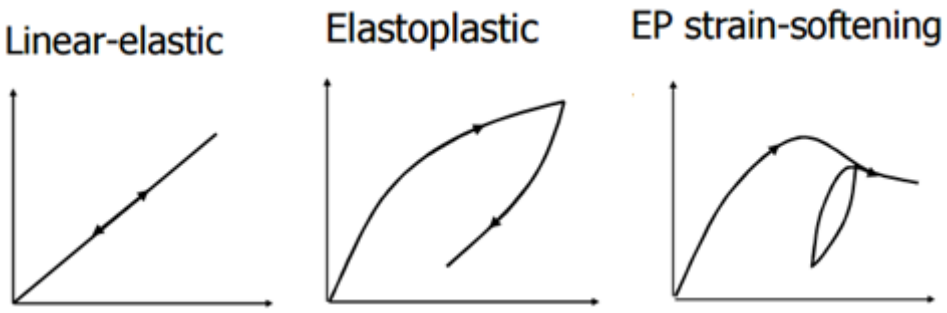

Figure A-14: Constitutive behaviour descriptions: Linear elastic (LE), elasto-plastic (EP) and EP strain softening (modified from: (Brinkgreve, 2015)).

The fracture work needed in reality is significantly smaller than for fully plastic material. The energy criterion G_{IC} can be used when considering that the area under the $\sigma - \epsilon$ diagram is equal to the total fracture energy G_f. Taking in mind the (uncertain) stress distribution in the material near the crack (Figure A-15), a linear elastic approach can only be used when the dimensions of the structure are large enough. The minimum dimension can be considered as three times the characteristic length $l_{ch} = \frac{G_F E}{f_t^2}$ according to Hillerborg et al. (1976) when using linear fracture mechanics. Hillerborg et al. (1976) states that using fracture mechanics, elastic deformations and crack opening, for concrete in FEM is better than using the tensile strength as only fracture/failure criterion.

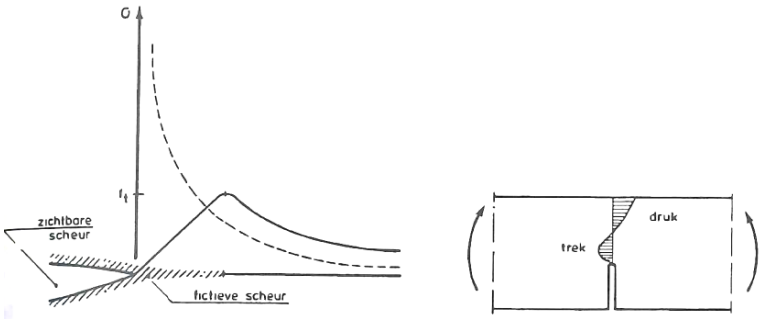

Figure A-15: The stress distribution according to the fictitious crack model near the crack and in the concrete (Reinhardt, 1985).

The fracture energy of concrete G_F [N/m] according to the CEB-FIP model code (2010) can be described as the required energy to propagate a tensile crack of unit area. This energy should be determined by uniaxial tension tests or three-point bend tests on notched beams. The fracture energy for normal weight concrete is determined by the size of a structural member, the depth of the ligament above the crack, water/cement ratio, the maximum aggregate size, the curing conditions and the age of concrete. Besides determining the fracture energy based on experimental data, it is also possible to relate the fracture energy to the mean compressive strength (equation A.6).

$$G_F = 73 * f_{cm}^{0.18} \ (A.6)$$

Two different types of crack models are currently used in numerical calculations: the discrete crack model and the smeared crack model (Figure A-16).

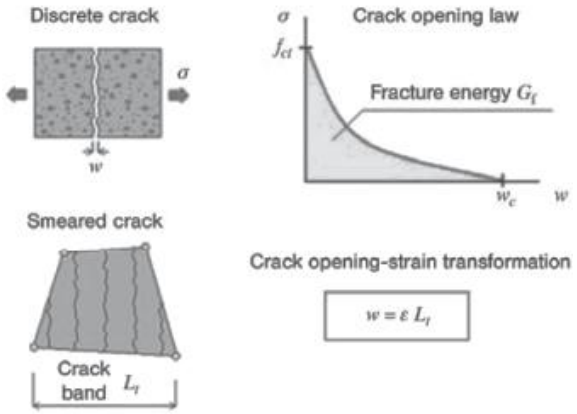

Figure A-16: Constitutive law of crack opening for discrete and smeared crack models (CEB-FIP, 2010).

In the discrete crack model, the crack is formed at the interface between two elements. When the crack opens, the boundary conditions will change. The fracture properties are described by a constitutive model. Modelling crack propagation requires re-meshing and mesh refinement near the crack tip. In the smeared crack model the crack is modelled by the concept of orthotropic damage in a certain area assigned to an element. When the crack propagates the tensile stresses are localised in a certain band width, therefore the crack is modelled by a crack band. The crack band is the result of the process of softening of the stress-crack opening law. When many cracks occur, which is often the case in practice, the smeared crack model is more suitable (CEB-FIP, 2010). Three parameters are needed in a smeared crack model to describe the constitutive behaviour: the tensile strength, the shape of the softening function and the fracture energy. The cracks are caused by strain localisation when the tensile strength is reached. The element size in reinforced concrete structures should be small, as small crack spacing can occur when the reinforcement is close to each other.

A model that could be used to describe crack propagation, by simulating the distribution of stresses around the crack tip more realistically, is a cohesive model (Reinhardt & Xu, 1999). A cohesive model is based on a traction-separation law. The crack extension resistance can be determined considering a cohesive force during the fracture process. The cohesive force can be described by the softening traction-separation law. This method is used, by for instance ABAQUS and DIANA, when reinforced concrete structures have to be modelled. The continuum elements in the model are not damaged when using a cohesive model. Instead cohesive interface elements are defined between the

continuum elements. These elements open when damage occurs and lose their stiffness at failure resulting in a disconnection of continuum elements (Scheider, Cohesive model for crack propagation analysis of structures with elastic-plastic material behaviour Foundations and implementation, 2001).

A.1.5 Multi-axial loading

Biaxial compressive loading, plane strain, reduces the potential of cracking, due to an additional "confining" pressure. Though when loading simultaneously in compression and tension will enlarge the cracking potential. During biaxial loading, failure caused by cracking will occur in the plane perpendicular to the plane which is not loaded. When considering the case that an element is subjected to a compressive load and a tensile load, cracking will occur perpendicular to the tensile stress. Under tri-axial loading cracking will be prevented due to the fact that the confining pressure counteracts the crack initiating force. The tensile stress is suppressed by the additional compressive load. Therefore an confining pressure will lead to an increase in axial strength.

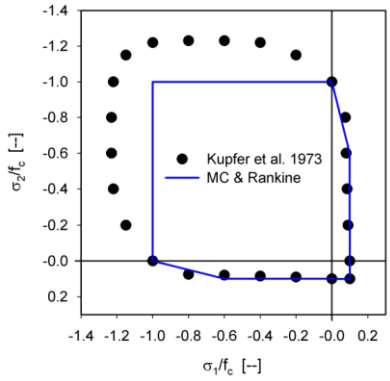

Figure A-17: Failure conditions under biaxial loading and the underestimation of strength when using the MC failure criterion (Schädlich & Schweiger, 2014b).

Behaviour under biaxial loading can be characterised by the principal stresses σ_1 and σ_2, the uniaxial compressive strength f_c and the tensile strength f_t. In Figure A-17 the failure surface in biaxial loading is visualised. It is shown that in the area loaded by two compressive loads an increase of strength takes place. The maximum strength (increase) can be found at the ratio $\frac{\sigma_1}{\sigma_2} = \frac{1}{2}$. If one load is tensile, it is shown that the strength decreases. The failure criterion for multiaxial loaded can be described by the ultimate strengths during uniaxial loading. The behaviour under compressive, respectively tensile loading can be described quite well using the Mohr-Coulomb criteria. The hypothesis by Mohr-Coulomb is that if the stress combination $\sigma - \tau$ touches the failure criterion (based on ϕ, c) failure occurs (Figure A-18).

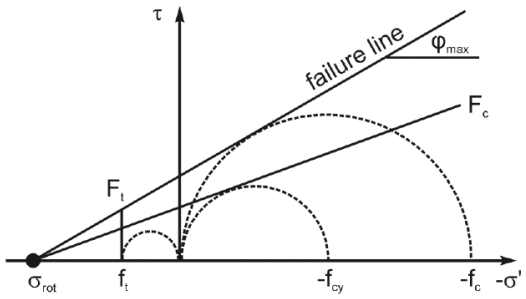

Figure A-18: Mohr-Coulomb yield (F_c, F_t)/ failure criterion with a tension cut-off (Schädlich & Schweiger, 2014b).

A tension cut-off (a circle in the tensile area) is often used to model behaviour more realistically. Modelling realistic stress-strain behaviour requires besides realistic failure criteria also a criterion at which yielding (plastic straining) starts to occur and a criterion describing the occurrence of instable growth of cracking.

A.1.6 Shear

Shear stresses are stresses perpendicular to normal (and principal) stresses in Cartesian, respectively principal stress space. In Figure A-5 the shear stresses are for instance represented by σ_{xy} and σ_{xz} on the plane of normal stress σ_{xx}.

In un-cracked material shear stresses do not exist, but are only used for calculation purposes. The behaviour of un-cracked material is governed by principal stresses. Nevertheless often shear stresses are taken into account. The reason is that on the one hand the stresses are determined in a fixed coordinate system, as can be seen in the Cartesian stress space (Figure A-5), and on the other hand because within the material often interfaces between different elements are present with a less stiff and strong behaviour. A crack is the result of an element being subjected to high tensile stresses or large deformations. A crack is a discontinuity in the material with different characteristics than the material itself. The stresses have therefore to be divided in normal stresses perpendicular and shear stresses parallel to the crack direction (Figure A-19). Shearing is dependent on the contact (area) and friction between grains. Together with the acting normal stress this determines the resistance against shearing.

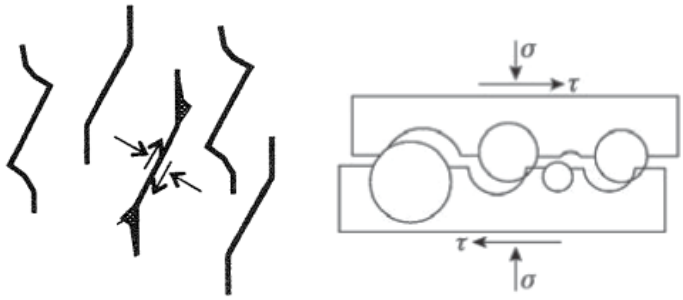

Figure A-19: Normal and shear stresses among a crack (modified from: (Reinhardt, 1985; CEB-FIP, 2010)).

The maximum resistance against shearing (shear stress) in a fracture surface is determined by the shear resistance of the reinforcement (Walraven & Reinhardt, 1981), as described in equation A.7.

$$\tau_{max} = 0.85\, f_{ck,cube}^{0.36} * \left(\rho * f_{sy}\right)^{0.09 f_{ck,cube}^{0.46}} \quad (A.7)$$

τ_{max} = shear strength

ρ = reinforcement percentage

f_{sy} = yield strength of steel

$f_{ck,cube}$ = Characteristic concrete cube compressive strength.

Increasing the amount of reinforcement will lead to an increase in (shear) strength. The normal forces on the fracture surface are excited by a confining pressure or the presence of rebar perpendicular to the crack direction. If the two sides of a fracture displace parallel to each other the

crack will always tend to open (dilatancy). Preventing the opening of such a crack by for instance rebar, the shear resistance is increased resulting in the fact that for further opening of the crack is only possible by a further increase in shear stress.

A.1.7 Shrinkage

Another cause of cracking are deformations induced by the phenomena of shrinkage or swelling. Both can be the result of chemical and physical processes. Cracking is only induced by these phenomena when the material movement (expansion or shrinkage) is constrained. Deforming during constraining conditions initiates tensile stresses when shortening, and compressive stresses when elongating. These stresses, by imposed deformations, often occur in statically undetermined structures. As shrinkage leads to tensile stresses and the concrete tensile strength is low, cracking is probable to occur. Reaching the ultimate compressive strength, by compressive stress induced by swelling, is not likely to occur and therefore swelling does seldom induce cracking (or even failure).

In more detail, shrinkage can be caused by many processes. The following types of shrinkage are distinguished:

- Capillary shrinkage
- Chemical shrinkage
- Autogenous shrinkage
- Hygric shrinkage (dehydration)
- Carbonic shrinkage

The CEB-FIP model code (2010) provides an estimation for shrinkage strains ($\epsilon_{cs,50y} * 10^3$) after a 50 year duration of drying for ordinary structural concrete and for normal weight high strength concrete (Table A-2 and Table A-3). The values in Table A-2 and Table A-3 are dependent on the atmospheric conditions as well as the notional size, which is on itself dependent upon the cross-sectional area A_c and the perimeter of the member in contact with the atmosphere u.

Table A-2: Estimation of total shrinkage strains $\epsilon_{cs,50y} * 10^3$ for ordinary structural concrete (till C50/60) with a 50 year reference period (CEB-FIP, 2010).

Dry atmospheric conditions (RH=50%)			**Humid atmospheric conditions (RH=80%)**		
Notional size $2A_c/u$ [mm]					
50	150	600	50	150	600
-0.60	-0.60	-0.49	-0.38	-0.38	-0.31

Table A-3: Estimation of total shrinkage strains $\epsilon_{cs,50y} * 10^3$ for normal weight high strength concrete (>C50/60) with a 50 year reference period (CEB-FIP, 2010).

Dry atmospheric conditions (RH=50%)			**Humid atmospheric conditions (RH=80%)**		
Notional size $2A_c/u$ [mm]					
50	150	600	50	150	600
-0.51	-0.51	-0.44	-0.37	-0.36	-0.32

A.1.8 Creep

Creep is besides initial, shrinkage and thermal strain another factor determining the total strain (equation A.8).

$$\epsilon_c(t) = \epsilon_{ci}(t) + \epsilon_{cc}(t) + \epsilon_{cs}(t) + \epsilon_{cT}(t) \quad (2.8)$$

Two different processes take place in time: creep and relaxation. Creep is the process of deformation in time under constant load. Relaxation is the stress relief in time under constant deformation. The magnitude of creep and relaxation are influenced by internal factors and external factors. The influencing internal factors are: kind of cement, the cement proportion, the water/cement ratio, the admixtures and additives, the moisture content, the hydration time and the geometry of the construction. The influencing external factors are: relative humidity, temperature (differences), loading configuration and the type of loading.

Two different types of strains are initiated from the beginning. Besides the elastic strains also creep strains are immediately initiated when loading (Figure A-20). Creep strains increase in time while elastic strains do not increase under constant load. The ratio between creep strains and elastic strains of concrete at an age of 28 days is defined as the creep coefficient $\phi_c = \delta_c/\delta_E$. The creep coefficient is a function of concrete composition, the environment and time. The relaxation coefficient can be defined as the ratio between the force needed at starting time to initiate a certain displacement and the force needed at an arbitrary point in time to initiate the same displacement ($\psi = \frac{F}{F_0} = \frac{\sigma}{\sigma_0}$). Creep will introduce additional displacement in time and can be seen as unfavourable, when not taken into account during the design process. In contrast, relaxation can be regarded as a favourable process due to the fact that by stress relief in time, cracking is less likely to occur.

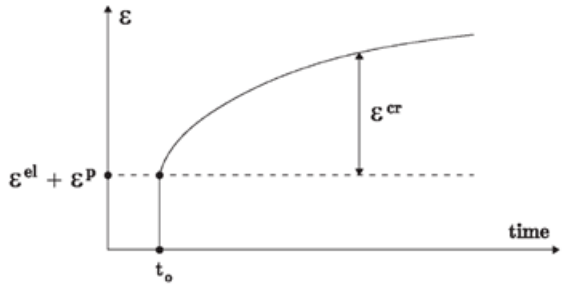

Figure A-20: Creep straining (Schütz, Potts, & Zdravkovic, Advanced constitutive modelling of shotcrete: model formulation and calibration, 2011).

Creep strains consist of two parts: creep recovery $\epsilon_{c,r}$ and irreversible $\epsilon_{c,ir}$ strains. The irreversible part represents the greatest proportion of the creep strains. The reversible part is the effect of uneven distribution of elastic strains of the gel particles within the concrete. The irreversible part is governed by the re-bonding of moved, due to loading, gel particles and by drying. When the creep strains are linear related to stress, the creep factor is constant (equation A.9).

$$\epsilon_{c,sp} = \frac{\epsilon_c}{\sigma} = \frac{\phi}{E} \quad (2.9)$$

This holds till an upper limit of $\sigma \leq 0.4\, f_{cm}$ is reached. When the stress exceeds 0.4 f_{cm} a non-linear relation between stress and creep strain is observed and has to be adopted in calculations. The cause of a observed non-linear relation when exceeding a particular percentage of the cylindrical strength

is the occurrence of micro-cracking at that point. Micro-cracking causes a more than proportional increase of creep.

Creep is mainly a long-term process. Long-term creep strains can be divided into basic creep and transient creep. Basic creep is a function of time, mixture properties, temperature and humidity, while in addition transient creep also concentration anomalies play a role. Initiated internal stresses have also to be taken into account when considering creep strains. These internal initiated stresses are caused by irregular distribution of humidity and temperature within the material. Locally this can lead to high stress areas causing cracking of the material, being also responsible for the fact that creep strains are non-linear.

Creep can be modelled with the use of rheological models. Rheological models use linear visco-elastic relations in combination with time dependent behaviour to describe material behaviour. Rheological models are based on integral and differential equations to describe visco-elastic behaviour and provide a (more) direct physical interpretation of the process. The Maxwell-element or the Voigt-Kelvin element (Figure A-21) are in most cases used to describe strain behaviour of concrete in time. The Maxwell element is based on the principle that under loading both components are loaded and deformed equally. When unloading, the spring relaxes while the dashpot remains in its deformed state. In the Kelvin element the stiffness of both components determines the load distribution over both components. At the start of loading, the deformation is equal to zero and the force is entirely taken by the dashpot. In time the dashpot is subsequently compressed, leading to loading of the spring element and (additional) deformation. In unloading, the deformation decreases gradually due to relaxation and after some time the deformation is completely recovered. Using more elements in a rheological model and introducing time dependent stiffness and strength of concrete, taking into account hydration, leads to a more realistic simulation of material behaviour under loading.

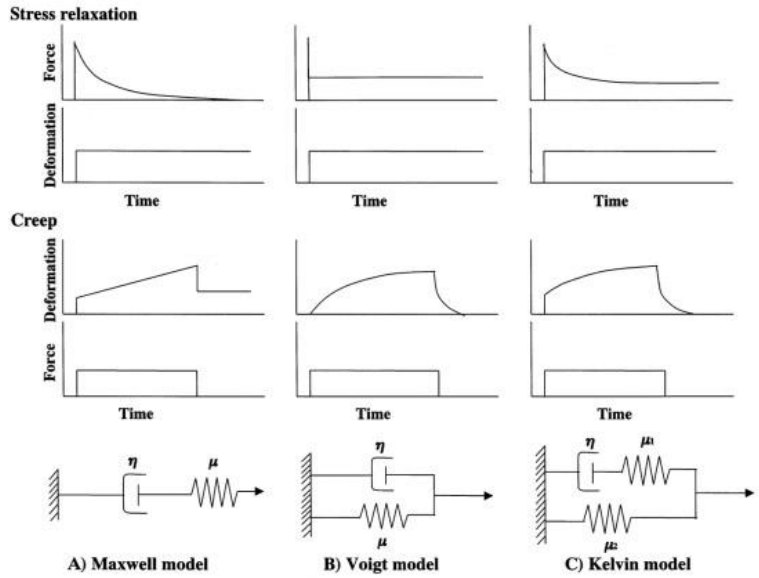

Figure A-21: Viscoelastic behaviour with rheological models; Maxwell, Voigt and Kelvin model (Tanaka & van Eijden, Biomechanical Behavior of the Temporomandibular Joint Disc, 2003).

In practice often the CEB-FIP model code (2010) is used to predict and model creep strains. In the CEB-FIP model code a detailed mathematical description to model the different parts of creep strain

is provided. Also the exact formulation of the visco-elastic constitutive equations to be used are considered. In the model code a distinction is made between basic creep and drying creep, which together determine the total creep (coefficient). For normal weight concrete (between C20 and C50) and for higher strength concrete (C60 - C100) the creep coefficient can be estimated according to Estimation of creep coefficients for ordinary structural concrete (till C50/60) after 50 years of loading Table A-4 and Table A-5, which are provided below.

Table A-4: Estimation of creep coefficients for ordinary structural concrete (till C50/60) after 50 years of loading (CEB-FIP, 2010)

Age at loading t_0 [days]	**Dry atmospheric conditions (RH=50%)**			**Humid atmospheric conditions (RH=80%)**		
	Notional size $2A_c/u$ [mm]					
	50	150	600	50	150	600
1	4.8	4	3.3	3.2	2.9	2.6
7	3.5	2.9	2.4	2.4	2.2	2
28	2.7	2.3	1.9	1.9	1.7	1.5
90	2.1	1.8	1.5	1.5	1.3	1.2
365	1.6	1.3	1.1	1.1	1	0.9

Table A-5: Estimation of creep coefficients for normal weight high strength (C50/60) concrete after 50 years of loading (CEB-FIP, 2010)

Age at loading t_0 [days]	**Dry atmospheric conditions (RH=50%)**			**Humid atmospheric conditions (RH=80%)**		
	Notional size $2A_c/u$ [mm]					
	50	150	600	50	150	600
1	2.3	2.0	1.7	1.7	1.6	1.5
7	1.7	1.5	1.3	1.3	1.2	1.1
28	1.3	1.1	1.0	1.0	0.9	0.9
90	1.0	0.9	0.8	0.8	0.7	0.7
365	0.7	0.7	0.6	0.6	0.5	0.5

A.1.9 Stiffness

Another important material property is stiffness. The material stiffness is described by the modulus of elasticity. The stiffness determines the strain behaviour of concrete under stress and is related to the strength. The modulus of elasticity is describing the stress-strain relationship in general, where creep is also an aspect of. The modulus of elasticity is according to the CEB-FIP model code (2010) directly dependent on the mean compressive strength, f_{cm}, at an age of 28 days. For normal strength concrete (<C55) the modulus of elasticity at the concrete age of 28 days can be calculated according to equation A.10.

$$E_{cm} = E_{ci} = 21500 * \alpha_E * \left(\frac{f_{cm}}{10}\right)^{\frac{1}{3}} \quad (A.10)$$

This formulation for the tangent modulus of elasticity at the origin of the stress-strain diagram is used in case of uniaxial compression and -tension. An approximation of the stiffness can be made by using the secant modulus of elasticity E_c between $\sigma_c = 0$ and $0.4\ f_{cm}$. For long-term loading, design

values and the according irreversible strains have be taken into account. A reduced or secant modulus of elasticity (equation A.11), depending on the concrete class, is used in those cases and can be calculated as follows:

$$E_c = \left(0.8 + 0.2 * \frac{f_{cm}}{88}\right) * E_{ci} = \alpha * E_{ci} \; when \; \sigma_c \leq 0.45 \, f_{ck}(t_0) \; (A.11)$$

$f_{ck}(t_0) =$ the characteristic compressive strength at an age t_0; the age at loading.

The different elasticity modulus can be visualised in a stress-strain diagram (Figure A-22).

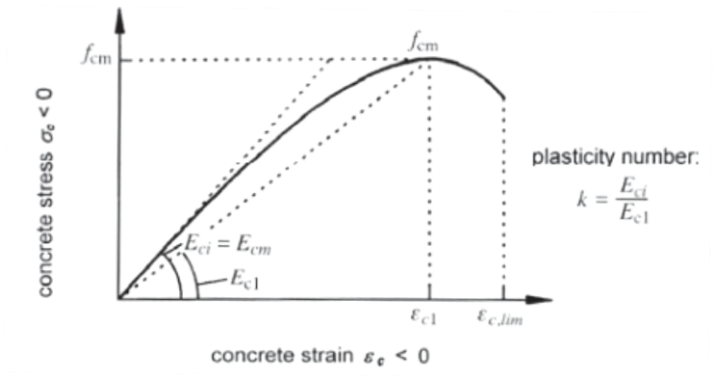

Figure A-22: Visualisation of different E-modulus in a stress-strain diagram (CEB-FIP, 2010).

The values for the tangent modulus and the reduced modulus of elasticity for normal strength concrete are given in Table A-6.

Table A-6: Tangent and reduced modulus of elasticity for normal strength concrete according to CEB-FIP model code (2010).

Concrete grade	**C12**	**C16**	**C20**	**C25**	**C30**	**C35**	**C40**	**C45**	**C50**	**C55**	**C60**
E_{ci} [GPa]	27.1	28.8	30.3	32.0	33.6	35.0	36.3	37.5	38.6	39.7	40.7
E_c [GPa]	22.9	24.6	26.2	28.0	29.7	31.4	33.0	34.5	36.0	37.5	38.9
α	0.845	0.855	0.864	0.875	0.886	0.898	0.909	0.920	0.932	0.943	0.955
Concrete grade	**C70**	**C80**	**C90**	**C100**	**C110**	**C120**					
E_{ci} [GPa]	42.6	44.4	46.0	47.5	48.9	50.3					
E_c [GPa]	41.7	44.4	46.0	47.5	48.9	50.3					
α	0.977	1.0	1.0	1.0	1.0	1.0					

When creep is taken into account another expression (equation A.12) for the stiffness has to be used. This expression is based on the creep factor and the tangent modulus at a concrete age of 28 days which is 1.05 times the mean secant modulus.

$$E_{c,lt} = \frac{E_{cm}}{1 + \phi} \; (A.12)$$

Under compression concrete acts as a non-linear ($\sigma - \epsilon$) material. Concrete will act elastically under compressive loading at first. The stresses occurring during SLS can be characterised by a quasi-elastic function. When the compressive load further increases, the stresses between the particles increase

and micro-cracks will start to grow. During this quasi-elastic behaviour the growth of cracks is stable, which means that without additional loading cracks will not grow. The upper-boundary of this process is determined by the smallest element volume, which occurs at 80-90% of peak strength. Increasing the load any further will lead to progressive cracking without additional loading. The stress-strain relation for different concrete classes is given in Figure A-23. The lowest line represents a concrete class of C20 while subsequently the concrete class/strength increases up to C80.

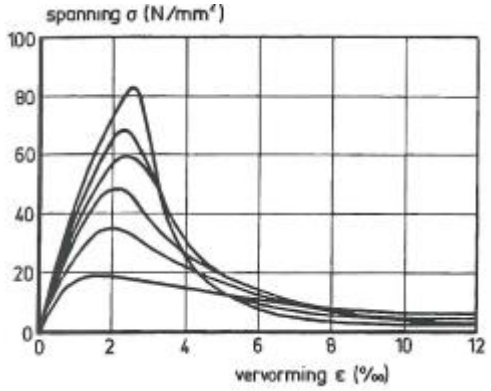

Figure A-23: Stress strain diagram for different concrete classes (Reinhardt, 1985).

The stress-strain behaviour of concrete can be described in different cases by different formulations. In Figure A-24(1) a non-linear function is described. This formulation (equation A.13) describes the behaviour of concrete when a uniaxial short-term load is experienced. Furthermore it describes the behaviour in the case that the quasi-permanent combination of stress, when creep strains play a significant role, exceeds 0,4 f_{ck}.

$$\frac{\sigma_c}{f_{cm}} = \frac{k\eta - \eta^2}{1 + (k-2)\eta} \quad (2.13)$$

With $\eta = \frac{\epsilon_c}{\epsilon_{c1}}$

ϵ_{c1} is the strain at maximum compressive stress can be determined with the help of table 3.1 NEN-EN 1992-1-1 (2011).

$k = 1.05 * E_{cm} * \frac{|\epsilon_{c1}|}{f_{cm}}$ with f_{cm} according to table 3.1 NEN-EN 1992-1-1 (2011).

For calculation of concrete cross-sections also a parabolic-rectangle stress-strain relationship could be used (Figure A-24(2)). Another stress-strain function that could be adopted in such a case is a bi-linear function (Figure A-24(3)), also called linear elastic-perfectly plastic (LEPP). The first, elastic, part is described by Hooke's law. The plastic part is determined by the limit of ($\sigma = f_{cd}$) and the ultimate compressive (failure) strength. The parabolic-rectangle and the bi-linear formulation both depend on design or characteristic strength values rather than the (higher) mean strength value. This leads to the fact that in such way there can be accounted for lower bending stiffness in the case when bending is the decisive design criterion. The according values for $\epsilon_{c1,2,3}$ respectively $\epsilon_{cu1,2,3}$ for different concrete classes can be found in table 3.1 of NEN-EN-1992-1-1 (2011) as well as in Table A-1 of this report. For higher concrete strengths than C50 the formulation slightly changes, accounting for different material response. Also the corresponding design strain values for higher strength can be found in Table A-1.

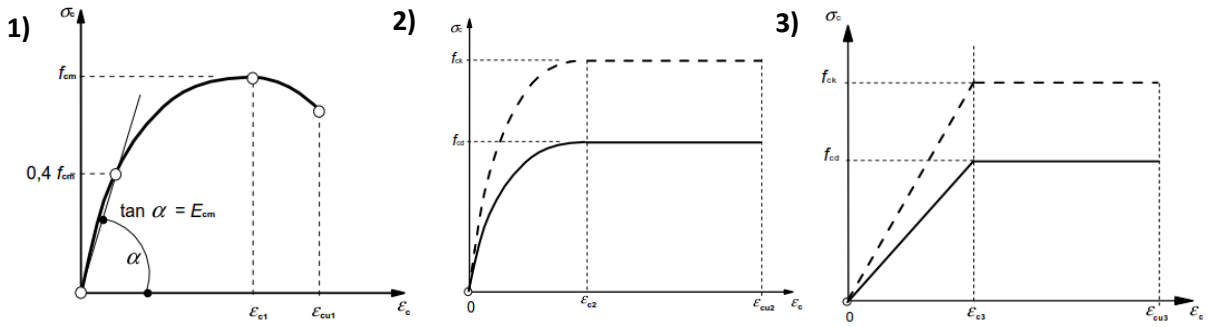

Figure A-24: Material behaviour of concrete in compression (NEN-EN 1992-1-1, 2011).

Considering confined concrete instead, the stress-strain diagram changes. Described in paragraph A.1.5, confinement leads to higher (allowable) obtained strength and strain values. The before described parabolic-rectangle stress-strain diagram can be modified such that also the behaviour taking into account confinement can be described. An addition to the superscript with the letter c for confinement, indicates the higher values for the characteristic and design strength respectively strain (Figure A-25).

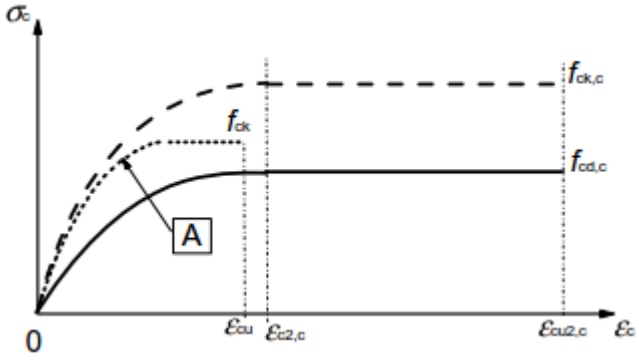

Figure A-25: Material behaviour of concrete in compression when confined (NEN-EN 1992-1-1, 2011).

A.1.10 Poisson's ratio

Another parameter describing the behaviour of concrete is Poisson's ratio. Poisson's ratio is the ratio between the axial and lateral straining under loading. Mathematical this is described in equation A.1. For a range of stresses $-0.6f_{ck} < \sigma_c < 0.8f_{ctk}$ the Poisson's ratio of concrete ν_c ranges between 0.14 and 0.26. The influence of crack formation at ultimate limit state (ULS) for designing is met by using a Poisson's ratio of 0.2.

A.2 Reinforced concrete

A.2.1 Crack limitation

Adding reinforcement to a structure subjected to bending increases the strength, due to the fact that failure does not occur at the moment when the concrete fails in tension (starts to crack). Failure occurs when the tensile strength of the reinforcement is reached, which is significantly higher. Though the fact that concrete has to crack in order to let the tensile forces to be taken up by the reinforcement also gives a risk. The risk of cracking is, as introduced before, that corrosion will occur causing failure if the crack is becoming too wide in a threatening environment. A threatening environment can be defined such that besides mechanical loads, the construction is also subjected to

physical and chemical conditions. Environmental circumstances and the effect on the (additional) concrete cover can be found in table 4.1 and 4.4 of NEN-EN-1992-1-1 (2011).

Another check has to be performed considering the limitation of cracking (NEN-EN 1992-1-1, 2011). A check regarding the yield stress, the diameter and the distance between the rebar has to be performed. Tensile stresses in the reinforcement have to be limited in order to prevent plastic strains, unacceptable initiation of cracking and excessive deformation. It may be assumed that as long as the yield stress in the reinforcement is below 0,8 f_{yk}, unacceptable cracking and deformation is prevented. Requirements of functionality of the structure can also play a role in limiting the maximum crack width. An example of such a requirement is that a structure has to be water tight. The check to be performed on the minimal concrete cover in this situation is based on serviceability limit state (SLS) (Braam & Lagendijk, 2010).

A minimum percentage of reinforcement is besides required as gradual cracking of the concrete is wished. The first crack will be initiated at the point where the concrete is the weakest. With an increase in load a second, third (and so on) crack will develop. In time over the full length of the concrete beam (and the reinforcement) small cracks will develop. At a certain moment the number of cracks will not increase any more, but the cracks will become wider when more tensile stress is experienced. A check according to NEN-EN-1992-1-1 (2011) has to be performed in order to have a safe cover as described before. In all cases the crack width has to be limited and a calculation of the minimum required reinforcement has to be performed. The amount of reinforcement required can be calculated by searching for an equilibrium between the equivalent compressive force in the concrete, before failure in compression occurs, and the tensile stress (equivalent force) in the rebar. In all cases brittle failure, failure of concrete in compression before yielding of the reinforcement, has to be avoided. The behaviour of elements under bending are governed by a un-cracked part and a cracked part at sufficient loading. In the next paragraph in more detail the influence of cracked and un-cracked concrete due to bending will be elaborated.

A.2.2 Bending stiffness

A good prediction of the behaviour of partly cracked and partly un-cracked concrete material behaviour (Figure A-26) can be formulated as in equation A.14 (CEB-FIP, 2010).

$$\alpha = \xi\alpha_{II} + (1-\xi)\alpha_I \quad (A.14)$$

α is the deformation parameter, for instance strain, a curvature, deformation or a rotation.
α_I, α_{II} are the parameters describing the behaviour of the α parameter in respectively un-cracked and cracked state.
ξ is the factor (taking tension stiffening into mind) which can be calculated as follows:

$$\xi = 1 - \beta\left(\frac{\sigma_{sr}}{\sigma_s}\right)^2$$

$\xi = 0$ for un-cracked sections.
β is the coefficient which takes the kind of loading (short-term, long- term or cyclic) on straining into account. With value 1 for short-term loading and 0,5 for long-term or cyclic loading.
σ_{sr} is the stress in the (tension) reinforcement of a cracked cross-section caused by the load-combinations which initiate the first crack.
σ_s is the stress in the (tension reinforcement) of a cracked cross-section.

In case of pure bending, $\frac{\sigma_{sr}}{\sigma_s}$ may be replaced by $\frac{M_r}{M}$.

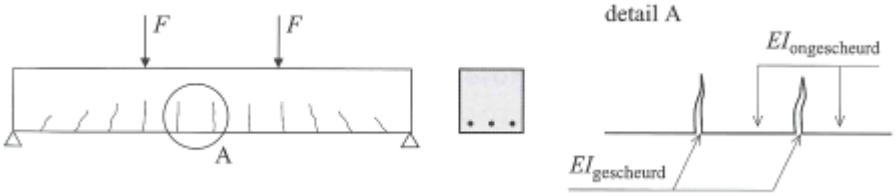

Figure A-26: Governing behaviour of uncracked and cracked part of a reinforced beam (Braam & Lagendijk, 2010).

A concrete beam is not only subjected to bending but also to shear forces. Due to the shear force excited by tensile stress or deformation, shear stresses develop in the material. In combination with bending of the beam, diagonal cracks will develop in the concrete. As is known from theory, in principal stress directions in the Cartesian stress space, perpendicular to those diagonal shear cracks, normal (tensile) stresses act on the beam. To prevent the concrete from (excessive) cracking also (shear) reinforcement has to be applied.

A.3 Shotcrete material model

A.3.1 Time dependency

Hydration of the cement paste results into an increase of stiffness and strength with time as mentioned in section 0. The shotcrete model uses the CEB-FIP model code (1990) to take an increase of the modulus of elasticity in time into account (Figure A-27). The CEB-FIP model code determines the modulus of elasticity during the hydration time by a ratio between the modulus of elasticity at day 1 and at day 28, which is the proposed time for hydration. A constant value for the modulus of elasticity is used in the shotcrete model before the start time of hydration (1 hour) and after 28 days. In reality after 28 days, as described in section 0, the concrete still gains stiffness and strength. Though in the model the material properties after 28 days remain constant. The uniaxial compressive strength is defined by a comparable expression to the evolution of the modulus of elasticity in time. The strength in time is determined by a ratio between the hydration time and the strength at day 1. As a lower bound for the strength a percentage of the strength of the material after 28 days is governing.

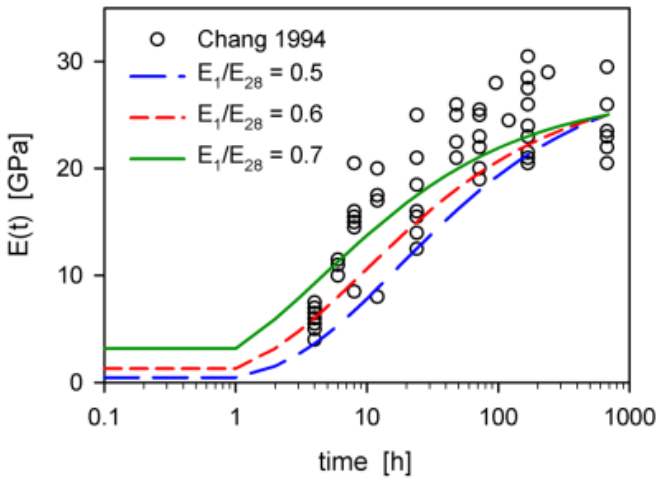

Figure A-27: Increase of modulus of elasticity in time by the Shotcrete material model using the CEB-FIP model code (1990) recommendations, matching experimental data (Schädlich & Schweiger, 2014a).

In the shotcrete model an increase in strength under straining, also called compaction or cap hardening is included. The cap of the Mohr-Coulomb yield surface grows under compressive stress . Every time the yield cap/criterion is reached, yielding (plastic straining) is initialised (in primary loading). When yielding occurs under compression the material strength increases by the fact that the major principal stress σ_3/f_c does not increase linearly with the axial strain $\epsilon_3/\epsilon_{cp}^p$. Adoption of this theoretical concept leads to the fact that the model can account for stress-strain (loading) history, the distinction between un- and reloading and the occurrence of plastic compaction in primary loading.

Another property of the model to be able to account for the ability of young shotcrete to withstand large deformations, besides the time dependent stiffness, is the plastic deformability. The high plastic ductility at early time stage is governed by a time dependent formulation of the plastic peak strain (Figure A-28). Meschke et al. (1996) proposed a tri-linear function in time to incorporate such behaviour. The plastic peak strength decreases stepwise in time and is assumed to be constant after 1 day. Hardening of the concrete results in more brittle behaviour, which is caused by an increase in stiffness and strength in time coinciding with a decrease of strain at peak strength.

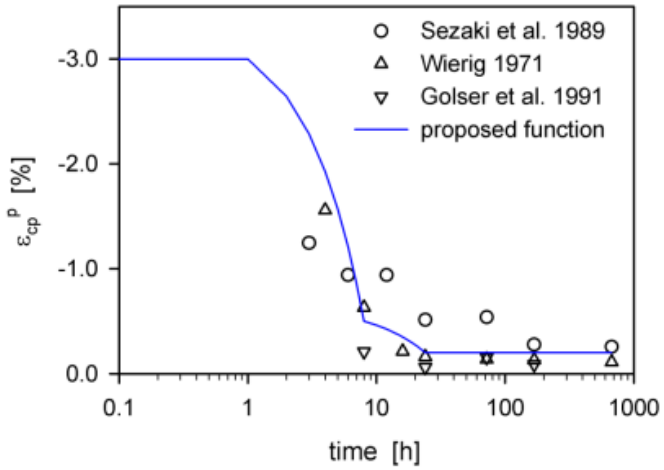

Figure A-28: Time dependency of plastic peak strain in the shotcrete model accounting for high plastic ductility at early time stage (Schädlich & Schweiger, 2014b).

Both the tensile and compressive failure strains are governed by a change of fracture energy and the final tensile respectively compressive strength. The fracture energy is regarded as input, it helps accounting for the theoretical behaviour of concrete in time. It accounts for the moment and effect of cracking when peak strength is reached. At peak strength the tensile stresses reduce while the displacement increases. The fracture energy can be defined as the energy needed to widen or start a crack per unit area and increases approaching the crack tip. The fracture energy is also a measure of the straining between the compressive strength f_{cp}^p and $f_{cf,n}$ and therefore accounts for strength reduction, depending on the magnitude of strain, during compression.

A.3.2 Other model properties

Another feature of the material model is to account for creep. Creep is modelled within the framework of visco-elasticity as is proposed by CEB-FIP (1990). Creep and relaxation are modelled according to a creep law, based on the rheology of a time-dependent Newton dashpot. The Newton dashpot is the dashpot component in the Voigt as well as in the Maxwell model (Figure A-21). The

relation between creep strains and stress is linear and determined by a creep factor as also is commended by CEB-FIP (1990). Though when material is loaded higher than 45% of the compressive strength a non-linear formulation has to be taken into account according to NEN-EN 1992-1-1 (2011), which is not adopted in the Shotcrete model. To account for shrinkage of the concrete, isotropic loss of volume with time, a formulation according to ACI 209-R92 (1992) is adopted in the model. This formulation is independent of stress state and accounts for deformation caused by the hardening and drying of the cement. Both creep and shrinkage strains are determined in the model with a reference value at half (magnitude and time) of the ultimate creep respectively shrinkage strain. Thermal deformation, expansion and contraction, due to hydration, at early ages is also accounted for. Thermal deformations at early age are modelled by a function of Schubert (1988). A function is adopted which describes the effect of temperature history (only) during cement hydration in terms of plastic straining. The thermal strains ϵ_{th} are determined by a coefficient of thermal expansion α_{th} which is constant in time and an incremental temperature parameter $\Delta T(t)$, describing the increase in hydration temperature in time. In Figure A-29 the adopted temperature history during cement hydration is given with a peak increase in temperature ΔT_{max}.

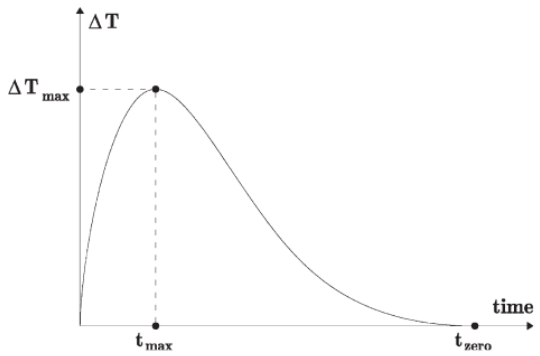

Figure A-29: Temperature history during hydration (Schütz, Potts, & Zdravkovic, Advanced constitutive modelling of shotcrete: model formulation and calibration, 2011)

Another feature included in the model are separate safety factors for the compressive and tensile strength. This gives the opportunity to do design calculations with the shotcrete model and evaluate the effects of additional safety. State variables are used in the model (during calculations) to give information about the progression of stress-strain behaviour, time dependency and creep.

A.4 Modelling diaphragm walls and piles

Diaphragm walls and piles can both be schematised as a transversely loaded beam in the subsurface, despite to geometrical and functional differences both have to modelled differently. A first difference between diaphragm walls and piles is that piles have a limited diameter (length), while diaphragm walls can be modelled as (endlessly) long elements in 2D. This difference in shape and geometry has the result that the area of influence is different. For piles a 3D soil area of 4 times the diameter below the pile and 8 times the diameter above the tip by axial loading (Xu, 2007; NEN-9997-1, 2012) and 8 times the diameter in lateral direction around the pile is influenced (Rollins, et al., 2006). While for diaphragm walls this concept is less applicable. Furthermore, flow of soil around the structure is a 3D problem as the pile has a limited diameter. Meanwhile when modelling diaphragm walls this does not play a role. To correctly model piles a 3D model should therefore be used. Though in engineering practice for a preliminary design a 2D approach can be used (Sluis, 2012). A single pile can be

modelled in 2D by a plate element, but in almost all cases more than one pile has to be considered for the design. Realistic pile modelling (in Plaxis) for different L/D ratios, the centre to centre distance between piles in a pile row and the pile diameter, is given in Figure A-30. In groups a load or deformation of a single pile has influence on the other piles, assuming a distance smaller than 8D between the areas. A diaphragm wall has an infinite length compared to a pile, wherefore plain strain (2D) modelling can be applied (realistically). Group effects do not play a role when modelling diaphragm walls.

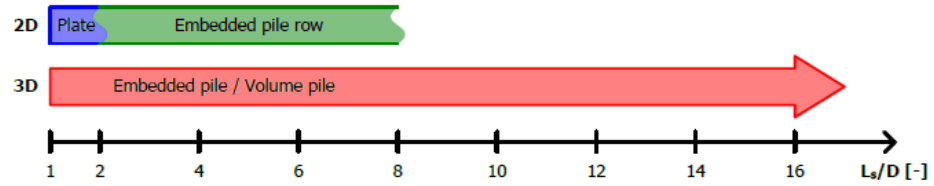

Figure A-30: Application area of modelling a pile row with various structural elements (in Plaxis 2D/3D) (Sluis, 2012).

Diaphragm walls are commonly used as a retaining wall; dealing with a relatively large lateral force compared to the normal force. In densely populated areas or near structures which are prone to cracking, installation vibrations have to be avoided (NEN-9997-1, 2012). In those situations diaphragm walls are used as retaining structure instead of a sheet pile wall, because the installation causes no vibrations and only little deformations.

The fact that diaphragm walls are reinforced and have bearing capacity, applying axial load on a diaphragm wall is possible. Two types of piles can be used, soil-displacing, installed by vibrating or hammering, and soil-removing piles, bored piles. Soil-removing piles have the advantage that vibrations and noise are limited, while soil displacing piles have a higher bearing capacity in general. Piles are commonly used as foundation, however in some cases piled walls are used as retaining structure or to provide surface stability by avoiding development of a shear plane in slopes and dikes. For foundations the axial capacity, to bear the super structure, and the lateral capacity, to take up the horizontal loads by wind or traffic on a structure, are both important (van Tol, 2006). In contrast to diaphragm walls the lateral load excited on the structure acts commonly on the pile cap rather than over the whole length of the pile. The difference in point of loading implies the use different calculation methods as different loading/deformation behaviour takes place. Furthermore the fact that the type of loading (axial, lateral or a combination of both) on a diaphragm wall and a pile can be different, the calculation methods/programs to be used is different.

Another difference when modelling laterally loaded piles and diaphragm walls are the effects of installation. A pile can be installed by using different techniques, hammering, vibrating, auguring and boring. Using soil displacing installation techniques, the behaviour of the soil after installation is influenced by for instance the densification around the shaft and at the base (van Tol, 2006). When boring piles, densification does not play a role but the relaxation of soil after removing the steel casing and the flow of bentonite/cement around the casing do have influence. A diaphragm wall can be compared to a bored pile, when considering installation techniques. Segments are dug while being filled and kept open with bentonite. After reaching the required depth and length, a casing (reinforcement) is lowered in the bentonite suspension. The segment is consequently filled with cement. The installation effects on soil properties of bored piles and (in-situ) diaphragm walls are limited (van Tol, 2006). Only minor effects of the bentonite (filter cake) and relaxation of the soil are of influence on the soil structure interaction. When soil-displacing piles (driving/vibrating) are used,

installation effects have to be taken into account when modelling as soil properties and therefore the soil-structure interaction changes.

A last aspect which influences the difference in modelling diaphragm wall structures and piles are reinforcement and anchoring. When expecting large lateral loads on a diaphragm wall, the wall has to be anchored. In normal practice piles are not anchored, however in the case of a piled wall anchors are used. The reinforcement of the diaphragm wall is such that at depth, where it is fixed, additional reinforcement is applied. Driven piles are commonly pre-stressed, but also bored piles are reinforced. Though due to the circular shape of a bored pile, the reinforcement is not the same as in diaphragm walls.

A.5 Calculation Methods

A.5.1 D-pile group & D-Sheet pile

In D-pile group the soil-structure interaction can be modelled with the use of axially and laterally loaded beams with (soil)springs. D-pile uses a 3D-space to model these situations as pile behaviour is a 3D problem. The soil springs can account for non-linear relationships according to API or Eurocode codes. D-pile group can use different soil-structure interaction models, to model this kind of behaviour. The following models can be used: Poulos model, Plasti-Poulos model, Cap model, Cap soil interaction model and a Cap layered soil interaction model.

D-sheet pile a 2D-space is used to model laterally loaded structures. The program is able to distinct passive and active lateral loads. The program is applicable to model 2D problems, in one direction endlessly long or symmetric or a single pile where the influence on the surrounding soil does not play a role. Beam elements on elasto-plastic springs are used to model soil-structure interaction, which is comparable to D-pile group.

A.5.2. Technosoft

Technosoft is a 2D software package consisting of different programs which uses the Eurocode and TGB 1990 for structural design. Different aspects can be calculated with the help of Technosoft: frameworks, beam grids, beams, reinforcement, sheet piles according to CUR 166 and piles (capacity). When modelling reinforced concrete beams it gives the opportunity to take a $M - \kappa$ diagram into account.

A.5.3 FEM: Plaxis

Integral subsurface modelling is commonly done with FEM programs. A FEM program is Plaxis 2D and 3D. FEM modelling is based on the concept of interconnection and coupling. A change in conditions in 1 element propagates through the whole mesh. Displacements and forces of soils and structures can be incorporated. By partial differential equations those two different (external) prescriptions can be taken into account. In Plaxis 2D two different model setups can be chosen for modelling the problem, plane strain or axisymmetric. Structures and foundations can be modelled by using plate elements, node-to-node anchors or embedded beams depending on the actual structure. Volume elements, given a material model, can also be used in the design. Specific (subsurface) material models are included to describe the behaviour of the modelled soil (layers) and structures realistically. Those material models use constitutive relations to capture the behaviour of real materials. Besides the modelling of mechanical behaviour also a thermal and flow analysis can be carried out. The possibility to add different construction stages with different calculation methods

(in-situ stress, drained/undrained, seepage and consolidation analysis) and the possibility to take into account loading history helps modelling situations more realistic.

A.5.4 FEM: DIANA

A structural modelling program which is also capable of modelling subsurface behaviour is DIANA. DIANA is a 2D-3D FEM software package. DIANA has the capabilities of modelling reinforced concrete structures in detail. The reinforced concrete concept is applicable in all element types namely, solids, plane stress, plane strain, axi-symmetric, shell and plate elements, beam elements and interface elements. Also for geotechnical DIANA includes features accounting for mechanical, thermal and flow loading conditions. Different material models, as the (modified) Mohr-Coulomb and modified Cam-Clay can be used for modelling the different types of soil/rock. As in Plaxis also, in-situ stress, a construction staged, drained/undrained, seepage and consolidation analysis can be carried out.

Appendix B: Modelling reinforced concrete structures

B.1 Mohr-Coulomb model

The Mohr-Coulomb model is a Linear Elastic-Perfectly Plastic model (LEPP). The input parameters of the Mohr-Coulomb model, explained in the list of symbols, are limited. Only c, ϕ, E, ν and ψ are required. A tension cut-off can be used to define different behaviour under tensile loading. Due the limited number of input parameters and a quite good representation of failure behaviour the model is often used a first order approximation. Though non-linear, time dependent and stress-dependency are not incorporated. The fact that simple hand-calculations make it possible to verify the outcome of the model gives the opportunity to test the Shotcrete model (simplified). Besides the Mohr-Coulomb model can give a first order approximation for the behaviour of a simple beam on two hinges subjected to bending and therefore a first guidance for the results of the Shotcrete model.

In chapter 3 it is mentioned that a concrete with the strength class of C30/37 is tested. The Mohr-Coulomb model input parameters are set such that the same properties concrete material properties are governing. An (effective) internal friction angle of 35 degrees is the first input, as proposed by literature (paragraph 2.2.3). The second important input parameter is the (effective) cohesion. The (effective) cohesion is another parameter defining the failure criterion as shown in equation A.2 (Brinkgreve, Kumarswamy, & Swolfs, 2016).

$$f_{2b} = \frac{1}{2}(\sigma'_3 - \sigma'_1) + \frac{1}{2}(\sigma'_3 + \sigma'_1)\sin\phi' - c'\cos\phi' \quad (A.15)$$

Under (uniaxial) compressive loading the following stress-strain curve (Figure A-31) is followed by the Mohr-Coulomb model.

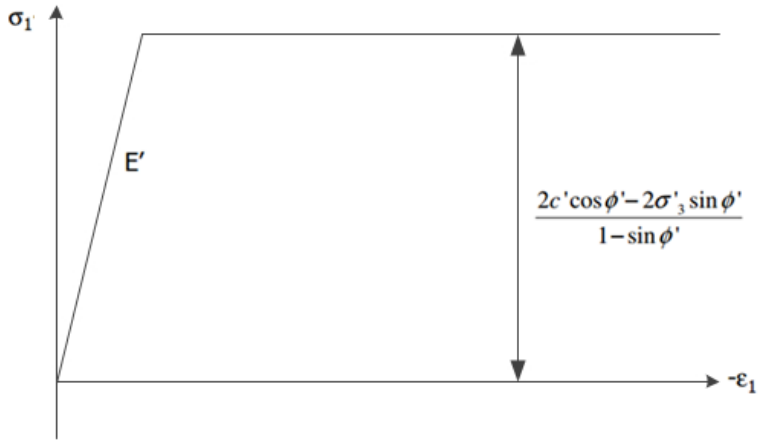

Figure A-31: Stress-strain curve Mohr-Coulomb model (theory) (modified from: (Brinkgreve, 2015)).

The value of the cohesion has to be defined such that the results in compression match C30/37 concrete material behaviour. Therefore the formulation of the elastic/plastic limit stress has to be calculated such that with an internal friction angle of 35 degrees a stress limit of 30 MPa is reached. Therefore the following formula (equation A.3) has to be solved.

$$c = (f_{ck} * (1 - \sin\phi) + 2 * \sigma_3 \sin\phi)/(2\cos\phi) \quad (A.16)$$

A value of 7808.5 kN/m^2 for the cohesion is obtained to match the compressive strength of 30 MPa. In Table A-7 the values of the initial Mohr-Coulomb model parameters are summarised.

Table A-7: Mohr-Coulomb model parameters.

Input Parameter	Value	Unit
c	7808.5	kN/m^2
ϕ	35	Deg
E	29.7E6	kN/m^2
ν	0.2	-
ψ	13	-
Tensile strength	2000	kN/m^2

In the Soil-test facility in Plaxis a uniaxial compression test is designed as a general test. The uniaxial compression test is simulated by the test configurations given in Table A-5 and Table A-6. The uniaxial compression test is strain driven rather than loaded until failure occurs. The results as shown in Figure A-32 are obtained with the Mohr-Coulomb model parameters. The major principal stress respectively strain, σ_1 and ϵ_1, are used to visualise the stress-strain behaviour. To give more insight in the deformation of the material a diagram of the volumetric strain (ϵ_v) versus the major principal strain is visualised. The major principal stress and strain consider the direction in which no shear stresses are present in the sample and besides consider the highest magnitude of the stress, respectively strain, occurring (in that direction). The volumetric strain gives the change in volume with respect to the original volume. Noted has to be that not the full 10% of compressive strain is showed. Focussed is on verifying the model outcome with the theory and therefore only the first 1% of compressive strain is regarded.

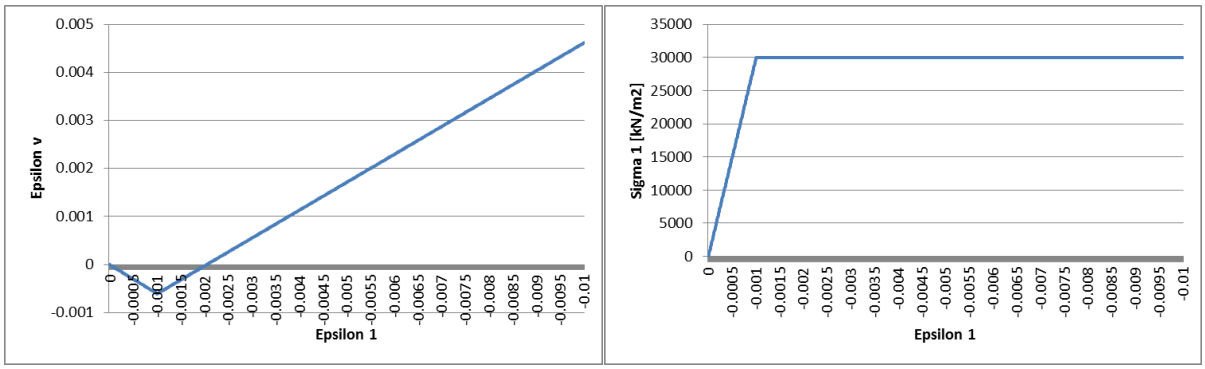

Figure A-32: Uniaxial compression test output, where the strain is a percentage of the sample (1).

The Mohr-Coulomb model reaches a compressive strength of 30 MPa when ongoing plasticity occurs. Also Poisson's ratio, the dilatancy and friction angle comply with the proposed/expected values. Poisson's ratio, dilatancy and friction angle can be back calculated by the following equation using the theory, described in Figure A-32. Comparing the tangents of the lines in Figure A-32 with the theoretical formulas and lines, considering , $\nu = 0.2$ and $\psi = 13°$, in Figure A-31 and Figure A-33 it can be concluded that the results match the theory.

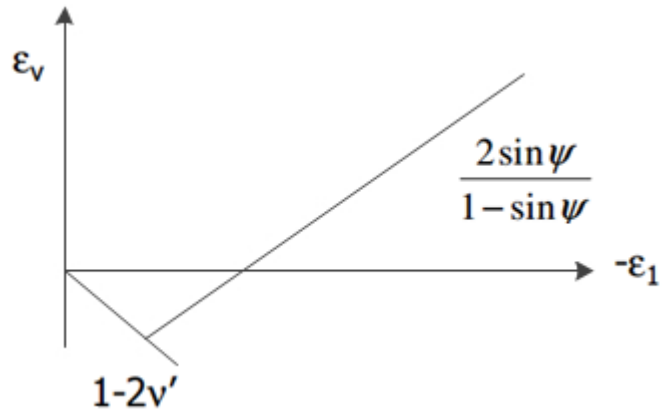

Figure A-33: Mohr-Coulomb model in ϵ_1 - ϵ_v space (modified from: (Brinkgreve, 2015)).

B.2 Shotcrete model matched with Mohr-Coulomb model

A first test for the Shotcrete material model, excluding non-linear, softening, hardening and time dependent behaviour, is to comply with the single stress-point modelling results of the Mohr-Coulomb model. The following parameter values (Table A-8) are used to comply with the Mohr-Coulomb model. The parameters below the thick line do not influence the results yet.

Table A-8: Input values Shotcrete model to match a Mohr-Coulomb model.

Parameter	Value	Unit
E_{28}	29.7E6	kN/m^2
ν	0.2	-
f_{c28}	30	MPa
f_t	2000	kN/m^2
ψ	13	Deg
E_1/E_{28}	1	-
f_{c1}/f_{c28}	1	-
f_{c0n}	1	-
f_{cfn}	1	-
f_{cun}	1	-
ϵ_{cp}^p	-0.0035	%
G_c	140.5	kN/m

The results of the Mohr-Coulomb (MC) and Shotcrete (SC) material model are visualised in Figure A-34. The input values for the Mohr-Coulomb model considering a concrete strength of C30/37 are given in Table A-8. It is shown that the results of both models are exactly similar results and comply with the expected values according to theory. Noted should be that in Figure A-34 a strain controlled uniaxial compression test up to 10% is considered.

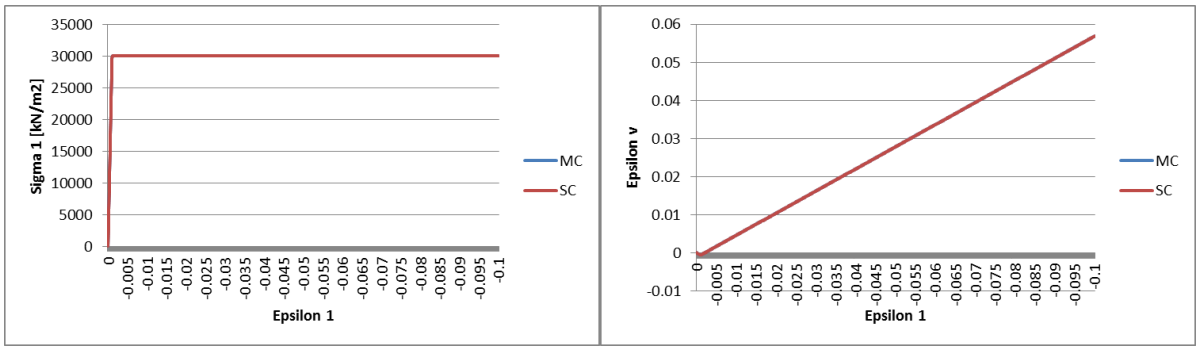

Figure A-34: Results of the Mohr-Coulomb (MC) and Shotcrete (SC) model.

B.3 Sensitivity analysis Shotcrete model

The parameter sensitivity analysis is also done with the help of the Plaxis soil-test facility. In compliance with the previous modelling, a general soil-test is used in order to simulate a uniaxial compression test (in time). To test time-independent model behaviour at first the time is progressed with specifying a load or displacement. After 1 day, a displacement is specified testing the whole range of stress-strain behaviour. The advantage of evaluating results after 1 day of hardening is that the ratio parameters (E_1/E_{28} and f_{c1}/f_{c28}) are taken with respect to day 1 and the end of hardening day 28. Therefore the influence of those parameters and simultaneously other model parameters is possible. The results of the previous model verification are taken as starting point (Table A-8), with the difference that ν and ψ are taken zero in the reference scenarios. In the sensitivity analysis each parameter is regarded subsequently. The parameters with most influence on the stress-strain relationship and the relation volumetric strain – major principal strain are evaluated and discussed below. The sensitivity analysis for all other parameters are given in Appendix A. A plausible range for each parameter is researched, taking also the proposed by literature values into account. In a further going analysis considering different tensile behaviour parameters in the case of giving reinforcement characteristics to concrete, a broader range of the tensile fracture energy, the tensile strength and relating parameters is tested.

B.3.1 Time dependent stiffness/strength parameters

Time dependent parameters in this paragraph include the hardening and stiffening of concrete in time. The parameters considered are E_1/E_{28} and f_{c1}/f_{c28}. As time evolving is excluded, at a set time (1 day), the results have only influence on the ratio of the final strength and stiffness reached. The parameter sensitivity is tested according to the scenarios given in Table A-9. Scenario 0 serves as a reference scenario for as well the Poisson's ratio as the stiffness ratio. Scenario 1 is different from scenario 0 by the means that the scenario serves as a reference in the case of analysing the sensitivity to the dilatancy angle.

Table A-9: Time dependent stiffness sensitivity analysis scenarios.

Parameter	Value	Scenario
ν	0.2	0 (reference)
ν	0	1-5
ψ	0	1 (reference)
ψ	13°	0, 2-5
E_1/E_{28}	1	0 (reference),1 and 2
E_1/E_{28}	0.8	3

E_1/E_{28}	0.6	4
E_1/E_{28}	0.4	5

The results of applying the scenarios (0-5) given in Table A-9 are visualised in two different graphs (Figure A-35) considering stress-strain behaviour and major principal strain versus volumetric strain behaviour. The lines in both graphs are numbered in the order of the scenarios which they are representing.

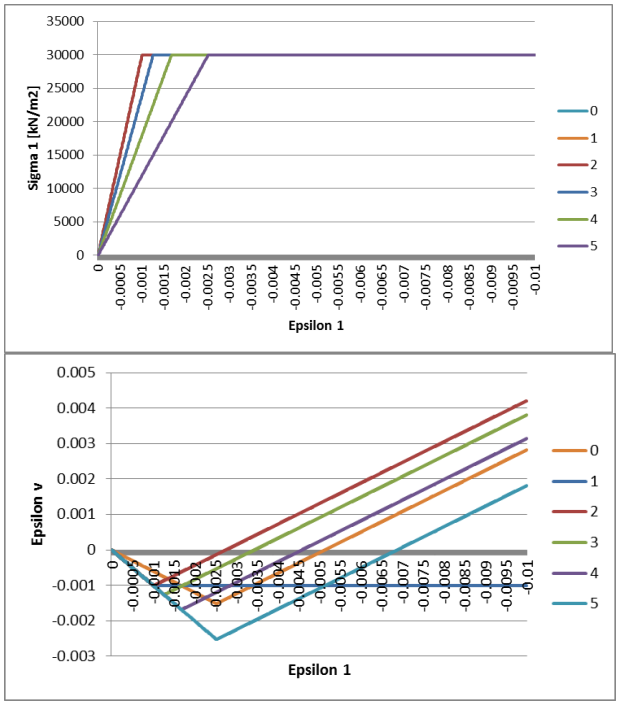

Figure A-35: Stress-strain (1%) and ϵ_1 - ϵ_v relations under scenario 0, 1-5 (Table A-9) regarding stiffness ratio E_1/E_{28}.

It is shown that the Poisson's ratio in scenario 0 (reference scenario) has influence on the $\epsilon_v - \epsilon_1$ diagram but no influence on the stress-strain behaviour, what is expected considering the theory described in the previous chapters. The downward going line in the $\epsilon_v - \epsilon_1$ diagram is for all other scenarios equal to a half, which is expected according to the theory in Figure A-33 and a Poisson's ratio of 0.The sensitivity analysis results are the same as the results to be expected. By the fact that the stiffness ratio at day 1 with respect to day 28 decreases the stiffness, the tangent of the stress-strain diagram, decreases and the slope becomes more gradual. The decrease in slope is proportionally inherent to the decrease in stiffness (ratio). Effect on the $\epsilon_v - \epsilon_1$ diagram is that the final strength is reached at lower (major principal) strain, wherefore the volumetric strain increases also at lower (major principal) strain values.

The scenarios for the f_{c1}/f_{c28} sensitivity analysis are given in Table A-10. The other parameters considered are with respect to the reference scenario, in this case scenario 4. The results of applying the different scenarios in the uniaxial compression test are given in Figure A-36. The strength at day 1 with respect to 28 days decreases with the ratio in the different scenarios. The effect on the $\epsilon_v - \epsilon_1$ diagram is as described before. When the final strength is reached at lower strain values, at lower (major principal) strain value the volumetric strain starts to increase. Taken in mind should be that this is only the fact when the same stiffness is regarded in the scenario, as is done in this sensitivity analysis.

Table A-10: Time dependent strength sensitivity analysis scenarios.

Parameter	Value	Scenario
ν	0.2	All scenarios
ψ	13°	All scenarios
E_1/E_{28}	0.6	All scenarios
f_{c1}/f_{c28}	1	4 (reference scenario)
f_{c1}/f_{c28}	0.8	6
f_{c1}/f_{c28}	0.6	7
f_{c1}/f_{c28}	0.4	8
f_{c1}/f_{c28}	0.25	9

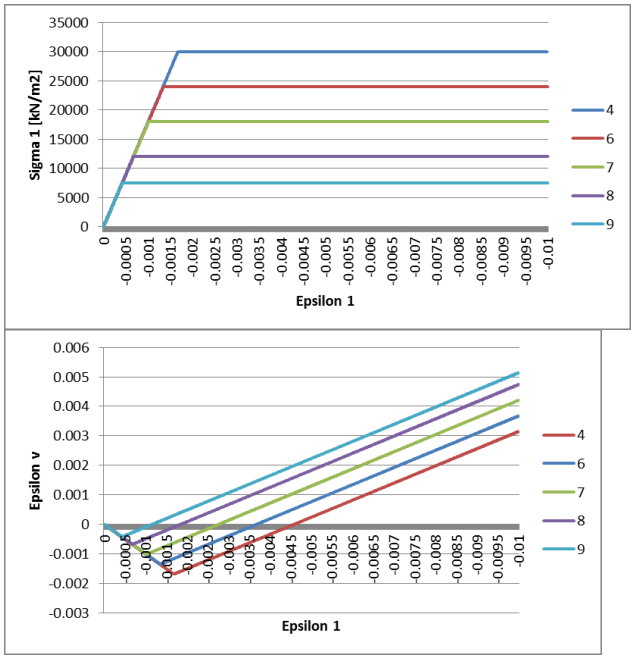

Figure A-36: Stress-strain (1%) and ϵ_1 - ϵ_v relations under scenario 4, 6-9 (Table A-10) regarding strength ratio f_{c1}/f_{c28}.

B.3.2 Plasticity

Till this point only linear elastic-perfectly plastic behaviour is considered. From now on when loading, plasticity is involved. This can be seen by the non-linear behaviour instead of linear elastic behaviour till perfectly plastic behaviour. As described in paragraph 2.2, in specific Figure 12, f_{c0n} is the ratio of the final (characteristic) compressive strength at which plastic strains are generated. Other parameters involving the determination of stress-strain behaviour is f_{cfn}, f_{cun} and the related parameters ϵ_{cp}^{p} and G_c. These model parameters are described in paragraph 2.2.3. In short, f_{cfn} is the ratio of the failure strength with respect to the peak (characteristic compressive) strength and f_{cfn} is the residual compressive strength and is also described by a ratio with respect to the peak compressive strength (characteristic compressive strength). In Table A-11 the parameters and corresponding scenarios considering plasticity are given.

Table A-11: Sensitivity analysis parameters regarding plasticity.

Parameter	Value	Scenario
ν	0.2	All scenarios
ψ	13°	All scenarios
E_1/E_{28}	0.6	All scenarios

f_{c1}/f_{c28}	0.25 ($f_c = 7.5\ MPa$)	All scenarios
f_{c0n}	1	10
f_{c0n}	0.8	11
f_{c0n}	0.5	12
f_{c0n}	0.33	13
f_{c0n}	0.1	14
f_{cfn}	1	15 (reference)
f_{cfn}	0.9	16
f_{cfn}	0.7	17
f_{cfn}	0.5	18
f_{cfn}	0.3	19
f_{cfn}	0.1	20
f_{cfn}	0	21
G_c	140.5 kN/m	22 (reference)
G_c	0.1 kN/m	23
G_c	10 kN/m	24
G_c	20 kN/m	25
G_c	50 kN/m	26
G_c	200 kN/m	27
f_{cun}	1	28 (reference)
f_{cun}	0.6	29
f_{cun}	0.3	30
f_{cun}	0.1	31
f_{cun}	0	32
ϵ_{cp}^{p}	-0.0035 %	33 (reference)
ϵ_{cp}^{p}	-0.0055 %	34
ϵ_{cp}^{p}	-0.01 %	35
ϵ_{cp}^{p}	-0.001 %	36
ϵ_{cp}^{p}	-0.0001 %	37

The first parameter considering plasticity investigated is f_{c0n}. In Figure A-37 the effect of varying the values for the point at which plastic strains are generated besides the elastic strains, as explained in more detail in paragraph 2.2.2. In the stress-strain diagram the influence is clearly visible. Especially the stress path in the region before reaching the plastic peak strain, at 3.5 ‰ in this case, is highly influenced by the value of this parameter. Reducing the value of f_{c0n} causes the fact that plastic strains are generated earlier. The result is that the slope becomes more non-linear, but still converges to the governing plastic peak strain. Due to the fact that in the NEN-EN-1992-1-1 (2011) the failure strain of concrete is approximated by 3.5 ‰, this parameter has to be treated with care. The plastic peak strain will therefore being reduced to a value such that the peak strain matches the 1.75 ‰, respectively 2.2 ‰ in another calculation method, proposed by NEN-EN-1992-1-1 (2011). The influence on the $\epsilon_v - \epsilon_1$ is not that significant, the moment that plastic strains are generated influence only the compressive and dilative behaviour slightly.

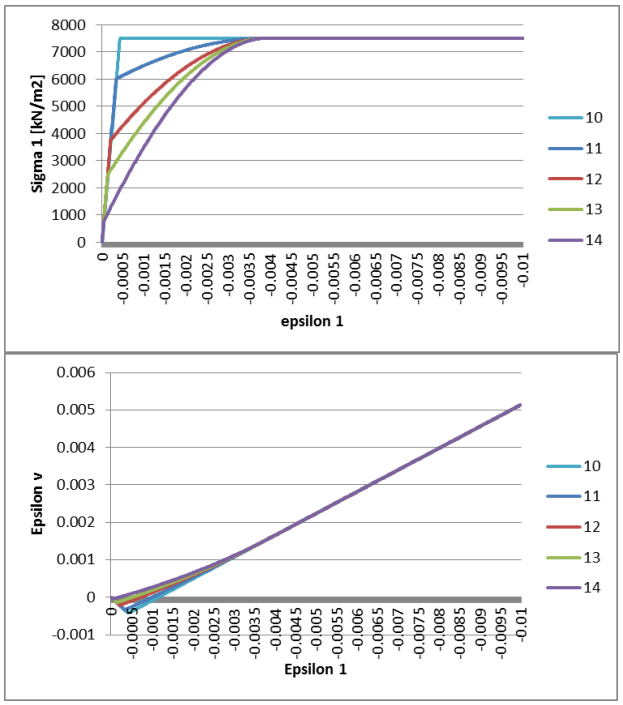

Figure A-37: The model sensitivity to f_{c0n} in a stress-strain (1%) and a $\epsilon_v - \epsilon_1$ diagram by scenarios 10-14 proposed in Table A-11.

Another parameter influencing plasticity and thereby the whole stress-strain curve is the failure strength f_{cfn}. This parameter is on its turn dependent on the fracture energy G_c, wherefore both parameters are evaluated simultaneous though individually analysed in terms of sensitivity. The failure strength determines the linear descending slope, as explained in literature (paragraph 2.2.2), of the stress-strain curve after reaching peak strength and is in specific the ratio of complete failure with respect to the peak strength. The fracture energy G_c influences on its turn the strain occurring between peak and failure strength. The larger the fracture energy G_c, the more strain is occurring between peak and failure strength. In Figure A-38 are the scenarios given (Table A-11) visualised with a constant fracture energy, with a proposed by literature value of 140.5 kN/m^2. Only the stress-strain diagram is displayed, while the $\epsilon_v - \epsilon_1$ is negligible influenced. Instead of strain values up to 1% of the sample, a strain up to 10% of the sample is applied, due to the influence of the magnitude of the fracture energy G_c. To match the failure criterion described by NEN-EN-1992-1-1 (2011), a strain of 3.5 ‰, a fracture energy $G_c$of 1.55 kN/m should be used in the Shotcrete material model. It must be noted that this is ten times smaller than proposed in literature. An equivalent length, back calculated from the bending beam model, of 0.03 meters is used to come to this fracture energy and results which match NEN-EN-1992-1-1 (2011).

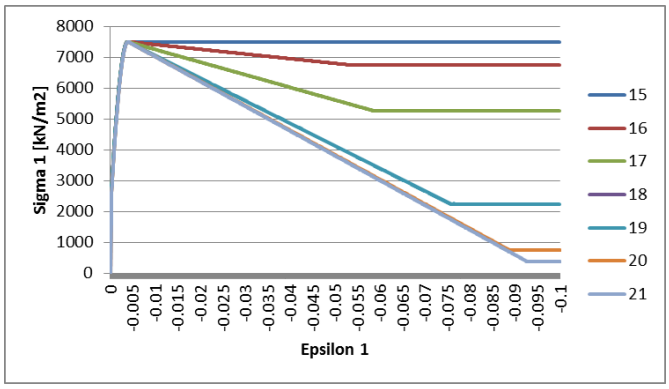

Figure A-38: The model sensitivity to f_{cfn} in a stress-strain (10%) diagram by scenarios (15-21) proposed in Table A-11.

In Figure A-38 it is shown that the influence of f_{cfn} is significant on the whole stress-strain behaviour, what also might be expect regarding literature and the specific model formulation. In scenario 15, which serves as a reference, no softening takes place. In all other scenarios, the described linear softening by literature in paragraph 2.2.2 is takes place. A curvature in this area of the stress-strain diagram is not possible due to the linear softening behaviour which is incorporated in the model. In scenario 21 softening should take place till zero strength is reached, though a strength of 375 kN/m^2 (approximately 5% of the peak) remains. The difference in strength values at a certain strain after peak strength is high, wherefore this parameter should be treated carefully. A realistic value of f_{cfn} should be obtained by fitting the stress-strain model curve to the results of a strain controlled uniaxial lab test or taking into account the proposed strain values for peak strength, 1.75 ‰ respectively 2.2 ‰, and 3.5 ‰ for failure strength by NEN-EN-1992-1-1 (2011).

As mentioned, the fracture energy G_c determines the distance between the peak strength and the failure strength. A value of 0.9 for f_{cfn} , a value of 0.1 for f_{cun} and a value of 3.5 ‰ for ϵ_{cp}^{p} is adopted for each scenario. Besides the values given in Table A-11, governing for all scenarios, are taken into account. The scenarios proposed in Table A-11 result in Figure A-39.

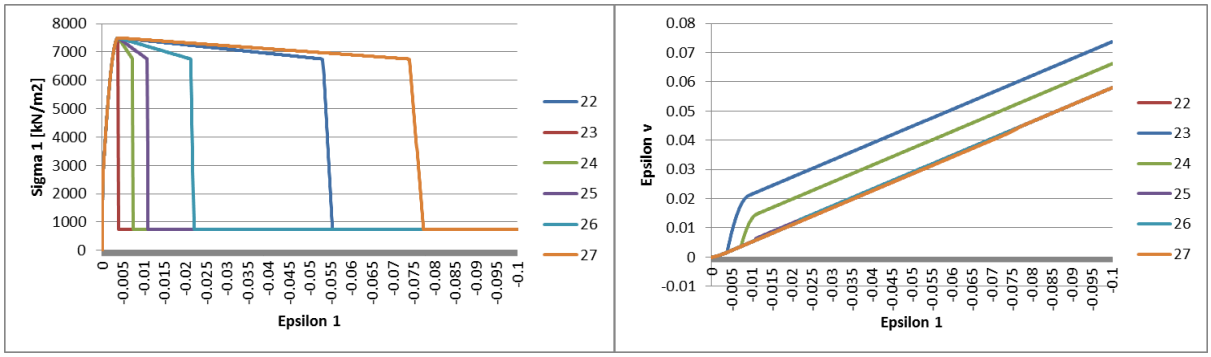

Figure A-39: Model sensitivity analysis to the fracture energy G_c by scenarios (22-27) with 10 % strain proposed in Table A-11.

The results of the stress-strain diagram are as might be expected from theory. The lower the fracture energy the smaller the area under the graph between peak and failure strength. By curve fitting to a lab test a right fracture energy should be obtained. Without results of a lab test, a value of 140.5 kN/m as proposed by literature can be used. It should be noted that a realistic upper bound for the maximum allowable strain, proposed in NEN-EN-1992-1-1 (2011), should be taken into account. The

results of the sensitivity analysis in the $\epsilon_v - \epsilon_1$ diagram is rather strange. An explanation for this is that the fracture process is not only dependent on the fracture energy but also on the equivalent length l_{eq} in numerical analysis.

The last parameter influencing the strength by a certain strain value specifically, determining the last phase of the stress-strain diagram in compression (paragraph 2.2.2), is f_{cun}. The residual strength after rapidly linear softening influences the value of strength at higher values of strain. A low value for the residual strength is probable according to theory and literature. Though the full range of possible values is covered in Figure A-40 according to the scenarios proposed in Table A-11. The lowest value, when is expected that the residual strength is zero ($f_{cun} = 0$), obtained is 375 kN/m^2 in scenario 26 (Table A-11). It is concluded that a lower boundary for the strength is implemented in the Shotcrete material model, probably to avoid numerical problems. The model sensitivity in the $\epsilon_v - \epsilon_1$ is negligible and therefore not displayed in Figure A-40.

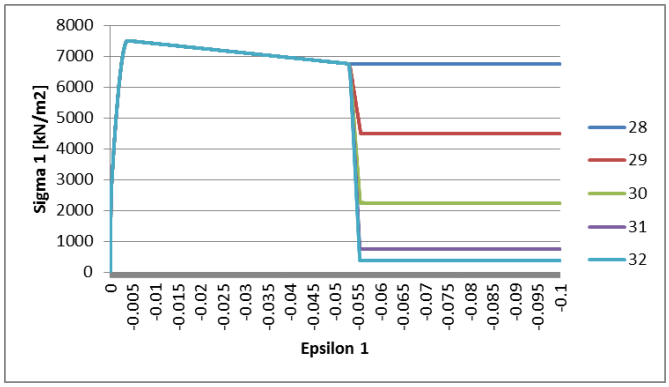

Figure A-40: Model sensitivity analysis regarding the residual strength f_{cun} by scenarios 28-32 with 10 % strain proposed in Table A-11.

The last parameter relating to direct plasticity in the model is the plastic peak strain ϵ_{cp}^{p}. The plastic peak strain determines at which strain value, taking also elastic strains into account, peak strength is reached. In Figure A-41 the scenarios (Table A-11) based on probable values for the plastic peak strain are visualised. Due to the fact that a uniaxial compression test is done with a set strain of 10% it seems that the influence is rather small, though the results should be treated with care as the proposed failure strain by NEN-EN-1992-1-1 (2011) is only 3.5 ‰. When using a value of 2.5 ‰ for the plastic peak strain, a strain of 3.5 ‰ is reached at peak strength indicating an elastic strain of 1‰. Negligible effect is found on the $\epsilon_v - \epsilon_1$ diagram (not visualised). To match NEN-EN-1992-1-1 (2011) it is concluded that the value for ϵ_{cp}^{p} has to be 0.75 ‰ when taking into account the LEPP diagram and 1.2 ‰ when taking into account the parabolic diagram. It is chosen, for safety, to consider 0.75 ‰ as the governing value for peak strength.

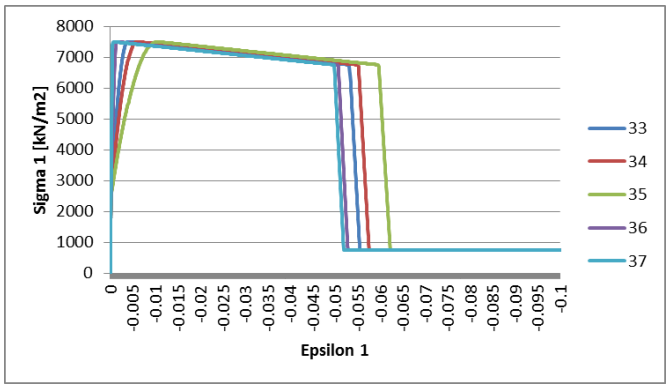

Figure A-41: Model sensitivity analysis to the plastic peak strain ϵ_{cp}^{p} with 10 % strain by scenarios 33-37 proposed in Table A-11.

B.3.3 Creep

Two creep parameters are included in the Shotcrete material model. It turned out that the creep factor has a major influence while the creep half time has a minor influence. The sensitivity analysis regarding the time when half of the creep strains is generated can be found in Appendix A.3. The creep factor has significant influence on as well the stress-strain as the $\epsilon_v - \epsilon_1$ development. The scenarios taken into account for the sensitivity analysis are summerised in Table A-12. The time dependent strength and stiffness ratios are taken to be 1, eliminating the effect of those parameters at the test date (1 day). The influence is of taking both time dependent parameters into account influences the behaviour significantly, as is demonstrated in scenario 48, which is only different from scenario 49 by taking proposed values of E_1/E_{28} (0.6) and f_{c1}/f_{c28} (0.25) into account.

Table A-12: Sensitivity analysis creep coefficient scenarios.

Parameter	Value	Scenario
ν	0.2	All scenarios
ψ	13°	All scenarios
E_1/E_{28}	1	All scenarios, except 48
f_{c1}/f_{c28}	1	All scenarios, except 48
f_{c0n}	0.33	All scenarios
f_{cfn}	0.9	All scenarios
f_{cun}	0.1	All scenarios
ϵ_{cp}^{p}	-0.0035 %	All scenarios
G_c	140.5 kN/m	All scenarios
ϕ_{cr}	0	38 (with realistic E_1/E_{28} (0,6) and f_{c1}/f_{c28} (0,25) values)
ϕ_{cr}	0	39 (reference)
ϕ_{cr}	1	40
ϕ_{cr}	1.9	41
ϕ_{cr}	2.3	42
ϕ_{cr}	2.7	43
ϕ_{cr}	3	44
ϕ_{cr}	5	45

For an appropriate range as proposed by literature in paragraph A.1.8, the model is not very sensitive to changes in the creep coefficient (Figure A-42). Also a non-realistic high value for the creep strain is used, $\phi_{cr} = 5$, in order to test the model sensitivity. The strain at peak strength increases only

slightly, taking into account low strain values (<1%). Though the $\epsilon_v - \epsilon_1$ relation is influenced more heavily (Figure A-42) due to additional straining of creep.

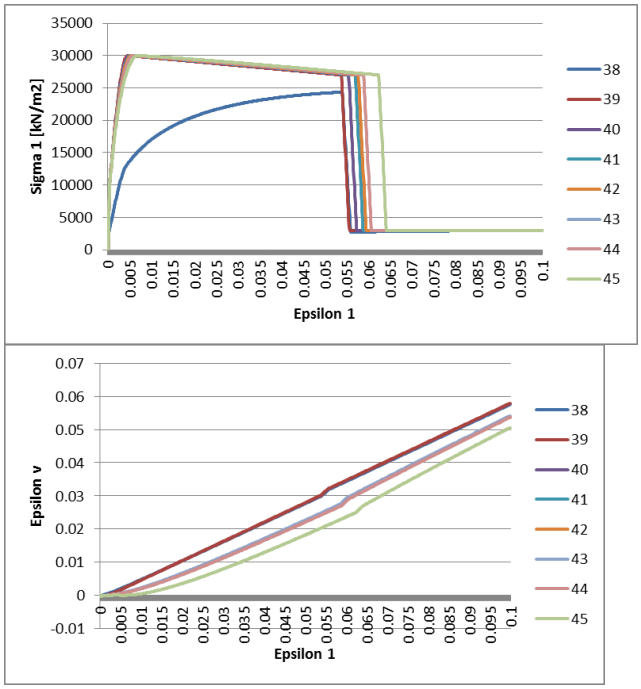

Figure A-42: Model sensitivity regarding the creep coefficient under 10% straining scenarios 38-45 proposed in Table A-12.

B.4 Results of using different models

B.4.1. Overview

Table A-13: Comparison between using Mohr-Coulomb, Shotcrete and a Linear elastic material model and calculations of unreinforced concrete respectively hand calculations.

Load [kN/m]	Parameter	MC	SC	LE	Unreinforced SC	Hand Calc. Unreinf.
14	u_y [m]	-2.57*10^{-3}	-2.48*10^{-3}	-2.57*10^{-3}	-2.77*10^{-3}	-2.80*10^{-3}
	σ_{xx} [kN/m^2]	1733/-1926	1733/-1926	1733/-1926	2059/-2061	±2058
	N [kN/m]	97	93	96.5	-	381
17	u_y [m]	-3.12*10^{-3}	-3.01*10^{-3}	-3.12*10^{-3}	-3.45*10^{-3}	-3.40*10^{-3}
	σ_{xx} [kN/m^2]	2019/-2341	2019/-2341	2019/-2341	1926/-2588	±2499
	N [kN/m]	117	118	117	-	535
30	u_y [m]	-6.39*10^{-3}	-6.53*10^{-3}	-5.51*10^{-3}	Model crack at 18.15 kN/m.	6.00*10^{-3}
	σ_{xx} [kN/m^2]	2000/-4667	1970/-2799	3713/-4129		±4410
	N [kN/m]	288	346	207		943
50	u_y [m]	-0.0143	-0.0179	-9.18*10^{-3}	-	-0.0100
	σ_{xx} [kN/m^2]	2000/-9057	2000/-10150	6189/-6883	-	±7350
	N [kN/m]	762	1318	345	-	1572
80	u_y [m]	-0.0284	-0.0367	-0.0147	-	-0.0160
	σ_{xx} [kN/m^2]	2007/-15680	959/-15130	9904/-11020	-	±11760
	N [kN/m]	1616	2362	552	-	2516
120	u_y [m]	-0.0483	-0,0619	-0.0221	-	-0.0240
	σ_{xx}[kN/m^2]	2000/-24390	1021/-21840	14860/-	-	±17640

				16530		
	N [kN/m]	2812	3686	829	-	3774
Failure load	Load [kN]	146.4	146.4	-	-	-
	u_y [m]	-0.06353	-0.1157	-	-	-
	σ_{xx}[kN/m^2]	2000/-30810	1355/-34720	-	-	-
	N [kN/m]	3720	4350	-	-	-

B.4.2 hand calculation rebar force

The rebar force can be back calculated with the help of a hand-calculated M-κ diagram. At different applied line loads the occurring moments can be calculated with the help of the Forget-me-nots ($\frac{1}{8} * q * l^2$). In figure 41 the M-κ diagram is given. The M-κ diagram is a method to calculate cracked reinforced concrete beams. At the different stages, uncracked, cracked, yielding of the rebar and yielding/failure of the concrete, the height of the compressive zone changes. The effective compressive cross-section decreases with increasing load. At all time, the rebar force has to be in equilibrium with the equivalent force of the compressive stress in the cross-sectional area, resulting in the fact that within the concrete beam the forces have to be balanced. To be conservative the distance between the force in the reinforcement and the balancing equivalent force in the concrete is taken to be on the safe side.

The rebar force N can be calculated by the occurring moment M and the distance z between the equivalent force due to compression in the concrete and the force in the rebar :

$$N_s = M/z$$

When considering uncracked concrete a distance of d between the rebar and the equivalent compressive concrete force is used. Where d is the distance of the rebar to the top of the beam.. The height of the compressive stress area in the concrete decreases with increasing load, wherefore the arm between the forces increases. Therefore, when a cracked cross-section is taken into account the distance between the forces is safely characterised by $z = d - 1/3x$. Where x is the height of the compressive stress area in the concrete. In Braam & Lagendijk (2010) it is suggested that this method is taken into account when the moment is higher than the yielding moment. Therefore the calculations after cracking are conservative with respect to the lowest occurring rebar force. In Table A-14 the results are given.

Table A-14: Hand calculated rebar force.

Line load [kN/m]	M [kNm]	z [m]	N_s [kN]
14	343	0.9	381
17	416,5	0.9 - 1/3*0.363 = 0.779	535
30	735	0.779	943
50	1225	0.779	1572
80	1960	0.779	2516
120	2940	0.779	3774
138.3	3388	0.779	4350

Appendix C: M-κ diagram calculations

C.1 M-κ diagram hand calculation

C.1.1 Rupture moment

The tensile strength of the concrete is reached, indicating rupture. At the rupture moment de compressive strength is small in means of far below 1.75‰. The elasticity of the concrete is determined with the characteristic value of C30/37.

$$E_c = \frac{f_{ck}}{1.75 * 10^{-3}} = \frac{30000}{1.75 * 10^{-3}} = 17142867\ kN/m^2$$

Subsequently the centre of gravity, and the corresponding enlargement factor of the reinforcement, has to be calculated.

$$n = \frac{E_s}{E_c} = \frac{210000}{17143} = 12.25$$

The area of the reinforcement has to be enlarged with this factor in the calculations of the M-k diagram.

The area of the concrete and rebar are as follows, including the distance x from the centre of the concrete respectively reinforcement to the top.

$$A_c = 1000 * 1000 = 1\ m^2$$

$$A_s = n * A_s = 12.25 * 1\% * A_c = 12.25 * 0.01 * 1 = 0.1225\ m^2$$

$$A_c * x_c = A_c * 0/5\ h = 1 * 0.5 * 1 = 0.5\ m^3$$

$$A_s * x_s = A_s * 0/9\ h = 0.1225 * 0.9 = 0.11025\ m^3$$

$$\sum A = 1/1225\ m^2; \sum A * x = 0/509\ m^3$$

$$x_{uncracked} = \frac{0.610}{1.1225} = 0.544\ m$$

The bending stiffness of the uncracked surface area is calculated with the moment of inertia below.

$$I_0 = \sum \left(I_{eig} + I_{steiner}\right)$$

$$= \frac{1}{12} * b_c * h_c^3 + b_c * h_c * (x_{uncracked} - x_c) + \frac{1}{12} * b_s * h_s^3 + b_s * h_s * (x_{uncracked} - x_s)$$

$$= 0.10\ m^4$$

$$(EI)_0 = 17143 * 10^3 * 0.1 = 1714.3 * 10^3\ kNm^2$$

The rupture moment M_r at the moment $f_{ck}$is reached can be calculated subsequently.

$$z_{under} = h - x_{uncracked} = 1 - 0.544 = 0.456\ m$$

$$M_r = f_{ctk} * W = f_{ctk} * \frac{I_0}{z_{under}} = 2000 * \frac{0.1}{0.456} = 441.74\ kNm$$

At that moment also the corresponding strains can be calculated.

$$\epsilon_{ct} = \frac{f_{ck}}{E_c} = \frac{2}{17143} = 0.12\ promille$$

$$\epsilon_s = \frac{h - x_{uncracked} - 0.9\,h}{h - x_{uncracked}} * \epsilon_{ct} = \frac{1 - 0.544 - 0.9}{1 - 0.544} * 0.12 = 0.09\ promille$$

$$\epsilon_c = \frac{x_{uncracked}}{z_{under}} * \epsilon_{ct} = \frac{0.544}{0.456} * 0.12 = 0.14\ promille$$

The curvature is:

$$\kappa_r = \frac{\epsilon_c + \epsilon_s}{d} = \frac{(0.09 + 0.14) * 10^{-3}}{1} = 2.56 * 10^{-4} m^{-1}$$

A check is performed if the calculation is correct.

$$\kappa_r = \frac{M_r}{(EI)_0} = \frac{441.74}{1714.3 * 10^3} = 2.56 * 10^{-4} m^{-1}$$

C.1.2 Yielding of the rebar

The load is increased such that the stress in the rebar is equal to the yield strength ($\sigma_s = f_{yd}$). A horizontal equilibrium in the reinforced concrete beam has to be found. The horizontal force in the rebar has to equal the horizontal force in the compressive (top) part of the beam. This equilibrium holds only when is proven that the strain in the concrete is smaller than 1.75 ‰.

$$N_c = N_s$$

$$\frac{1}{2} * b * x * \sigma_c = A_s * \sigma_s$$

If divided by σ_s the x can be found in the formula

$$\left(\frac{1}{2} * b * x^2\right) + (n * A_s) * x - (n * A_s * d) = 0$$

$$\left(\frac{1}{2} * 1 * x^2\right) + (12.25 * 0.01) * x - (12.25 * 0.01 * 0.9) = 0$$

This holds for a value of 0.363 m of $x_{cracked}$. It can be concluded that the height of the compressive zone in the beam is decreased to 363 mm. The corresponding strains are as follows:

$$\epsilon_s = \epsilon_{sy} = \frac{f_{yd}}{E_s} = \frac{435}{210000} = 2.07\ promille$$

$$\epsilon_c = \frac{x_{cracked}}{d - x_{cracked}} * \epsilon_s = 1.40\ promille$$

The assumption of $\epsilon_c < 1.75\ promille$ was therefore right.

The curvature at yielding of the rebar is:

$$\kappa_y = \frac{\epsilon_c + \epsilon_s}{d} = \frac{(2.07 + 1.40) * 10^{-3}}{0.9} = 3.85 * 10^{-3} m^{-1}$$

The moment at which this curvature occurs is called the yielding moment.

$$M_y = A_s * f_{yd} * \left(d - \frac{1}{3} * x_{cracked}\right) = 0.01 * 435000 * \left(0.9 - \frac{1}{3} * 0.363\right) = 3387\ kNm$$

At yielding the stiffness reduced from $1714.3 * 10^3$ kNm^2 to:

$$(EI)_y = \frac{M_y}{\kappa_y} = \frac{3387}{3.85 * 10^{-3}} = 879 * 10^3\ kNm^2$$

C.1.3 Concrete yielding

Yielding of concrete occurs at a strain of 1.75‰, wherefore in this stage the load is increased to the moment this occurs. Again the way of searching for a horizontal equilibrium of forces within the beam is used to find the height of the compressive zone and subsequently the corresponding strains.

$$\sum H = 0$$

$$N_c = N_s$$

$$\frac{1}{2} * b * x * \sigma_c = A_s * f_{yd}$$

At $\epsilon_{c3} = 1.75\ promille \rightarrow\ \sigma - c = f_{ck} = 30\ N/mm^2$

Therefore:

$$\frac{1}{2} * 1 * x * 30000 = 0.01 * 435000 \rightarrow x = 0.29\ m$$

It is shown that the height of the compressive area within the concrete beam again is decreased, which is also to be expected. The strain in the rebar can be calculated and has to be checked afterwards if the occurring strain is below the failure (allowable) strain in the rebar.

$$\epsilon_s = \frac{d - x}{x} = \frac{0.9 - 0.29}{0.29} * 1.75 = 3.7\ promille$$

According to NEN-EN-1992-1-1 (2011) the strain has to be limited to:

$$\epsilon_s < \epsilon_{ud} = 0.9\epsilon_{uk} = 0.9 * 25 = 22.5\ promille\ (> 3.7\ promille)$$

The curvature is:

$$\kappa_{c,pl} = \frac{\epsilon_{c3} + \epsilon_s}{d} = \frac{(1.75 + 3.7) * 10^{-3}}{0.9} = 6.04 * 10^{-3} m^{-1}$$

The corresponding moment is

$$M_{c,pl} = A_s * f_{yd} * \left(d - \frac{1}{3} * x_{cracked}\right) = 0.01 * 435000 * \left(0.9 - \frac{1}{3} * 0.29\right) = 3493\ kNm$$

The bending stiffness is reduced to:

$$(EI)_{c,pl} = \frac{M_{c,pl}}{\kappa_{c,pl}} = \frac{3493}{6.04 * 10^{-3}} = 578.5 * 10^3\ kNm^2$$

C.1.4 Failure

The reinforced concrete beam fails when the criterion of a strain 3.5‰ is reached in the concrete according to NEN-EN-1992-1-1 (2011). The load will increased such that a strain of 3.5‰ is obtained in the concrete material. Again a horizontal equilibrium is used to determine the height of the compressive zone at this particular moment.

$$\sum H = 0$$

$$N_c = N_s$$

$$\frac{3}{4} * b * x * \sigma_c = A_s * f_{yd}$$

At $\epsilon_{c3} = 3.5\ promille \rightarrow\ \sigma - c = f_{ck} = 30\ N/mm^2$

Therefore:

$$\frac{3}{4} * 1 * x * 30000 = 0.01 * 435000 \rightarrow x_u = 0.193\ m$$

It is shown that the height of the compressive area within the concrete beam is again decreased. The strain in the rebar can be calculated and has to be checked afterwards if the occurring strain is below the failure (allowable) strain in the rebar.

$$\epsilon_s = \frac{d - x_u}{x_u} = \frac{0.9 - 0.193}{0.193} * 3.5 = 12.8\ promille$$

According to NEN-EN-1992-1-1 (2011) the strain has to be limited to:

$$\epsilon_s < \epsilon_{ud} = 0.9\epsilon_{uk} = 0.9 * 25 = 22.5\ promille\ (> 12.8\ promille)$$

The curvature is:

$$\kappa_{Rd} = \frac{\epsilon_{cu3} + \epsilon_s}{d} = \frac{(3.5 + 12.8) * 10^{-3}}{0.9} = 18.11 * 10^{-3} m^{-1}$$

The corresponding moment is

$$M_{Rd} = A_s * f_{yd} * \left(d - \frac{7}{18} * x_u\right) = 0.01 * 435000 * \left(0.9 - \frac{7}{18} * 0.193\right) = 3586\ kNm$$

The bending stiffness is reduced to:

$$(EI)_{Rd} = \frac{M_{Rd}}{\kappa_{Rd}} = \frac{3586}{18.11 * 10^{-3}} = 4348\ kNm^2$$

C.2 Example calculating kappa Plaxis bending reinforced beam

As mentioned in the report, it is not possible to directly output the curvature of the reinforced concrete bending beam. The curvature is often calculated based on the concrete strain at the top in the middle of the beam and the strain occurring in the reinforcement in the middle. Those are averaged over the height to get the curvature at the neutral line in the middle. The Shotcrete material model gives the opportunity to include the cracking process in Plaxis. For the modelling of cracking a, the smeared cracking concept is used. The result of incorporating cracking in the bending beam model is that the concrete strain is varying from millimetre to millimetre. Besides in Plaxis it is not possible to directly output the strain in the reinforcement (plate element). Therefore it is chosen to use a dummy element (stiffness is zero) to calculate the curvature. The dummy element is located at the neutral line of the beam, in case of absence of normal force this is in the middle.

From mathematics it is known that the curvature is the second derivative of the deformation (function). Interest is paid to the maximum curvature, which is occurring in the middle of the beam. In Figure A-43, the middle of the beam is at x = 9. Though on forehand it is not known which is the function of the deformation. Therefore a higher order polynomial function has to be fitted to the deformation. The expression for the 4th order polynomial function of the deformation at a applied line load of 100 kN/m is given in Figure A-43, as well as the corresponding line. The reliability of the fit is given with the R-value. The R-value approximates 1, which indicates a "perfect" fit.

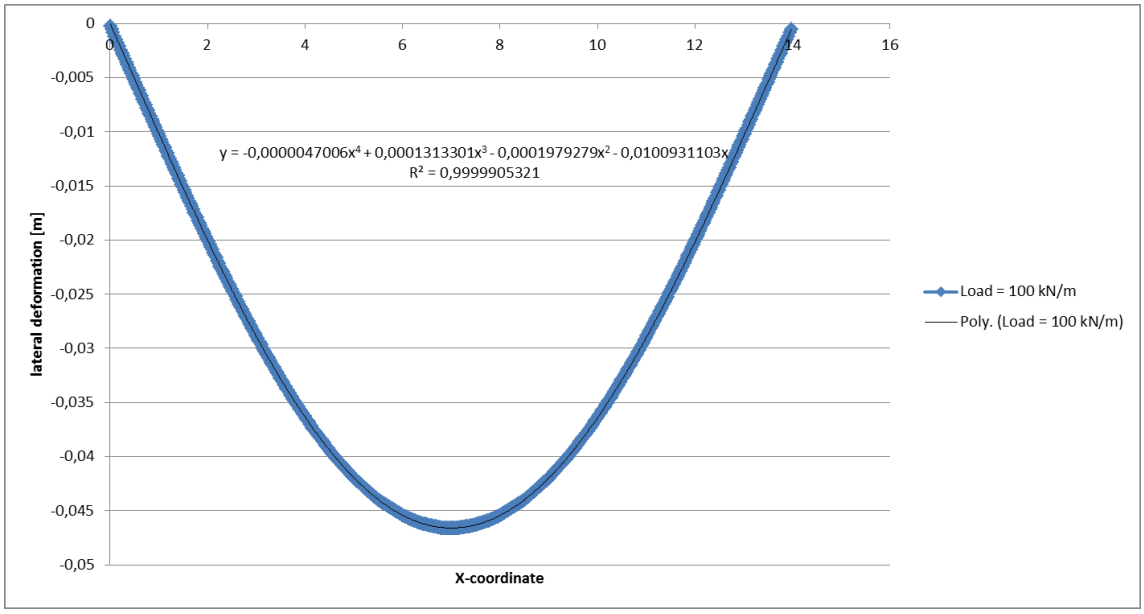

Figure A-43: Deformation of bending beam at a applied line load of 100 kN/m and the according fourth order polynomial fit.

The fourth order polynomial function is derived twice, resulting in the following equation where y indicates the curvature and x the x-coordinate of the beam.

$$y\,(deformation) = -4{,}7 * 10^{-6}\,x^4 + 0{,}000131x^3 - 0{,}000198x^2 - 0{,}010x$$

$$y' = -1{,}88 * 10^{-5}\,x^3 + 0{,}00039x^2 - 0{,}000396x$$

$$y"(curvature) = -5{,}64 * 10^{-5}\, x^2 + 0{,}000788x - 0{,}000396$$

Subsequently the x-coordinate of the middle of the beam can be filled (x= 7) in and a curvature of 0,002356 m^{-1} is obtained. This procedure is used for different applied loads. The deformation differs for each load wherefore also the derivatives of the function differ and the obtained curvature differs.

Appendix D: Modelling soil structure interaction

D.1 Obtaining the bending moment for a reinforced non-linear concrete structure in Plaxis

In this appendix several opportunities to output the bending moment of a non-linear reinforced concrete structure are investigated. The first opportunity researched is the dummy element method. Often in practice when a linear volume element is used in Plaxis, a plate element with a stiffness which is a thousand times smaller than the volume element is placed in the middle of the beam. Plaxis is possible to directly output the moments for such an element. The moments obtained in the dummy plate element should be multiplied by a thousand to obtain the bending moment in the volume element. This option for a non-linear reinforced concrete beam is researched at first.

Thereafter a recently updated possibility to output the moments directly by Plaxis itself is researched. This option in Plaxis is able to output the bending moment directly by integrating the stresses over the height of the volume element, but does it work when the volume element is reinforced and how does it deal with non-linear material behaviour including cracking.

Another option is use mechanics to calculate the bending moment when dealing with non-linear and reinforced volume element behaviour. This can be done by using the centre of gravity of the compressive stress zone as point at which the bending moment can be calculated. However the forces, with arm to this point, in the reinforcement have to be added, to the residual tensile stress after cracking and its arm to the centre of gravity of the compressive zone. Another possibility to calculate the bending moment in the normative cross-section is to calculate the bending moment at the neutral line by adding the equivalent (stress) force in the cross-section multiplied with the arm to the neutral line to the normal forces in the reinforcement and their arm with respect to the neutral line.

D.1.1 Dummy element analysis

In this appendix the correctness of the use of the dummy element when analysing the results of a volume element will be researched. In a volume element it is not possible to directly output for instance bending moments and an accurate prediction of the deformation. For this purpose a dummy element is often used in practice (in case of linear elastic material behaviour). Dummy elements are given such properties that the plate deforms with the bending structure and does not influence the behaviour of the reinforced concrete structure. To achieve such features a plate element with a stiffness equivalent to the stiffness of the structure divided by thousand is created in the centre of the structure. The bending moment that can be found from the plate element have to multiplied by a thousand to get the real occurring moment in the bending volume element. A remark has to be made that the tolerated error in Plaxis is set 1% wherefore slight differences in calculations will occur.

For linear elastic volume elements a dummy element with $1/1000^{th}$ of the stiffness will properly do its work. However when analysing a Shotcrete volume element where cracking and therefore a reduction in stiffness occurs, a linear elastic plate element will not work. To overcome this problem the stiffness of the dummy element has to simultaneously decrease with the decreasing bending stiffness of the structure. The solution is to apply a M-κ material model for the dummy element. At cracking and yielding the stiffness is reduced. To not influence the behaviour of the structure, the

moments from the M-κ diagram matching the structures behaviour have to be divided by a factor 1000.

Another feature of the Shotcrete material model brings difficulties with obtaining accurate results by using a dummy element. The fact that the neutral line, at the height of the beam where it does not experience compressive neither tensile stresses, changes with increasing load. The most accurate result is to replace the dummy element in each calculation phase at the obtained neutral line from Plaxis calculations. This implies the use of a iteration step, which is not wanted. A practical solution is to only use a dummy element at the neutral line at almost failure, or at the neutral line at the start of loading.

As illustration for the dummy element obtained moment results the soil-structure interaction case as presented in chapter 4 is used. For simplicity four different cases are researched to evaluate both defined problems and solutions.

- Linear elastic dummy element in Shotcrete volume element.
- Eccentric (failure neutral line) linear elastic dummy element in Shotcrete volume element.
- M-κ diagram based dummy element in Shotcrete volume element.
- Eccentric (failure neutral line) M-κ diagram based dummy element in Shotcrete volume element.

The results of the research are given in Figure A-44 and Figure A-45. In Figure A-44 the difference between using a linear elastic and a M-κ based dummy element can be seen. In Figure A-45 the result of introducing eccentricity for the dummy element in order to take into account the moving neutral line is shown. For comparison reasons also a linear elastic volume element and linear elastic, respectively M-κ plate element are given in the figures.

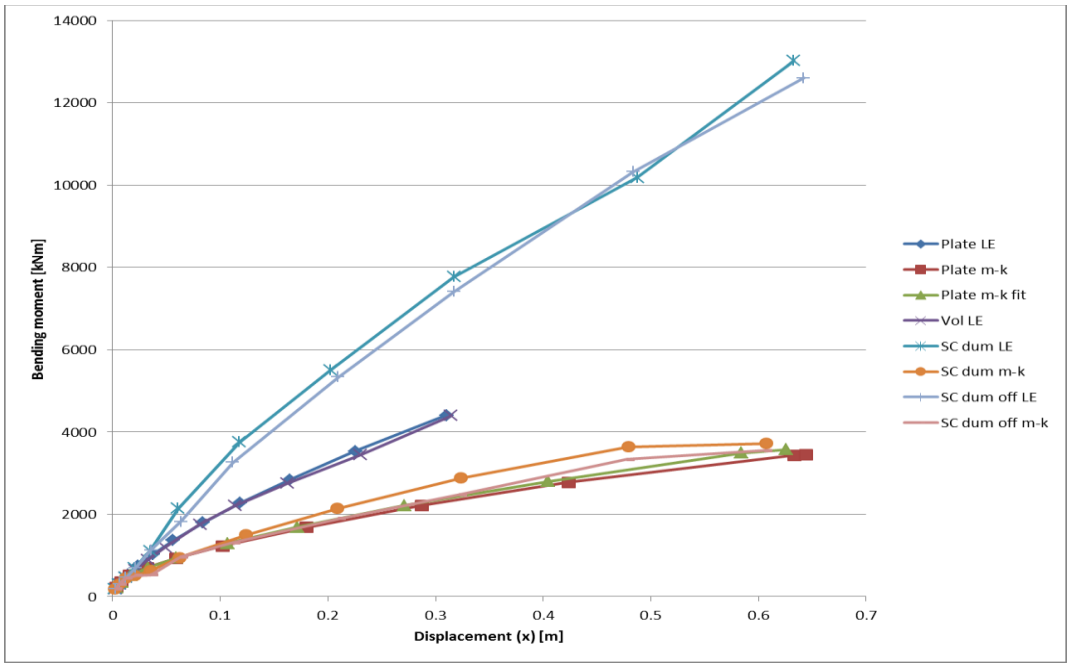

Figure A-44: All case results for dummy element analysis.

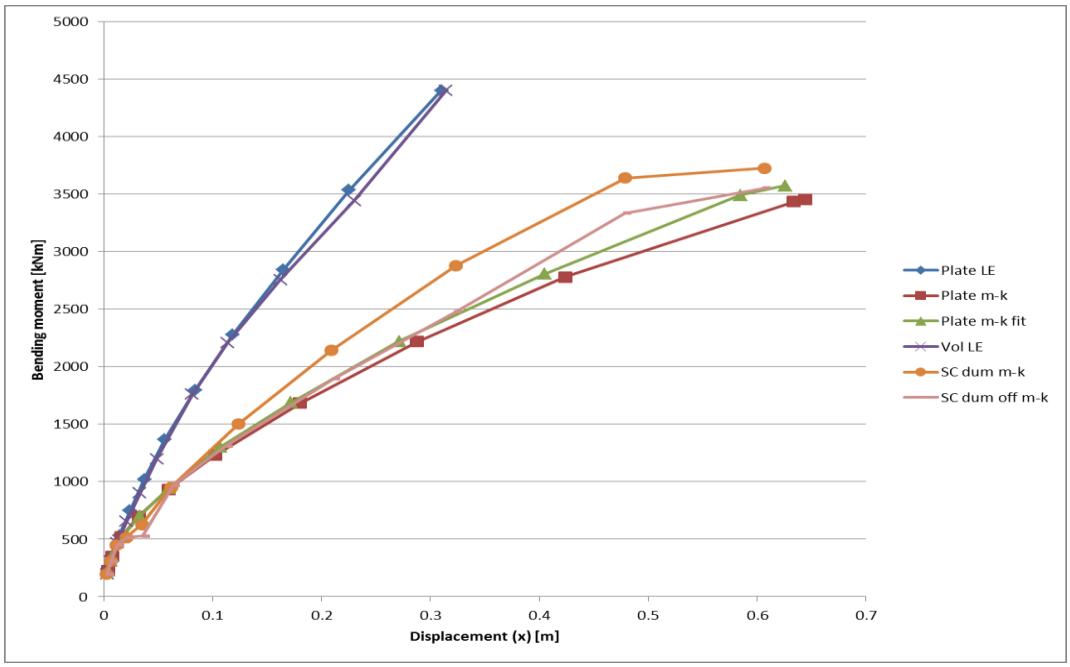

Figure A-45: Only M-kappa dummy element results of dummy element analysis.

The results in Figure A-44 show that using a linear elastic dummy element in a cracking volume element leads to a huge overestimation of the occurring moment at equal displacement. It can therefore be concluded that a M-κ based dummy plate element has to be used to get reasonable bending moment results for a Shotcrete volume element. Figure A-45 shows that using an eccentric M-κ dummy element approximates the results of a plate element. However this will not be better by definition, due to the fact that there is a difference in calculation method and features of Plaxis the Shotcrete model with respect to the hand calculated M-κ diagram. Optimising the location of the dummy due to the movement of the neutral line in the concrete leads to an almost perfect correspondence of the volume and plate element results. However during the whole process of deformation the neutral line moves in the cross-section, decreasing the compressive zone, which implies that in Plaxis also the dummy element should be corrected at each displacement. This is not feasible in practice as in a lot of cases the displacement is not known on forehand, wherefore the location of the neutral line is not known. Besides the curvature is different at the neutral line with respect to the centre line, causing an incorrect moment curvature relationship. For a conservative and correct calculation the dummy element has to be located in the centre of the beam.

However there is a large deviation with respect to reality found. When pre-calculating an equivalent to the moment curvature relation of the reinforced concrete structure M-κ dummy element, the second order effect, the self-weight of the structure, the deforming cross-section and the influence of the wall friction (interface shear stresses) resulting from the surrounding soil are not taken into account. These forces acting on the structure in a complex situation like this soil-structure interaction case have a significant influence on the behaviour and resulting bending moment. Therefore this method can be regarded as inappropriate and invalid for complex situations like soil-structure interaction cases. To make the deviation visible in Figure A-49 and Figure A-50 the obtained bending moments by this method are compared to the other methods, still to be researched. A schematisation of this method to obtain the bending moment in given in Figure A-46.

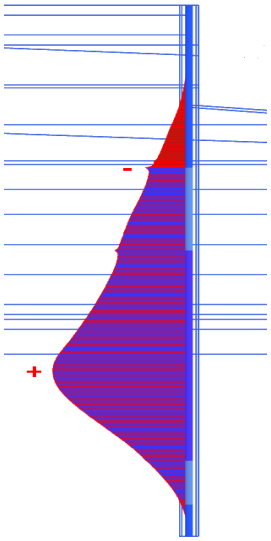

Figure A-46: Bending moment in a diaphragm wall with difference in reinforcement over the height in the crest of a dike (KIS project).

D.1.2 Plaxis moment output

It is (recently) possible to output the moments of a volume element in Plaxis. This function integrates the stresses over the height and calculates the corresponding moment at the center line of the volume element. Due to the fact the diaphragm wall is reinforced by means of plate elements, the moment should be obtained by adding the corresponding normal forces in the reinforcement multiplied by the arm to the neutral line to the considered moment in the volume element. The neutral line can be found when drawing a cross-section in Plaxis at the normative structural cross-section and find the transition of compressive to tensile stresses (ie. Where the stress is zero).

For a linear elastic element this method works properly. However using this method for a cracking Shotcrete volume element can lead to difficulties. The wizard function calculates the moment at the central line of the volume element, while due to cracking the central line is not the neutral line anymore. This could lead to some deviations. Though due to numerical integration the moment obtained over the height should not differ. The statically determined bending beam test showed that the moment obtained by this method is not appropriate when using a reinforced Shotcrete volume element, the deviation is larger than 10 % for high bending moments. To test the applicability of this function in combination with adding the normal forces in the reinforcement and their arm to the neutral line to obtain the correct moment also a calculation is done with the help of concrete mechanics. In Figure A-47 a schematisation of the cross-section of the diaphragm wall used in the KIS project is given. On the left side the outputted bending moment from the volume element by Plaxis is visible. On the right side the normative cross-section with the normal forces (N) in the reinforcement and their arms (a)to the neutral line are mentioned.

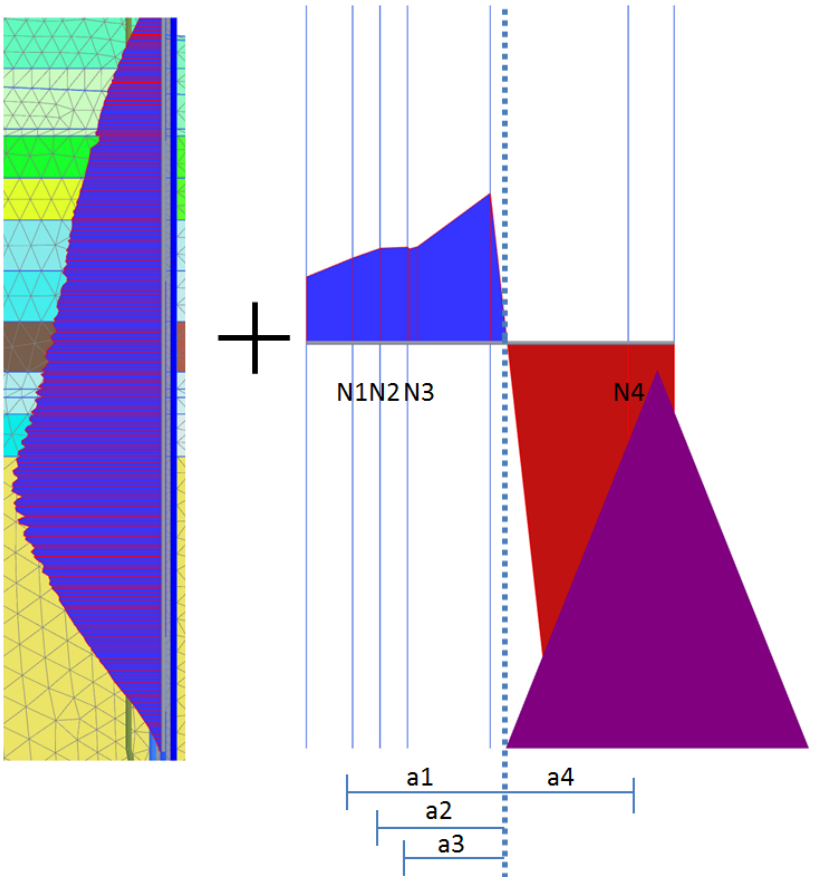

Figure A-47: On the left the by Plaxis calculated center line bending moment in the volume element. On the right the Normal forces (N) with their arm (a) to the neutral line. Together representing the total occurring bending moment.

D.1.3 Moment calculation by concrete mechanics

The first way in which concrete mechanics can be used is by taking the center of gravity of the compressive stress zone as base point (Figure A-48 (left)). Around this point the normal forces in the reinforcement and the residual tensile stress cause the bending moment when multiplied with the arm to this point (Figure A-48 (left)). The disadvantage of this method is that or an equivalent stress to the residual tensile stress should be taken for not fully cracked concrete, disregarding the variation in magnitude in the height of the tensile zone. Another option is to disregard the tensile stress in its whole and assume that the tensile stress remaining in the normative cross-section is of minor influence or even zero. This method will be tested for both the soil-structure interaction case as the KIS project.

The second way in which concrete mechanics can be used to determine the moment in the normative cross-section is to search for the neutral line and subsequently take the moment caused by the normal forces in the reinforcement and add the equivalent force of the stress profile in this cross section with its arm to the neutral line (Figure A-48 (right). The validity of this option is first checked on the reinforced concrete beam subjected to bending. This proved that the results approximately matched (± 2 %) the statically determined structural moment $M = \frac{1}{8} * q * l^2$. An exact match is not possible due to the fact that Plaxis also takes shear deformation into account.

A schematisation of both methods to obtain the bending moment by using concrete mechanics are given in Figure A-48.

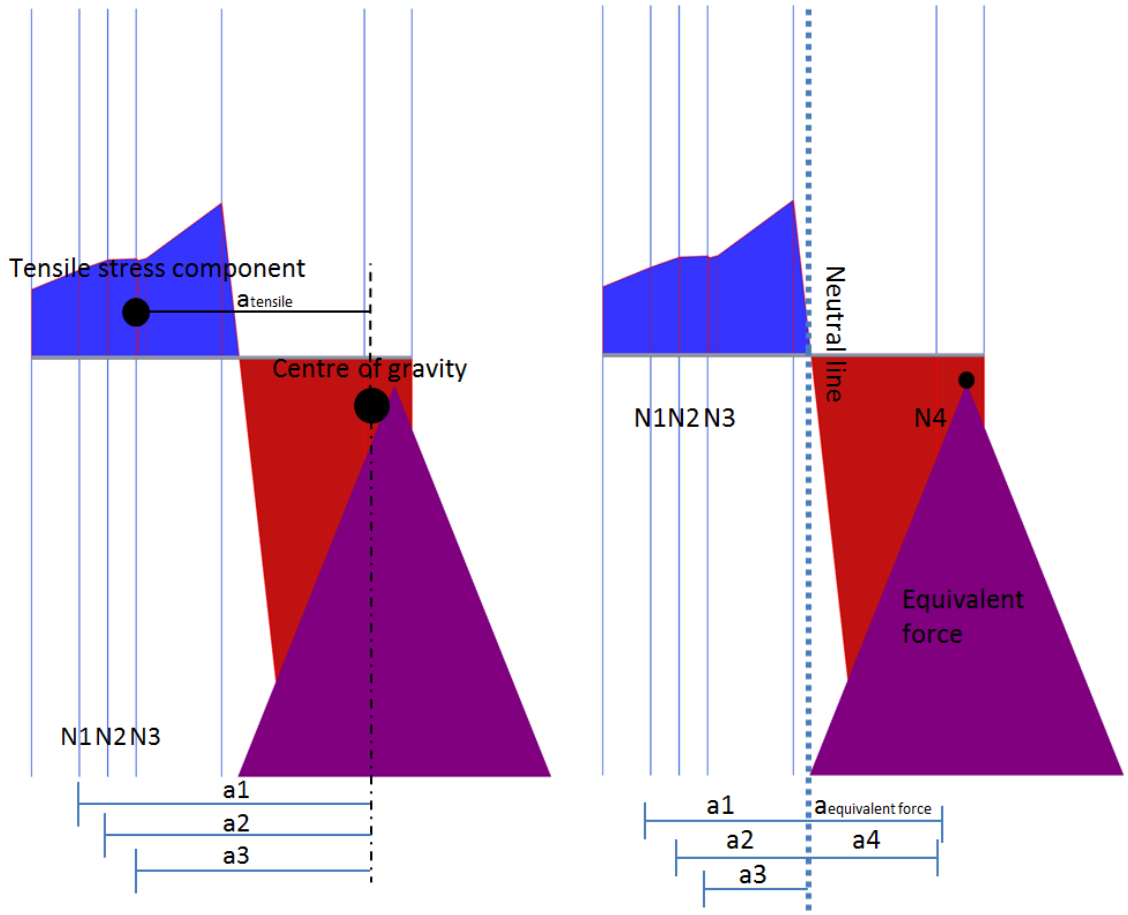

Figure A-48: On the left the first mechanical equilibrium method (centre of gravity) and on the right the second mechanical equilibrium method (equivalent force/neutral line) to calculate the bending moment.

D.1.4 Soil-structure interaction case

Below in Figure A-49 the bending moments for the single plate reinforced diaphragm wall outputted to the excavation depth are given for the four possibilities to obtain the bending moment in the normative cross-section. It is already found that only the method by mechanics gives realistic bending moments for a statically determined structure. To clarify the differences however all methods to obtain the bending moment in the structure are visualised in Figure A-49.

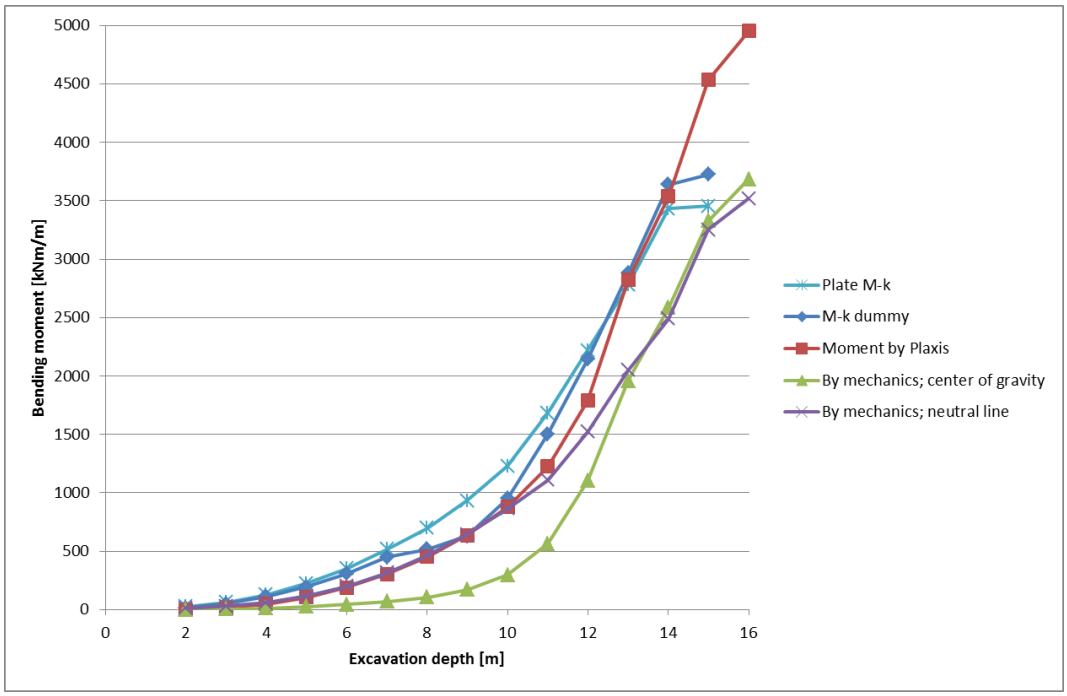

Figure A-49: Bending moment for progressing excavation depth given by a M-κ plate element and a reinforced Shotcrete volume element considering four different back calculation methods to obtain the bending moment.

The method used by Plaxis overestimates the moment capacity very highly. The maximum bending moment according to Plaxis is 4950 kNm/m. It is shown in chapter 3.3.2 that when a normal force of 2 MPa is applied a maximum bending moment of 4839 kNm/m can be obtained. The hand calculated maximum moment of the structure is 3586 kNm/m without taking into account the second order effect, a deforming cross-section, the self-weight of the structure and shear forces acting on the structure. Though these will not lead to a normal force higher than 2 MPa in the structure. Therefore the moment obtained can be regarded as not appropriate for modelling with a reinforced Shotcrete volume element.

Furthermore it is shown that using the dummy M-κ element gives an underestimation of the bending capacity of the diaphragm wall. Without dummy element the Shotcrete model is able to resist a meter deeper excavation without failure. Influence of a deforming cross-section, shear forces acting on the wall and self-weight of the structure causes the difference between the plate element calculation and the Shotcrete volume element calculation. This confirms the added value of using the Shotcrete model to design reinforced concrete structures.

The correct failure moment of the Shotcrete diaphragm wall can be obtained by using the mechanical equilibrium calculation. When using the centre of gravity approach it under estimates the bending moment when the cracking pattern is not fully developed yet, due to the remaining tensile capacity. Approaching failure leads to an increasingly more correct obtained moment due to the decreasing effect of tensile capacity in the tensile zone. It is shown that it converges with the neutral line method by mechanics. This takes the tensile capacity into account during the whole process of loading. The failure bending moment in 3516 kN/m which is almost equal to the hand calculated maximum moment capacity. The verification of this method on the statically determined bending beam showed that it only differs 2 % from the hand calculation which does not take shear

deformation into account. The observation in this case proves the reliability of using this method to determine the bending moment.

For more insight, in Figure A-50 also the obtained bending moments by the different methods versus the displacement of the diaphragm wall are given. It is shown that by mechanics neutral line method gives the most reliable results from uncracked to fully cracked to failure of the reinforced concrete wall. However a small remark must be made about the not completely smooth progression of the bending moment with increased displacement.

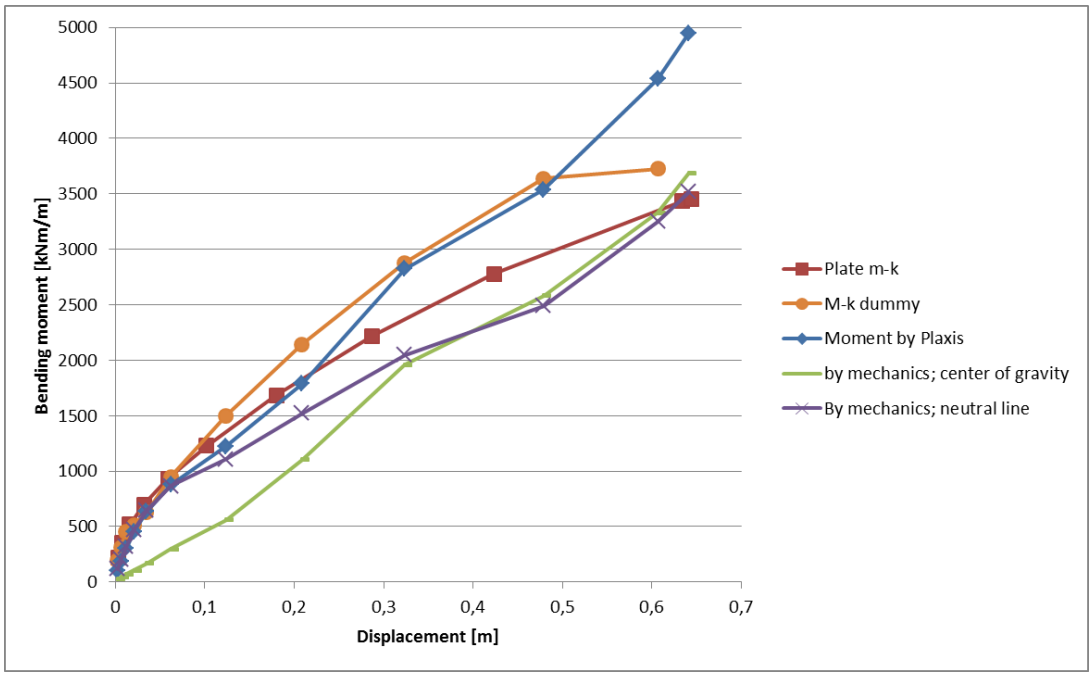

Figure A-50: Bending moment obtained at different displacements of the diaphragm wall given by a M-κ plate element and a reinforced Shotcrete volume element considering four different back calculation methods to obtain the bending moment.

D.1.5 KIS project

Also for the KIS project the four different methods of obtaining the bending moment of the reinforced Shotcrete volume element can be compared. It is already concluded that only the equilibrium by forces on the neutral gives accurate moment predictions for a statically determined structure and therefore also for the excavation case next to the diaphragm wall. However to clarify the need of the proposed moment calculation method and to illustrate the effect on the obtained bending moment using the other calculation methods also the KIS project is evaluated.

In Table A-15 the obtained bending moments for the different calculation methods, indicated by: M-κ dummy, Plaxis moment, equilibrium centre of gravity and equilibrium neutral line, are given. The differences are given with respect to the reference, linear elastic plate element with reduced stiffness of 20.000 MPa, case.

Table A-15: Obtained bending moment in a plate reinforced Shotcrete volume element by four different methods, compared to the bending moment in a linear elastic plate element with reduced stiffness.

Calculation method	Bending moment [kNm/m]	Difference with respect to reference [%]
M-κ dummy	1175	-38.9
Plaxis moment	1525	-20.7
Equilibrium centre of gravity	1751	-9.0
Equilibrium neutral line	1594	-17.2

In Table A-15 it is shown that every method gives a reduction in bending moment with respect to the linear elastic plate element case, taking into account reduced stiffness, for the same deformation. Taking in mind the fact that the (force) equilibrium at the neutral line gives realistic results, the effect of using the other methods for designing can be evaluated. The approach with the equilibrium of forces at the neutral line gives a reduction of 17.2 % in bending moment with respect to the reference case.

The force equilibrium at the centre of gravity approach leads to an overestimation of the moment with respect to the one at the neutral line. Overestimation is conservative but also disregards the advantage of using a reinforced Shotcrete volume element over a simple linear elastic plate element calculation. The overestimation of the moment is the effect of taking a crude approximation of the remaining tensile stresses in the tensile zone.

The calculation of the moment by using the integrated function in Plaxis to output the bending moment in the volume element and add by hand the moment caused by the normal force in the reinforcement underestimates the moment slightly. This means that this method is not conservative in the design and as mentioned before the results will differ a lot when structural failure is reached.

Using the conventional way in obtaining moments, by an equivalent to the structure including reinforcement M-κ based plate element, will cause a huge underestimation of the occurring bending moment in the diaphragm wall. This way of calculating the moment can therefore be regarded as not conservative and inappropriate when accounting for non-linear material behaviour including cracking.

D.1.6 Conclusion

In this appendix it shown there is only one correct way to back calculate the bending moments of a reinforced (by plate elements) Shotcrete volume element. Due to the fact that the Shotcrete material model accounts for non-linear material behaviour and softening by means of cracking two commonly used methods will not give realistic results. The dummy element works properly for a linear elastic volume element but using an equivalent M-κ dummy element is not satisfying for a statically determined bending beam test as well as for more complicated (soil-structure interaction) cases. Furthermore the option to output the moments by Plaxis does not give appropriate results in case of using a by plates reinforced Shotcrete volume element in the case of a statically determined bending beam test and more complex cases. The equilibrium method regarding the centre of gravity of the compressive zone as point at which the bending moment can be back calculated, disregards or crudely approximates the effect of remaining tensile strength (stress) after cracking and in between cracking. This method is therefore only accurate in case of almost complete failure of the structure. The equilibrium method considering the equivalent force, with its arm to the neutral line, and the

normal force in the reinforcement with its arm to the neutral line results in obtaining the correct moment for a statically determined structure. The results of using this method are shown for as well an excavation next to a diaphragm wall as the KIS case study. This method is used for the results stated in the main report.

D.2 Guide for using the Shotcrete material model

Using the Shotcrete material model in a soil-structure interaction case requires a sequence of steps to be followed. Below the steps to be followed are explained.

1. Input proposed parameter values for normal strength structural concrete

In this research standard input parameter values for normal strength structural concrete of different strength classes are found. These are given below in Table A-16. These values consider also time dependent behaviour, despite this is excluded in further research. When excluding time dependent behaviour the parameters E_1/E_{28} and $f_{c,1}/f_{c,28}$ have to be set equal to 1. The other time dependent parameters as, ϕ_{cr}, t_{50}^{cr}, ϵ_{∞}^{shr}, t_{50}^{shr} and t_{hydr} have to be set equal to 0.

Table A-16: Standard input parameters for the Shotcrete model in case of modeling normal strength structural concrete.

Parameter	Proposed value for normal strength structural concrete (time dependent modelling)	Proposed value for normal strength structural concrete (time independent modelling)	Unit
ν	0.2	0.2	--
ψ	13	13	Deg
E_1/E_{28}	0.6	1	--
$f_{c,1}/f_{c,28}$	0.25	1	--
f_{c0n}	0.33	0.33	--
f_{cfn}	0.85	0.85	--
f_{cun}	0.10	0.10	--
f_{tun}	0	0	
$G_{t,28}$	0.15	0.15	kN/m
l_{eq}	--	--	--
a	No confinement	No confinement	--
ϕ_{max}	35	35	Deg
ϕ_{cr}	1.9 – 2.7	0	--
t_{50}^{cr}	3	0	d
ϵ_{∞}^{shr}	-0.00049 – -0.00061	0	%
t_{50}^{shr}	200	0	d
γ_{fc}	--	--	--
γ_{ft}	--	--	--
t_{hydr}	28	0	d

2. Input concrete specific parameters

Besides there are concrete parameters which are specific for each case. The difference in input value is caused by the concrete class, the parameter consideration (characteristic or design values) and the stress-strain design method. The first parameters to be inputted are the modulus of elasticity (after 28 days), uniaxial compressive and tensile strength, respectively E_{28}, f_c and f_t. In the Eurocode 2 for each concrete class these parameters are stated. The characteristic values for the strength and stiffness parameters are given in Table A-1. For design values these values have to be divided by a factor of 1.5. Other parameters to be inputted are the plastic peak strain ϵ_{cp}^{p} and the fracture energy G_c. These are needed to fit the model to the by Eurocode 2 described (different) stress-strain diagram(s).

3. Fitting the peak and failure strain according to Eurocode 2 recommendations in the soil-test facility in Plaxis

The soil-test facility, modelling a uniaxial compression test, in Plaxis is needed to fit a stress-strain diagram for the concrete material behaviour by the Shotcrete material model, which is in accordance to Eurocode 2 recommendations. A correct fit is required in order to give a good representation of the concrete behaviour and be able to use the model to design a structure. The parameters needed to fit the Shotcrete material model are the plastic peak strain ϵ_{cp}^{p} and the fracture energy G_c. Fitting of the plastic peak strain is necessary to fit the peak strength at a certain value of strain. The peak strength has to occur at 1.75 ‰ strain when method 1 (Linear elastic-Perfectly plastic) in Eurocode 2 is used to describe the concrete stress strain behaviour and a strain of 2.2 ‰ (for C30/37) when parabolic stress-strain behaviour is considered.

The fracture energy G_c is needed to fit the strain at which material failure occurs correctly to Eurocode recommendations. The strain at which failure occurs is defined in the Eurocode 2 as 3.5 ‰. The fracture energy G_c determines the area under the stress-strain graph between peak and failure strength and therefore the strain at which failure occurs. In the soil-test facility in Plaxis it is possible to calibrate the fracture energy G_c such that failure occurs at a strain of 3.5 ‰ in a uniaxial compression test.

4. Plate elements as reinforcement with equivalent surface area and determining of moment of inertia of reinforcement

For reinforcement of the Shotcrete volume element plate elements will be used. An elastoplastic plate element should be used such that yield strength (435 N/mm^2) of the reinforcement can be inputted. The input for a plate element furthermore consists of a EA and EI. The modulus of stiffness of the steel reinforcement can be considered as a fixed value of 210 000 000 kN/m^2. However other types of reinforcement (according to other guidelines) can relate to another magnitude. The area of the reinforcement can be determined by tables which give an equivalent area for different reinforcement configurations, the diameter of the reinforcement bars and the number of reinforcement bars. The moment of inertia has be fitted such that the thickness of the plate element is equal to the ratio of area of the reinforcement with respect to the area of the cross-section. To coop with different reinforcement beds on one side of the structure, one equivalent (sectioned) plate can be calculated. The equivalent plate can be calculated based on the strain in each individual reinforcement bed and the distance to the neutral line, by means of a ratio. This ratio has to be

multiplied with the characteristics of the concerned reinforcement bed and has to be added to the first reinforcement bed (furthest away from the neutral line) in the section where the multiple beds are present.

5. Dimensioning the reinforced concrete structure in Plaxis

Drawings of the reinforced concrete structure form the basis of the model. Different reinforcement plates need to be created with for instance a differentiation of compressive and tensile reinforcement. These different plate elements have to be created in the equivalent to the drawings concrete cross-section.

6. Calculate the situation correctly
7. Obtaining the bending moments of the structure

In appendix D.1 a description of the different possibilities to output the bending moments of the structure are evaluated. It is concluded that the bending moment can only be obtained correctly by using an internal force equilibrium at the neutral line of the normative cross-section. The neutral line changes with a change in load wherefore at every governing load step in the normative cross-section a cross-section has to be drawn. The normative cross-section can be found by evaluating the normal force in the plate element(s). The normative cross-section is at the point where the normal force in the plate element is maximum. Drawing a cross-section at that point gives information about the equivalent force of the stresses in that cross-section and its coordinates with respect to the neutral line. Multiplying the equivalent force in the cross-section with the arm to the neutral line and add the normal force in the reinforcement (plate element) in that cross-section with its arm to the neutral line will give the correct governing bending moment. For engineering convenience this method can be used, however it is also possible to rely on failure criteria which are directly outputted by Plaxis. A check on the bending moment is equal to a check on the occurring normal force in the reinforcement and the strain in the compressive zone of the structure.

8. Evaluate results such as bending moments, deformation of the structure and normal forces in the reinforcement.

The last step consists, as in every other calculation, of analysing and evaluating the results. Not only the structural part but also the geotechnical part including factors such as shear stresses at the interface have to be regarded.

Appendix E: Modelling results

E.1 Sensitivity analysis

E.1.1 Poisson's ratio results

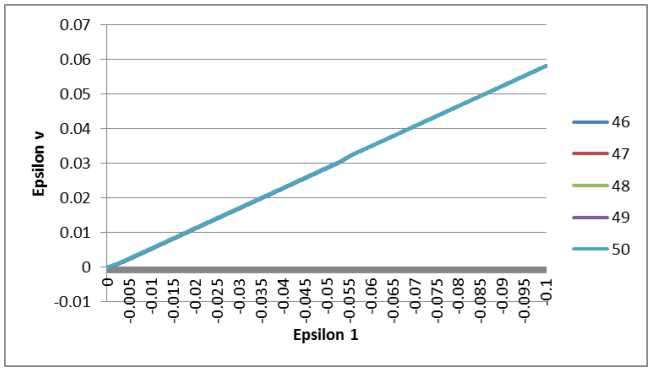

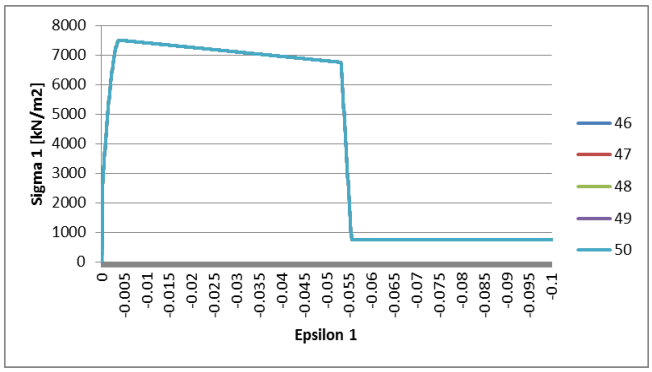

E.1.2 Angle of internal friction results

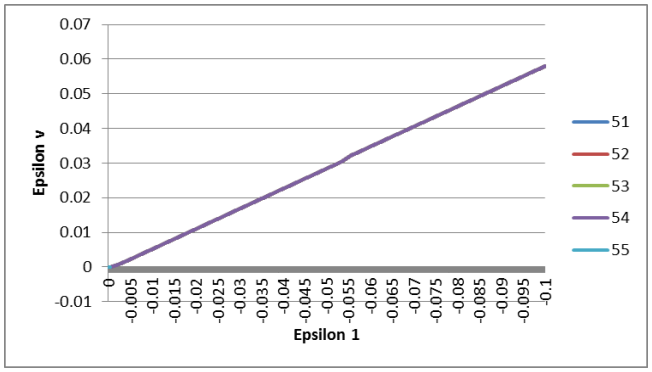

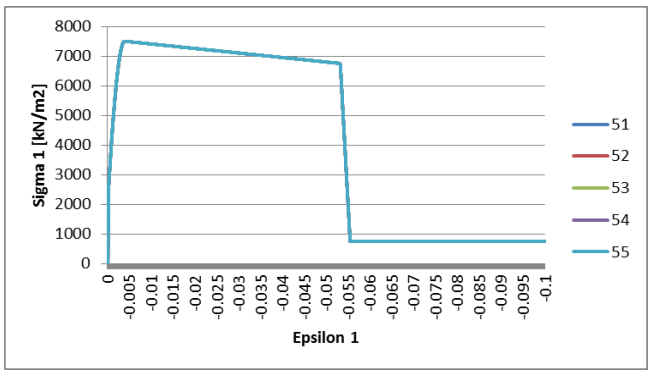

E.1.3 Time at which half of the creep strains have occurred results

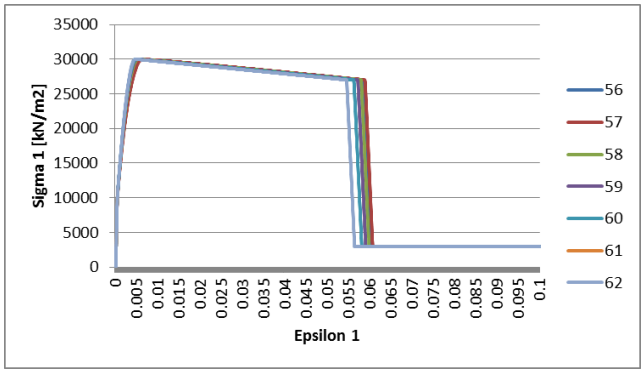

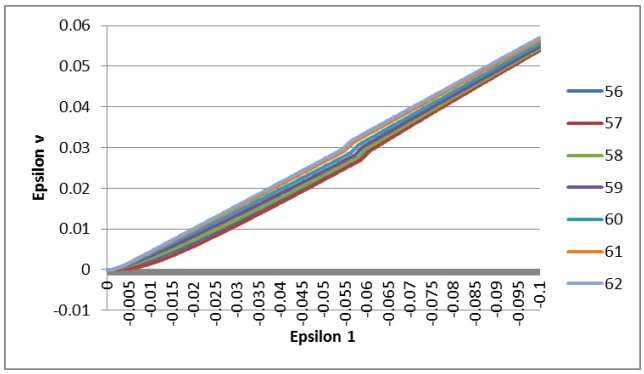

E.2 Single plate reinforced Mohr-Coulomb model results

E.2.1 Results applied line load of 10 kN/m

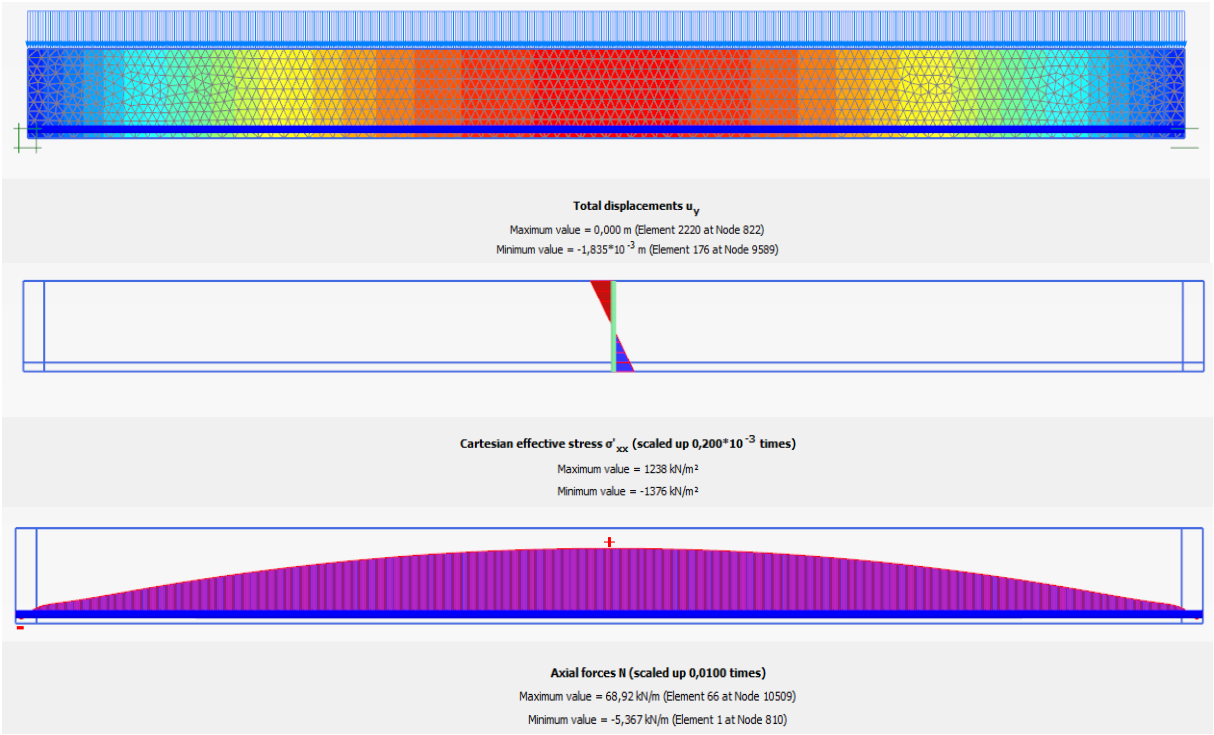

E.2.2 Results applied line load of 14 kN/m

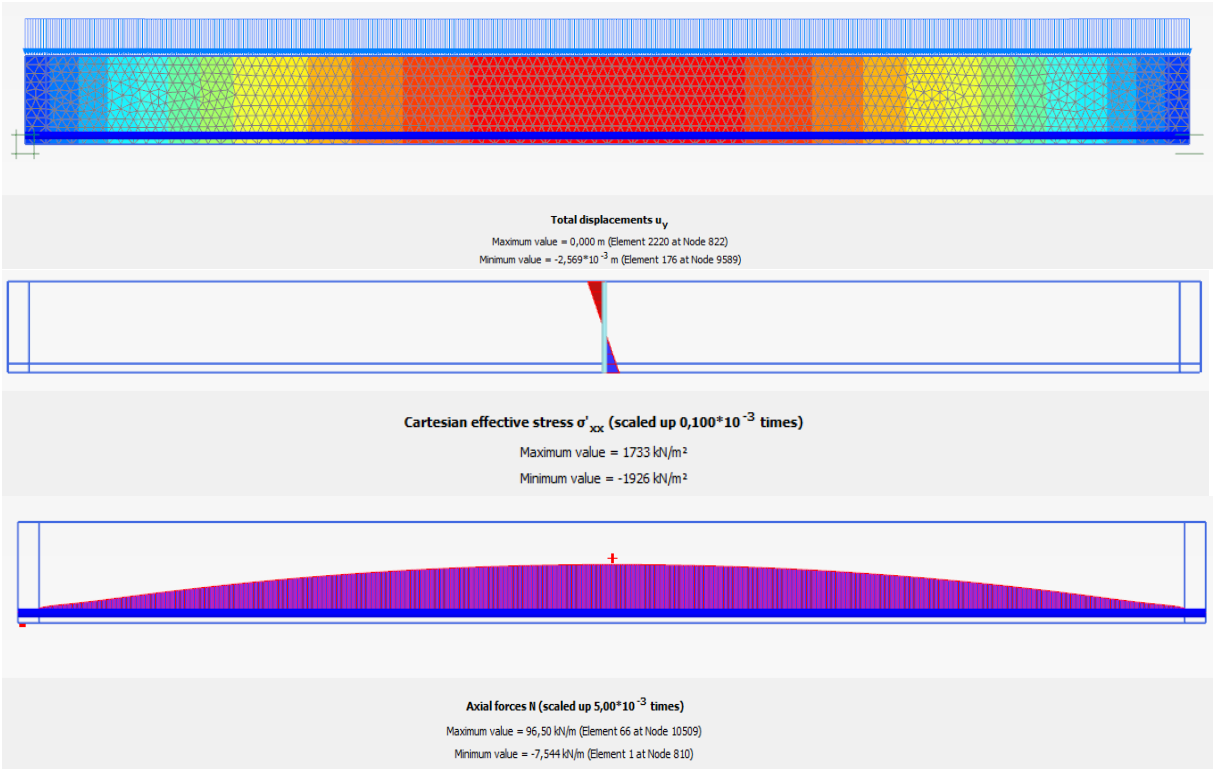

E.2.3 Results applied line load of 15 kN/m

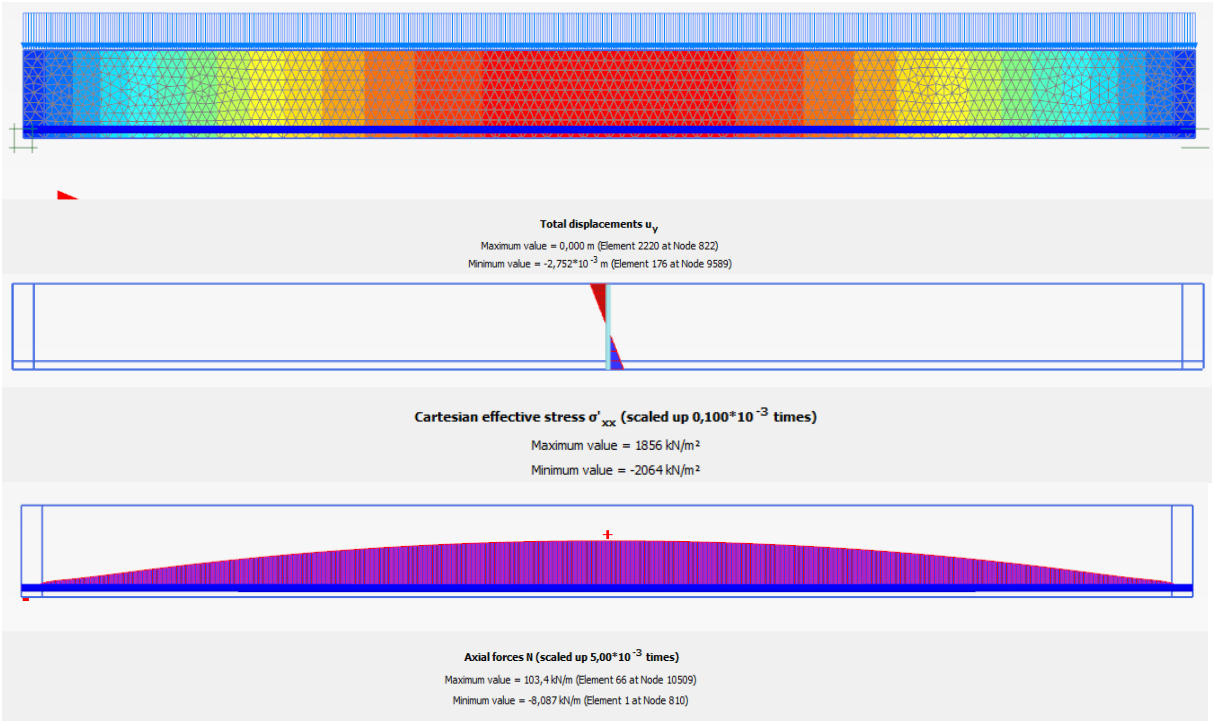

E.2.4 Results applied line load of 16 kN/m

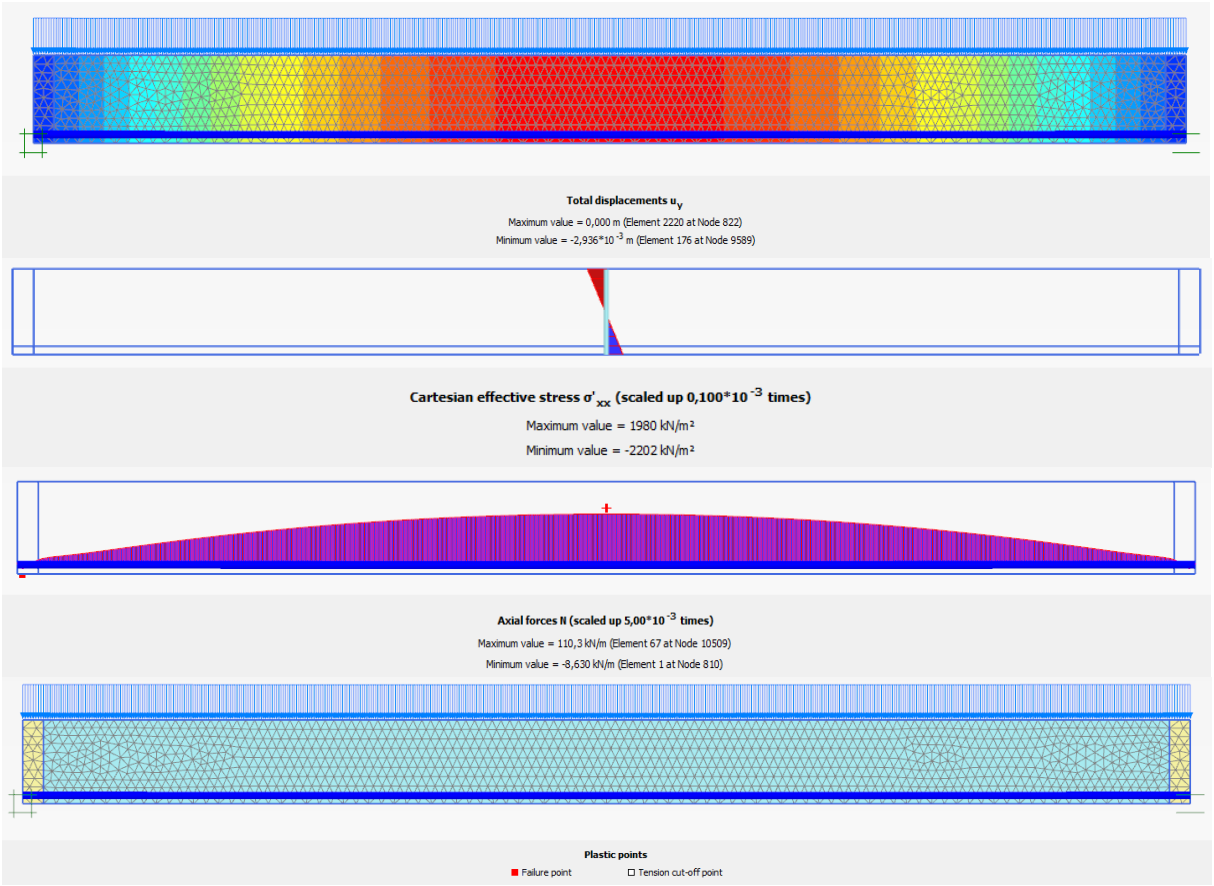

E.2.5 Results applied line load of 17 kN/m

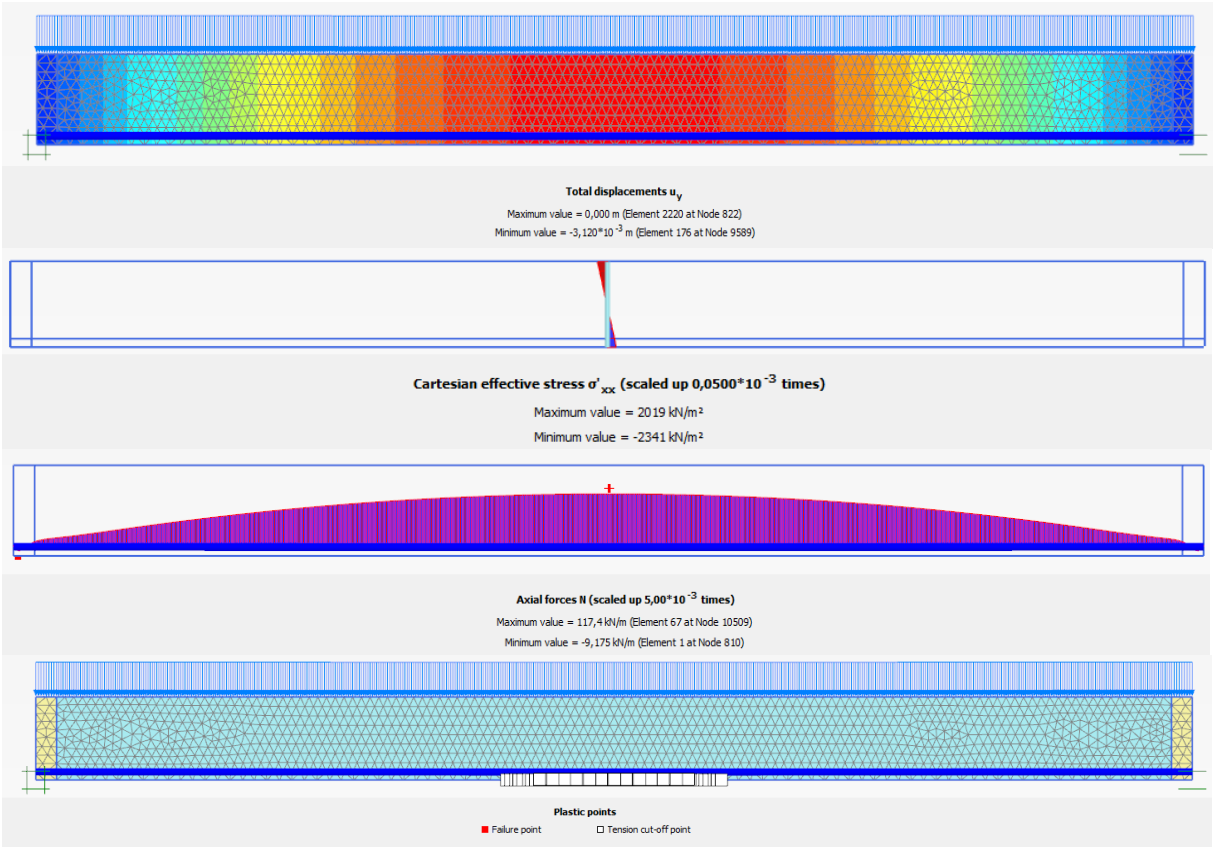

E.2.6 Results applied line load of 20 kN/m

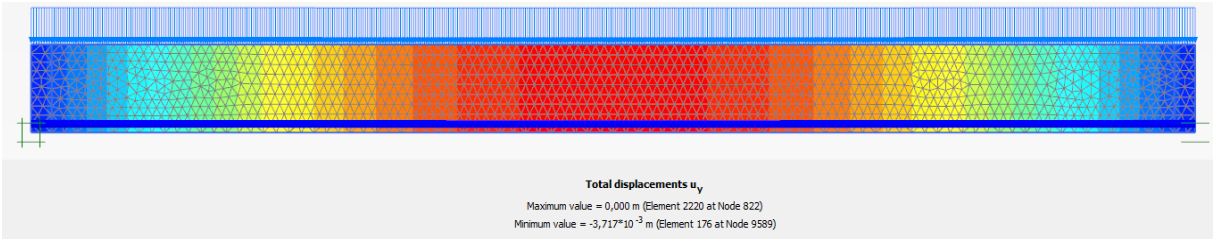

Total displacements u_y

Maximum value = 0,000 m (Element 2220 at Node 822)

Minimum value = -3,717*10^{-3} m (Element 176 at Node 9589)

Cartesian effective stress σ'_{xx} (scaled up 0,0500*10^{-3} times)

Maximum value = 2030 kN/m²

Minimum value = -2797 kN/m²

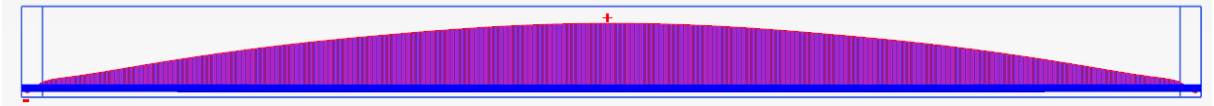

Axial forces N (scaled up 5,00*10^{-3} times)

Maximum value = 143,6 kN/m (Element 66 at Node 10437)

Minimum value = -10,82 kN/m (Element 1 at Node 810)

E.2.7 Results applied line load of 30 kN/m

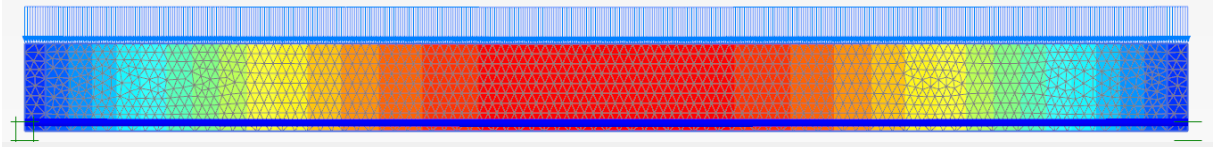

Total displacements u_y

Maximum value = 0,000 m (Element 2220 at Node 822)

Minimum value = -6,385*10^{-3} m (Element 176 at Node 9589)

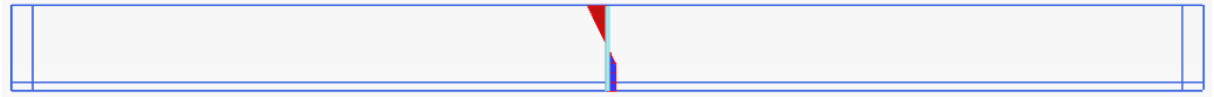

Cartesian effective stress σ'_{xx} (scaled up 0,0500*10^{-3} times)

Maximum value = 2000 kN/m²

Minimum value = -4664 kN/m²

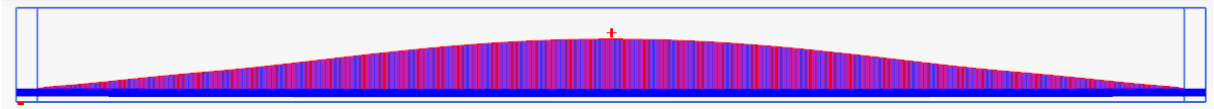

Axial forces N (scaled up 2,00*10^{-3} times)

Maximum value = 287,6 kN/m (Element 67 at Node 10509)

Minimum value = -16,06 kN/m (Element 1 at Node 810)

E.2.8 Results applied line load of 40 kN/m

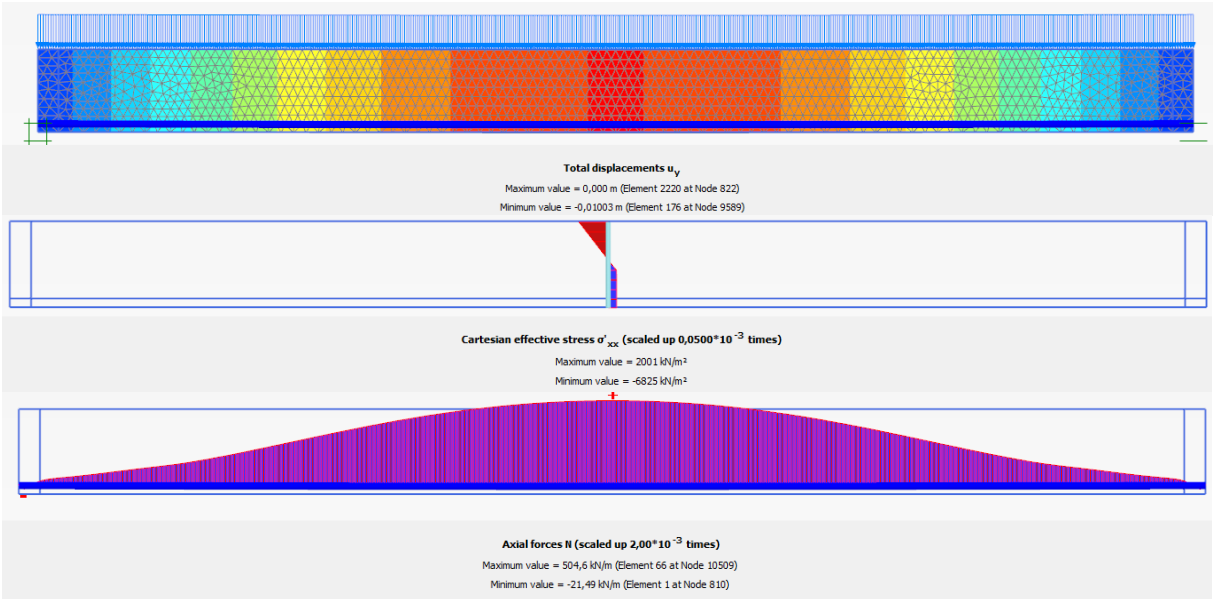

E.2.9 Results applied line load of 50 kN/m

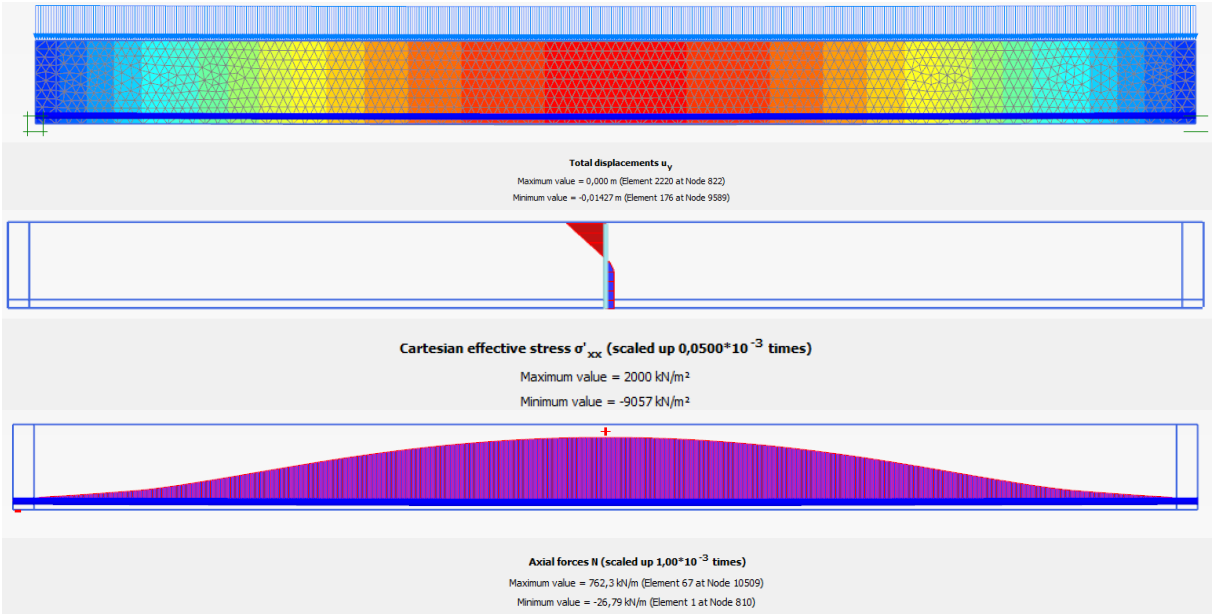

E.2.10 Results applied line load of 70 kN/m

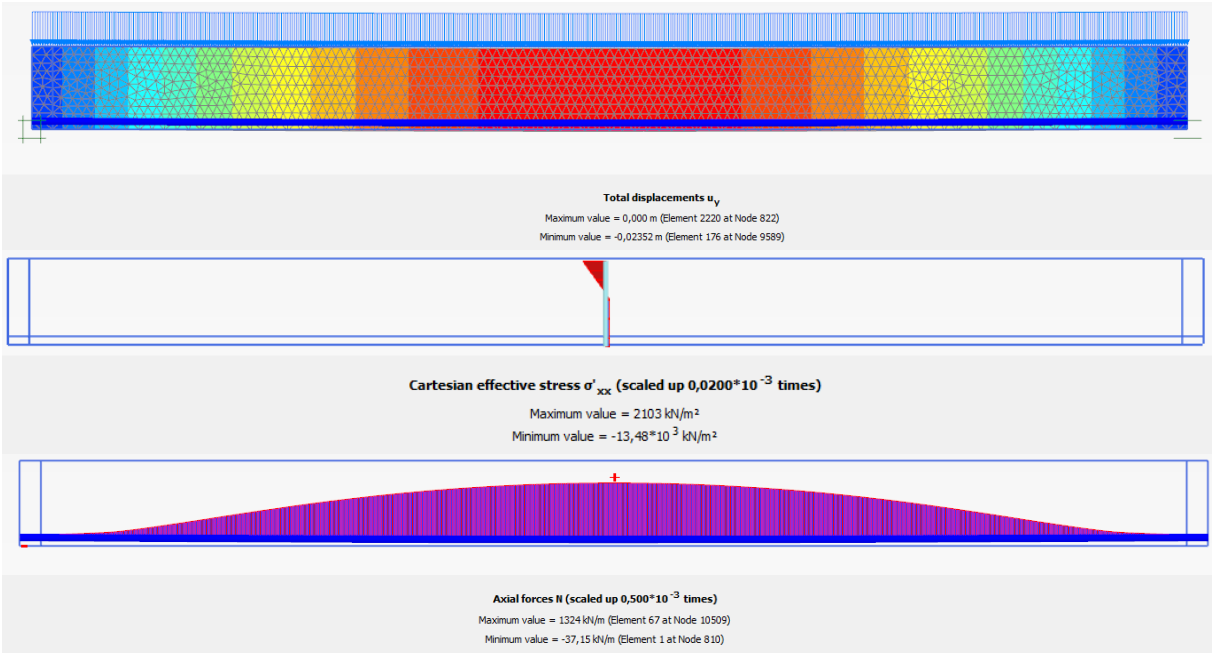

E.2.11 Results applied line load of 80 kN/m

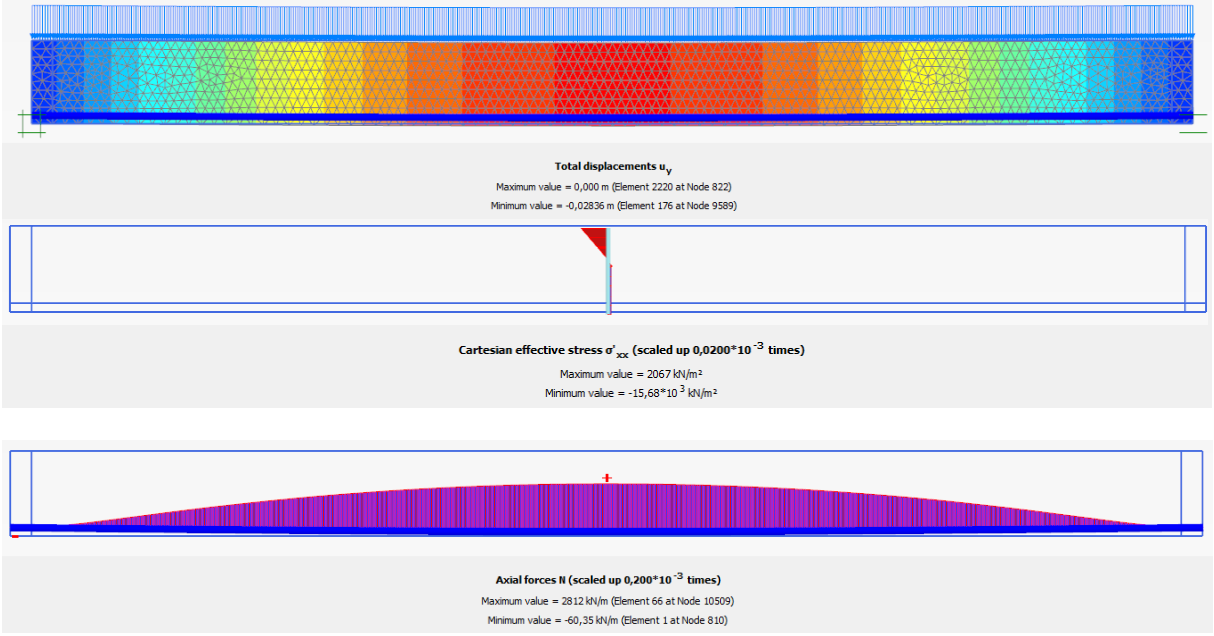

E.2.12 Results applied line load of 120 kN/m

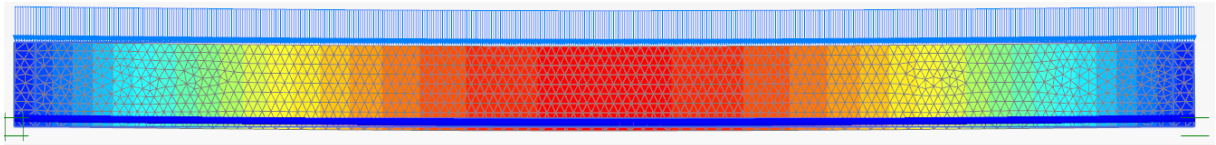

Total displacements u_y
Maximum value = 0,000 m (Element 2220 at Node 822)
Minimum value = -0,04826 m (Element 176 at Node 9589)

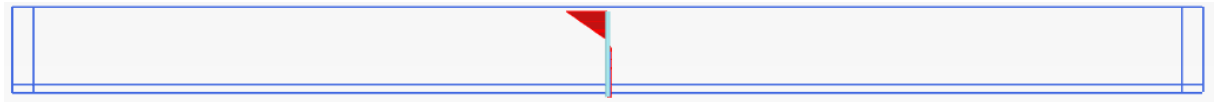

Cartesian effective stress σ'_{xx} (scaled up $0{,}0200*10^{-3}$ times)
Maximum value = 2000 kN/m²
Minimum value = $-24{,}39*10^{3}$ kN/m²

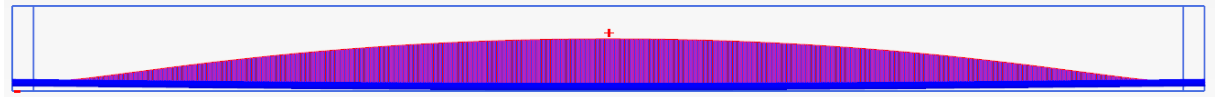

Axial forces N (scaled up $0{,}200*10^{-3}$ times)
Maximum value = 2812 kN/m (Element 66 at Node 10509)
Minimum value = -60,35 kN/m (Element 1 at Node 810)

E.2.13 Results applied line load of 138.3 kN/m (yielding)

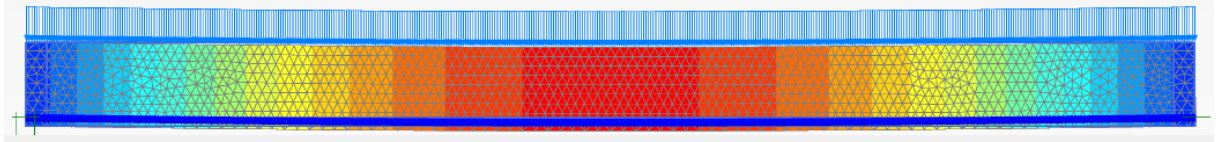

Total displacements u_y
Maximum value = 0,000 m (Element 2220 at Node 822)
Minimum value = -0,05761 m (Element 176 at Node 9589)

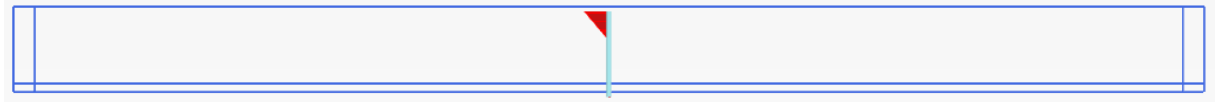

Cartesian effective stress σ'_{xx} (scaled up $0{,}0100*10^{-3}$ times)
Maximum value = 2009 kN/m²
Minimum value = $-28{,}38*10^{3}$ kN/m²

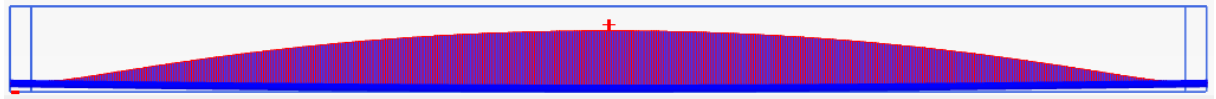

Axial forces N (scaled up $0{,}200*10^{-3}$ times)
Maximum value = 3369 kN/m (Element 66 at Node 10509)
Minimum value = -68,87 kN/m (Element 1 at Node 810)

E.2.14 Results applied line load of 142.5 kN/m (concrete yielding)

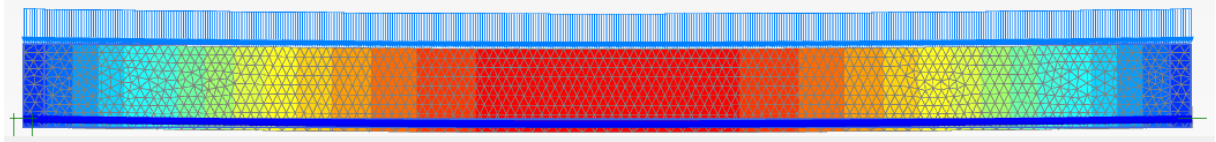

Total displacements u_y
Maximum value = 0,000 m (Element 2220 at Node 822)
Minimum value = -0,05970 m (Element 176 at Node 9589)

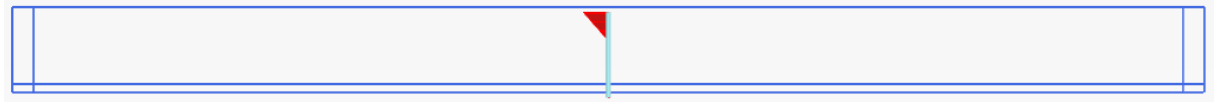

Cartesian effective stress σ'_{xx} (scaled up $0{,}0100*10^{-3}$ times)
Maximum value = 2010 kN/m²
Minimum value = $-29{,}26*10^{3}$ kN/m²

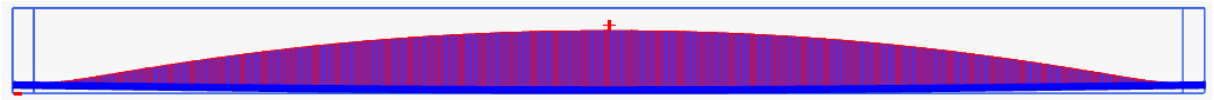

Axial forces N (scaled up $0{,}200*10^{-3}$ times)

Maximum value = 3493 kN/m (Element 67 at Node 10509)

Minimum value = -70,77 kN/m (Element 1 at Node 810)

E.2.15 Results applied line load of 146.4 kN/m (failure)

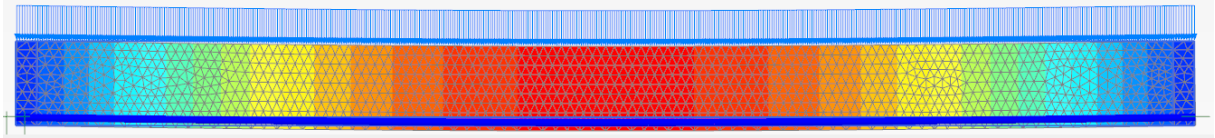

Total displacements u_y

Maximum value = 0,000 m (Element 2220 at Node 822)

Minimum value = -0,06170 m (Element 176 at Node 9589)

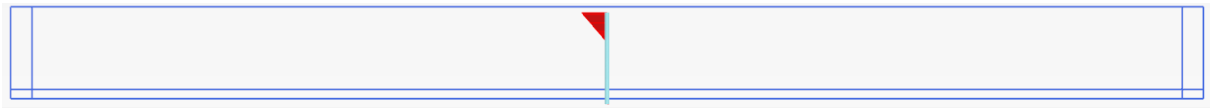

Cartesian effective stress σ'_{xx} (scaled up $0{,}0100*10^{-3}$ times)

Maximum value = 2011 kN/m²

Minimum value = $-30{,}11*10^{3}$ kN/m²

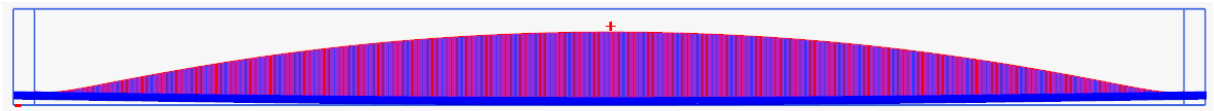

Axial forces N (scaled up $0{,}200*10^{-3}$ times)

Maximum value = 3611 kN/m (Element 66 at Node 10509)

Minimum value = -72,58 kN/m (Element 1 at Node 810)

E.2.16 Results applied line load of 150 kN/m (model failure)

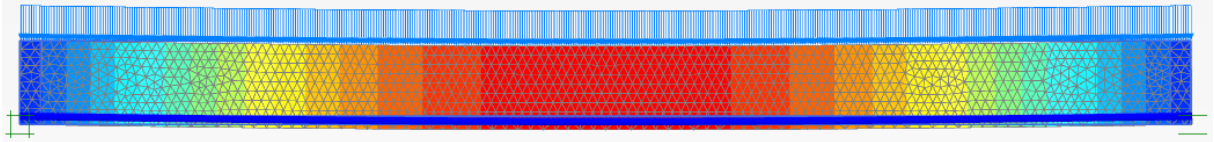

Total displacements u_y

Maximum value = 0,000 m (Element 2220 at Node 822)

Minimum value = -0,06353 m (Element 176 at Node 9589)

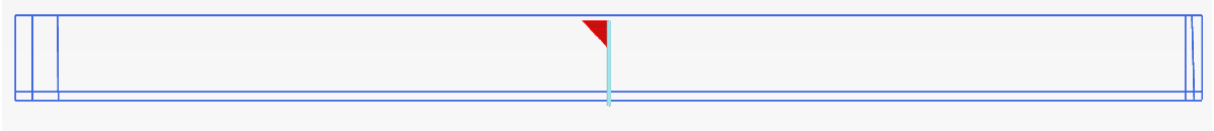

Effective normal stresses (cross section) σ'_N (scaled up $0{,}0100*10^{-3}$ times)

Maximum value = 2000 kN/m²

Minimum value = $-30{,}81*10^{3}$ kN/m²

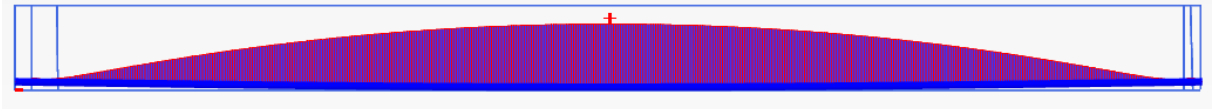

Axial forces N (scaled up $0{,}200*10^{-3}$ times)

Maximum value = 3720 kN/m (Element 68 at Node 11824)

Minimum value = -51,33 kN/m (Element 1 at Node 690)

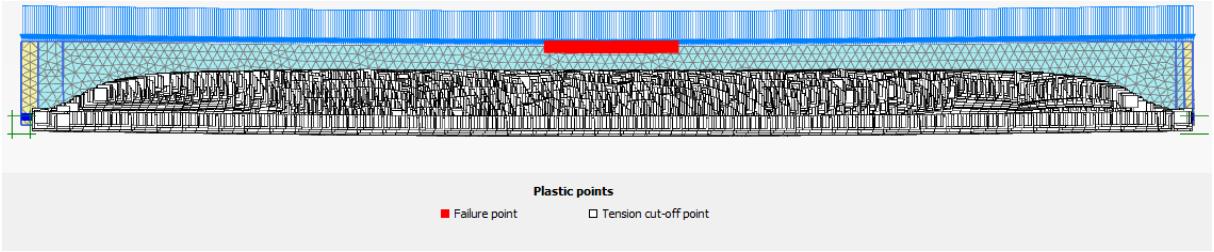

E.3 Single plate reinforced Shotcrete model results

E.3.1 Results applied line load of 10 kN/m

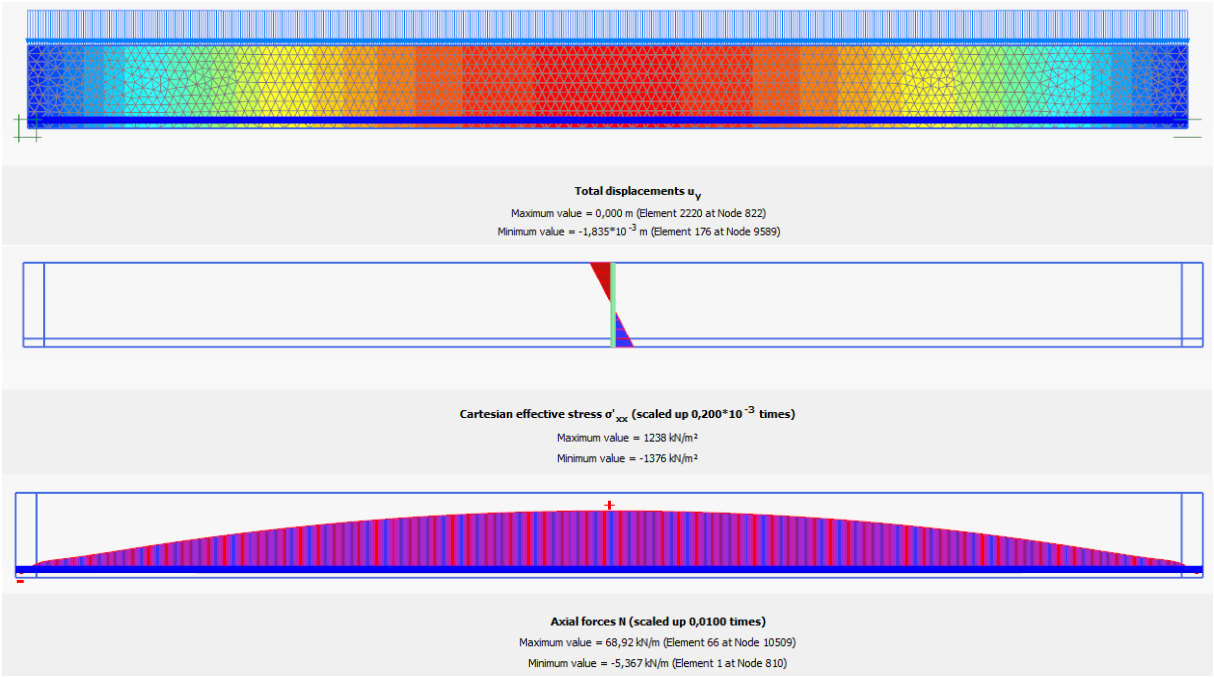

E.3.2 Results applied line load of 14 kN/m

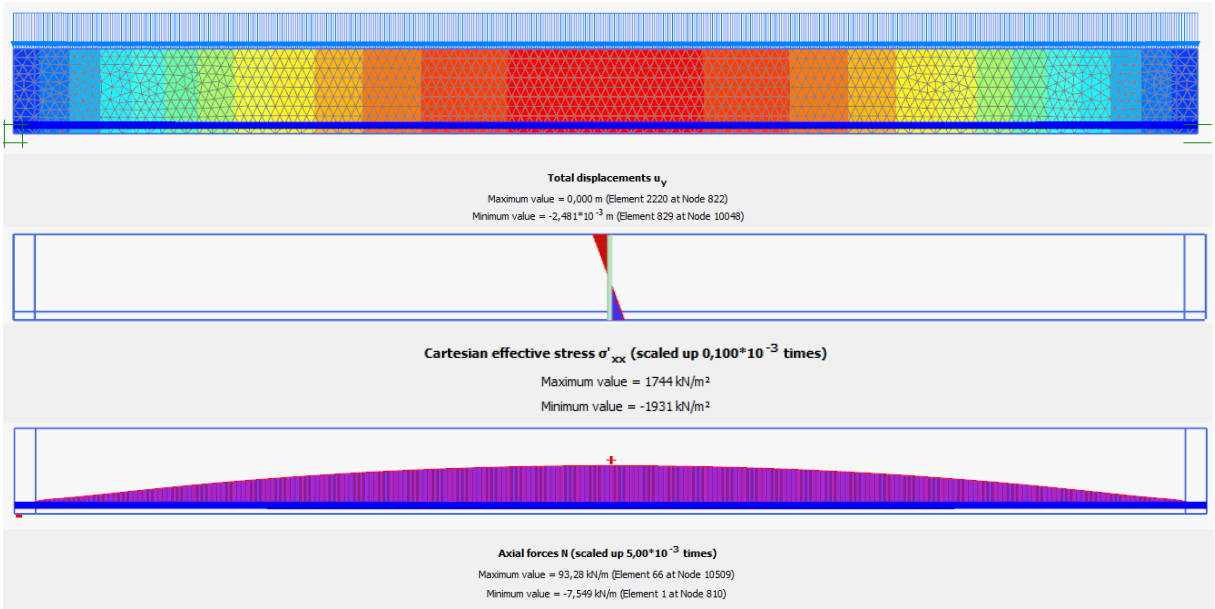

E.3.3 Results applied line load of 15 kN/m

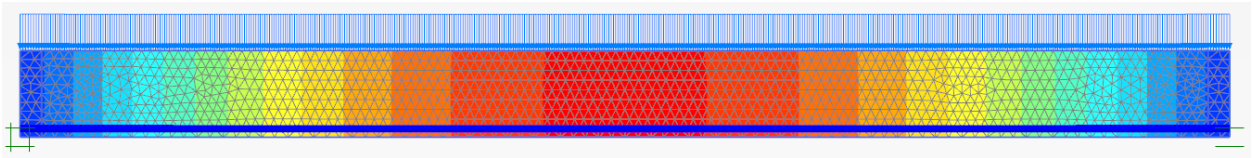

Total displacements u_y

Maximum value = 0,000 m (Element 2220 at Node 822)

Minimum value = -2,658*10^{-3} m (Element 829 at Node 10048)

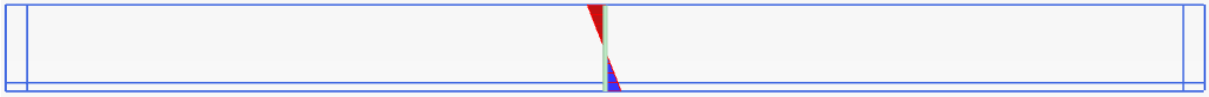

Cartesian effective stress σ'_{xx} (scaled up 0,100*10^{-3} times)

Maximum value = 1868 kN/m²

Minimum value = -2069 kN/m²

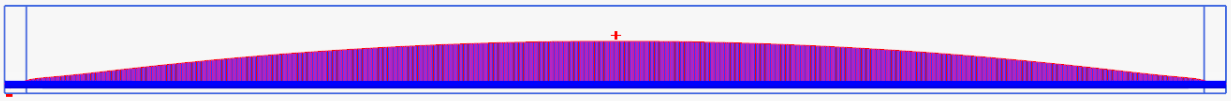

Axial forces N (scaled up 5,00*10^{-3} times)

Maximum value = 99,94 kN/m (Element 67 at Node 10509)

Minimum value = -8,093 kN/m (Element 1 at Node 810)

E.3.4 Results applied line load of 16 kN/m

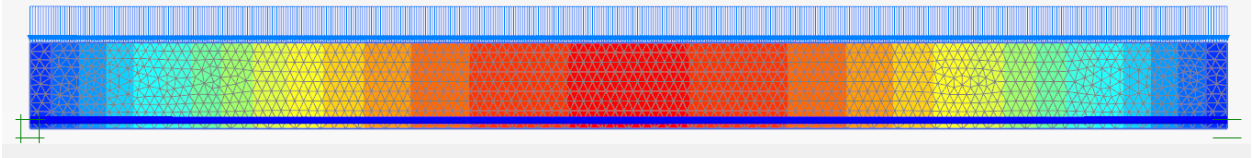

Total displacements u_y

Maximum value = 0,000 m (Element 2220 at Node 822)

Minimum value = -2,835*10^{-3} m (Element 829 at Node 10048)

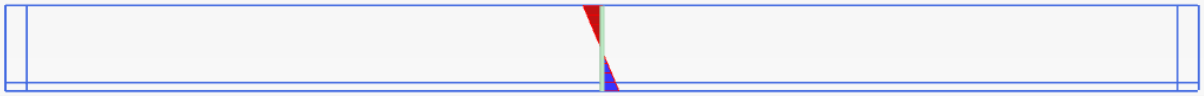

Cartesian effective stress σ'_{xx} (scaled up 0,100*10^{-3} times)

Maximum value = 1993 kN/m²

Minimum value = -2207 kN/m²

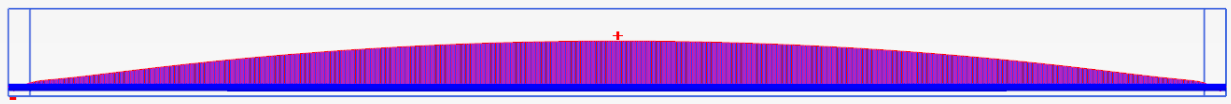

Axial forces N (scaled up 5,00*10^{-3} times)

Maximum value = 106,6 kN/m (Element 67 at Node 10509)

Minimum value = -8,638 kN/m (Element 1 at Node 810)

E.3.5 Results applied line load of 17 kN/m

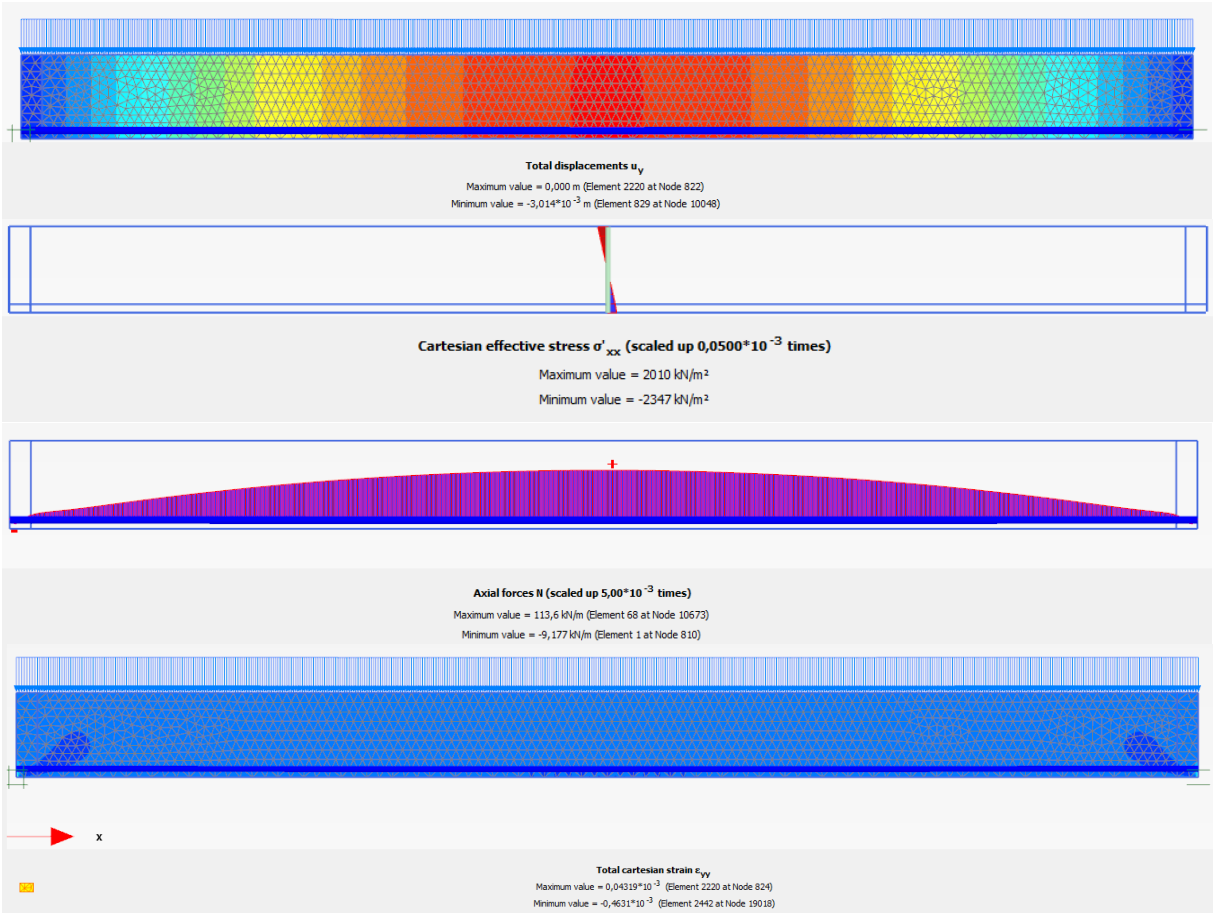

E.3.6 Results applied line load of 20 kN/m

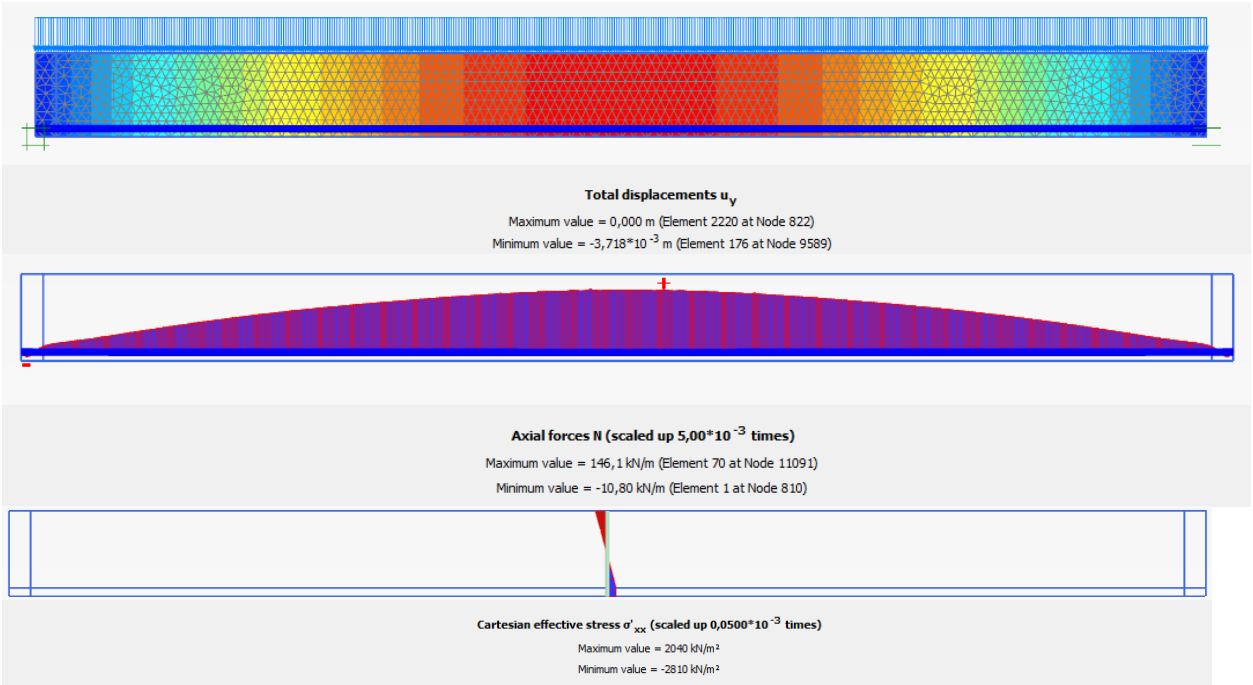

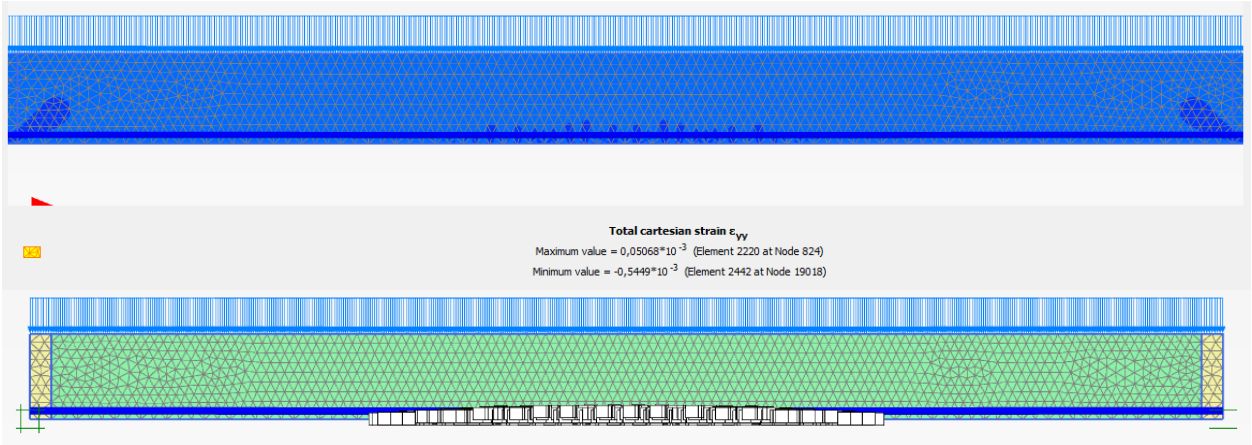

E.3.7 Results applied line load of 30 kN/m

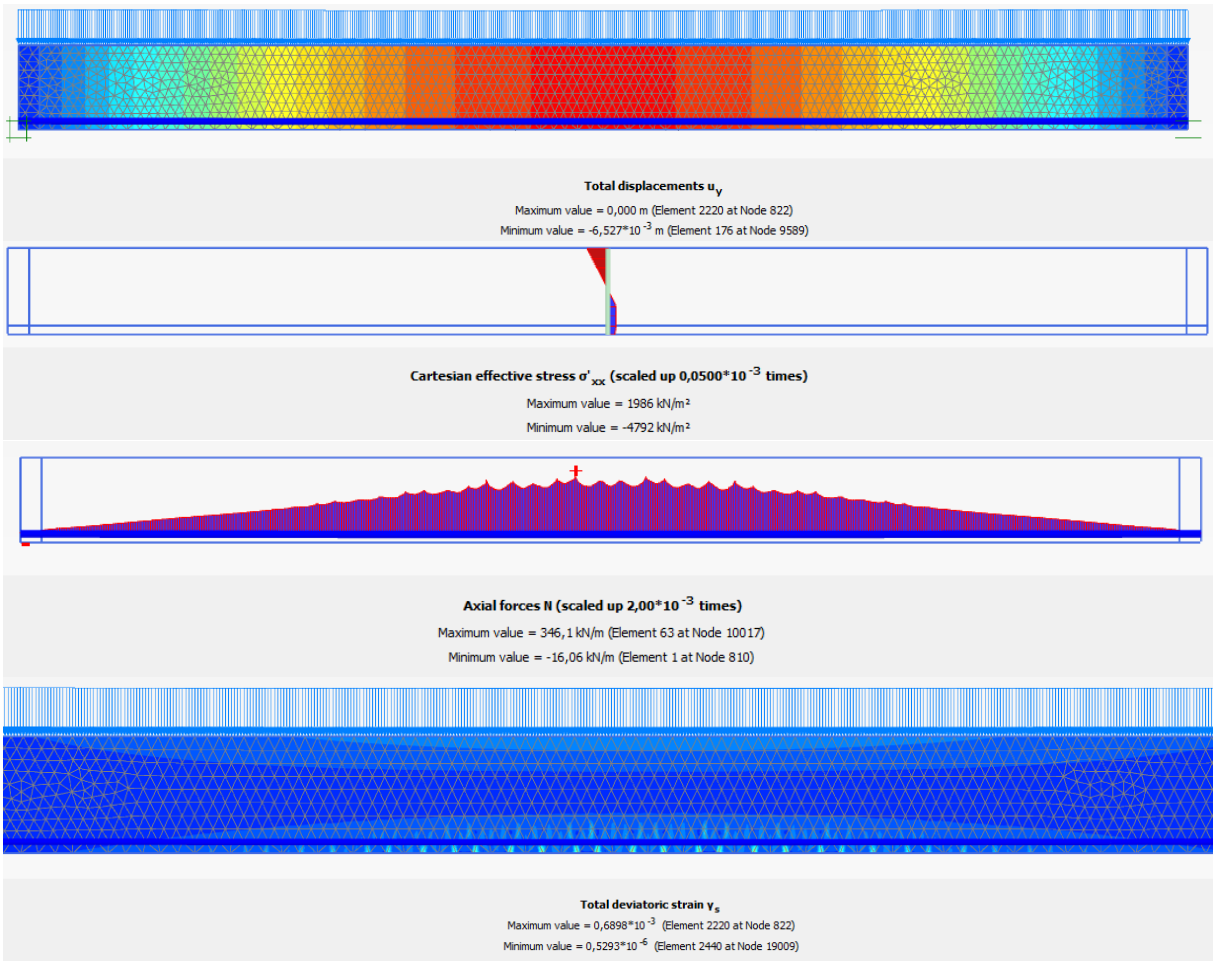

E.3.8 Results applied line load of 40 kN/m

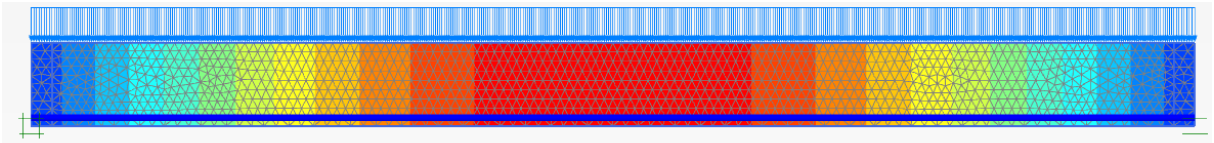

Total displacements u_y

Maximum value = 0,000 m (Element 2220 at Node 822)

Minimum value = -0,01193 m (Element 2265 at Node 10637)

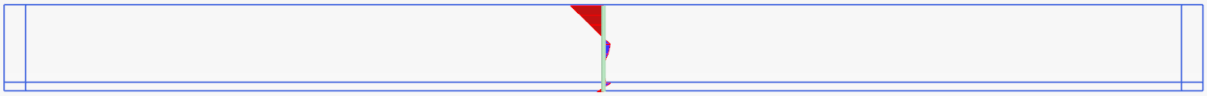

Cartesian effective stress σ'_{xx} (scaled up $0{,}0500*10^{-3}$ times)

Maximum value = 1770 kN/m²

Minimum value = -7758 kN/m²

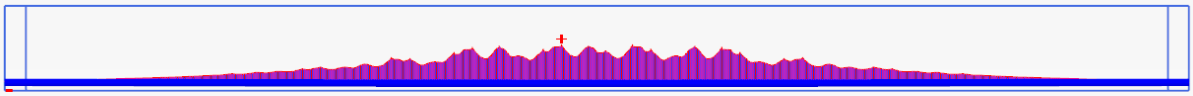

Axial forces N (scaled up $0{,}500*10^{-3}$ times)

Maximum value = 920,7 kN/m (Element 63 at Node 10017)

Minimum value = -21,61 kN/m (Element 1 at Node 810)

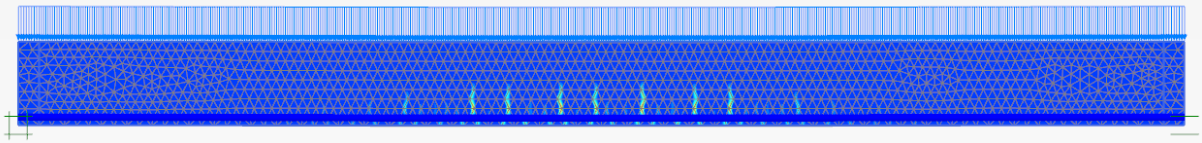

Total deviatoric strain γ_s

Maximum value = $2{,}566*10^{-3}$ (Element 434 at Node 11059)

Minimum value = $1{,}802*10^{-6}$ (Element 2440 at Node 19009)

E.3.9 Results applied line load of 50 kN/m

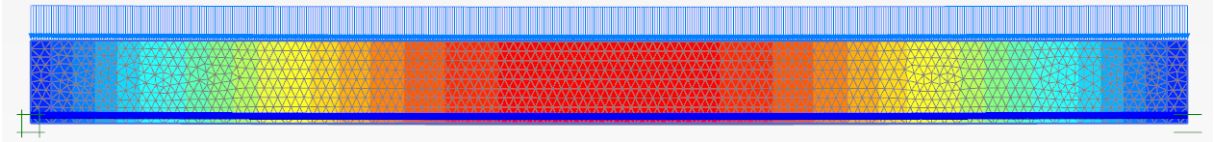

Total displacements u_y

Maximum value = 0,000 m (Element 2220 at Node 822)

Minimum value = -0,01788 m (Element 2264 at Node 10429)

Cartesian effective stress σ'_{xx} (scaled up $0{,}0500*10^{-3}$ times)

Maximum value = 1199 kN/m²

Minimum value = $-10{,}15*10^{3}$ kN/m²

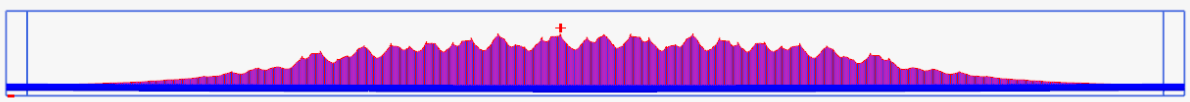

Axial forces N (scaled up $0{,}500*10^{-3}$ times)

Maximum value = 1318 kN/m (Element 63 at Node 10017)

Minimum value = -26,77 kN/m (Element 1 at Node 810)

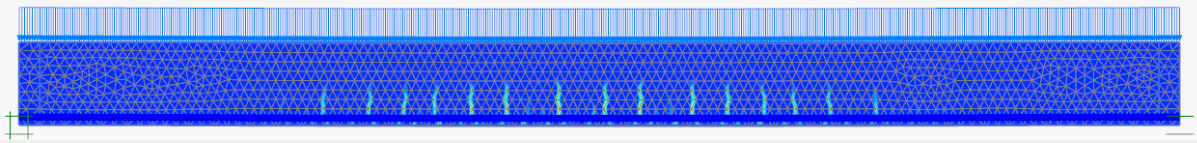

Total deviatoric strain γ_s

Maximum value = $4{,}158*10^{-3}$ (Element 433 at Node 9619)

Minimum value = $2{,}268*10^{-6}$ (Element 1354 at Node 14322)

E.3.10 Results applied line load of 70 kN/m

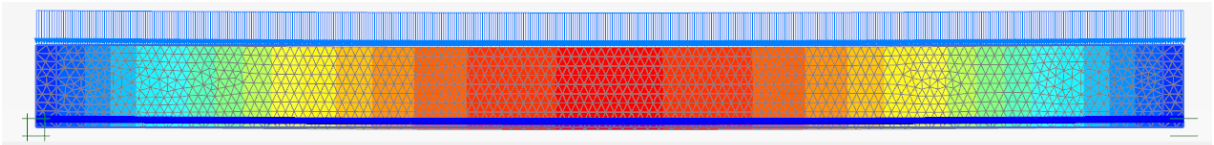

Total displacements u_y

Maximum value = 0,000 m (Element 2220 at Node 822)

Minimum value = -0,03038 m (Element 2264 at Node 10439)

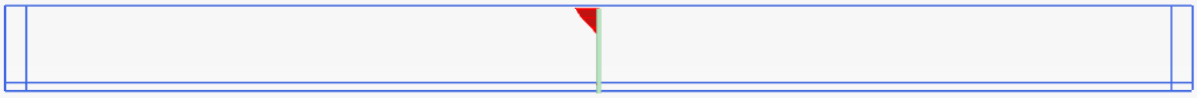

Cartesian effective stress σ'_{xx} (scaled up $0{,}0200*10^{-3}$ times)

Maximum value = 1128 kN/m²

Minimum value = $-13{,}63*10^{3}$ kN/m²

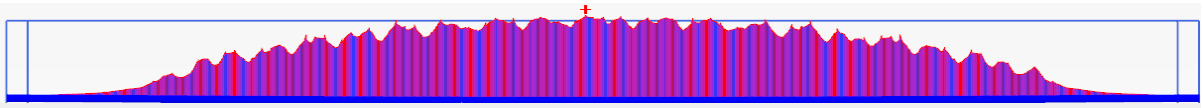

Axial forces N (scaled up $0{,}500*10^{-3}$ times)

Maximum value = 1991 kN/m (Element 65 at Node 10239)

Minimum value = -37,16 kN/m (Element 1 at Node 810)

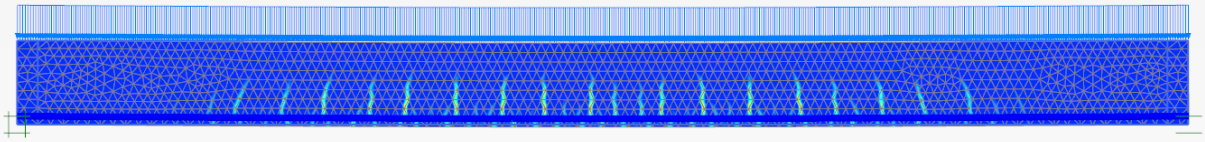

Total deviatoric strain γ_s

Maximum value = $6{,}768*10^{-3}$ (Element 447 at Node 9275)

Minimum value = $1{,}278*10^{-6}$ (Element 1634 at Node 3759)

E.3.11 Results applied line load of 80 kN/m

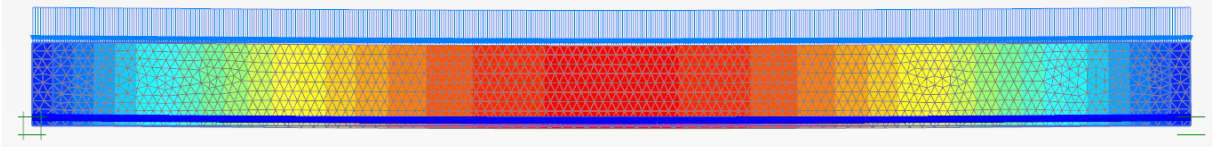

Total displacements u_y

Maximum value = 0,000 m (Element 2220 at Node 822)

Minimum value = -0,03669 m (Element 2264 at Node 10439)

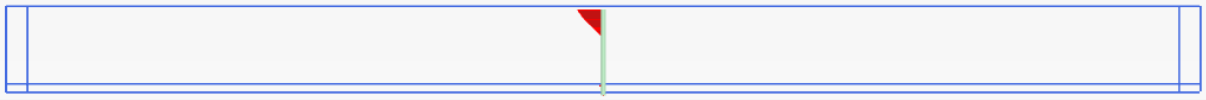

Cartesian effective stress σ'_{xx} (scaled up $0{,}0200*10^{-3}$ times)

Maximum value = 959,7 kN/m²

Minimum value = $-15{,}12*10^{3}$ kN/m²

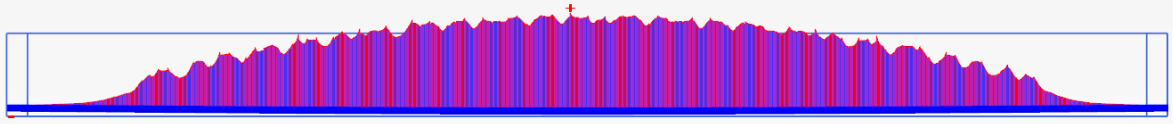

Axial forces N (scaled up $0{,}500*10^{-3}$ times)

Maximum value = 2362 kN/m (Element 65 at Node 10239)

Minimum value = -41,72 kN/m (Element 1 at Node 810)

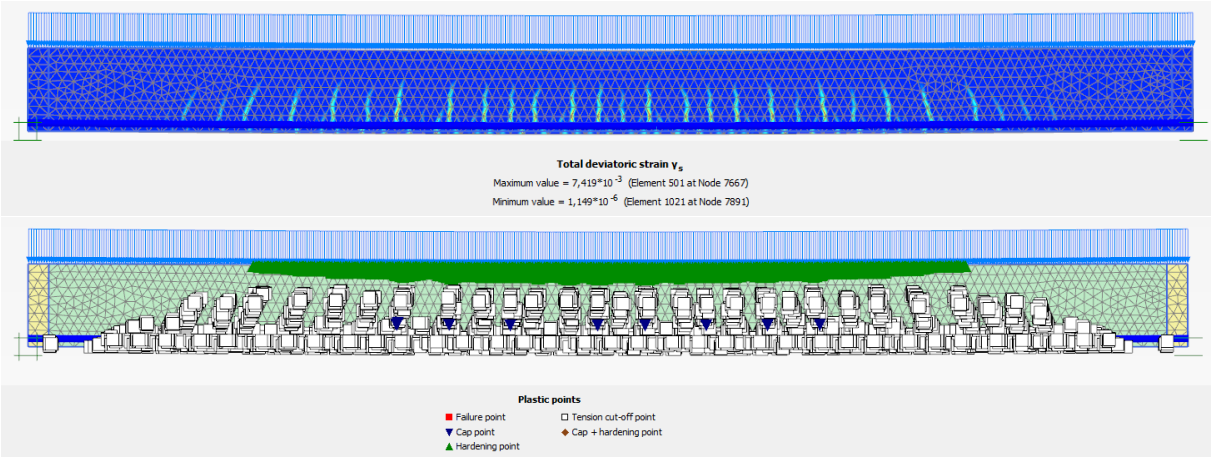

E.3.12 Results applied line load of 120 kN/m

E.3.12.1 G_t=0.1kN/m

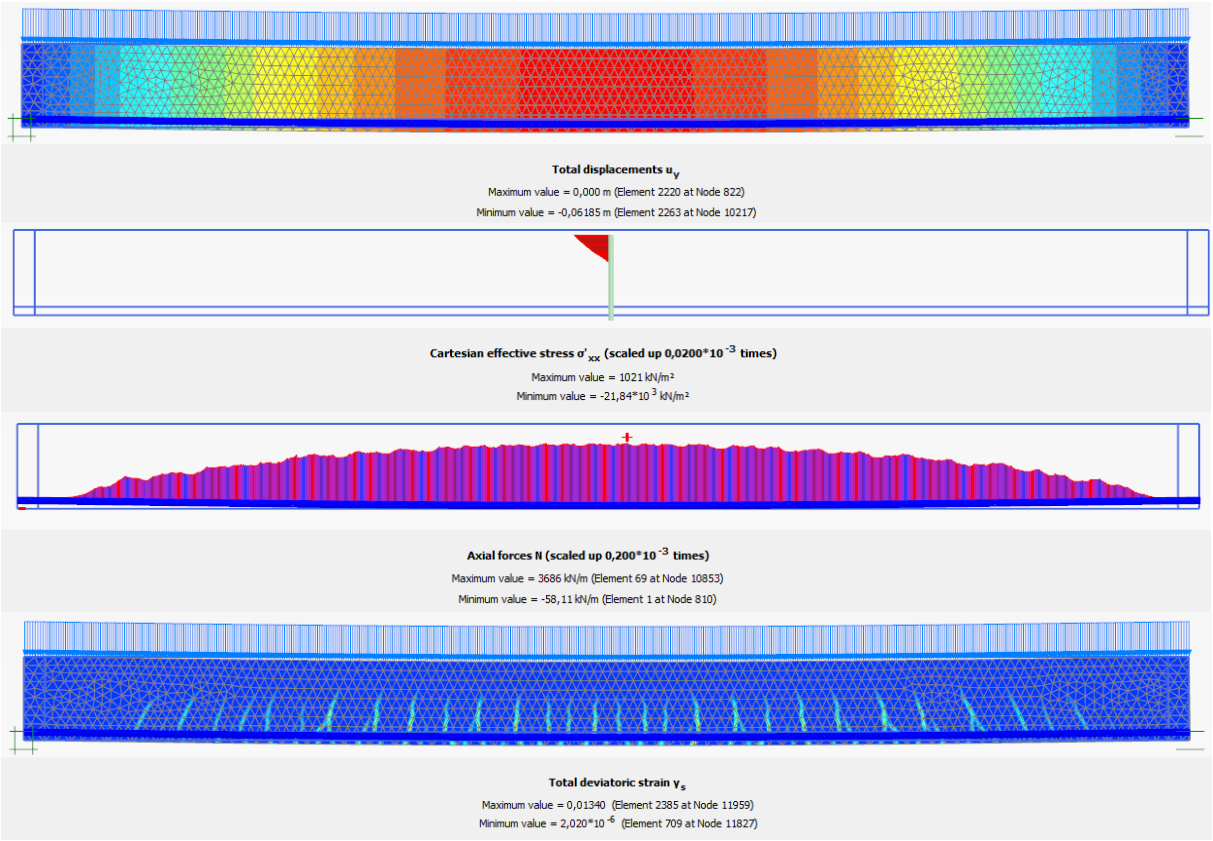

E.3.12.2 G_t=0.15kN/m

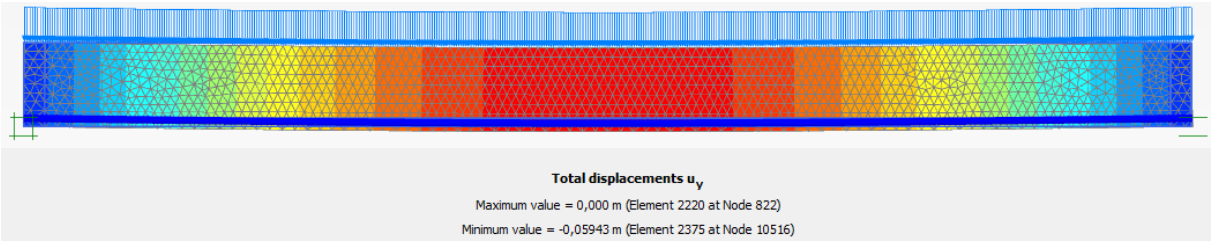

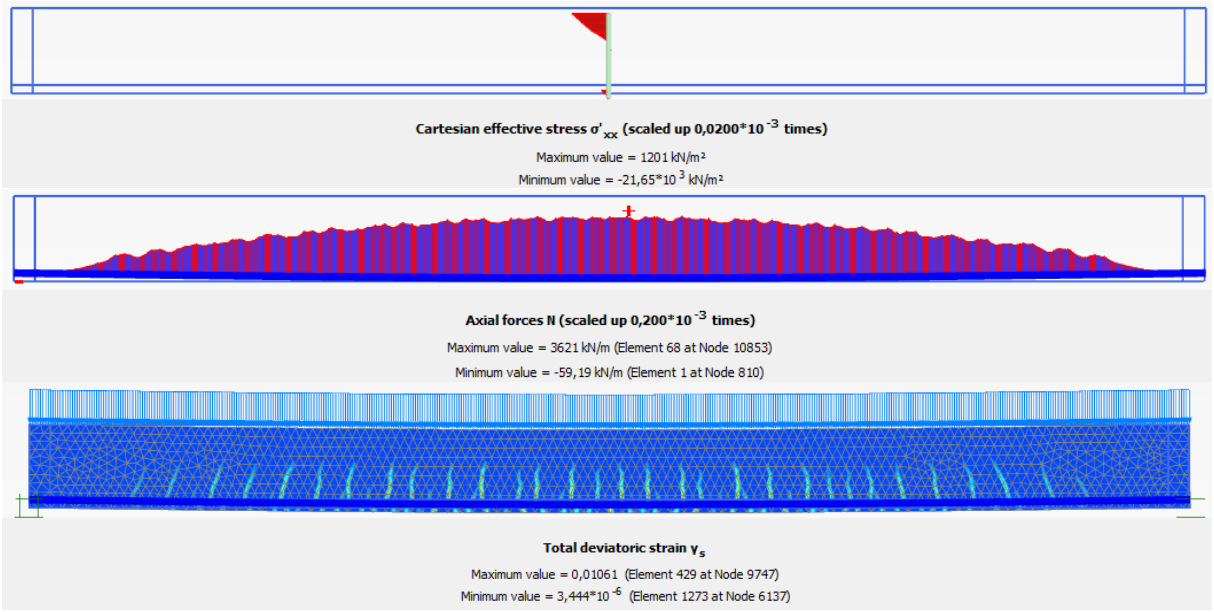

E.3.13 Results applied line load of 138.3 kN/m (yielding) (G_t=0.15 kN/m)

E.3.13.1 Linear elastic reinforcement

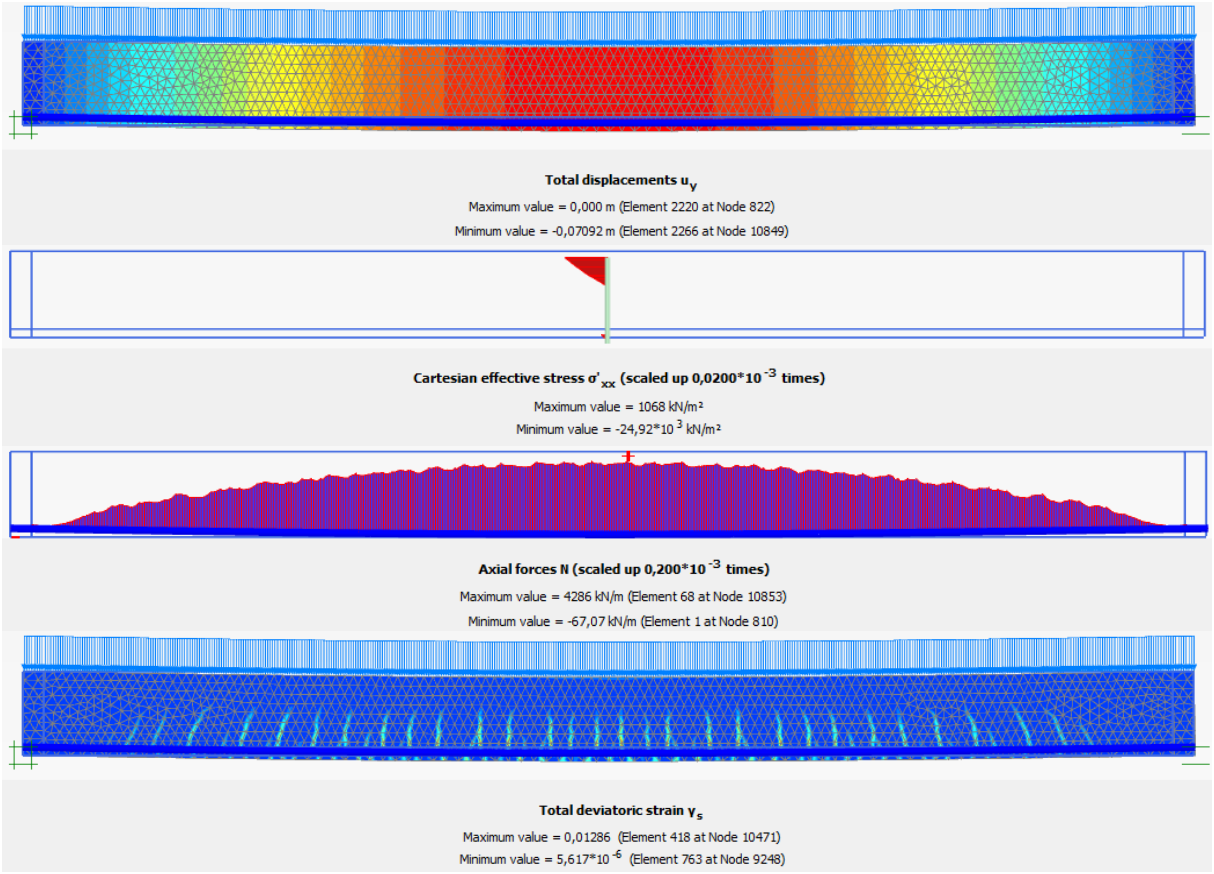

E3..13.2 Elasto-plastic reinforcement

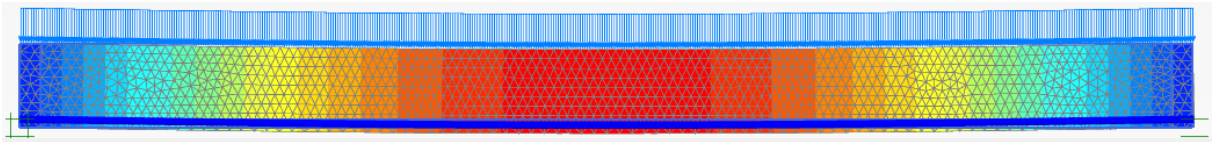

Total displacements u_y
Maximum value = 0,000 m (Element 2220 at Node 822)
Minimum value = -0,07090 m (Element 2266 at Node 10849)

Cartesian effective stress σ'_{xx} (scaled up 0,0200*10^{-3} times)
Maximum value = 1068 kN/m²
Minimum value = -24,91*10^{3} kN/m²

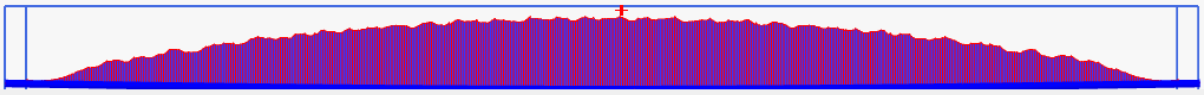

Axial forces N (scaled up 0,200*10^{-3} times)
Maximum value = 4285 kN/m (Element 68 at Node 10853)
Minimum value = -67,06 kN/m (Element 1 at Node 810)

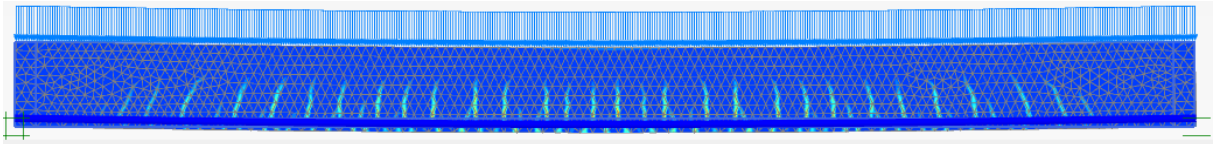

Total deviatoric strain γ_s
Maximum value = 0,01286 (Element 418 at Node 10471)
Minimum value = 5,615*10^{-6} (Element 763 at Node 9248)

E.3.14 Results applied line load of 140 kN/m (model yielding) (G_t=0.15 kN/m)

E3..14.1 Linear elastic reinforcement

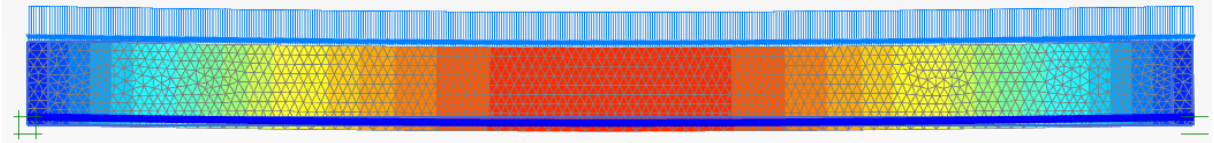

Total displacements u_y
Maximum value = 0,000 m (Element 2220 at Node 822)
Minimum value = -0,07194 m (Element 2263 at Node 10217)

Cartesian effective stress σ'_{xx} (scaled up 0,0200*10^{-3} times)
Maximum value = 973,9 kN/m²
Minimum value = -25,19*10^{3} kN/m²

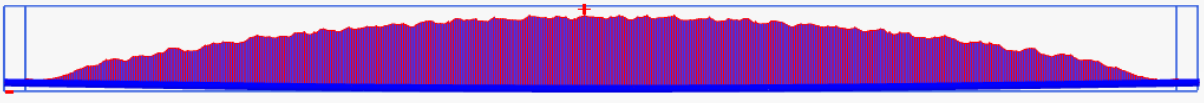

Axial forces N (scaled up 0,200*10^{-3} times)
Maximum value = 4337 kN/m (Element 65 at Node 10239)
Minimum value = -67,74 kN/m (Element 1 at Node 810)

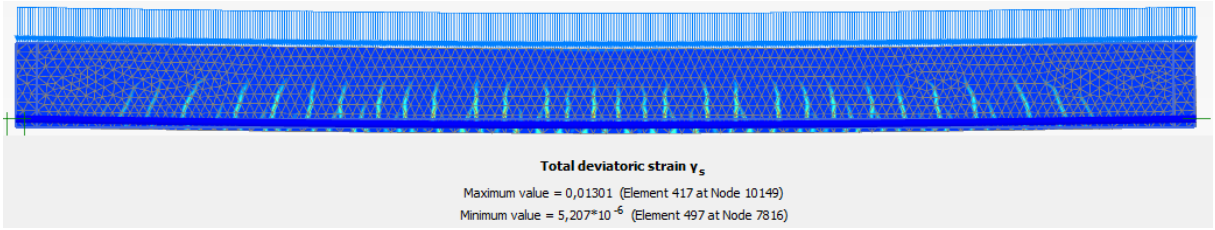

Total deviatoric strain γ_s

Maximum value = 0,01301 (Element 417 at Node 10149)

Minimum value = $5{,}207*10^{-6}$ (Element 497 at Node 7816)

E.3.14.2 Elasto-plastic reinforcement

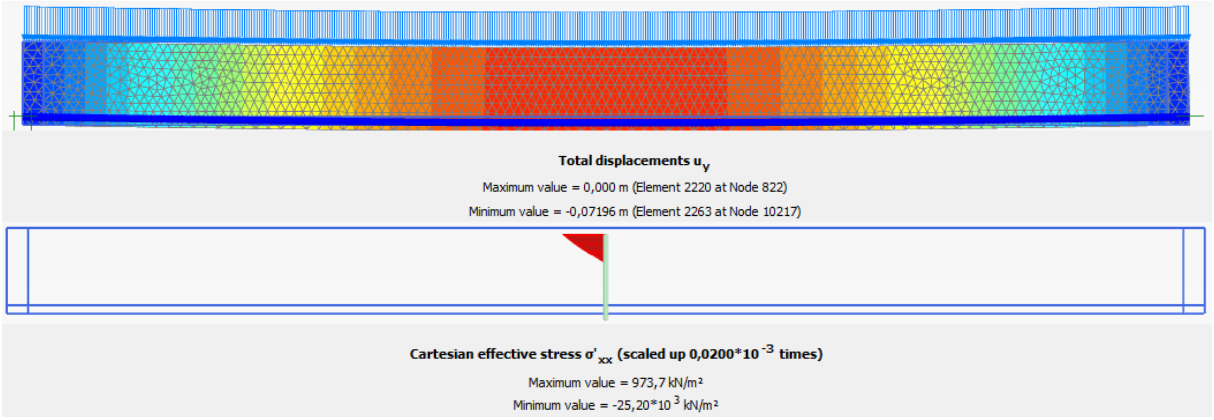

Total displacements u_y

Maximum value = 0,000 m (Element 2220 at Node 822)

Minimum value = -0,07196 m (Element 2263 at Node 10217)

Cartesian effective stress σ'_{xx} (scaled up $0{,}0200*10^{-3}$ times)

Maximum value = 973,7 kN/m²

Minimum value = $-25{,}20*10^{3}$ kN/m²

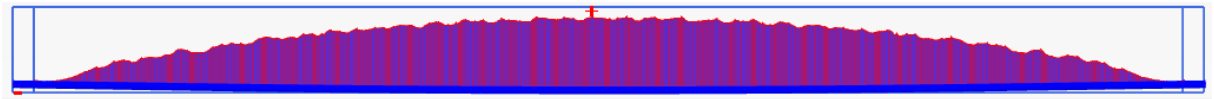

Axial forces N (scaled up $0{,}200*10^{-3}$ times)

Maximum value = 4338 kN/m (Element 65 at Node 10239)

Minimum value = -67,75 kN/m (Element 1 at Node 810)

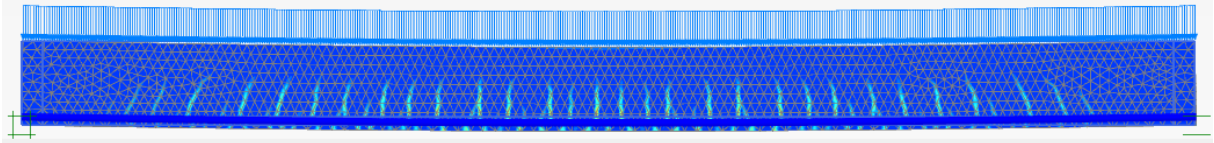

Total deviatoric strain γ_s

Maximum value = 0,01302 (Element 417 at Node 10149)

Minimum value = $5{,}204*10^{-6}$ (Element 497 at Node 7816)

E.3.15 Results applied line load of 142.5 kN/m (ϵ_c=3.5 ‰) (G_t=0.15kN/m)

E.3.15.1 Linear elastic reinforcement

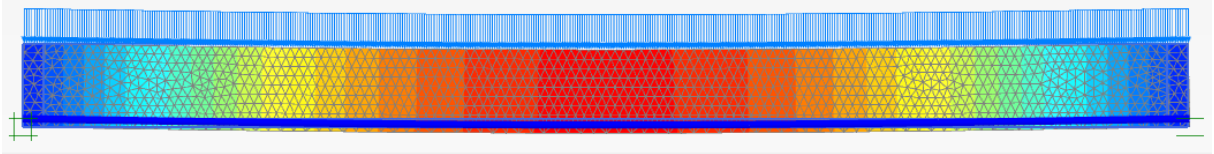

Total displacements u_y

Maximum value = 0,000 m (Element 2220 at Node 822)

Minimum value = -0,07345 m (Element 2373 at Node 10512)

Cartesian effective stress σ'_{xx} (scaled up $0{,}0200*10^{-3}$ times)

Maximum value = 1188 kN/m²

Minimum value = $-25{,}30*10^{3}$ kN/m²

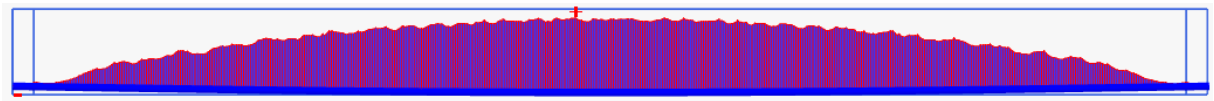

Axial forces N (scaled up 0,200*10 $^{-3}$ times)

Maximum value = 4405 kN/m (Element 63 at Node 10017)

Minimum value = -68,77 kN/m (Element 1 at Node 810)

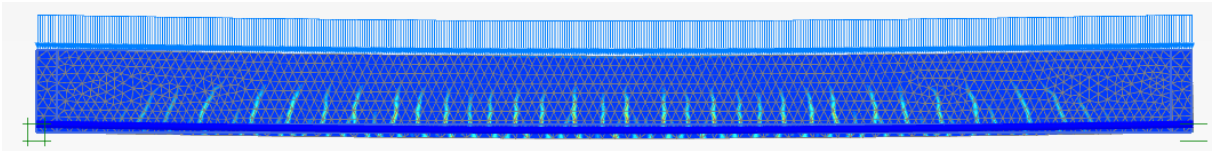

Total deviatoric strain γ_s

Maximum value = 0,01332 (Element 418 at Node 10471)

Minimum value = 1,640*10 $^{-6}$ (Element 821 at Node 8396)

E.3.15.2 Elasto-plastic reinforcement

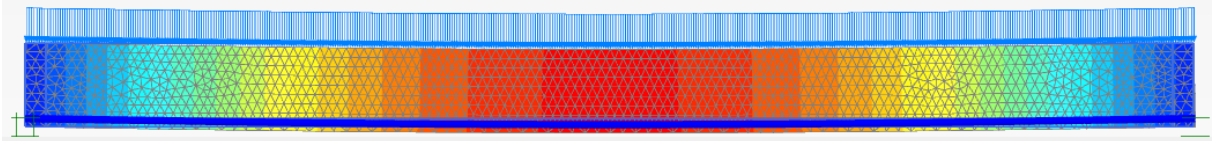

Total displacements u_y

Maximum value = 0,000 m (Element 2220 at Node 822)

Minimum value = -0,07344 m (Element 2373 at Node 10512)

Cartesian effective stress σ'_{xx} (scaled up 0,0200*10 $^{-3}$ times)

Maximum value = 1188 kN/m²

Minimum value = -25,30*10 ^{3} kN/m²

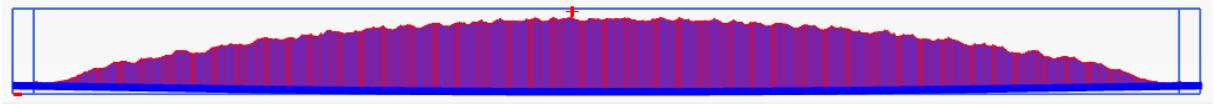

Axial forces N (scaled up 0,200*10 $^{-3}$ times)

Maximum value = 4387 kN/m (Element 63 at Node 10017)

Minimum value = -68,77 kN/m (Element 1 at Node 810)

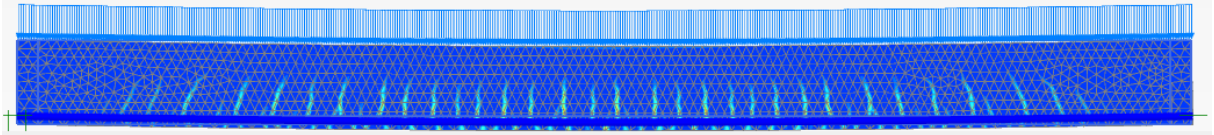

Total deviatoric strain γ_s

Maximum value = 0,01332 (Element 418 at Node 10471)

Minimum value = 1,638*10 $^{-6}$ (Element 821 at Node 8396)

E.3.16 Results applied line load of 146.4 kN/m (failure) (*Gt=0.15 kN/m)*

E.3.16.1 Linear elastic reinforcement

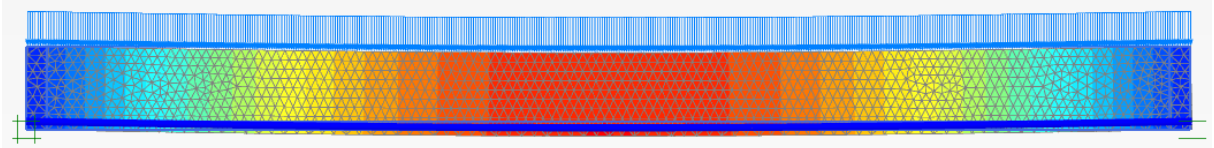

Total displacements u_y

Maximum value = 0,000 m (Element 2220 at Node 822)

Minimum value = -0,07613 m (Element 2263 at Node 10217)

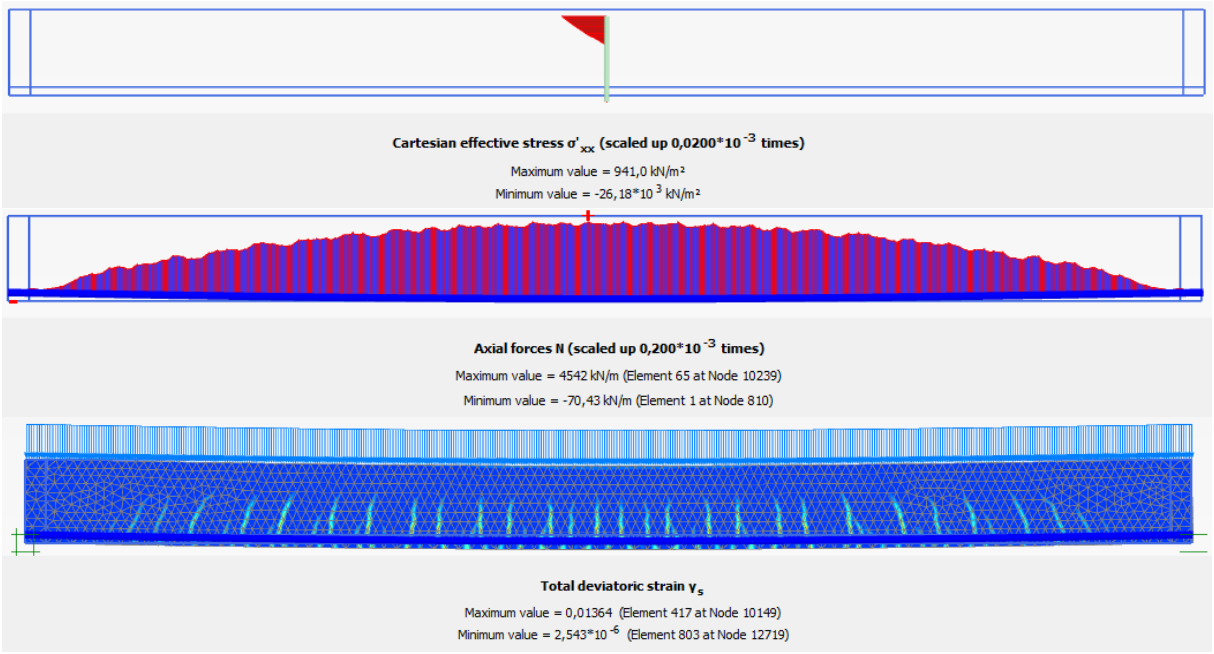

E.3.16.2 Elasto-plastic reinforcement

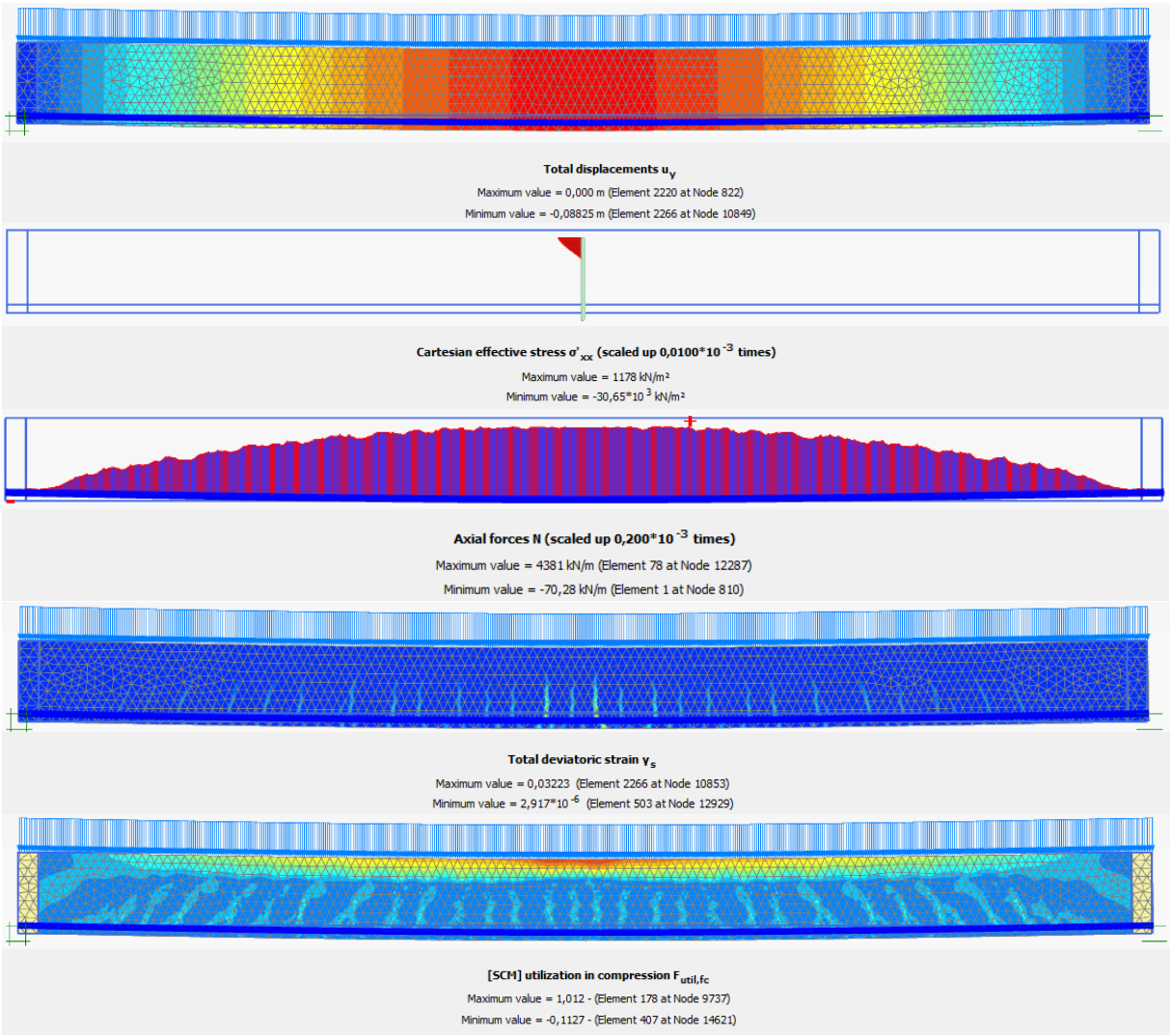

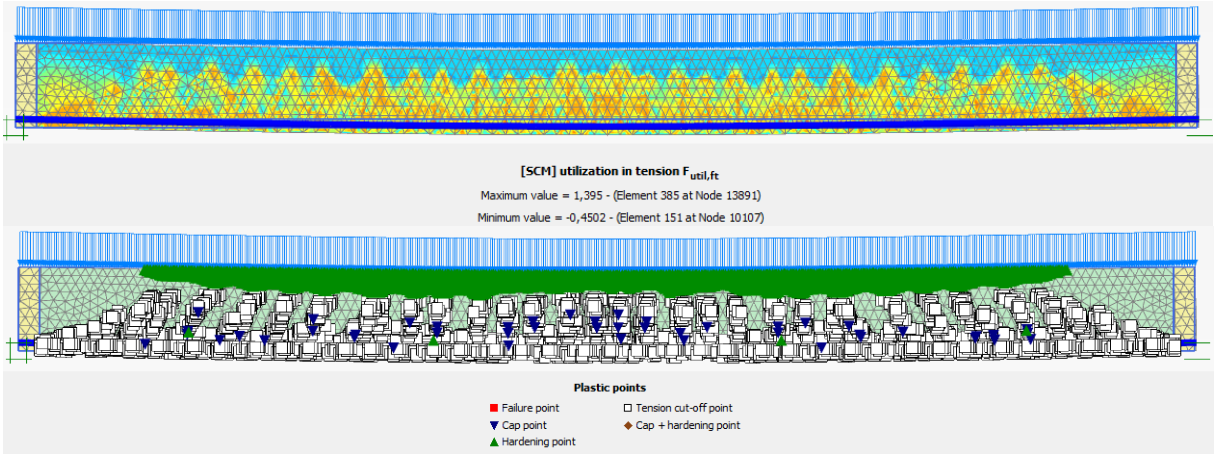

E.3.17 Results of model failure line load (Gt= 0.15 kN/m)

E.3.17.1 Linear elastic reinforcement (150 kN/m) (Still no failure)

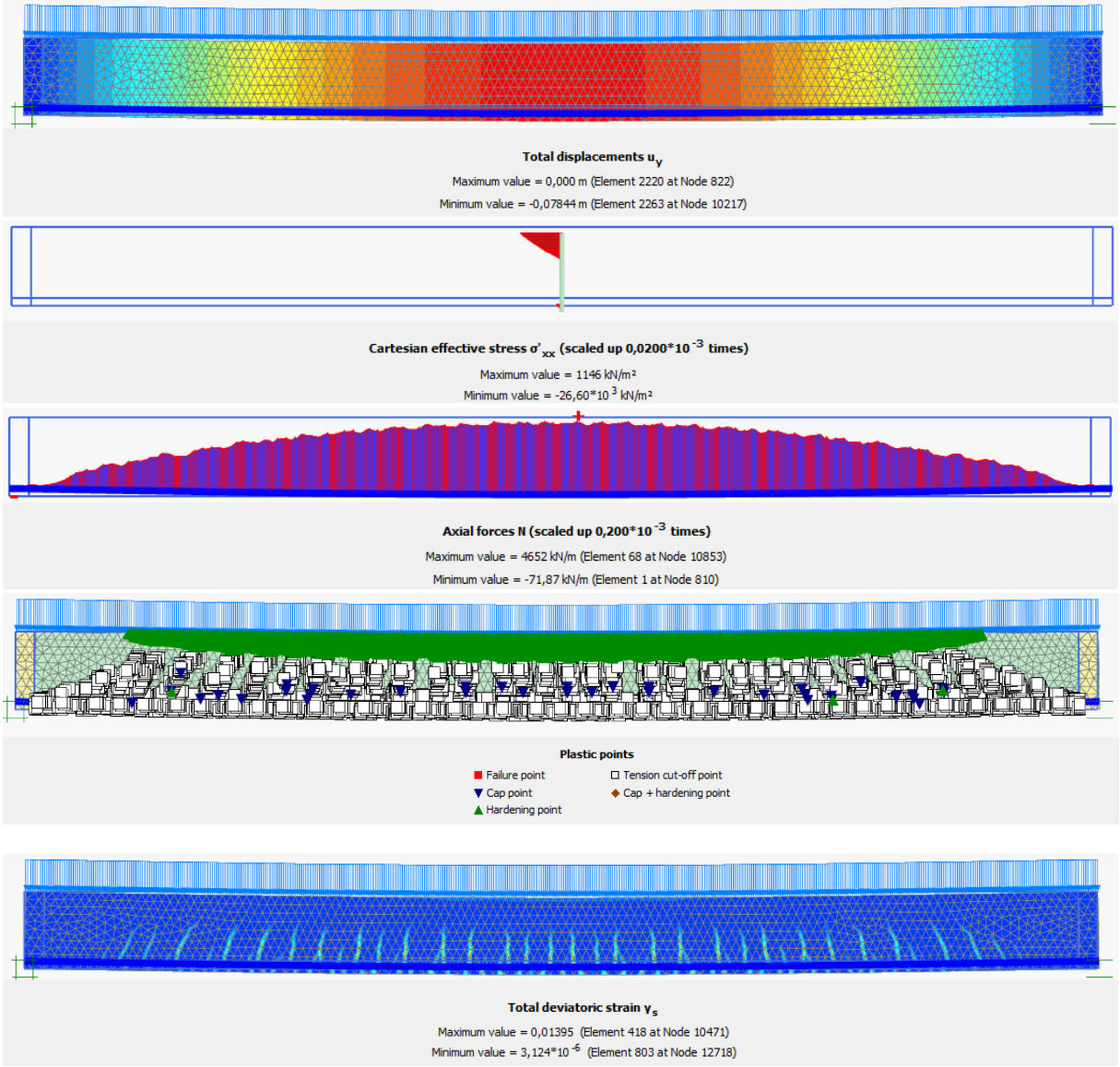

E.3.17.2 Elasto-plastic reinforcement (Failure at 146.4 kN/n)

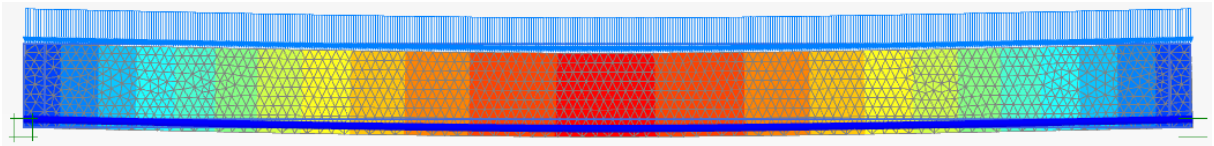

Total displacements u_y

Maximum value = 0,000 m (Element 2220 at Node 822)

Minimum value = -0,1157 m (Element 2263 at Node 10217)

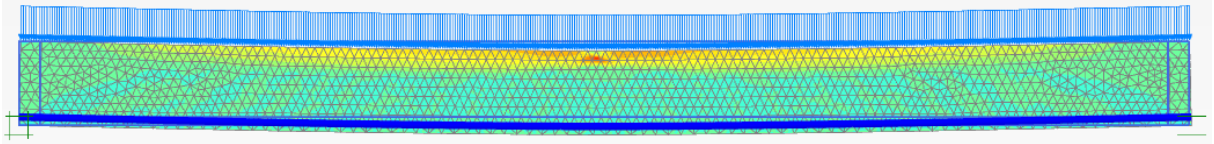

Cartesian effective stress σ'_{xx}

Maximum value = $36{,}23*10^{3}$ kN/m² (Element 2220 at Node 823)

Minimum value = $-45{,}49*10^{3}$ kN/m² (Element 297 at Node 9382)

Cartesian effective stress σ'_{xx} (scaled up $0{,}0100*10^{-3}$ times)

Maximum value = 1355 kN/m²

Minimum value = $-34{,}72*10^{3}$ kN/m²

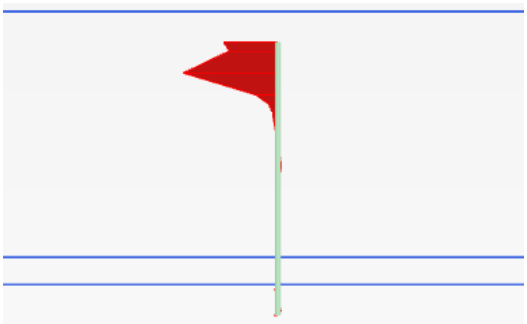

Cartesian effective stress σ'_{xx} (scaled up $0{,}0100*10^{-3}$ times)

Maximum value = 1355 kN/m²

Minimum value = $-34{,}72*10^{3}$ kN/m²

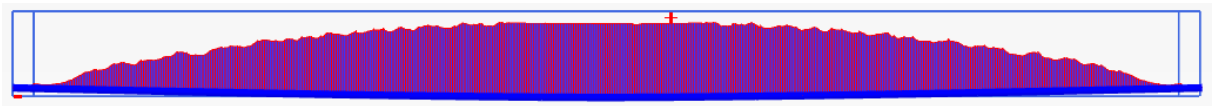

Axial forces N (scaled up $0{,}200*10^{-3}$ times)

Maximum value = 4374 kN/m (Element 73 at Node 11557)

Minimum value = -70,12 kN/m (Element 1 at Node 810)

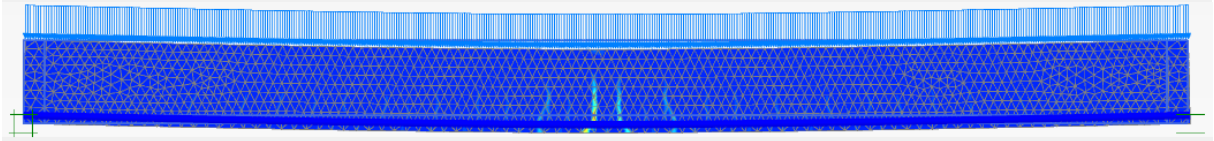

Total deviatoric strain γ_s

Maximum value = 0,07726 (Element 153 at Node 10229)

Minimum value = $4{,}739*10^{-6}$ (Element 856 at Node 10597)

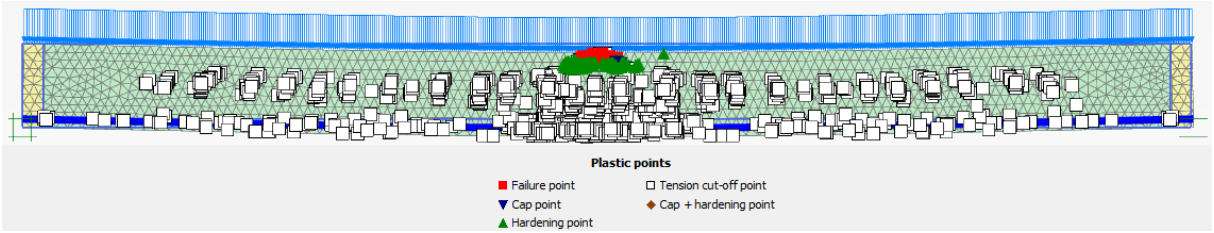

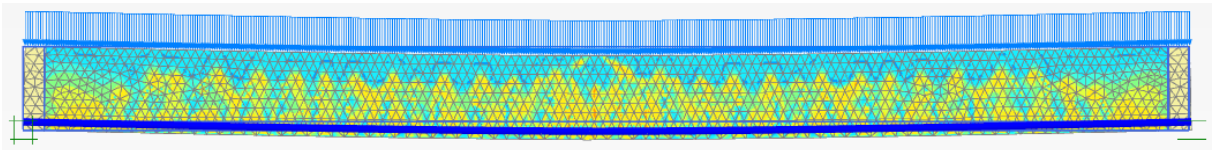

[SCM] utilization in tension $F_{util,ft}$

Maximum value = 1,484 - (Element 299 at Node 10239)

Minimum value = -0,5319 - (Element 133 at Node 8985)

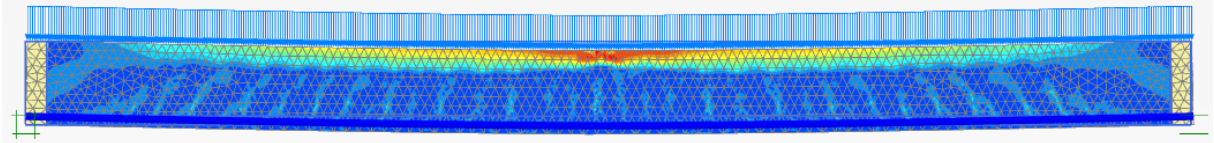

[SCM] utilization in compression $F_{util,fc}$

Maximum value = 1,044 - (Element 176 at Node 9384)

Minimum value = -0,07475 - (Element 243 at Node 16505)

E.4 Double plate reinforced shotcrete model results

E.4.1 Results applied line load of 17 kN/m

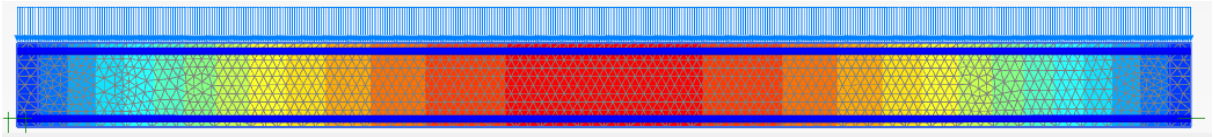

Total displacements u_y

Maximum value = 0,000 m (Element 2368 at Node 842)

Minimum value = -2,690*10 $^{-3}$ m (Element 1065 at Node 10769)

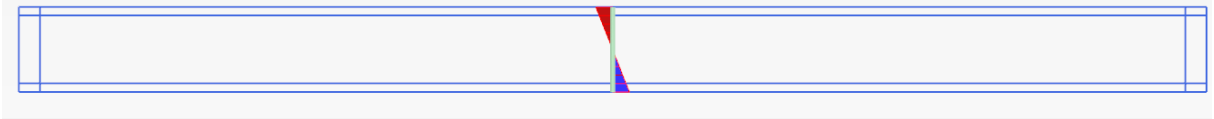

Cartesian effective stress σ'_{xx} (scaled up 0,100*10 $^{-3}$ times)

Maximum value = 1986 kN/m²

Minimum value = -1987 kN/m²

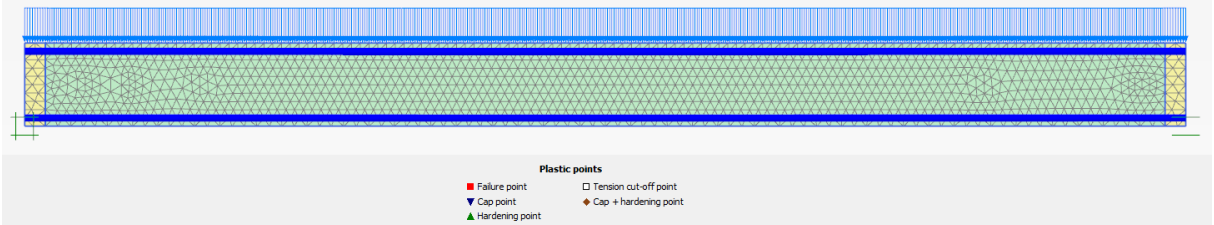

E.4.2 Results applied line load of 18 kN/m

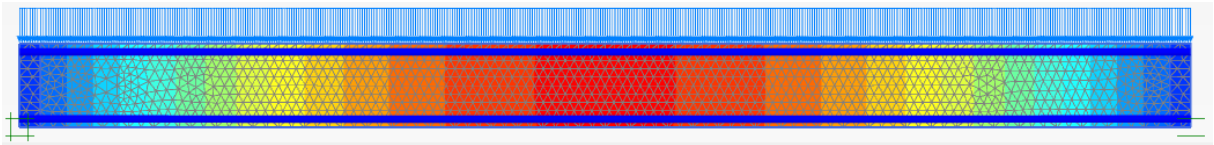

Total displacements u_y

Maximum value = 0,000 m (Element 2368 at Node 842)

Minimum value = -2,849*10^{-3} m (Element 1065 at Node 10769)

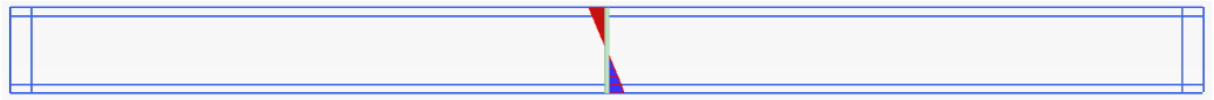

Cartesian effective stress σ'_{xx} (scaled up 0,100*10^{-3} times)

Maximum value = 2013 kN/m²

Minimum value = -2106 kN/m²

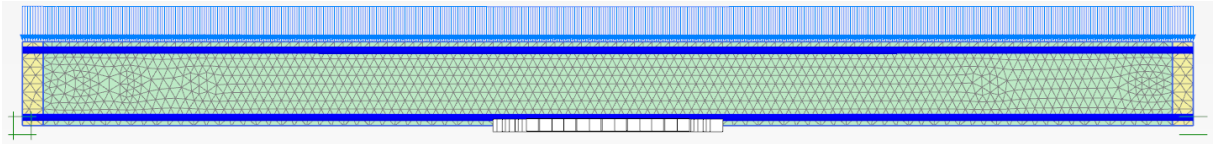

Plastic points

Failure point | Tension cut-off point

Cap point | Cap + hardening point

Hardening point

E.4.3 Results applied line load of 30 kN/m

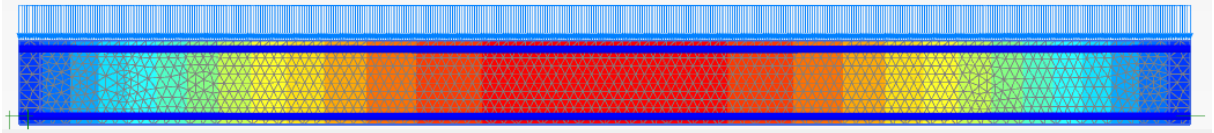

Total displacements u_y

Maximum value = 0,000 m (Element 2368 at Node 842)

Minimum value = -5,506*10^{-3} m (Element 1066 at Node 10566)

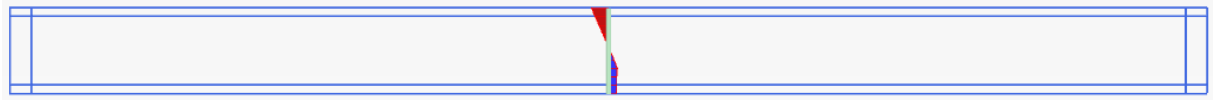

Cartesian effective stress σ'_{xx} (scaled up 0,0500*10^{-3} times)

Maximum value = 2014 kN/m²

Minimum value = -3966 kN/m²

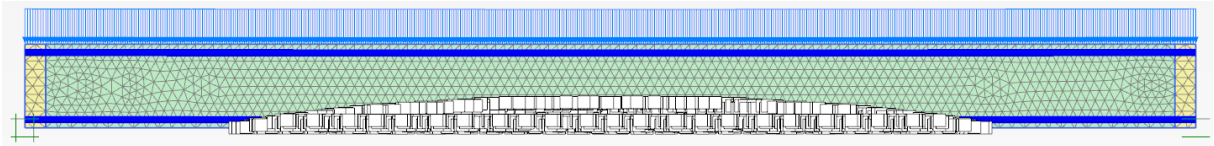

Plastic points

Failure point | Tension cut-off point

Cap point | Cap + hardening point

Hardening point

E.5 Mesh sensitivity analysis results

E.5.1 Results at a line load of 40 kN/m

E.5.1.1 Very Fine

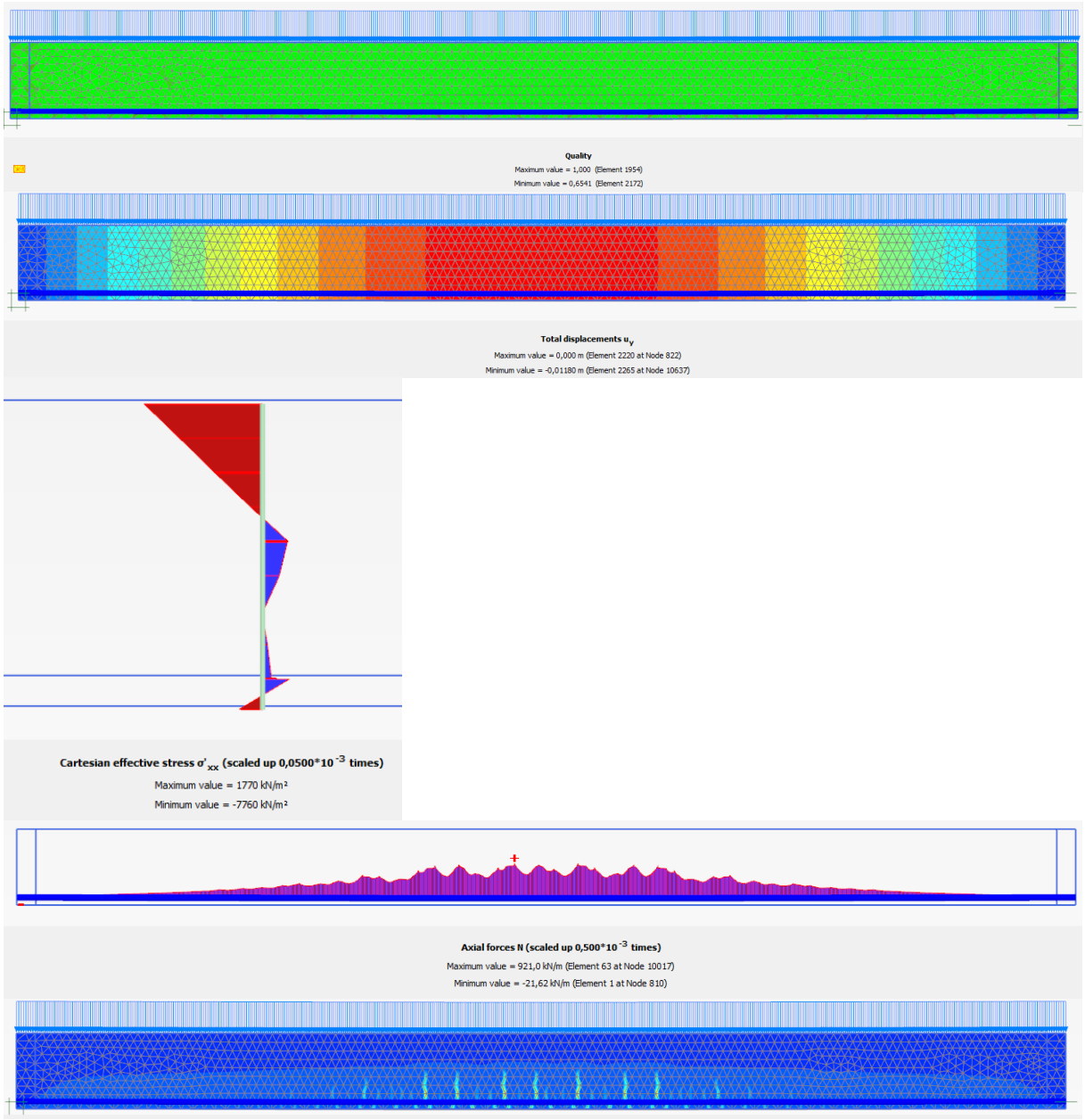

E.5.1.2 Fine

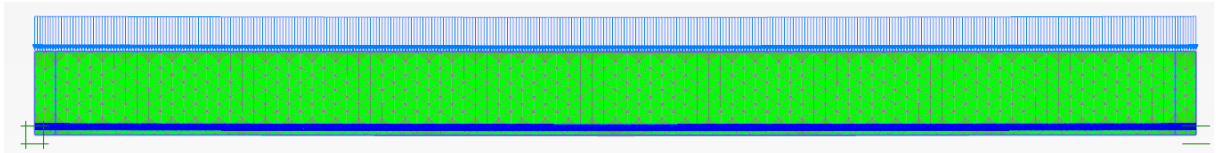

Quality

Maximum value = 1,000 (Element 46)

Minimum value = 0,7889 (Element 1239)

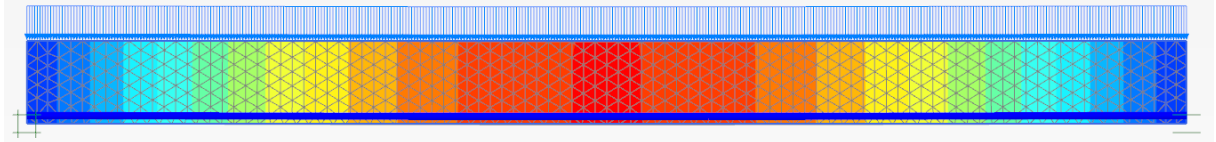

Total displacements u_y

Maximum value = 0,000 m (Element 1104 at Node 126)

Minimum value = -0,01206 m (Element 1148 at Node 5354)

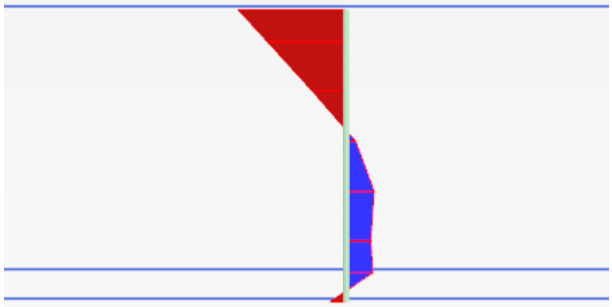

Cartesian effective stress σ'_{xx} (scaled up 0,0500*10^{-3} times)

Maximum value = 1920 kN/m²

Minimum value = -7388 kN/m²

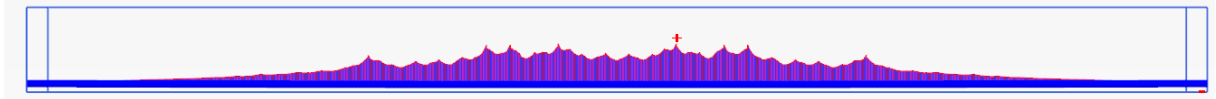

Axial forces N (scaled up 0,500*10^{-3} times)

Maximum value = 970,5 kN/m (Element 55 at Node 5999)

Minimum value = -22,15 kN/m (Element 100 at Node 10710)

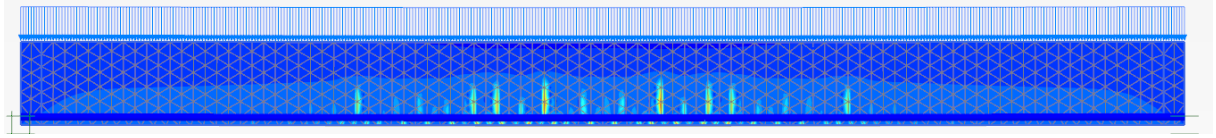

E.5.1.3 Medium

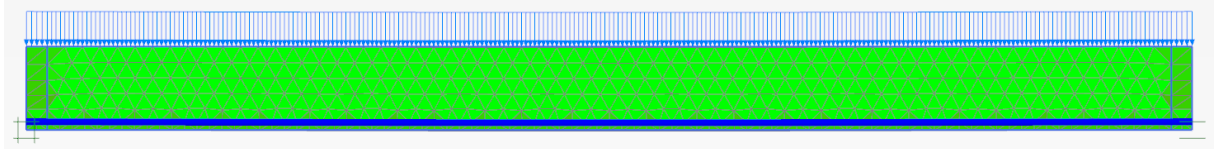

Quality

Maximum value = 1,000 (Element 123)

Minimum value = 0,7431 (Element 398)

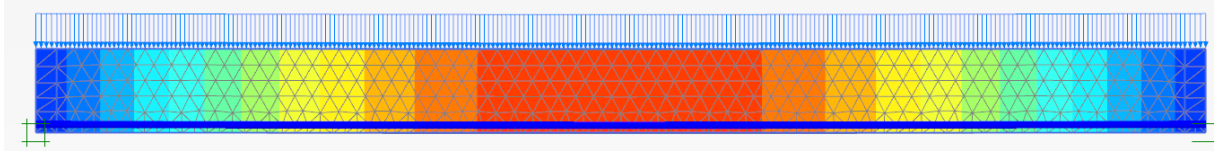

Total displacements u_y

Maximum value = 0,000 m (Element 689 at Node 159)

Minimum value = -0,01199 m (Element 777 at Node 3635)

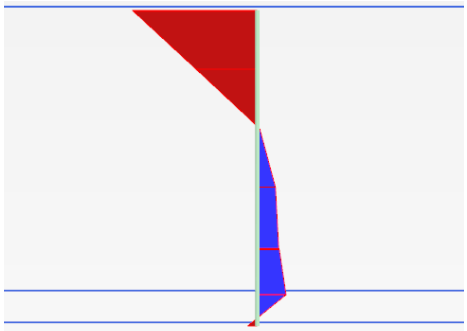

Cartesian effective stress σ'_{xx} (scaled up $0{,}0500*10^{-3}$ times)

Maximum value = 1825 kN/m²

Minimum value = -7923 kN/m²

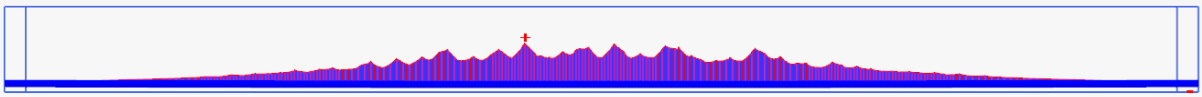

Axial forces N (scaled up $0{,}500*10^{-3}$ times)

Maximum value = 978,8 kN/m (Element 41 at Node 3287)

Minimum value = -20,94 kN/m (Element 94 at Node 7326)

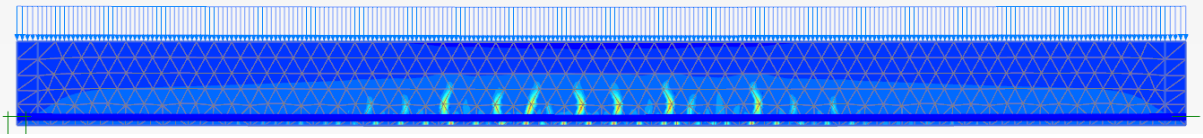

E.5.1.4 Coarse

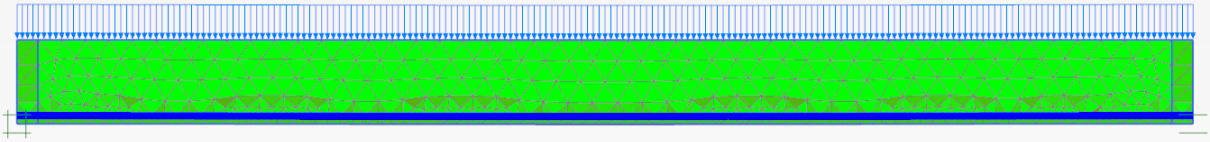

Quality

Maximum value = 1,000 (Element 159)

Minimum value = 0,5280 (Element 449)

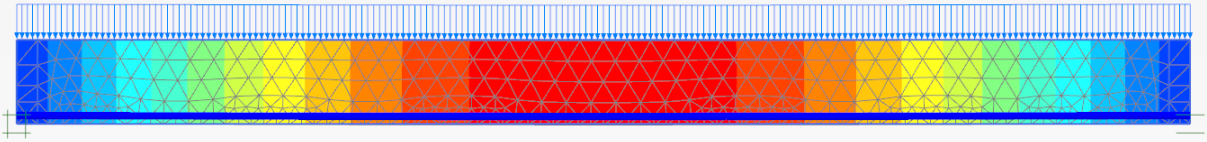

Total displacements u_y

Maximum value = 0,000 m (Element 563 at Node 17)

Minimum value = -0,01185 m (Element 653 at Node 3124)

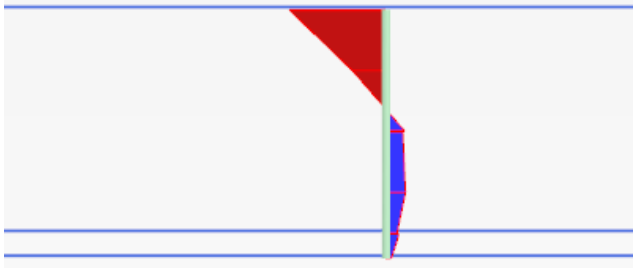

Cartesian effective stress σ'_{xx} (scaled up $0{,}0500*10^{-3}$ times)

Maximum value = 1564 kN/m²

Minimum value = -7798 kN/m²

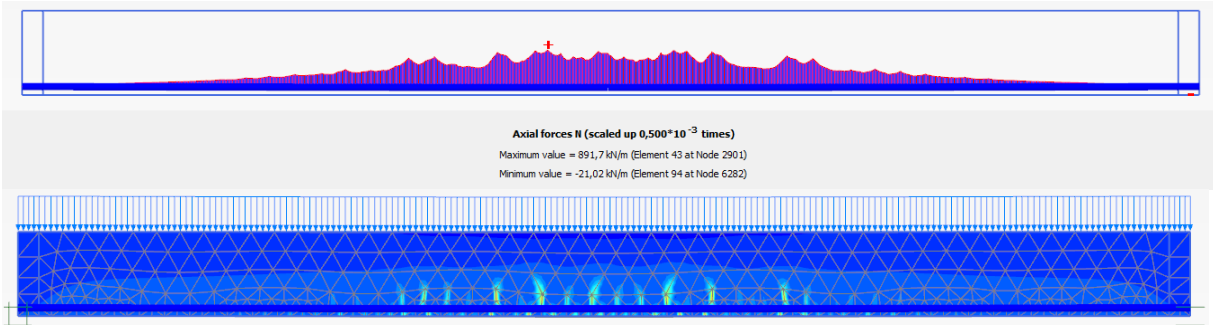

Axial forces N (scaled up 0,500*10 $^{-3}$ times)

Maximum value = 891,7 kN/m (Element 43 at Node 2901)

Minimum value = -21,02 kN/m (Element 94 at Node 6282)

E.5.1.5 Very Coarse

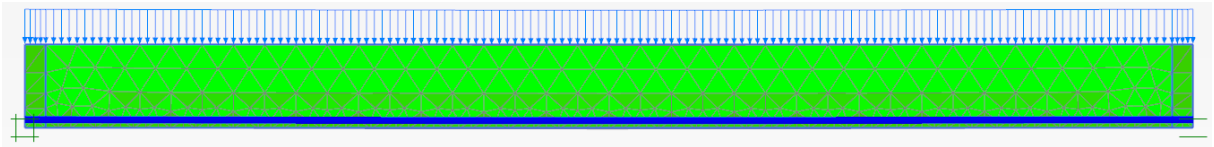

Quality

Maximum value = 0,9993 (Element 418)

Minimum value = 0,7505 (Element 400)

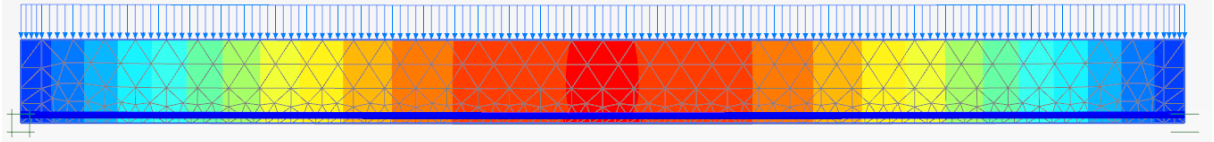

Total displacements u_y

Maximum value = 0,000 m (Element 439 at Node 13)

Minimum value = -0,01207 m (Element 531 at Node 2630)

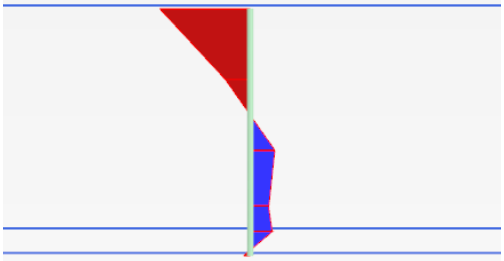

Cartesian effective stress σ'_{xx} (scaled up 0,0500*10 $^{-3}$ times)

Maximum value = 2005 kN/m²

Minimum value = -7347 kN/m²

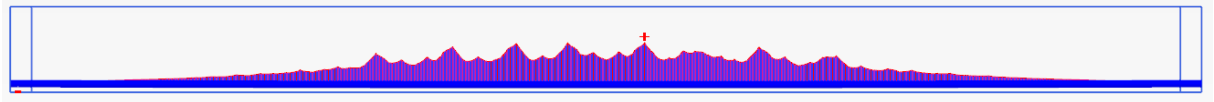

Axial forces N (scaled up 0,500*10 $^{-3}$ times)

Maximum value = 994,7 kN/m (Element 51 at Node 2855)

Minimum value = -20,90 kN/m (Element 1 at Node 33)

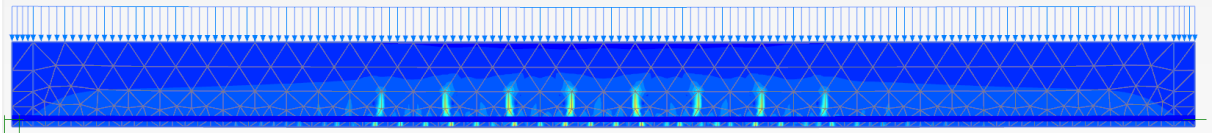

E.5.2 Results at a line load of 60 kN/m

E.5.2.1 Very Fine

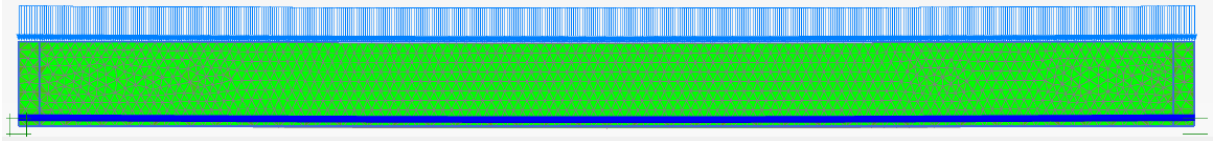

Quality

Maximum value = 1,000 (Element 1954)

Minimum value = 0,6541 (Element 2172)

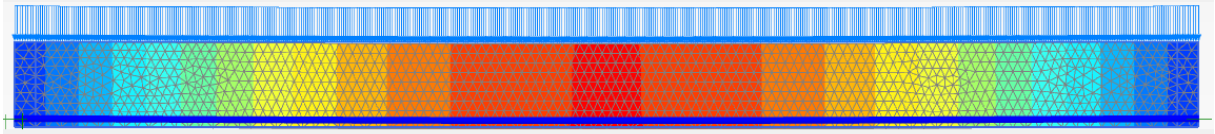

Total displacements u_y

Maximum value = 0,000 m (Element 2220 at Node 822)

Minimum value = -0,02416 m (Element 2264 at Node 10429)

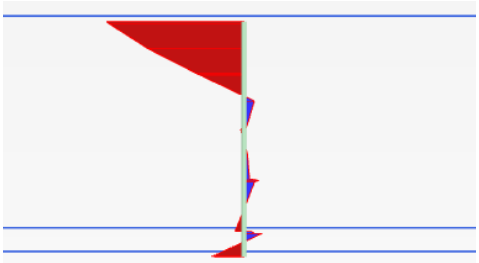

Cartesian effective stress σ'_{xx} (scaled up $0{,}0500*10^{-3}$ times)

Maximum value = 1559 kN/m²

Minimum value = $-11{,}73*10^{3}$ kN/m²

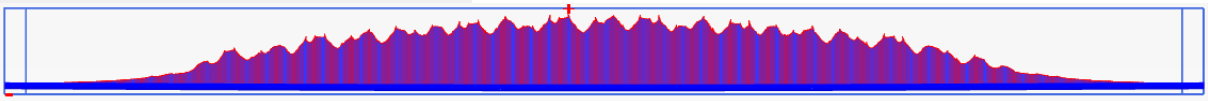

Axial forces N (scaled up $0{,}500*10^{-3}$ times)

Maximum value = 1709 kN/m (Element 63 at Node 10017)

Minimum value = -32,11 kN/m (Element 1 at Node 810)

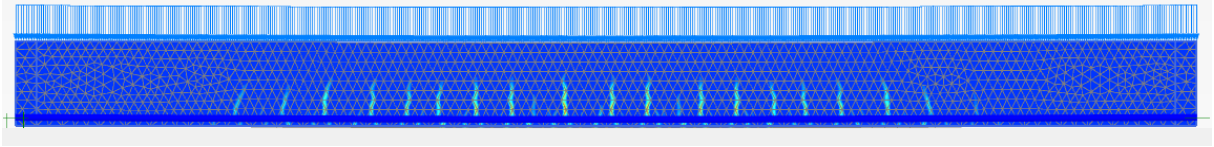

E.5.2.2 Fine

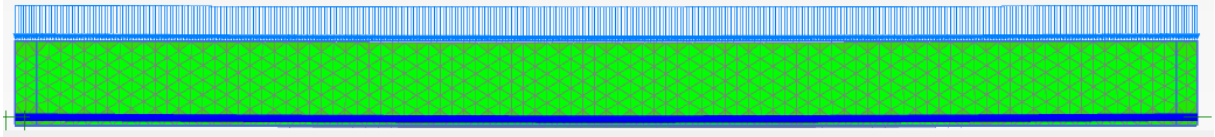

Quality

Maximum value = 1,000 (Element 46)

Minimum value = 0,7883 (Element 1241)

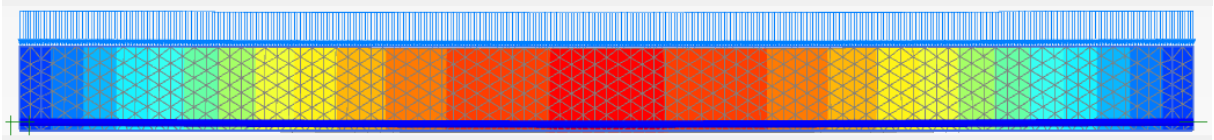

Total displacements u_y

Maximum value = 0,000 m (Element 1104 at Node 126)

Minimum value = -0,02432 m (Element 1239 at Node 5464)

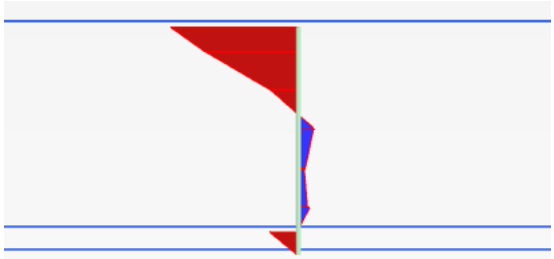

Cartesian effective stress σ'_{xx} (scaled up $0{,}0500*10^{-3}$ times)

Maximum value = 1406 kN/m²

Minimum value = $-11{,}31*10^{3}$ kN/m²

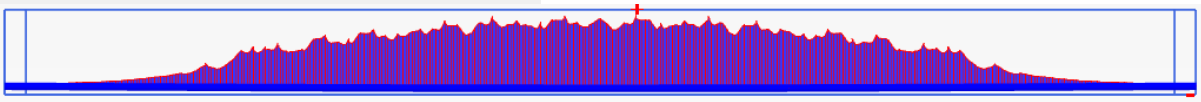

Axial forces N (scaled up $0{,}500*10^{-3}$ times)

Maximum value = 1725 kN/m (Element 53 at Node 5783)

Minimum value = -33,02 kN/m (Element 100 at Node 10710)

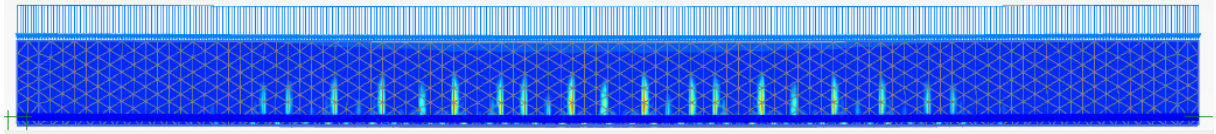

Total deviatoric strain γ_s

Maximum value = $3{,}510*10^{-3}$ (Element 985 at Node 5763)

Minimum value = $2{,}179*10^{-6}$ (Element 1138 at Node 4189)

E.5.2.3 Medium

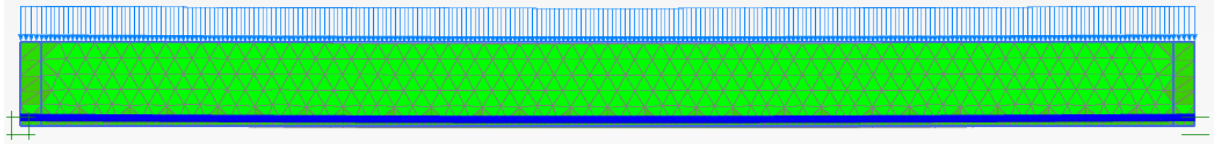

Quality

Maximum value = 1,000 (Element 123)

Minimum value = 0,7431 (Element 398)

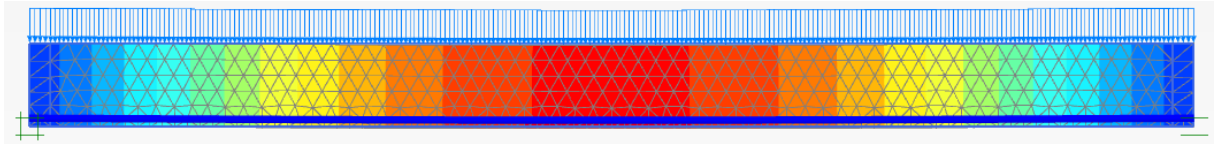

Total displacements u_y

Maximum value = 0,000 m (Element 689 at Node 159)

Minimum value = -0,02462 m (Element 781 at Node 3755)

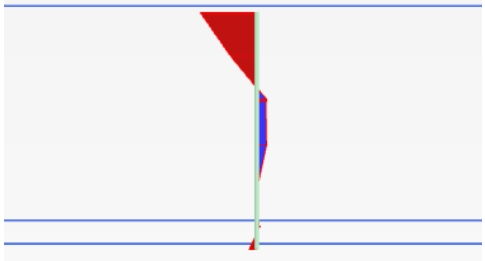

Cartesian effective stress σ'_{xx} (scaled up $0{,}0200*10^{-3}$ times)

Maximum value = 2135 kN/m²

Minimum value = $-11{,}88*10^{3}$ kN/m²

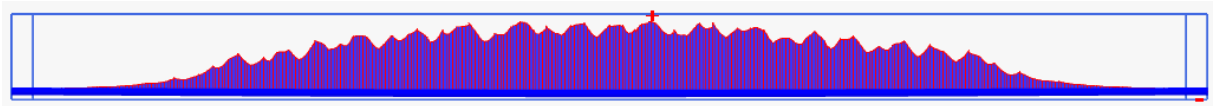

Axial forces N (scaled up 0,500*10 $^{-3}$ times)

Maximum value = 1674 kN/m (Element 51 at Node 3976)

Minimum value = -31,04 kN/m (Element 94 at Node 7326)

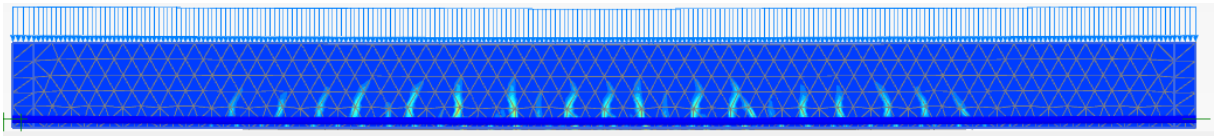

E.5.2.4 Coarse

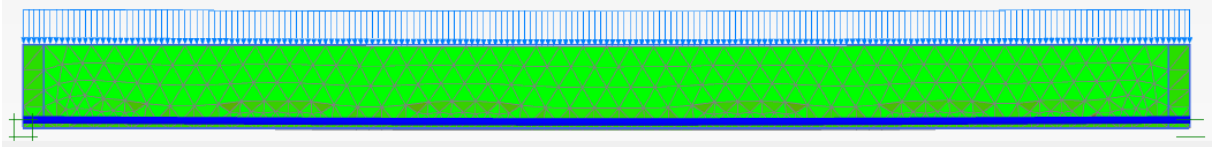

Quality

Maximum value = 1,000 (Element 159)

Minimum value = 0,5280 (Element 449)

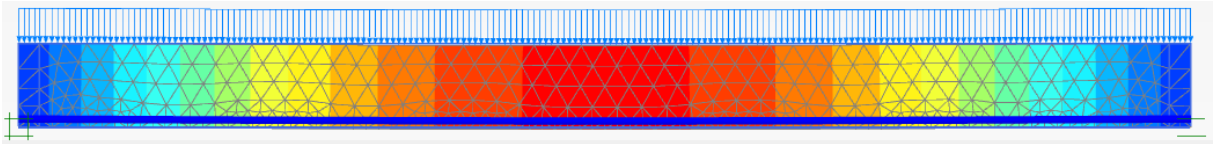

Total displacements u_y

Maximum value = 0,000 m (Element 563 at Node 17)

Minimum value = -0,02468 m (Element 653 at Node 3127)

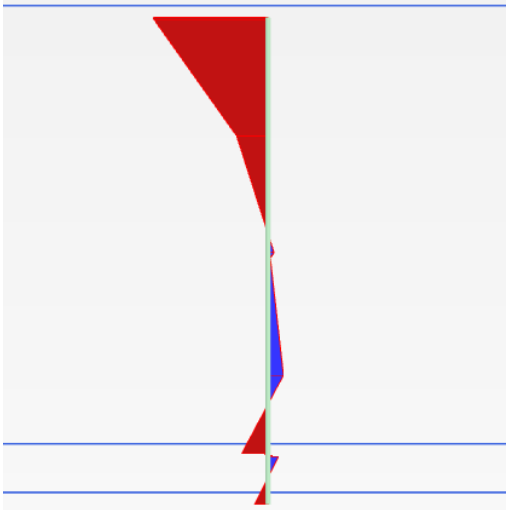

Cartesian effective stress σ'_{xx} (scaled up 0,0200*10 $^{-3}$ times)

Maximum value = 1603 kN/m²

Minimum value = -11,79*10 ^{3} kN/m²

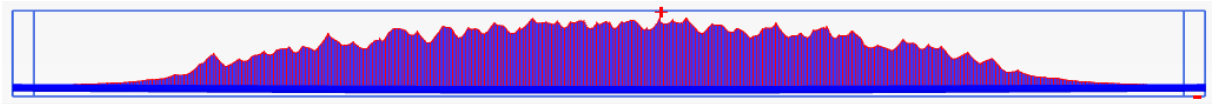

Axial forces N (scaled up 0,500*10 $^{-3}$ times)

Maximum value = 1708 kN/m (Element 51 at Node 3383)

Minimum value = -31,09 kN/m (Element 94 at Node 6282)

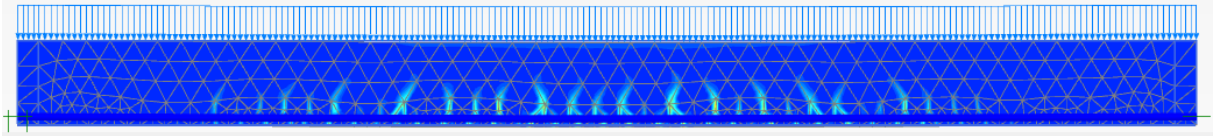

Total deviatoric strain γ_s

Maximum value = 4,547*10 $^{-3}$ (Element 665 at Node 3461)

Minimum value = 2,145*10 $^{-6}$ (Element 270 at Node 3041)

E.5.2.5 Very Coarse

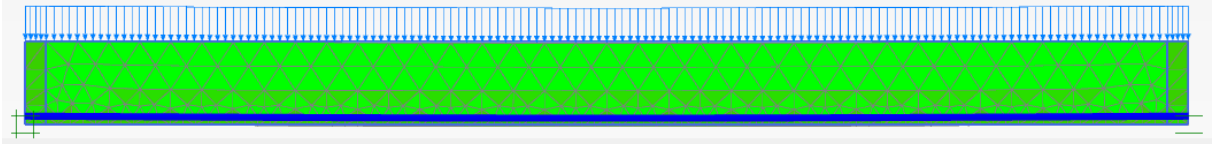

Quality

Maximum value = 0,9993 (Element 418)

Minimum value = 0,7505 (Element 400)

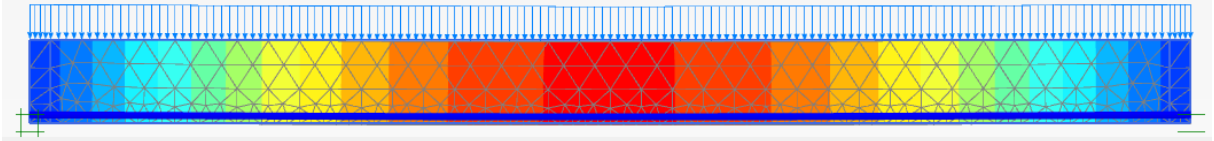

Total displacements u_y

Maximum value = 0,000 m (Element 439 at Node 13)

Minimum value = -0,02445 m (Element 525 at Node 2478)

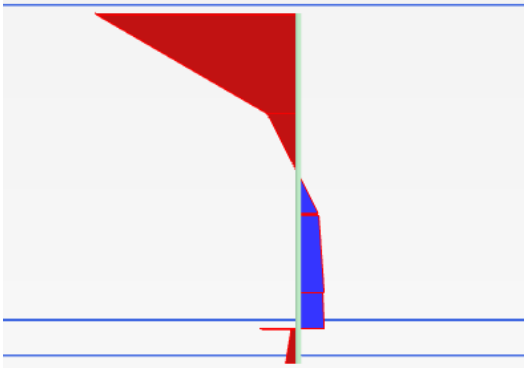

Cartesian effective stress σ'_{xx} (scaled up 0,0500*10 $^{-3}$ times)

Maximum value = 1484 kN/m²

Minimum value = -11,58*10 ^{3} kN/m²

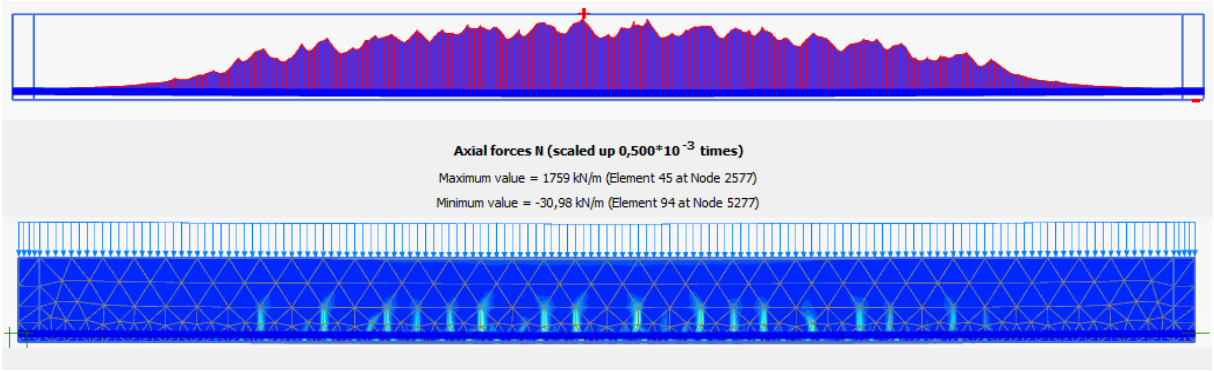
Axial forces N (scaled up 0,500*10 -3 times)
Maximum value = 1759 kN/m (Element 45 at Node 2577)
Minimum value = -30,98 kN/m (Element 94 at Node 5277)

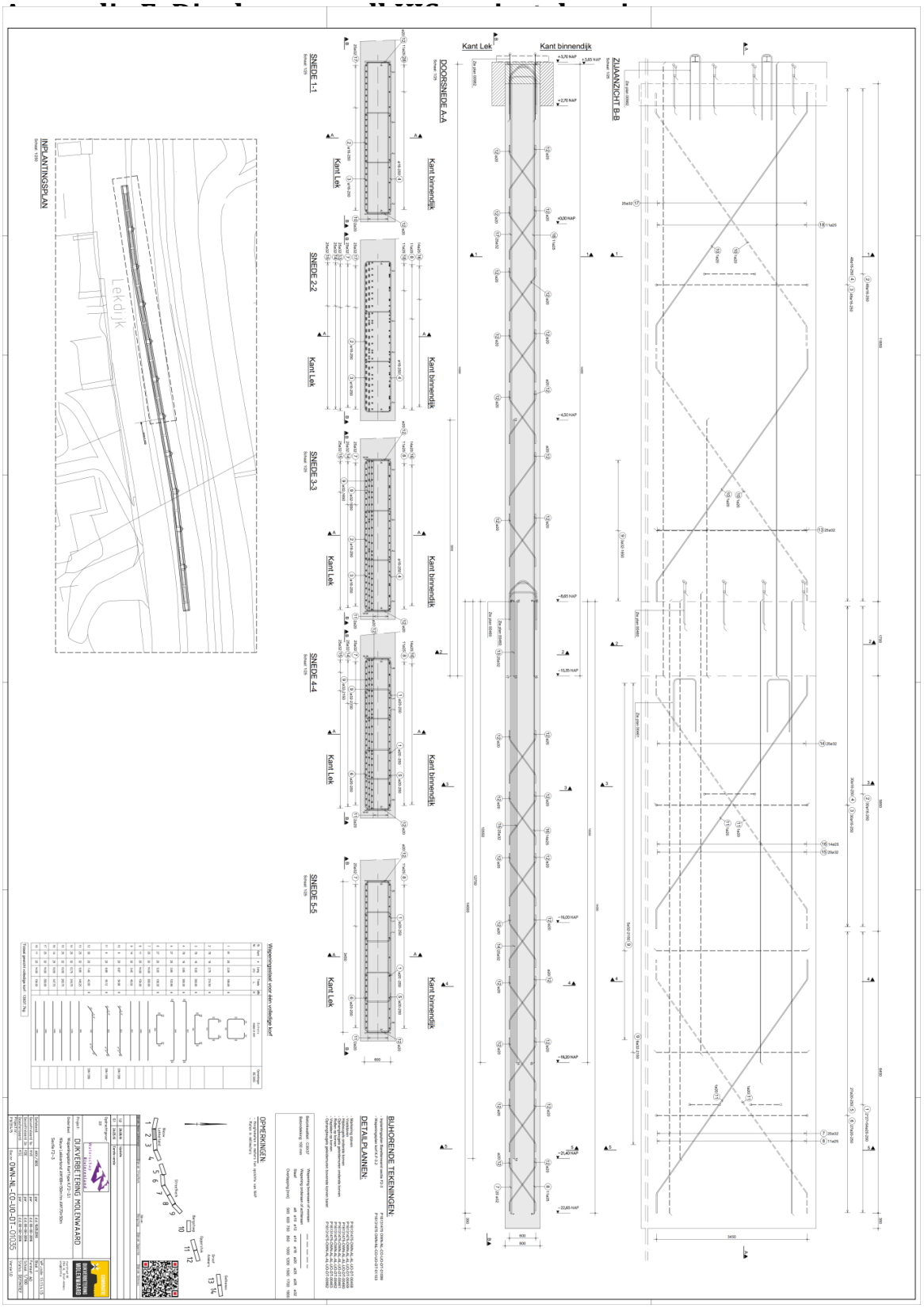

Drawing by: Mourik Groot-Ammers/ Besix